Forschungszentrum Karlsruhe

Technik und Umwelt

Wissenschaftliche Berichte

FZKA 6557

INFLUENCE OF HUMIC ACIDS ON THE MIGRATION BEHAVIOUR OF RADIOACTIVE AND NON-RADIOACTIVE SUBSTANCES UNDER CONDITIONS CLOSE TO NATURE

Final Report

C.M. Marquardt (Editor)

Institut für Nukleare Entsorgung

in collaboration with:

Institut für Kernchemie, Universität Mainz

Institut für Anorganische und Analytische Chemie und Radiochemie, Universität des Saarlandes

Forschungszentrum Rossendorf e.V., Institut für Radiochemie

Forschungszentrum Karlsruhe GmbH, Karlsruhe

2000

The work performed in this report is supported by funding from the German Federal Ministry for Education and Research (BMBF) under the Contract No. 02 E 8795 8 and 02 E 8815 0. The authors are solely responsible for the content of this publication.

BMBF Project No.: 02 E 8795 8

Partner No. 1:	Institut für Kernchemie, Universität Mainz
Partner No. 2:	Institut für Anorganische und Analytische Chemie und Radiochemie, Universität des Saarlandes
	Duration of the project: 11.95 – 01.99

BMBF Project No.: 02 E 8815 0

Partner No. 3:	Forschungszentrum Rossendorf e.V.,
	Institut für Radiochemie
	Duration of the project: 11.95 – 02.99

External Partner

Partner No 4:	Forschungszentrum Karlsruhe GmbH,
	Institut für Nukleare Entsorgung

Foreword

The present report summarizes the progress and the final results obtained within the BMBF-Project "INFLUENCE OF HUMIC ACIDS ON THE MIGRATION BEHAVIOUR OF RADIOACTIVE AND NON-RADIOACTIVE SUBSTANCES UNDER CONDITIONS CLOSE TO NATURE". This project, which has continued for 3 years, was conducted in the frame of a BMBF supporting program directed towards the assessment of final repositories / underground disposal facilities in deep geological formations.

The report contains an executive summary of three final reports prepared by the individual financially supported partners. The more detailed information is found in the final reports given by the partners in three appendices hereby enclosed. The summary intends to give an overview of the covered topics and the corresponding results without going into details, but wants to point out relationships among the different studies. Readers, who are interested in details, also need to consult the appendices.

The report reflects the excellent co-operation of different scientific groups, which were integrated in the "cost shared research project" of the BMBF. The elaborated results are important contributions to elucidate the mechanisms of radionuclide and heavy metal-ion behaviour in natural systems, which can be introduced into the safety assessment of nuclear and toxic waste disposal in deep geologic formations.

The following abbreviations are used in the text for each partner:

- Institut für Kernchemie, Universität Mainz: UMz
- Institut für Anorganische und Analytische Chemie und Radiochemie, Universität Saarbrücken: USb
- Institut für Radiochemie, Forschungszentrum Rossendorf e.V.: FZR
- Institut für Nukleare Entsorgung, Forschungszentrum Karlsruhe GmbH: FZK

Content

Executive Summary

INFLUENCE OF HUMIC ACIDS ON THE MIGRATION BEHAVIOUR OF RADIOACTIVE AND NON-RADIOACTIVE SUBSTANCES UNDER CONDITIONS CLOSE TO NATURE

Final Report

BMBF Project No.: 02 E 8795 8

and

BMBF Project No.: 02 E 8815 0

C.M. Marquardt

(FZK/INE)

Content of the Executive Summary

Introduction

For the long-term safety assessment of waste repositories, detailed knowledge about the geochemical behaviour of radioactive and toxic metal ions in the environment (geologic matrix and aquifer system) is necessary. The geochemical behaviour and thus, mobilisation or immobilisation of radioactive and toxic metals can be largely determined by humic acids (HA) due to their ability of complexation and colloid formation. With this background the present project was supported by the Bundesministerium für Bildung und Forschung (BMBF) in the frame of a program concerning the assessment of final repositories / underground disposal facilities in deep geological formations. The project started at 11.95 and lasted three years. The work program has encompassed the characterization of natural humic acid (Aldrich HA, Fluka HA, Kranichsee HA), synthesis, ^{14}C-labelling and characterization of synthetic humic acids (M1, M42), complexation studies of metal ions (Pb^{2+}, Cd^{2+}, Zn^{2+},Sm^{3+}, Cm^{3+}, NpO_2^{+}, UO_2^{2+}) with humic acids as well as batch and column experiments of metal ions in a water/sediment system under near-natural conditions.

Humic acids are organic macromolecules with undefined structure and large heterogeneity in composition depending on their origin. In order to understand binding mechanisms, the synthesis of simpler model substances for humic acids was developed [1]. Alkali-soluble and acid-insoluble melanoidin fractions were chosen as model substances for humic acids, because the molecules show both structural and also functional similarities with natural HA. The melanoidin synthesis is considered as one possible way for the formation of humic substances in the environment [2]. By variation of the precursor substances for melanoidins, manifold special model substances for HA are available. These “simple” HA have been used for metal complexation studies and have been compared with natural HA.

Another objective of the project was to study the metal ion complexation with humic acids in order to deliver reliable thermodynamic data, which can be introduced into migration modelling and safety assessment calculations. In order to maintain comparability of the results, the examinations were limited to a few humic acids, which were investigated by all partners. Aldrich humic acid was chosen as a natural reference humic acid and two synthetic humic acids (M1 and M42), prepared by FZR, served as well-defined model humic acids.

The next step on the way from well defined laboratory systems to nature has been tackled in more complex laboratory experiments: batch and column experiments with natural material under near-natural conditions. A humic-acid rich groundwater and a sandy sediment from the Gorleben site were taken to examine the mobility of metal ions.
In the following Table, the activities within this project are summarized.

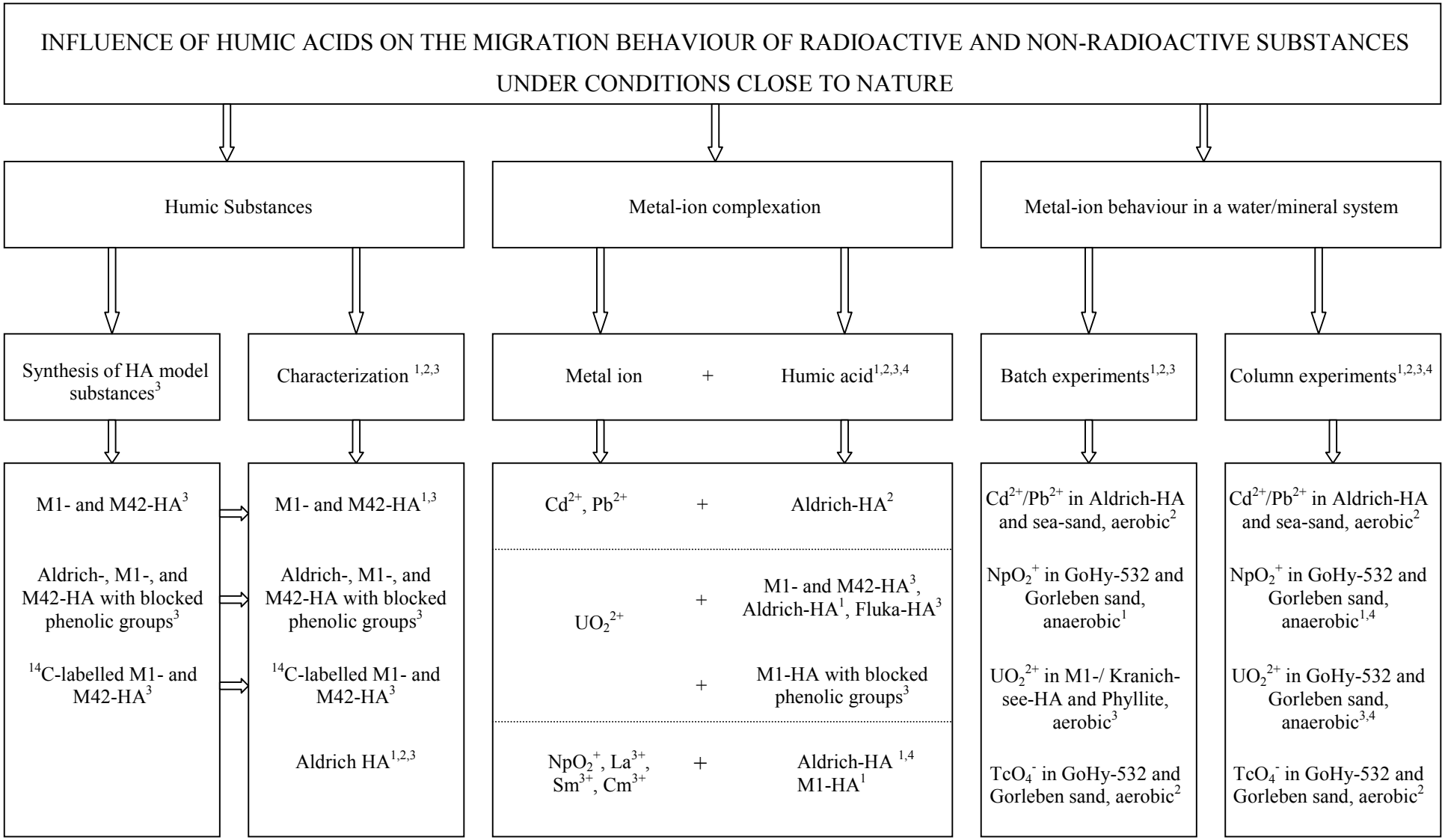

Fig.1: Schematic description of the project; foot notes mean: 1: UMz; 2: USb; 3: FZR; 4: FZK

1. Experimental

1.1 Methods

Within the project, a broad variety of methods was used and is summarized in the following section. Details are not mentioned in this section, but can be found in the contributions of the partners (appendices 1 to 3, experimental parts).

For the characterization of humic acids, elemental analysis, size exclusion chromatography (SEC), ultrafiltration (UF), capillary and free flow electrophoresis were used. The content of functional groups, carboxylic and phenolic, of humic acids was determined radiometrically after derivatization with [^{14}C]diazomethane as well as by direct potentiometric titration, and the calcium acetate and barium hydroxide method. In order to obtain structural information, FTIR spectroscopy, ^{13}C-CP/MAS-NMR spectroscopy and Pyrolysis-gas chromatography/mass spectrometry (Py-GC/MS) were performed.

Complexation studies for metal ions with humic acids were done by anion/cation exchange (AIX/CIX), continuous electrophoretic ion focusing (EIF), ultrafiltration (UF), anodic stripping voltammetry (ASV), absorption (VIS) and time-resolved laser-induced fluorescence spectroscopy (TRLFS).

For complexation studies at trace and ultratrace concentrations very sensitive radiometric methods were applied after previous chemical separation of complexed and uncomplexed metal ion species. Samarium-153 (as Sm^{3+}), Lanthanum-140 (as La^{3+}), Neptunium-239 (as NpO_2^+), which can be measured very sensitively by γ-spectrometry, and Neptunium-237 (as NpO_2^+), Uranium-232/235 (as UO_2^{2+}) detectable by α- spectrometry, liquid scintillation counting, or by delayed-neutron activation analysis (DNAA) were used in those experiments. The determination of plutonium at very low concentrations can be achieved by resonance ionization mass spectrometry (RIMS) down to about 10^7 atoms.

In order to explain the mechanism of the complexation of metal ions with humic colloids, the structural parameters of metal-humates were investigated by capillary (CE) and free-flow electrophoresis (FFE), EXAFS, and FTIR spectroscopy.

1.2 Batch and column experiments

Batch and column experiments were performed under aerobic and anaerobic conditions (glove-boxes with Argon-atmosphere / 1% CO_2). In aerobic batch experiments, the influence of humic acids on the uranium(VI) sorption to phyllite, a site-specific rock material associated with uranium mining areas in East Germany, and uranium(VI), were determined. The natural

Kranichsee HA, isolated from the bog "Kleiner Kranichsee" [3] and the ^{14}C-labelled synthetic humic acid type M1 (^{14}C-M1) were used for the experiments.

For batch and column experiments the well characterized groundwater GoHy-532 [4] from the Gorleben area was used together with a pleistocene aeolian quartz sand from the near aquifer surface as the solid phase. In this system, the behaviour of uranium(VI) and neptunium(V) under anaerobic conditions, and the technetium(VII) under aerobic conditions was studied. The experiments to investigate the migration behaviour of cadmium and lead were conducted under aerobic conditions with Aldrich-HA solution and purified sea-sand from Merck.

1.3 Humic material

Natural humic acids

For this project, the commercially available natural humic acid from Aldrich was used in purified form as reference humic acid by all partners. In some cases, the commercially available Fluka humic acid was taken in the experiments for comparison. For site-specific investigations (Appendix 3, chapter 14), the original Kranichsee HA, isolated from the bog 'Kleiner Kranichsee' [3], was applied.

Synthetic humic acids

One of the most extensive issues of the project was the synthesis and characterization of well defined humic acid model substances in order to use them in metal-ion complexation studies and to elucidate the complexation mechanism. The synthesis of five defined humic acids was developed and improved by FZR. In this chapter, the different types of humic acids are only listed. Background information, synthesis and characterization are described in chapter 2.
The following model substances were synthesized, characterized, and used for metal complexation studies:

- M1, a substance with low content of carboxylic groups and a high amount of aromatic structural elements.
  - Two types of the M1 were synthesized, a pure and an ultra pure humic acid regarding the metal content.
- M42, a substance which has a carboxylic group content more comparable to most natural humic acids.
- A nitrogen-free humic acid.
- Three humic acids with phenolic OH groups blocked by permethylation.
  - M1, M42 and Aldrich HA were modified.
- ^{14}C-labelled humic acids of type M1 and type M42. The labelling was performed with different ^{14}C-labelled amino acids.

The characteristics of all humic acid model substances are listed in Table 1 (more details in appendix 3, chapter 6-8).

Natural humic acids for migration experiments

For migration experiments, a Gorleben groundwater designated as GoHy-532 was used which originally contained 30 mg/l DOC (dissolved organic carbon) and was generally handled under an atmosphere of argon/1% CO_2 [4] in order to maintain the anaerobic characteristics of the groundwater, except in the case of the Tc(VII)-experiments.

2. Synthesis and characterization of humic acids

2.1 Synthetic humic acids

The alkali soluble and acid insoluble fractions of melanoidins are suitable as functionality model for humic acids because the molecules show both structural and also functional similarities with natural humic acids. The synthesis of humic acid model substances is based on the preparation of a "standard melanoidin" according to Enders and Theis [2] starting from a mixture of α-amino acid, sugar, and water in the heat under reflux in a nitrogen stream. Humic acid model substances of manifold functionality can be synthesized by varying the precursor substances as well as their relative proportions. Thus, starting from xylose, glycine, and phenylalanine results in a synthetic humic acid type M1 having a high amount of mono-substituted aromatic structural elements and only a low number of carboxylic groups. By starting from xylose and glutamic acid, it is possible to synthesize a humic acid (M42), which shows a carboxylic group content comparable to most natural humic acids. Beside the functional group content, the elemental composition of the synthetic humic acids can also be varied. A nitrogen-free synthetic humic acid model substance was synthesized from an aqueous glucose solution.

Comparison of the humic acid-like melanoidins with the natural Aldrich humic acid reveals very similar functional and structural properties. Nevertheless, the melanoidins show a higher homogeneity (smaller charge-to-size ratio distribution) regarding their structural composition and a lower amount of inorganic constituents than their natural analogous. By using very pure precursor substances and a apparatus made of Teflon, "ultra-pure" humic acid can be prepared in order to study the influence of inorganic impurities and constituents on humic acid properties, for instance on the complexation behaviour. The used precursors, their proportions and special requirements of the synthesis are summarized in Appendix 3, paragraph 6, which deals with the synthesis and characterization of the specific humic acid types. In Table 1 of this chapter, some characteristics of all investigated humic acids are listed.

Table 1: Summary of humic acids investigated within this project and some of their characteristics. Details are found in Appendix 3.

Humic acid	**Functional groups, (meq/g)**			**Precursor** substances	**Elemental analysis (%)**					**Fe content**
	COOH:	Phenolic-OH:	PEC[5]:	for synthesis	C	H	O	N	ash content	ppm
HA M1	1.3±0.1[1]	2.3 ± 0.1[1]	1.36±0.08[4]							
	1.02±0.06[2]	2.02±0.99[3]		Xylose	63.92±0.72	4.75±0.26	22.51±0.53	5.34±0.07	0.7	<250
saponified	2.03±0.02	1.7±0.1	2.12±0.06	+ Phenylalanine	-	-	-	-	-	-
permethylated	<0.1[1]	0.3	-	+ Glycine	-	-	-	-	-	-
blocked phenolic OH	1.91±0.07	1.1±0.2	1.94±0.13		-	-	-	-	-	-
ultra pure M1	1.36±0.08[2]	2.5±0.3[3]	-		-	-	-	-	<0.05	n.d.
HA M42	3.72±28[1]	2.30±0.36[1]	3.90±0.18[4]							
	4.10±0.10[2]		-	Xylose	58.41±0.53	4.30±0.22	27.24±0.53	4.54±0.12	0.3	<20
permethylated	<0.1[1]	0.6±0.1	-	+ Glutamic acid	-	-	-	-	-	-
blocked acidic OH	3.21±0.08	0.6±0.3	3.28±0.18		-	-	-	-	-	-
nitrogen-free HA	2.38±0.14[1]	4.86±0.83[1]	-	Glucose + Na_2CO_3	57.55±0.03	5.26±0.01	37.14±0.03	n.d.	-	-
	2.64±0.12[2]		-							
Aldrich HA	4.0±0.4[1]	3.2±0.7[1]	5.33±0.12[4,6]	Natural	54.47±1.42	3.82±0.14	29.26±1.53	0.75±0.04	3.7	3651 ± 224
	4.74±0.05[2]	2.71±0.34[3]	-	Substances	-	-	-		-	
permethylated	<0.1	0.6±0.3	-	-	-	-	-	-	-	-
blocked phenolic OH	3.25±0.05	1.1±0.4	3.58±0.21	-	-	-	-	-	-	-
∅ literature [1]	1.5-5.7	2.1-5.7	-	Natural Substances	50-60	4-6	30-35	2-6	-	-

1: Radiometric methods; 2: Ca-acetate exchange; 3: $Ba(OH)_2$ –method; 4: Direct titration; 5: PEC = Proton exchange capacity; 6: Charge from UMz = 4.60 meq/g, from USb = 3.88 meq/g; n.d.= not detectable; – : not determined.

Blocking of phenolic hydroxyl groups

In order to elucidate the role of phenolic OH groups in the metal-complexation reaction, the M1, M42 and Aldrich humic acids were modified by blocking the phenolic groups in a two-step process, a) the permethylation of carboxylic and phenolic OH groups with diazomethane resulting in methyl ester and methyl ether groups and b) the hydrolysis of the ester groups in alkaline solution. The permethylated humic acids and the humic acids with blocked phenolic OH groups were characterized for their functional group content using different methods. Synthesis and results are discussed in Appendix 3 (chapter 7). Nevertheless, the modified HA M1 with blocked phenolic OH groups, designated as M1-b, was included in metal complexation studies.

Synthesis of isotopically labelled humic acids

For those migration experiments, where the interaction of humic acid itself with sediments is studied, it is desired to use radiolabelled humic material. The synthesis of HA with ^{14}C-labelled precursor substances, e.g., α-amino acids according to the melanoidin concept was investigated (Appendix 3, chapter 8). In this way, a stable labelling of the humic acid in the backbone structure without any changes in the humic acid functionality was obtained. ^{14}C-labelled humic acids of type M1 and type M42 were synthesized according to the melanoidin synthesis procedure. The highest labelling (radioactivity) yields for the humic acid type M1 are achieved using [2-^{14}C]glycine, and for M42 using [U-^{14}C]glutamic acid as precursor substances (Appendix 3, chapter 8). Calculations, by taking into consideration the maximal reachable specific activity of ^{14}C-labelled HA M1, have shown that 1 µg/L humic acid can be detected. This detection limit allows the use of ^{14}C-labelled humic acid in batch and migration experiments.

2.2 Natural humic acids

Size characterization by UF and SEC

The size distribution of Aldrich-HA was determined by ultrafiltration (UF) and size exclusion chromatography (SEC)(Appendix 2, chapter 3). In the SEC, polystyrene sulfonic acids standards were used for size calibration of the divinyl benzene-based column. The results are listed in the following:

	Ultrafiltration		Size exclusion chromatography	
	>100000 Dalton	>1000 Dalton	>100000 Dalton	>1000 Dalton
Aldrich-HA	10 %	85 %	< 5%	>95%

The Aldrich humic acid consists of a small fraction of very large molecules (>100000 Dalton) and a large fraction of small molecules (distribution maximum around 3000 Dalton in the SEC). Within the experimental error of the methods due to different non-specific interactions of the humic acid colloids with the equipment surfaces (ultrafilter membranes, size exclusion resin), both results are in good agreement.

Characterization by electrophoresis methods

Different electrophoresis methods were used to investigate the mobilities of humic acids in solution, which are determined by their charge to size ratios. By capillary electrophoresis, it is possible to separate the humic acids in the presence of hydroxycarboxylic acids, e.g. tartaric acid, malic, or citric acid, into two or three fractions, which are attributed to species of fast and slow mobilities. The migration times of fast and slowly moving species of Aldrich and Fluka humic acid differ noticeably. It is found, that in the presence of a dicarboxylic acid instead of the hydroxycarboxylic acid only broad bands appear with no occurrence of shape peaks attributable to different species of distinct mobility. Esterification of the hydroxyl groups of the hydroxycarboxylic acids with carboxyl groups of humic acid molecules may explain the generation of different species with distinct mobilities.

Capillary zone electrophoresis (CZE) reveals a significant effect of increasing metal loading on the mobility distribution of the humates. A generally decreased mobility of colloids upon increased metal ion loading is observed. By another method, the micellar electrokinetic chromatography (MEKC), the influence of metal ion loading on the hydrophily of humic acid constituents was illustrated. A co-ordination of the heavy-metal cations to different functional groups obviously decreases the hydrophily of humic acids.

The studies with different electrophoretic methods showed some influences on the electrophoretic mobilities by changing the experimental conditions. However, explanations are sometimes difficult and ambiguous, because many influences due to e.g. pH shifts in the apparatus during the separation, hydrolysis, and carbonate complexation of metal ions at higher pH values, cannot be assessed without additional experiments in the future.

3. Interaction of metal ions with different humic acids

3.1 Metal ion humate complexation studies

Table 2: Summary of the complexation constants log β_{LC} for metal humate complexation (Aldrich HA). Log β_{LC} is deduced according to the neutralization model by introducing the loading capacity of the humic acid for each metal and experimental conditions.

Metal	[Me] (mol/L)	Ionic strength	pH	log β_{LC}	Method
Divalent:					
Pb^{2+}	~1 x 10^{-4}	0.1	5.0	5.2 – 6.4	EIF, ASV,UF
		<0.01	6.0	5.6 – 6.1	EIF, ASV,UF
Cd^{2+}	~1 x 10^{-4}	<0.01	5.0	4.0 – 5.0	EIF, ASV,UF
			6.0	4.1 – 5.5	EIF, ASV,UF
Zn^{2+}	~1 x 10^{-4}	<0.01	5.0	3.9	EIF
			6.0	4.2	EIF
Trivalent:					
Sm^{3+}	5 x 10^{-7}	0.001	5.0	7.99	EIF
		0.001	6.0	9.04	EIF
		0.001	7.0	9.69	EIF
	6.6 x 10^{-7}	0.001	5.0	6.40	AIX
Cm^{3+}	1 x 10^{-7}	0.001	5.0	6.54	TRLFS
			6.0	6.52	
Pentavalent:					
NpO_2^{+}	1 x 10^{-13}	0.001	6-8	5.3	EIF, AIX, UF
	1 x10^{-8}	0.001	6-8	5.1	EIF, AIX, UF
	1 x10^{-7}	0.001	6-8	4.5	EIF, AIX, UF
	1 x 10^{-5}	0.001	6-8	3.0	EIF
	1 x 10^{-5}	0.001	6-8	4.1	UF, VIS
Hexavalent:					
UO_2^{2+}	(0.02-9.7) x 10^{-6}	0.1 (0.004)	4-5	6.1	AIX, EIF
	(0.65-8.3) x 10^{-6}	0.1	4	5.9	TRLFS
	(0.48-1.8) x 10^{-5}	0.1	7	6.35	TRLFS

One goal of this project was to investigate the humate complexation of metal ions with respect to their oxidation state, concentration, pH value and ionic strength. Aim of the study is the

evaluation of a complexation constant in order to create a thermodynamic database, which is required for geochemical modelling of the metal-ion behaviour in the environment.
In Table 2, the investigated metal ions and the corresponding concentration ranges, ionic strengths, and pH values are shown. Different methods were used for differentiation between free metal ions and metal humate complexes.

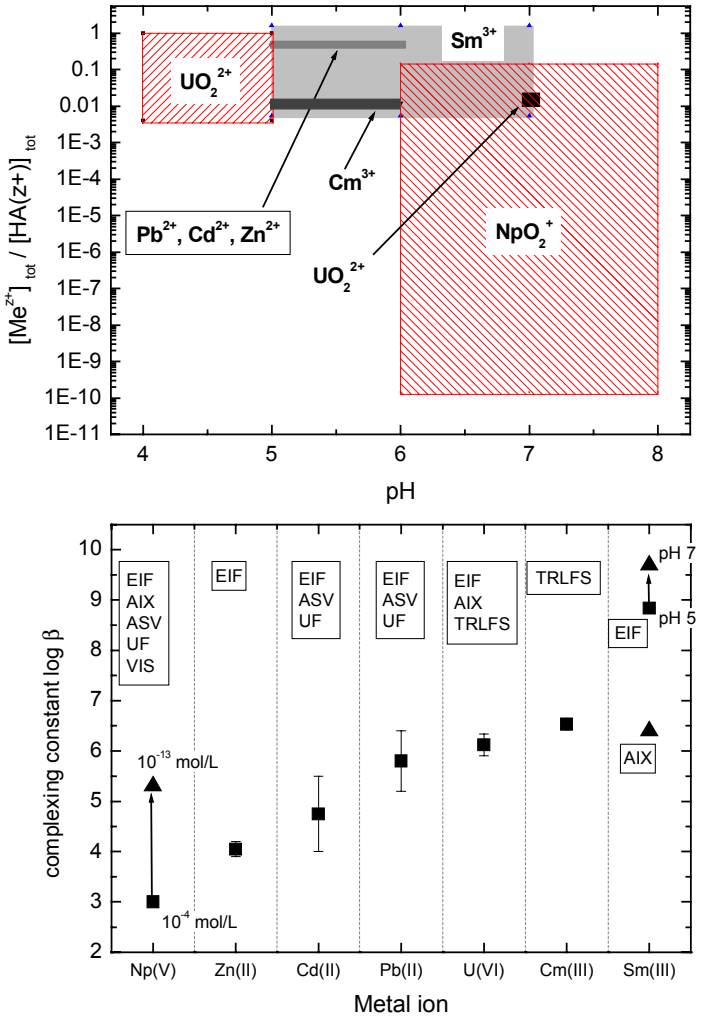

Fig. 2: Illustration of the experimental conditions ($[Me^{z+}]_{tot}/[HA(z+)]_{tot}$ ratios, pH) used for metal-ion complexation studies in the present project (upper part) and the obtained complexation constants log β_{LC} for metal complexation with Aldrich humic acid for each metal ion (bottom part; EIF: electrophoretic ion focusing; AIX: anion exchange; UF: ultrafiltration; ASV: anodic stripping voltammetry; VIS: absorption spectroscopy; TRLFS: time resolved laser-induced fluorescence spectroscopy.

For calculation of the complexation constant log β_{LC} (LC stands for loading capacity), the charge neutralization model according to [5] was mainly applied in order to estimate the actual free humic acid concentration. In Fig. 2, the metal loading of the humic acid expressed as the ratio $[Me^{z+}]_{tot}/[HA(z+)]_{tot}$ is illustrated for each metal ion as a function of pH. For each

metal ion a box is plotted, which encloses all investigated metal loadings of humic acid within the present project. For most metal ions the loading varied from about 1% up to near saturation, with the exception of the neptunyl ion, where the investigations are extended to very low $[Me^{z+}]_{tot}/[HA(z+)]_{tot}$ ratios. In the lower figure, the mean complexation constant is plotted for each metal ion which was evaluated from all complexation data determined by different methods at different conditions. Generally, the complexation constants log β_{LC} are independent of the pH values for a given method in a narrow concentration range, however, with the exception of ion focusing data of Sm^{3+}. Adsorption of trivalent metal ions at low concentrations in the electrophoretic apparatus as well as hydrolysis and carbonate complexation are responsible for this pH dependence. It is obvious, that for most metal ions a wide range of log β_{LC} is found. For lead and cadmium, different complexation constants are found depending on the speciation method applied (**u**ltra**f**iltration, **a**nodic **s**tripping **v**oltammetry, **e**lectrophoretic **i**on **f**ocusing). This finding suggests, that systematic artefacts accompany the methods. The wide range of log β_{LC} in case of neptunium is caused by an increase of log β_{LC} from 3 to 5.4 with decreasing concentration from 10^{-4} to 10^{-13} M which is obtained consistently by EIF, AIX, and UF. Using the absorption-spectroscopy and the electrophoretic technique in the concentration range between 10^{-5} and 10^{-4} mol/l $[NpO_2^+]_{tot}$ the results show a discrepancy, indicating again that the speciation method based on chemical separation might be affected by artefacts. On the other hand, similar experiments at very low neptunium concentrations < 10^{-8} mol/l with different methods (EIF, AIX and UF) give consistent log β_{LC}-values. The change of the log β_{LC} = 4.4 at 10^{-5} to 10^{-4} mol/l $[NpO_2^+]_{total}$ to log β_{LC} > 5 below 10^{-8} mol/l is still unexplained.

Independent of the experimental method (AIX, EIF, TRLFS), well corresponding log β_{LC} values were obtained for UO_2^{2+} resulting in a mean log β_{LC} of 6.0. In one experiment at pH 7, where uranium is partly hydrolysed, a log β_{LC} for $UO_2(OH)HA(I)$ of 6.35 was deduced by taking into consideration the two hydrolysed uranyl species, $UO_2(OH)_2$ and $UO_2(OH)^+$.

Generally, the complexation strength for the actinides follows the order: $NpO_2^+ < UO_2^{2+} < Cm^{3+}/Sm^{3+}$ and reflects the mean charge of the metal ion. For the heavy metal ions lead, cadmium, and zinc a complexation strength order of $Zn^{2+} < Cd^{2+} < Pb^{2+}$ is found. However, the log β_{LC} values vary by one order of magnitude depending on the separation method.

One prerequisite for the calculation of log β_{LC} is the knowledge of the loading capacity (LC) for each metal ion at given experimental conditions. In Fig. 3, the LC is shown as a function of pH for different metal ions (Np(V) data are from [6]). The LC increases with the pH value, but the degree of change depends systematically on the nature of the metal ion.

It must be emphasized, that the artificial humic acids M1 and M42 reveal similar complexation behaviour as natural humic acid (Aldrich HA) under the experimental conditions, but details have to be investigated in the future.

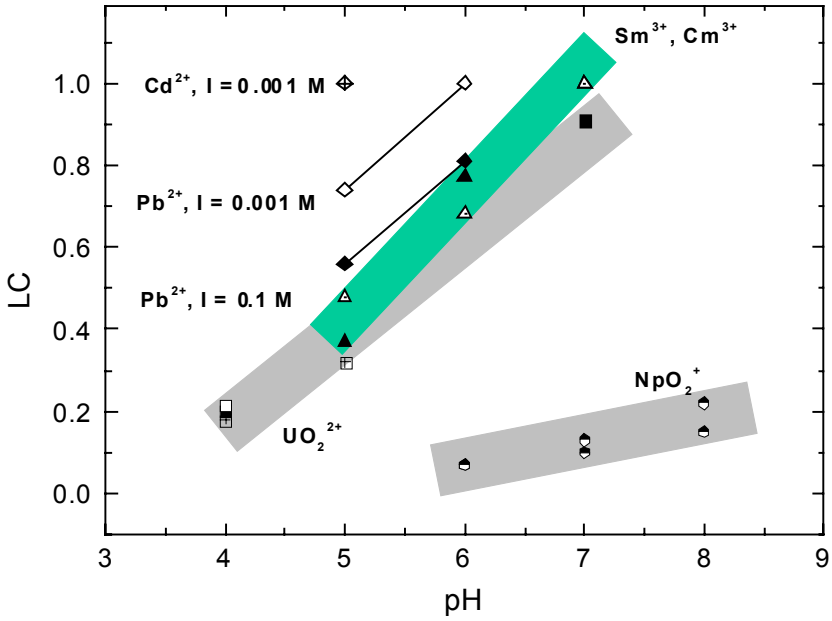

Fig. 3: Loading capacities (LC) of humic acids (Aldrich HA and GoHy-573) as a function of pH. The LC for NpO_2^+ was determined with GoHy-573 and depicted from [6].

In Appendix 3, chapter 11, the role of phenolic OH groups in the metal-humate complexation is discussed. In complexation experiments of U(VI) with HA M1, the loading capacity decreases from 0.34±0.03 to 0.18±0.02 (pH 4) when the phenolic OH groups are blocked by methylation. From these results one can conclude that phenolic OH groups may be involved in the complexation process with UO_2^{2+} ions under the applied conditions. To confirm this assumption, experiments with other synthetic HA as well as EXAFS studies are planned.

3.2 Structural parameters of uranyl(VI) humates

The objective of EXAFS and FTIR investigations was to obtain information on the structure of uranyl-humate complexes, in particular on the binding of the UO_2^{2+} ion to humic acid at different experimental conditions. From FTIR spectroscopic studies of humic acid and uranyl humate, the interrelated decrease in carbonyl band intensity (C=O 1720 cm^{-1}; C-O, 1200 cm^{-1}) and increase in COO^- band intensity (1560, 1520 and 1380 cm^{-1}) strongly suggest a direct interaction/complexation of uranyl ions with the carboxyl group of the humic acid by displacement of protons.

The EXAFS as well as the FTIR studies reveal that synthetic humic acids M1 and M42 show similar interactions with U(VI) as the natural humic acid. EXAFS studies have shown no

influence of the metal loading of the humic acid on the U-O bond distances. Furthermore, the structural parameters obtained for the sample prepared by sorption of UO_2^{2+} onto a suspension of natural humic acid are similar to those of the samples prepared from humic acid in solution. The samples measured as a wet paste show the same results as the samples measured in dried form. This indicates that the presence of excess water does not change the average equatorial bond distance in the surrounding of uranium in the uranyl humate complexes.
It can be concluded from EXAFS and FTIR measurements, that a monodentate and/or bridging carboxylate complex is mainly formed with the uranyl cation.

4. Metal-ion behaviour in a water/mineral system

4.1 Effect of humic acid on the uranium(VI) sorption onto phyllite

Phyllite was chosen as one site-specific rock material, which is a low-grade metamorphic rock mainly composed of the minerals quartz, muscovite, chlorite, and albite. Phyllite is closely associated with the uranium deposits of the uranium mining areas in East Germany.
Batch experiments with Kranichsee humic acid and a ^{14}C-labelled synthetic humic acid type M1 (^{14}C-M1) showed that both humic acids are sorbed on the phyllite over the entire pH range (below pH 8 up to 94 % and 88 % for Kranichsee humic acid and ^{14}C-M1, respectively). The strong uranyl sorption on phyllite (95 - 97 % in the absence of humic acid) is not significantly changed by the presence of humic acid in the pH range from 6 to 7.5.
The strong humic acid and uranyl sorption is attributed to phyllite sites and a coating consisting of ferrihydrite sites. The ferrihydrite phase is formed in the course of the sorption experiments due to Fe(II) oxidation.
At lower pH values (3.5-6.0) the sorption of uranyl is slightly enhanced by humic acid. At higher pH values (> 7.5) the Kranichsee-HA reduces and the synthetic M1-HA increases the uranyl sorption on the phyllite. Explanations for sorption at low and high pH values are found in appendix 3.

4.2 Migration behaviour of metal ions

The present studies focus on flow-through column experiments to investigate the migration behaviour of lead(II), cadmium(II), neptunium(V), uranium(VI), and technetium(VII) in a solid/water system with a sandy sediment and a water rich in humic colloids. Gorleben groundwater GoHy-532 and Aldrich humic acid solution as mobile phase, as well as a Gorleben sandy sediment and a Merck sea sand as solid phase, were taken. The original groundwater Gohy-532 and the Aldrich humic acid solution contain 30 mg/L and 27 mg/L dissolved organic carbon (DOC), respectively. Prior to the column experiments, the behaviour of metal ions was investigated in batch experiments in order to determine adsorption isotherms for the sorption of metal ions, humic acid, and metal humate onto the sand. The batch experiments revealed that the free metal ion as well as humic acid and metal humate are sorbed onto the solid depending on the experimental conditions. The metal-ion migration behaviour was investigated as a function of metal ion/groundwater equilibration time before

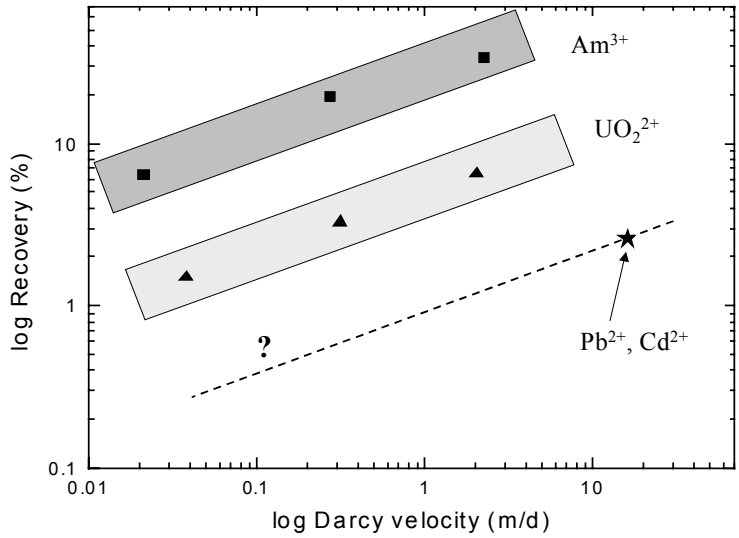

Fig. 4: Influence of the Darcy velocity (~ residence time) on the recovery of the metal ion in humic acid containing water passing a sand-filled column. It may assumed, that lead and cadmium follow the same trend as americium and uranyl ions, but this must be proven in further experiments.

injection into the column, groundwater flow velocity, and column length. By ultrafiltration experiments the size distribution of humic colloid bound metal ion was determined before and after permeation through the columns.

Independent of the metal ion (with exception of TcO_4^-), all column experiments show the general trends: the colloid-bound metals move up to 5% faster than an ideal tracer because of size exclusion effects. The migration behaviour of metal ions is strongly influenced by kinetically controlled processes. Furthermore, the recovery of humic colloid-borne metal ion depends on the residence time of the species in the column and on the metal-ion/groundwater equilibration time prior to the injection into the column. The recovery decreases with decreasing Darcy velocity, which is demonstrated for UO_2^{2+} and Am^{3+} in Fig. 4 (Am^{3+} data from [2]). Unfortunately, for Pb^{2+} and Cd^{2+} no experiments with flow velocity variation were performed, but it may be assumed that the two metal ions follow the same trend. This assumption has to be proven in further experiments. It is obvious, that the differences in the recovery for the metal ions is related to the nature of the metal ions.

Furthermore, the recovery increases with increasing pre-equilibration time (Fig. 5), which is attributed to a time-dependent change of strength of lead, cadmium, and uranium binding to the humic colloids. The recovery varies again with the nature of the metal ion, reflecting the mean charge of the metal ion ($UO_2^{2+} < Am^{3+} < Np^{4+} \sim Th^{4+}$). The recoveries for the divalent metal ions cannot be compared with all other recoveries, because these column experiments were performed at a much higher Darcy velocity than all other experiments. As shown in

Figure 4, the recovery depends on the Darcy velocity, and it may be assumed that the values for Pb^{2+} and Cd^{2+} shown in Figure 5 are too high. Nevertheless, the recoveries of Pb^{2+} and Cd^{2+} also depend on the equilibration time.

In case of neptunium, the initial pentavalent neptunyl ion is reduced to tetravalent neptunium during the equilibrium time before injection on the column and its residence time in the column, resulting in a higher recovery due to stronger humate complexation of Np(IV) as compared to NpO_2^+. This higher recovery for tetravalent actinides is confirmed by other column experiment with Th(IV) by Artinger et al [7]. In batch experiments with Np(V) in the system GoHy-532 groundwater/Gorleben sand under argon/ 1 % CO_2 atmosphere, up to 40% of Np(V) are removed from the solution and adsorbed onto the sand within a period of 300 hours. Liquid-liquid extraction leads to the conclusion that the increasing adsorption with time is due to the slow reduction reaction of Np(V) to Np(IV).

The metal ions which are not bound to the humic colloids are retarded on the column depending on the residence time, nature of the metal ion, pH, and sediment in the experiment. Free metal ions can reach retardation factors of about 10000 compared to an ideal tracer, as it was observed for Am(III) [4].

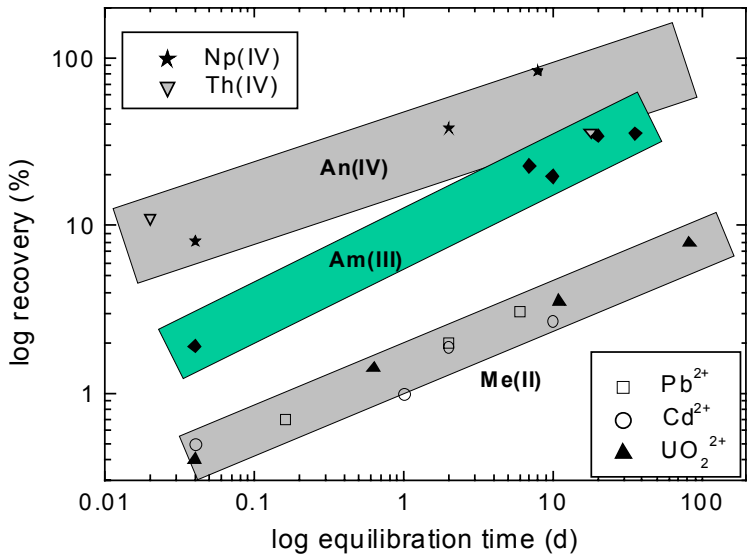

Fig. 5: Recovery of each metal ion as a function of the equilibration period of the metal ion with humic acid containing water before injection into the column. Am(III)-data from [4] and Th from [7].

The column experiments carried out within this project reveal important kinetic effects controlling the humic colloid-borne migration of uranium, neptunium, lead, and cadmium. These kinetic effects are comparable to those found for instance for the migration behaviour of Am(III) [4]. For the divalent Pb^{2+} and Cd^{2+}, details of the kinetic effects still have to be examined in future experiments. Consequently, one can conclude that the K_D-concept, which is based on thermodynamic equilibrium, is not suitable to describe the humic colloid-borne

metal-ion migration. Therefore, the metal-ion migration experiments provide a first basis to describe and to predict the subsurface migration of colloidal metal-ion species in natural aquifers. Additionally, they showed impressively that the migration of humic colloid bound metal ions cannot be described solely by relying on equilibrium approaches, but additionally requires inclusion of kinetics.

5. Outlook

Great progress has been achieved within the present project concerning the metal-ion humate interactions. The amount of basic humate interaction data has been extended and improved and brings forward the understanding of basic processes. Despite of this progress, numerous issues still need further attention in order to yield a reliable safety assessment of nuclear and toxic waste disposal. Theses issues may be summarized as follows:

There is still need for additional data on:

1. Humate complexation with synthetic humic acids on specificically designed binding sites to elucidate the metal-ion complexation mechanism
2. Humate complexation at very low metal ion concentrations
3. Tetravalent actinide humate interactions
4. Mixed complexes
5. Kinetics of metal ion humate interactions

Metal-ion transport investigations:

1. Improvement of existing data including redox-sensitive metal ions
2. Investigation of humic substances mediated inorganic colloid transport

Model development:

1. Implementation of metal-humate complexation models into improved geo-chemical modelling programs
2. Predictive modelling of the humic-borne metal-ion transport

6. References

[1] Pompe, S. Entwicklung huminsäureähnlicher Melanoidine als Funktionalitätsmodelle für Huminsäuren und ihr Vergleich mit Fluka-Huminsäure hinsichtlich ihres Komplexbildungsverhalten gegenüber Uran(VI), Dissertation 1997, TU Dresden.

[2] Enders, C. and Theis, K.: Die Melanoidine und ihre Beziehung zu den Huminstoffen, Brennstoff Chemie, **19**, 360 (1938).

[3] Schmeide, K., Zänker, H., Heise, K. H., and Nitsche, H.: Isolation and Characterization of Aquatic Humic Substances from the Bog "Kleiner Kranichsee", Scientific report FZKA 6124, Karlsruhe (1998).

[4] Artinger, R., Kienzler, B., Schüßler, W., and Kim, J. I.: Effects of Humics Substances on the ^{241}Am Migration in a Sandy Aquifer: Column Experiments With Gorleben Groundwater / Sediment Systems, J. Contam. Hydrology, **35**, 261 (1998).

[5] Kim, J. I. and Czerwinski, K. R.: Complexation of Metal Ions with Humic Acid: Metal Ion Charge Neutralization Model, Radiochim. Acta, **73**, 5 (1996).

[6] Marquardt, C. and Kim, J. I.: Complexation of Np(V) with Humic Acid: Intercomparison of Results from Different Laboratories, Radiochim. Acta, **80**, 129 (1998).

[7] Artinger, R., Schäfer, T., and Kim, J. I.: Actinide Transport in Column Experiments: Influence of Humic Colloids, to be published (2000).

Appendix 1

Complexation Studies of Actinides with Humic Acids at Very Low Metal Concentrations

A. Mansel[1], G. Montavon[1], A. Seibert[1], R. Artinger[2], H. Keller[1], J.I. Kim[2], J.V. Kratz[1], C. Marquardt[2], F. Scherbaum[2], N. Trautmann[1]

[1] Institut für Kernchemie, Universität Mainz

[2] Institut für Nukleare Entsorgung, Forschungzentrum Karlsruhe

Zusammenfassung

Das Komplexierungsverhalten von dreiwertigen (Am, Cm), fünfwertigen (Np) und sechswertigen (U) Aktiniden sowie der dreiwertigen Lanthaniden (La, Sm) mit natürlichen und synthetischen Huminsäuren wurde im umweltrelevanten pH-Bereich (pH 5 bis 8) bei mittleren und sehr geringen Metallionenkonzentrationen (10^{-14} bis 10^{-4} mol/l) studiert. Die eingesetzten Bestimmungsverfahren für die Komplexierungskonstanten waren die kontinuierliche, trägerfreie Durchflußelektrophorese (EIF), Anionen- und Kationenaustausch (AIX, CIX), Ultrafiltration (UF) in Verbindung mit radiometrischen Messungen sowie ICP-MS, UV/VIS-Spektroskopie und die zeitaufgelöste, laserinduzierte Fluoreszenzspektroskopie (TRLFS).

Weiterhin wurden Batch- und Säulenexperimente mit Np(V) und der Gorlebenhuminsäure GoHy-532 an Gorlebensand durchgeführt.

Die Komplexierung von Aktinidionen und Huminsäuren wurde mit dem „Konzept der Ladungsneutralisation von Metallionen“ und der Korrektur für unterschiedliche Beladungsgrade (loading capacity, LC) oder mit Hilfe des Deprotonierunggrades α beschrieben [Kim96], [Tor84]. Die Ermittlung von Komplexierungskonstanten für die Metallion-Humatkomplexe durch das Ladungsneutralisations-Modell ermöglicht einen Vergleich der Ergebnisse für verschiedene Huminsäuren unter variierenden experimentellen Bedingungen und mit Literaturdaten.

Bei der Verwendung von Kationaustauschern wurden für die dreiwertigen Metallionen zu niedrige log β_{LC} – Werte ermittelt (2.73), da der Kationenaustauscher in das Metallion-Humatkomplexierungsgleichgewicht eingreift. Anionenaustauschermaterialien zeigen dagegen eine geringe Tendenz, das freie Metallkation zu adsorbieren (log $\beta_{LC,Sm}$ = 6.40).

Die Untersuchungen mittels der kontinuierlichen Durchflußelektrophorese zeigten zunächst, daß Metallion-Humatkomplex und freies Metallion an unterschiedlichen Oberflächen der Apparatur adsorbiert wurden. Nach einer Modifizierung der Elektrophoresekammer konnten die Adsorptionsverluste jedoch minimiert werden. Trotzdem zeigte diese Methode eine pH-Abhängigkeit der log $\beta_{LC,An(III)}$-Werte (7.99 bei pH 5, 9.04 bei pH 6 und 9.69 bei pH 7). Für Metallionkonzentrationen kleiner 10^{-6} mol/l An(III) ist diese Methode nicht einsetzbar. Die synthetische Huminsäure vom Typ M1 zeigte ein ähnliches Komplexierungsverhalten wie die Aldrich-Huminsäure.

In Zusammenarbeit mit dem INE, Forschungszentrum Karlsruhe, wurden mittels einer direkten Speziationsmessung, der zeitaufgelösten laserinduzierten Fluoreszenz-Spektroskopie (TRLFS), log β_{LC}-Werte von 6.54 (pH 5) und 6.52 (pH 6) für Cm und Aldrich-Huminsäure bestimmt.

Für Neptunium(V) ist auch bei sehr niedrigen Metallionenkonzentrationen die Adsorption an Oberflächen der Elektrophoresekammer vernachlässigbar (< 5%). Es zeigte sich ein Gang in den Komplexierungskonstanten in Abhängigkeit von der Metallionenkonzentration (10^{-14} bis 10^{-4} mol/l).

Um diese Abhängigkeit der Komplexbildungskonstanten von der Metallionenkonzentration zu überprüfen, wurden Versuche mittels Anionenaustausch und Ultrafiltration durchgeführt, die ebenfalls auf eine höhere Komplexbildungskonstante für Kationenkonzentrationen < 10^{-8} mol/l hindeuten. Die starke Erniedrigung der Bildungskonstanten bei Konzentrationen > 10^{-6} mol/l, die bei den Untersuchungen mit der EIF auftrat, ließ sich mittels AIX und UF nicht bestätigen. UV-VIS-Messungen in diesem Bereich deuten auf einen log $\beta_{LC,Np(V)}$ von 4.4 hin. Es steht hier aber noch die Bestimmung der Loading Capacity für Aldrich-Huminsäure und Neptunium(V) aus.

Die synthetischen Huminsäuren M1 und M1b (FZ Rossendorf) [Pom96] zeigten für Neptunium in geringer Konzentration (10^{-13} mol/l) ähnliche Komplexbildungskonstanten wie die Aldrich-Huminsäure.

In Zusammenarbeit mit dem INE, Forschungszentrum Karlsruhe, wurden Durchlaufsäulenexperimente im System GoHy-532/Gorlebensand und Neptunium(V) durchgeführt, die Aussagen über die Mobilität von Aktinid-Huminstoffkolloiden erlauben. Die Migrationsexperimente wurden in einer Ar / 1% CO_2-Atmosphäre auf einer 25 cm Säule durchgeführt, die unter anaeroben Bedingungen über mehrere Monate konditioniert worden war. Variiert wurden die Np(V)-Konzentration (2 x 10^{-10} bis 3 x 10^{-4} mol/l) und die Konditionierungszeit (1 h bis 8 Tage). Die Retardation der mobilen Np-Spezies betrug R_f = 0,98 gegenüber dem wechselwirkungsfreien Tracer HTO. Bei einer Konditionierungszeit von 1 h ergab sich ein geringer Wiedererhalt (< 10 %). Erhöhte man die Konditionierungszeit zwischen Neptunium und Grundwasser vor Aufgabe auf die Säule, ergaben sich Wiedererhalte bis zu 85 %, was auf eine Reduktion des Neptunylkations in den vierwertigen Oxidationszustand und die dadurch bedingte stärkere Humatkomplexierung zurückgeführt werden kann. Der Nachweis der Reduktion konnte sowohl UV-VIS-spektroskopisch als auch mittels Flüssig-flüssig-Extraktion erbracht werden.

Experimentelle Daten aus Anionenaustauschexperimenten zur Humatkomplexierung von U(VI) ($5x10^{-6}$ bis $1x10^{-8}$ mol/l) ließen sich durch das Ladungsneutralisations-Modell gut beschreiben, wenn die Werte für LC mit einem neuartigen Ansatz ermittelt wurden, in dem das Vorliegen von Hydrolysespezies nicht berücksichtigt werden muß. Die Experimente mit U(VI) dienen als Modell für zukünftige Experimente mit Pu(VI).

Die Untersuchung der Uran-Humat-Wechselwirkung mit der EIF-Technik war nicht zu verwirklichen.

Weiterhin wurde in Zusammenarbeit mit dem Institut für Physik der Johannes Gutenberg-Universität Mainz ein neuartiges Festkörper-Lasersystem aufgebaut, das aus einem leistungsstarken, gepulsten Nd:YAG-Pumplaser mit hoher Repetitionsrate (1 bis 17 kHz) sowie drei Ti:Saphir-Lasern besteht. Die Ti:Saphir-Kristalle wurden in einem Z-förmigen Resonator integriert, in dem weitere optische Elemente zur Wellenlängenabstimmung und Einengung der Laserbandbreite (Lyotfilter und passende Etalons) eingebaut wurden. Auf diese Weise konnte ein kontinuierlich durchstimmbarer Wellenlängenbereich von 725 nm bis 895 nm realisiert werden. Durch den Aufbau einer Frequenzverdoppelung für einen der Ti:Saphir-Laser können Wellenlängen von 365 nm bis 445 nm erzeugt werden. Die Linienbreite von 2 bis 3 GHz liegt in der Grössenordnung der Linienbreite der

dopplerverbreiterten Resonanzen bei der optischen Anregung des Plutoniums. Mit diesem System wurden erstmals spektroskopische Messungen an ^{239}Pu durchgeführt und ein effizientes Anregungsschema für die dreistufige Resonanzionisation etabliert. Die Anregungsleiter mit λ_1 = 420.764 nm, λ_2 = 847.277 nm und λ_3 = 767.529 nm erreicht im ersten und zweiten Anregungsschritt mehrfache, im dritten einfache Sättigung. Mit der neuen Apparatur zur Resonanzionisations-Spektrometrie wurden Nachweiseffizienzen von ca. 8 x 10^{-6} erreicht, was einer Nachweisgrenze von 1 x 10^7 Atomen entspricht. Damit ist die Leistungsfähigkeit des neuen Festkörpersystems vergleichbar mit der des alten Kupferdampf-Farbstofflaser-Systems. Vorteile des neuen Systems sind seine kompakte Bauweise, der viel geringere Aufwand an Wartung und Instandhaltung und die einfachere Handhabung. Inzwischen wird das System routinemäßig zum Nachweis von Plutonium im Ultraspurenbereich eingesetzt.

Summary

The complexation of actinides as well as trivalent lanthanides as model elements for the trivalent actinides with natural and artifical humic acids was studied under environmental conditions (pH 4 to 8) over a wide range of metal-ion concentrations (10^{-14} to 10^{-4} mol/l). The experimental methods used for the determination of the complexation constants were continuous electrophoretic ion focusing (EIF), anion and cation ion exchange (AIX, CIX) and ultrafiltration (UF), in combination with radiometric measurements as well as ICP-MS and UV/VIS-spectroscopy and time-resolved laser-induced fluorescence spectroscopy (TRLFS).
Batch and column experiments were carried out with Np(V), Gorleben humic acid (GoHy-532) and Gorleben sand.
The interaction between actinides and humic acids was described either with the charge neutralization model including a correction for different loading capacities (LC) [Kim96] or a model which considers different degrees of deprotonation (α) [Tor84]. The calculation of complexation constants for metal-ion humic acid complexes with the charge neutralization model makes possible the comparison of results for various humic acids at various experimental conditions and data published in the literature.
Cation exchange experiments with trivalent metal-ions resulted in low log β_{LC}-values (2.73) because the cation exchanger disturbs the metal-ion humic acid complexation equilibrium. The anion exchanger adsorbed only small amounts of the free cation. The calculated log $\beta_{LC,Sm}$-value was 6.40.
Experiments with the continuous electrophoretic ion focusing revealed strong adsorption of the humic acid complex and the free cation on different surfaces of the apparatus. After a modification of the electropheric apparatus, the adsorption was minimized. Nevertheless the log $\beta_{LC,An(III)}$-values showed a dependence on pH (7.99 at pH 5, 9.04 at pH 6, 9.69 at pH 7). Thus, the continuous electrophoretic ion focusing is not suitable for trivalent metal-ion concentrations below 10^{-6} mol/l.
Therefore, in coorperation with INE, Forschungszentrum Karlsruhe, direct speciation measurements with the TRLFS were performed yielding log β_{LC}-values of 6.54 (pH 5) and 6.52 (pH 6) for the complexation of curium with Aldrich humic acid.
The adsorption for Np(V) in the electrophoretic chamber was negligible (< 5 %) even at low metal-ion concentrations. Nevertheless the calculated complexation constant varied with the metal-ion concentration (10^{-14} to 10^{-4} mol/l).
The dependence of the complexation constant on the metal-ion concentration was checked and verified with anion exchange and ultrafiltration at concentrations below 10^{-8} mol/l. The log β_{LC}-values were quite similar to those determined in the EIF-experiments. The decrease of the log β_{LC}-values at concentrations > 10^{-6} mol/l could not be confirmed with AIX and UF. UV/VIS-measurements resulted in log β_{LC}-values around 4.4 at these concentrations. The loading capacities for Aldrich humic acid and Np(V) have still to be determined.

At very low metal-ion concentrations (10^{-13} mol/l) the complexation behaviour of the artificial humic acids M1 and M1b (supplied from FZ Rossendorf) [Pom96] was similar to that of Aldrich humic acid.

In coorperation with INE, Forschungszentrum Karlsruhe, column experiments were carried out with the system GoHy-532/Gorleben sand and Np(V). They should give information about the mobility of actinide humic colloids in the natural aquifer system. The migration experiments were performed in a glovebox with an argon/1 % CO_2 atmosphere. The column had a length of 25 cm and was preconditioned several months under anaerobic conditions with GoHy-532. The total Np(V) concentration (2×10^{-10} to 3×10^{-4} mol/l) and the equilibration time (1 hour to 8 days) before injection were varied. The retardation of the mobile Np-species was 0.98 compared to the interaction free tracer HTO. The yield of recovery was low (10 %) after an equilibration time of 1 hour. An increase of the equilibration time before injection resulted in 85 % recovery because the Np(V) was reduced to Np(IV), and Np(IV) forms much stronger complexes with humic acids. The presence of Np(IV) was proven by UV/VIS-spectroscopy and liquid/liquid extraction.

Experimental data on the humate complexation of U(VI) by anion exchange have been obtained for uranium concentrations as low as 10^{-8} M. They can be well described by the charge neutralization model with loading capacity values determined by a new approach allowing to exempt from the presence of hydrolysis species. The U(VI) experiments serve as a model for future experiments with Pu(VI).

The investigation of the system U(VI):HA by continuous electrophoretic ion focusing has failed.

Furthermore, in collaboration with the Physics Institute of the Johannes Gutenberg University a newly designed solid-state laser system was constructed that consists of a powerful, pulsed Nd:YAG pump laser and three titanium-sapphire (Ti:Sa) lasers. The Ti:Sa crystals were integrated into a Z-shaped resonator, in which further optical elements for the selection of the wavelength and the narrowing of the laser band width (Lyot filter and associated etalons) were incorporated. In this way, a continuously variable region of wavelengths from 725 nm to 895 nm could be realized. By frequency doubling of one Ti:Sa laser wavelengths of 365 nm to 445 nm are available. The line widths of 2 to 3 GHz are in the order of the line width of the Doppler-broadened resonances in the optical excitation of plutonium. With this system, first ever spectroscopic measurements with ^{239}Pu were carried out and an efficient excitation scheme for the three-step resonance ionization was established. The stepwise excitation with λ_1 = 420.764 nm, λ_2 = 847.277 nm, and λ_3 = 767.529 nm reaches multiple saturation in steps 1 and 2, and single saturation in the third step. Detection efficiencies of the new resonance ionization mass spectrometry apparatus of about 8×10^{-6} were achieved, corresponding to a detection limit of 1×10^{7} atoms. Thus, the performance of the new solid-state laser system is comparable to that of the old copper-vapour dye laser system. Advantages of the new system are its compactness, the much lower need for maintenance and service and the simpler operation. Meanwhile, the system is routinely used for the detection of plutonium at the ultra-trace level.

Content

1. Introduction

The chemical and migration behaviour of actinides and heavy metals in aquifer systems is important in the context of safety assessments of underground repositories.

In addition to the complexation with inorganic substances in the aquifer and adsorption/ desorption phenomena on surfaces, the interaction between these metal cations and humic substances is of particular interest.

In natural waters, humic substances can exist in concentrations up to several mg/l. Humic substances are naturally occurring polyelectrolytes with non-uniform structural and chemical characteristics that depend on their origin. Their complexing functional units are carboxylic and phenolic groups. Humic substances can be divided into three groups: fulvic acids which are soluble over the entire pH range (lower molecular weight fraction), humic acids which are only soluble in near neutral to alkaline solution, and humin which is insoluble over the entire pH range (highest molecular weight fraction).

The irregular nature of humic substances results in different approaches to explain their complexation with metal cations. The models agree in that pH and ionic strength are main factors which influence the complexation of metal cations with humic acid. However, it is difficult to compare the calculated complexation constants due to different experimental conditions and the interpretation of the complexation reaction process.

For investigations at very low metal-ion concentrations, direct speciation methods like spectroscopic techniques are not suitable because they require metal-ion concentrations in excess of 10^{-8} mol/l.

Therefore, our studies are based on indirect speciation methods by combining chemical separation procedures with radiometric, mass spectrometric or laser spectroscopic detection methods. For the separation of the species the following methods have been used:

- Continuous electrophoretic ion focusing (EIF)
- Anion exchange (AIX)
- Cation exchange (CIX)
- Ultrafiltration (UF)

The radiometric methods used were liquid scintillation counting, α- and γ-spectroscopy and β-delayed neutron counting. For the determination of Np-237, besides liquid scintillation counting, the inductively coupled plasma mass spectrometry (ICP-MS) was applied.

Laserspectroscopic methods were used for the speciation of curium (time-resolved laser-induced fluorescence spectroscopy, TRLFS) and the determination of plutonium at very low concentrations (resonance ionisation mass spectrometry, RIMS).

2. Experimental Section

Chemicals and Radionuclides

All chemicals were purity grade „pro analysis“. Filtered and purified water (Milli-Q-System, Millipore, Molsheim, France) was used.

Uranium-235/238: Uranium was purified as described elsewhere [Cze94]. In experiments carried out with uranium concentrations above 10^{-7} mol/l, 235U was mixed with ^{238}U ($UO_2(NO_3)_2 \cdot 6H_2O$, < 0.3 % $_{235}U$, MERCK).

Neptunium-239: Uranylnitrate ($UO_2(NO_3)_2 \cdot 6H_2O$, < 0.3 % $_{235}U$, MERCK) was irradiated in the Mainz TRIGA-Reactor for 4 hours with 7 x 10^{11} n / s cm^2 to obtain ^{239}U ($T_{1/2}$ = 23.5 min) which decays into 2.35-d ^{239}Np. Several hours after irradiation the sample was dissolved in 8 M HCl and neptunium was separated via anion exchange with BIO RAD AG 1-X8. After elution of the fission products, ^{239}Np was eluted with 4 M HCl/0.05 M HF. The eluate was evaporated in a teflon beaker, fumed three times with 1 M $HClO_4$ and dissolved in distilled water.

Neptunium-237: The stock solution (diluted HNO_3) was fumed to dryness and dissolved in 8 M HCl. The solution was purified via anion exchange (BIO RAD AG 1-X8). After a washing step with several ml of 8 M HCl, plutonium-contaminants were removed with fresh 150 mg NH_4I in 5 ml 8 M HCl, and then neptunium was eluted with 4 M HCl/0.05 M HF. The eluate was evaporated to dryness in a teflon beaker and fumed three times with 1 M $HClO_4$ to obtain Np(V), which could be stored in distilled water as stock solution for several days at pH 3.

Americium-241 / Curium-248: The stock solutions (HCl or HNO_3) were fumed two times with $HClO_4$ and finally dissolved in 1 x 10^{-3} M $HClO_4$.

Samarium-153: Enriched Samarium (98.1% ^{152}Sm) dissolved in 1 x 10^{-3} M HNO_3 was irradiated in the Mainz TRIGA-Reactor for six hours at a flux of 4.2 x 10^{12} n / s cm^2:

$$^{152}\text{Sm (n,}\gamma\text{) } ^{153}\text{Sm} \xrightarrow[46.27\,\text{h}]{\beta^-} ^{153}\text{Eu}$$

The resulting activity was about 300 MBq ^{153}Sm / mg ^{152}Sm.

Lanthanum-140: Enriched Uranium-235 (90%) was irradiated in the Mainz TRIGA-Reactor for 30 hours to produce with a rather high radioactivity ^{140}Ba ($T_{1/2}$ = 12.75 d) among the fission products. The irradiated uranium was dissolved in 8 M HCl, and this solution was passed through an anion exchange column filled with BIO RAD AG 1-X8 (200-400 mesh). The eluate was evaporated to dryness, 20 mg Ba-carrier were added and $BaCl_2$ was precipitated with concentrated HCl at 0°C. The precipitation step was repeated, and the $BaCl_2$ was dissolved in 0.01 M HNO_3 at 60°C. Carrier-free ^{140}La ($T_{1/2}$ = 40.272 h) was separated from the ^{140}Ba-generator after a waiting time of six days by liquid/liquid extraction with bis(2-ethylhexyl)-phosphate (HDEHP) and back-extracted from the organic phase with 6 M HNO_3. The aqueous solution was washed three times with cyclohexane to remove traces of HDEHP. After evaporation, the residue was fumed two times with $HClO_4$ and dissolved in 1 x 10^{-3} M $HClO_4$. The resulting activity was about 3.2 MBq ^{140}La (1.1 pmol).

Humic Acids

The commercially available Aldrich-Humic acid (sodium salt, Charge No. 01816-054) was purified as described in the literature [Kim88].

The artificial humic acids M1 (charge No. FR-R36/95) and M1b were synthesized at the Institut für Radiochemie of the Research Center Rossendorf (FZR) by the Maillard reaction, purified by dialysis [End38] [Pom96] and put to our disposal.

In all experiments, a contact time of 24 hours was maintained in order to reach complexation equilibrium before the separations were performed.

The Gorleben groundwater GoHy-523 originally contained 30 mg/l DOC (dissolved organic carbon) and was only handled under an atmosphere of argon/1% CO_2 [Art98].

Table 1: Characteristics of the humic acids used for the experiments [Mar96], [Pom96], [PomPers.Com.]. PEC = proton exchange capacity, α = degree of deprotonation.

	Aldrich HA	M1 HA	M1b HA
PEC (meq/g)	4.60	1.36	1.94
carboxylic groups (meq/g)	4.70	1.28	2.06
phenolic OH-groups (meq/g)	2.90	2.31	1.06
α_{pH5}	0.45	0.41	-
α_{pH6}	0.70	0.75	-
α_{pH7}	0.85	0.94	-
α_{pH8}	0.98	1.00	1.0

Anion / Cation Exchange

Two different approaches were used in this study.

I. Column experiments:

1. glass columns (5 x 150 mm) filled with the cation exchangers BioRex 70 and BioRad AG 50 WX 12 (both from BioRad, München) ; the flow rate was about 1 ml/min.
2. glass columns (6 x 80 mm) filled with the anion exchangers Sephadex DEAE-25 (Fluka) and BioRad AG 1 X 8; flow rate: 2 ml/min.

II. Batch experiments:

The batch experiments were performed with the Sephadex DEAE-25 material. 100-500 mg of the resin were mixed with 2 ml of the analyte solution. After a shaking time of 20 s and centrifugation, an aliquot of the supernatant solution was radiometrically analyzed.

In both approaches, the resins were equilibrated to the desired pH and ionic strength before the experiments were carried out. For the pH adjustment suitable buffers were used (see Table 2). The ionic strength was adjusted by adding $NaClO_4$.

Continuous Electrophoretic Ion Focusing

The electrophoresis method is used to separate charged particles in an electric field and operates continuously in solution without any carrier. The apparatus was developed by Wagner et al. [Wag89] and can accept some liters of analyte solution within a reasonable time. In the electrophoretic technique, a conductivity-jump is used to focus the ions in the boundary zone between the zones AA and LF (see Figure 1). The separation chamber is

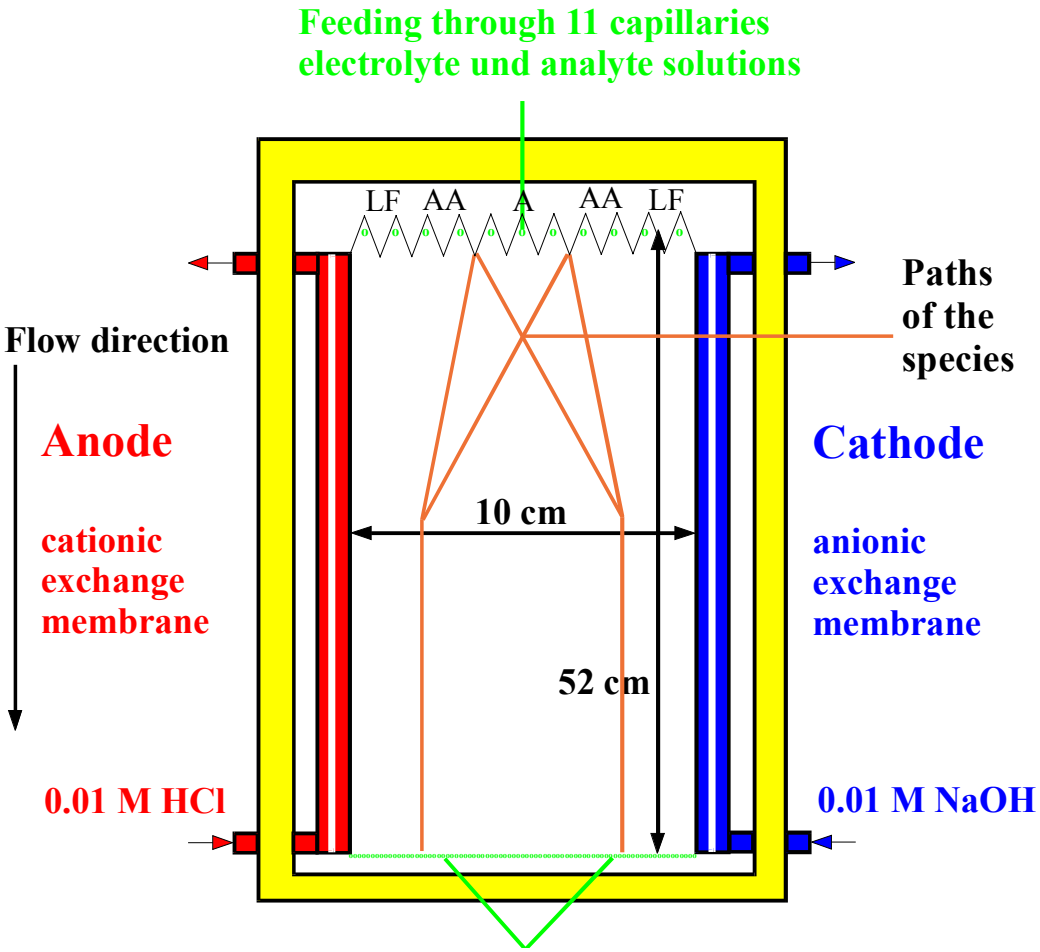

Figure 1: Schematic of the electrophoretic apparatus.

formed by two parallel plates (lower plate: glass, upper plate: acrylic glass; in the modified version teflon and PCTFE). The two plates are kept at a distance of 0.5 mm by a spacer thus forming a separation chamber of 100 x 520 mm x 0.5 mm. The lower plate is cooled to 4°C to avoid thermal convection. The upper plate contains eleven holes for capillaries (d_o: 2.5 mm; d_i: 1.57 mm) to feed the electrolyte (AA, LF) and analyte (A) solutions. At the end of the separation chamber are 89 capillaries (d_o: 1.0 mm; d_i: 0.5 mm) to collect the separated fractions. The electrode space containing the platinum wires is separated from the separation

chamber by ion exchange membranes. The electrode spaces are washed continuously with 0.01 M NaOH (cathode) and 0.01 M HCl (anode) to guarantee a high conductivity and to remove the gas bubbles which are formed during the experiments. The electrodes are connected to a high voltage of 500 – 700 V; the electric field is orthogonal to the flow direction. With a flow rate of 6.5 ml / min, the residence time in the chamber is about four minutes.

Separation with Continuous Electrophoretic Ion Focusing

The analyte solution (A) is fed through one or three capillaries in the centre of the inlet part of the chamber. An analogous solution (AA) with the same pH and the same buffer concentration as the analyte solution but without the metal ion and the humic acid is fed next through two (three) capillaries. Buffers were added to all solutions to stabilize the pH during the electrophoresis. The buffer must have two characteristics: the pH should not deviate more than 0.5 units from the desired value and there should be no or very low interaction with the metal-ions. The buffers used are given in Table 2.

Table 2: Buffers used for electrophoresis and anion / cation exchange

Buffer	pK_a - value	Used at pH
2 –Morpholinoethanesulfonic acid (MES)	6.10	5 and 6
2-[4-Hydroxyethyl)-1-piperazinyl]-ethanesulfonic acid (HEPES)	7.48	7
Imidazole	6.95	8

The anionic complex and the free cation are driven under the influence of the electric field to the electrodes (separation). A solution with the same pH but with a higher ionic strength and thus a higher conductivity (LF) is fed through the border capillaries. The velocity of migration towards the electrodes in these zones is strongly decreased by this conductivity jump (focusing). The conductivity is adjusted with $NaClO_4$ and must be more than 20 times higher than in the analyte solution to get an acceptable focusing. As an example, the distribution of pH, conductivity and separated species in the outlet fractions is shown in Figure 2.

Ultrafiltration Experiments

For these experiments the MicroSep^{TM} centrifugal concentrators (PallFiltron, Northborough) were used. Here, a separation due to the different size of the molecules and not due to their charge occurs. With a 1 K membrane the humic acid molecules are nearly completely hold back whereas the free cations pass through.

From 1 ml analyte solution, 100-200 µl were centrifuged through the membrane and the activity in an aliquot of the centrifugated solution was radiometrically determined.

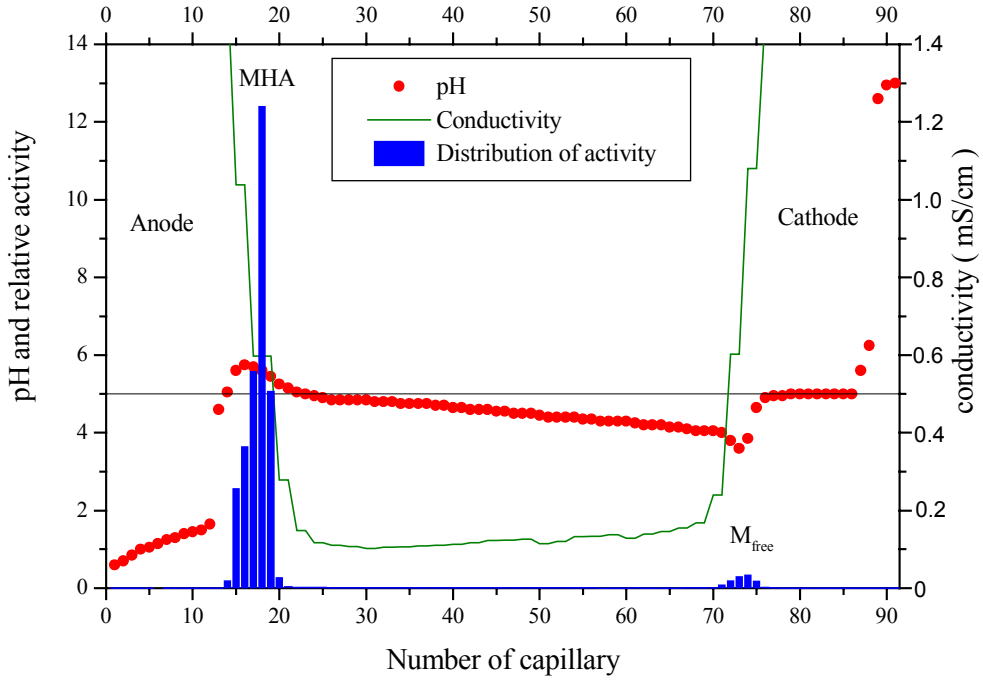

Figure 2: Distribution of pH, conductivity and metal species for a typical electrophoretic procedure; 1 x 10^{-7} mol/l La^{3+}; 20 mg/l Aldrich-HA ; 0.05 mol/l MES ; pH 5.

Batch and Column Experiments under Natural Aquifer Conditions

Batch and column experiments were performed under anaerobic conditions (Ar/1% CO_2) in glove-boxes in the pre-equilibrated groundwater/sand-system. The well characterized groundwater GoHy-532 [Art98] from the Gorleben area was used with a pleistocene aeolian quartz sand from the near aquifer surface as the solid phase. Details on the characteristics of the groundwater are summarized in Table 3.

Table 3: Characteristics of the groundwater GoHy-532. GoHy-532 is the original groundwater, GoHy-532 equil. has been equilibrated under anaerobic conditions (Ar/1% CO_2) with the aeolian quartz sand by pumping it over the column for several months.

	GoHy-532	GoHy-532 equil.
Depth (m)	65-68	
Stratification	Elster	
pH	8.9	7.4
E_h (mV)	-160	< -200
DOC (mg/l)	29.9	38.3
Cations (mg/l)		
Na	212.9	226.1
K	0.99	2.03
Ca	1.87	0.82
Fe	0.29	4.06
Anions (mg/l)		
Cl	131.7	130.8
F	0.6	0.8
HCO_3^-	334.1	322.8
Phosphate	2.4	0.5

In the batch experiments, a liquid/solid ratio of 10 ml groundwater to 2.5 mg sand was used, and the neptunium-239 concentration was chosen between 10^{-12} and 10^{-11} mol/l. The reaction time was up to 2 weeks.

The column experiments were carried out at the INE, FZ Karlsruhe. The experimental set-up for a flow through experiment is shown in Figure 3. A column of 25 cm length and 5 cm in diameter was tightly packed with the sand and equilibrated with the GoHy-532 groundwater for several months. Tritiated water (HTO) was used as tracer to determine the hydraulic properties of the system in each experiment.

The breakthrough curves of neptunium (^{237}Np and ^{239}Np as radiotracers) were measured on-line with a NaI-detector. Furthermore, at certain times, fractions of the eluate were taken for γ-spectrometric analysis and liquid scintillation counting to determine the Np- and tritium-activity and to enable a further characterisation of the eluate by means of ultrafiltration. Data

processing of the NaI-detector and the balance as well as the controlling of the sample collector were carried out by a personal computer.

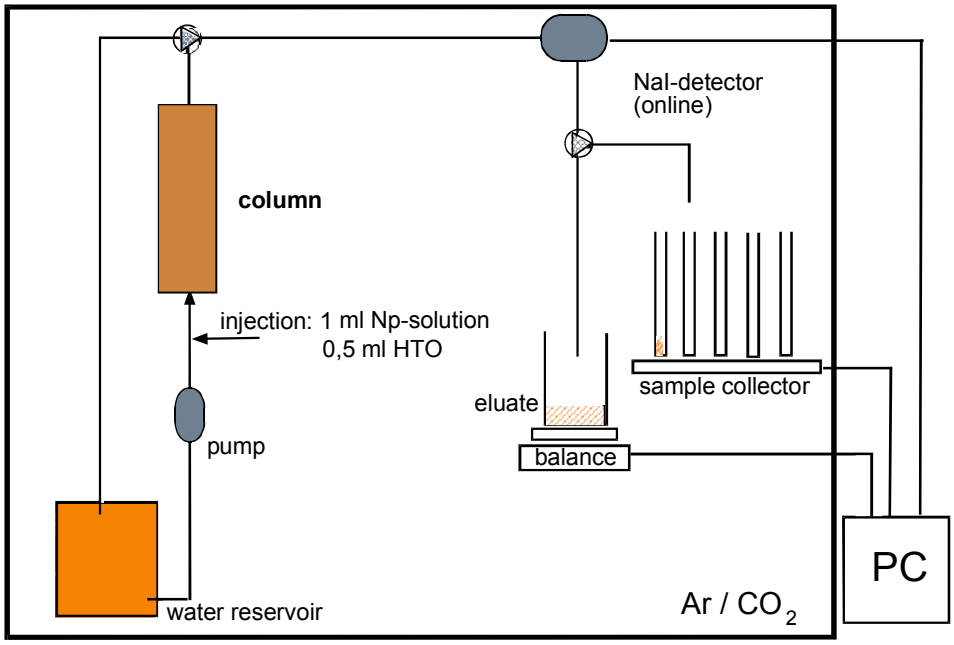

Figure 3: Experimental set-up for the column experiments.

Time Resolved Laser Induced Fluorescence Spectroscopy

The time resolved laser induced fluorescence spectroscopy is a suitable method for direct speciation [Kim91], [Kim93], [Kle91], [Mou92], [Pan96]. The experimental detection system used for fluorescence spectroscopy is shown schematically in Figure 4. A pulsed excimer (λ = 308 nm) pumped dye-laser system (Lambda Physic: COMPEX 205 / Scanmate 2; repetition rate: 20 Hz) is used to excite the sample solution at a wavelength of 375 nm (dye: QUI). To avoid strong photodegradation of the humic material, the original pulse energy of the dye-laser is reduced to about 1 mJ by a variable attenuator (Newport: M-935-5-OPT02). Sample solutions investigated are placed in rectangular silica cells (HELLMA: h·w·d = 46·12.5·12.5 mm^3). Perpendicular to the exciting laser pulse, the fluorescence emission of the sample solution is transferred onto the entrance slit (slit width: 1 mm) of a polychromator (Acton Research, Spectra Pro 275; grating: 1200 lines/mm) by a fibre cable and an appropriate optical equipment. Spectrally resolved fluorescence emission is detected by an intensified, time gated photo diode array detector (Princeton Instr., OSMA IRY 700 GR, 1024 linear

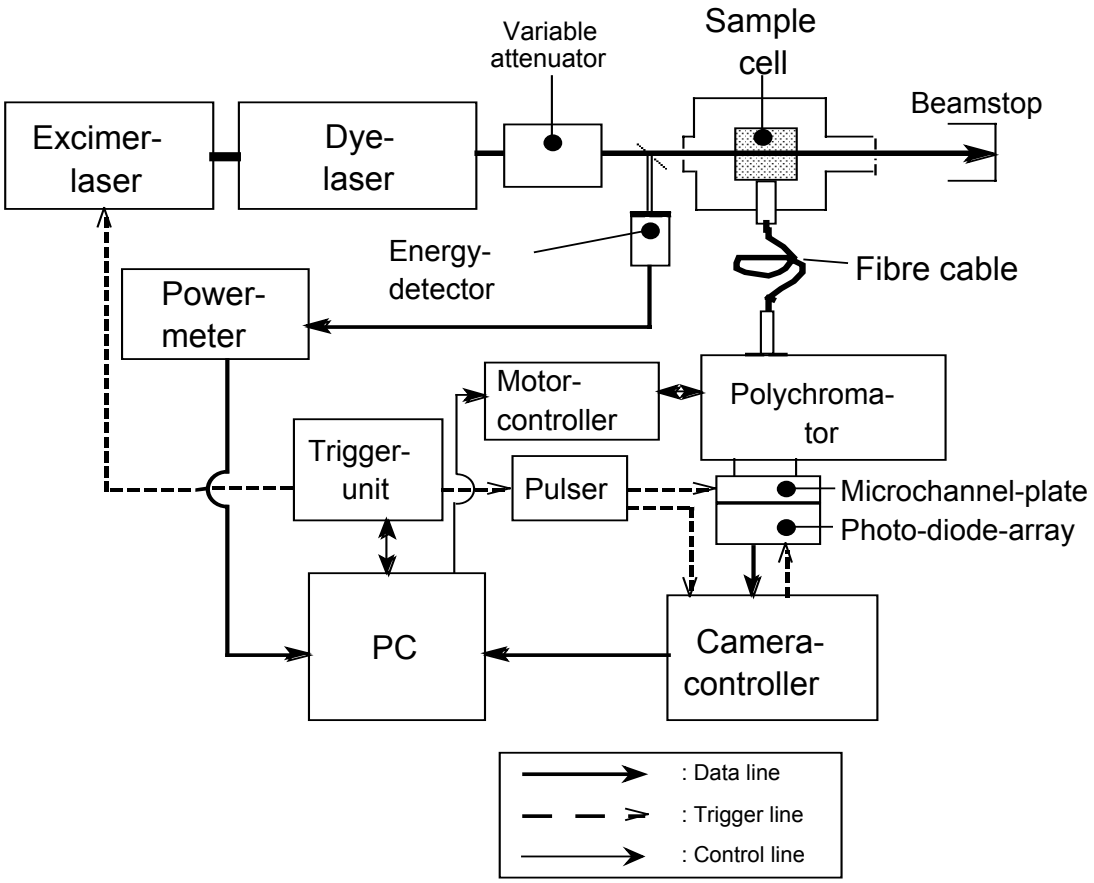

Figure 4: Experimental set-up for the time resolved laser induced fluorescence spectroscopy (TRLFS).

arranged Si photo diodes). Dependent on the fluorescence intensity of the solution, the investigated fluorescence emission, corresponding up to 2500 exciting laser pulses, is accumulated for each fluorescence spectrum. For normalization of the resulting spectra, the energy of the exciting laser pulse is monitored by reflecting (beam splitter) a small portion (~9 %) of the laser pulse onto a calibrated pyroelectric detector (Newport: 818J-09B) connected to a power meter (Newport: 818J-09B). Recording and digitizing of the data from the camera (photo diode array detector) is controlled by an ST180 camera controller (Spectroscopy Instruments). The system components are synchronised in time by a digital delay/pulse generator (Stanford Research Systems: DG535) used as the master trigger unit. With the software POSMA (Spectroscopy Instruments), an IBM compatible PC is used to control the system and to evaluate the data.

Resonance Ionisation Mass Spectrometry (RIMS)

For ultratrace analysis of plutonium, a pulsed laser system in combination with a time-of-flight (TOF) mass spectrometer is applied. A commercially available, Q-switched and intra-cavity doubled Nd:YAG pump laser (Clark-MXR ORC-1000) with a repetition rate of 1 – 25 kHz, a power of up to 50 W at 532 nm and a pulse length of approximately 400 ns is used to pump three titanium-sapphire (Ti:Sa) lasers simultaneously. The design of the optical system involves a Z-shaped laser resonator geometry to compensate for the astigmatism of the Ti:Sa-crystal. With one single set of mirrors, the laser is continously tuneable from 725 to 900 nm. For wavelength selection, a three plate birefringent filter and a thin etalon of d = 0.33 mm, corresponding to a free spectral range of 300 GHz are installed inside the resonator. This arrangement reduces the linewidth to 2 – 6 GHz. The set-up of the pulsed laser system is shown in Figure 5.
The temporal length of the Ti:Sa pulse is 60 – 150 ns. An intracavity Pockels cell is used as a Q-switch to optimize the temporal overlap of the pulses of all three lasers. It allows to shift the Ti:Sa pulses for 3.2 μs relative to the pump pulse, corresponding to the fluorescence lifetime of the excitated state of the Ti:Sa crystal.

As the ionisation energies of the actinides are approximately 6 eV, it is necessary to double the frequency of one laser in order to use a three step ionisation scheme. This is done with an external, single pass set-up applying a BBO crystal. Conversion efficiencies of up to 7 % are reached. All three laser beams are coupled into an optical fibre and finally focused into the source region of the TOF for optimum spatial overlap with the atomic beam.

After a number of principal tests of the performance of the laser system, first measurements of the system on ^{239}Pu were carried out with the following procedure: an atomic beam of plutonium is produced by evaporation from a sandwich filament. The atoms are ionised by two step resonant exitation and non-resonant and resonant ionisation. The photoions are subsequently mass analysed in a reflectron time-of-flight mass spectrometer with a mass resolution of $m/\Delta m \approx 600$. It serves for isotope selectivity and efficient background suppression.

After exploring the most promising excitation scheme, measurements of the overall efficiency of the new laser system combined with the TOF mass spectrometer for plutonium have been

carried out. The repetition rate of the lasers has been set to 3.3 kHz. With a laser power of 20 mW at $\lambda_1 = 421$ nm, 260 mW at $\lambda_2 = 847$ nm and 465 mW at $\lambda_3 = 756$ nm in the interaction region of the laser with the atomic beam, it could be demonstrated that the transitions of all three steps were saturated. Figure 6 shows a time-of-flight spectrum of a ^{239}Pu sample, where the filament contained 3.25 x 10^{11} atoms of plutonium. Pu^+ can be clearly seen. The oxide PuO^+ is suppressed by more than three orders of magnitude.

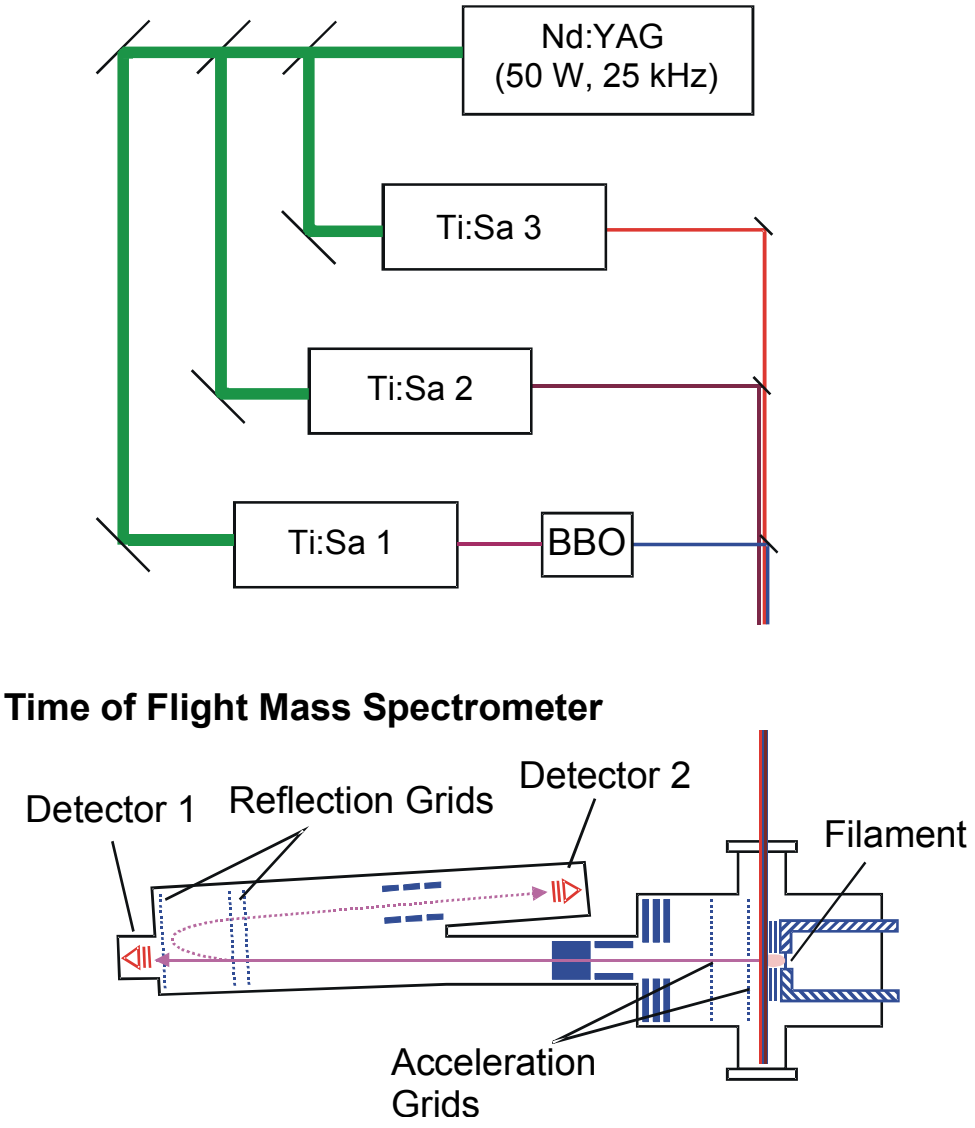

Figure 5: Experimental set-up of the laser system together with the time-of-flight mass spectrometer.

A total number of 2.6 x 10^6 ions of $^{239}Pu^+$ have been detected during a measuring time of 2.5 hours. Thus, an overall efficiency of $\varepsilon = 8.0 \times 10^{-6}$ is obtained. The background was less than 30 counts per mass-channel. Taking the background into account, a detection limit of

approximately 1 x 10^7 atoms of plutonium is derived at a confidence level of 99.7 % (3σ). This is comparable to the detection limit obtained with the previously used Cu-vapor/dye laser system. The new laser system is now routinely used for the determination of plutonium at the ultra-trace level.

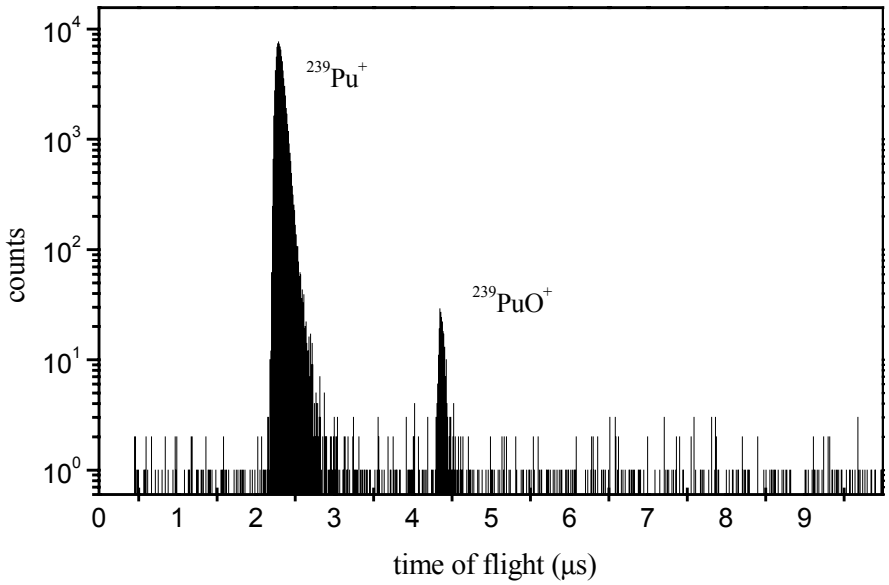

Figure 6: Time-of-flight spectrum of a plutonium-239 sample.

3. Results and Discussion

Determination of the complex stability constants

Two different procedures were applied for the determination of the free cation and the metal humic acid complex in solution. Indirect methods with a separation (ion exchange, EIF, ultrafiltration) of the species followed by the measurement of the content of the obtained fractions by radiometry (γ-spectrometry, liquid-scintillation-counting, β-delayed neutron counting), inductively coupled plasma mass spectrometry (ICP-MS) and direct optical methods (UV-VIS-spectroscopy, TRLFS).

For the complexation reaction M + HA ⇋ MHA the stability constant K is defined by:

$$K = \frac{[MHA]}{[M]_{free} \cdot [HA]_{free}}$$

The free humic acid concentration $[HA]_{free}$ can be calculated either with the charge neutralization model [Kim96] or the degree of deprotonation [Tor84].

In the charge neutralization model, it is assumed that in a metal-ion charge neutralization process the metal-ion occupies the number of proton exchange sites equal to its charge z^+. Thereby, the group of the complexing sites needed to neutralize the metal-ion is considered as one humic acid complexation unit.
The reaction is described as: $M^{z+} + HA(z) \leftrightarrow MHA(z)$. Thus, the complexation constant β becomes:

$$\beta = \frac{[MHA(z)]}{[M^{z+}]_{free} \cdot [HA(z)]_{free}}$$

The concentrations of MHA(z) and M^{z+} can be measured with the different methods mentioned above. $[HA(z)]_{free}$ is calculated by $[HA(z)]_{total} - [MHA(z)]$ with $[HA(z)]_{total}$ given by:

$$[HA(z)]_{total} = \frac{[HA]_{g/l} \cdot PEC \cdot LC}{z}$$

PEC is the proton exchange capacity in eq/g which is determined through pH titration. The loading capacity, LC, must be determined for each pH, metal-ion M^{z+}, ionic strength and humic acid. This leeds to β_{LC}- or $\log \beta_{LC}$-values.

Alternatively, with the degree of deprotonation, α, the humic acid concentration $[HA(z)]_{total}$ results as

$$[HA(z)]_{total} = \frac{[HA]_{g/l} \cdot PEC \cdot \alpha}{z}$$

By using the degree of protonation, $\log \beta_{\alpha}$-values are obtained.

The two calculations obviously differ in the concentration of available functional groups which are suitable for metal-ion complexation.

3.1 Trivalent Actinides and Lanthanides

Samarium and lanthanum were used as model elements for americium and curium, because of their similar charge to radius ratio. The lanthanides were used at higher (10^{-9} - 10^{-5} mol/l) and the actinides at lower (10^{-11} - 10^{-7} mol/l) metal-ion concentrations.

Ion exchange

Column experiments were carried out with anion and cation exchangers. The experiments with the weak cation exchanger BioRex 70, Aldrich humic acid and lanthanum resulted in a stoichiometrical coefficient for humic acid of 0.62 ± 0.08 and a log β_{LC}-value of 2.73 ± 0.44 (see Figure 7). This can be explained due to a competition between the humic acid ligands and the –COOH groups of the exchanger yielding a lower percentage of the lanthanum humate in the eluate, i.e. the cation exchange resin interferes with the humate complex formation equilibrium.

Experiments with the anion exchange resin Sephadex DEAE A-25 (Figure 8) delivered log β_{LC}-values which are in good agreement with data in the literature [Cze96], [Kim91], [Kim93]. However 5% of the free cation is adsorbed in absence of humic acid at pH 5.

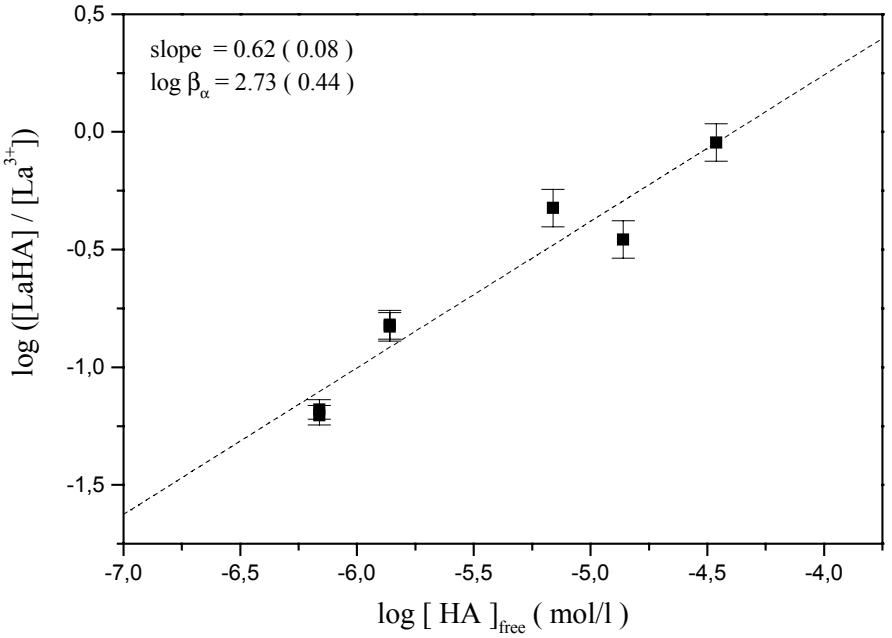

Figure 7: Determination of the stoichiometrical coefficient for humic acid and the log β_{LC}-value with BioRex 70; 5.4 x 10^{-6} mol/l La^{3+}; 1 x 10^{-3} mol/l $NaClO_4$; pH 5; Aldrich humic acid.

Continuous Electrophoretic Ion Focusing

The first experiments were performed under conditions similar to those described in [Fra97]. The two plates of the chamber were fabricated of glass and acrylic glass. The optimal voltage was determined to be 500 V for trivalent ions. Best focusing was achieved at a residence time in the apparatus of four minutes. The ionic strength was limited up to 5 x 10^{-2} mol/l; at higher ionic strenghts a voltage of only 240 V can be applied resulting in a bad focusing.

A log β_α-value of 7.21 ± 0.58 for pH 5 and a La^{3+} concentration of 5.4 x 10^{-7} mol/l with variable Aldrich-HA concentrations was determined (see Figure 9). The slope is 1.88 instead of 1.0 expected for a 1:1 stoichiometry and the yields of recovery are only 50-85 %, depending on the HA-concentration. The synthetic HA (type M1; charge No. FR-R36/95) showed a similar behaviour and the log β_α-value was 7.29 ± 0.28 under these conditions.

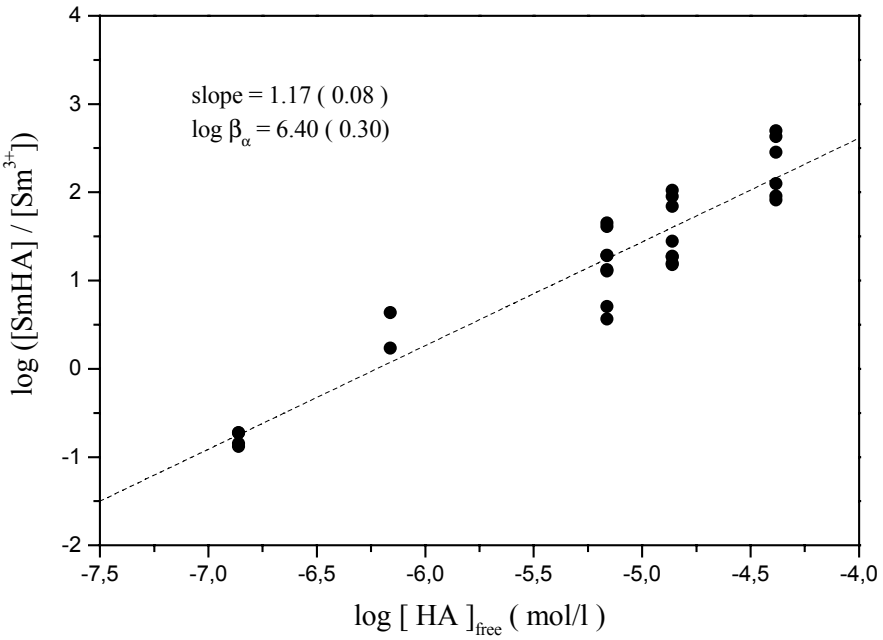

Figure 8: Determination of the stoichiometrical coefficient for humic acid and the log β_{LC}- value with Sephadex DEAE A-25; 6.6 x 10^{-7} mol/l Sm^{3+}; 1 x 10^{-3} mol/l $NaClO_4$; pH 5; Aldrich humic acid.

At low metal-ion concentrations both species are adsorbed on the surfaces and so the log β_{LC} - value was not correctly determined. To check this in detail, the chamber was operated for three hours with a analyte solution of 5.4 x 10^{-7} mol/l Sm^{3+} and 1 mg/l HA at pH 5. Every 30

minutes, samples were taken and measured (Figure 10). As can be seen, the yield of recovery is increasing with time.

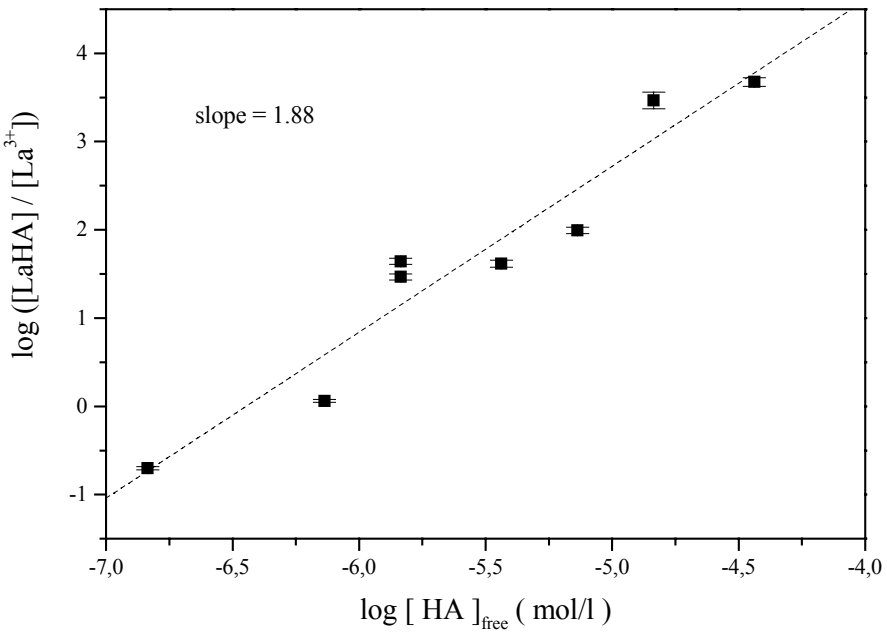

Figure 9: Dependence of log ([LaHA] / [La^{3+}]) on log [HA]; 5.4 x 10^{-7} mol/l La^{3+}; pH 5; 1 x 10^{-3} mol/l $NaClO_4$; surfaces of the chamber: glass and acrylic glass; log β_{LC} = 7.21 (Aldrich HA).

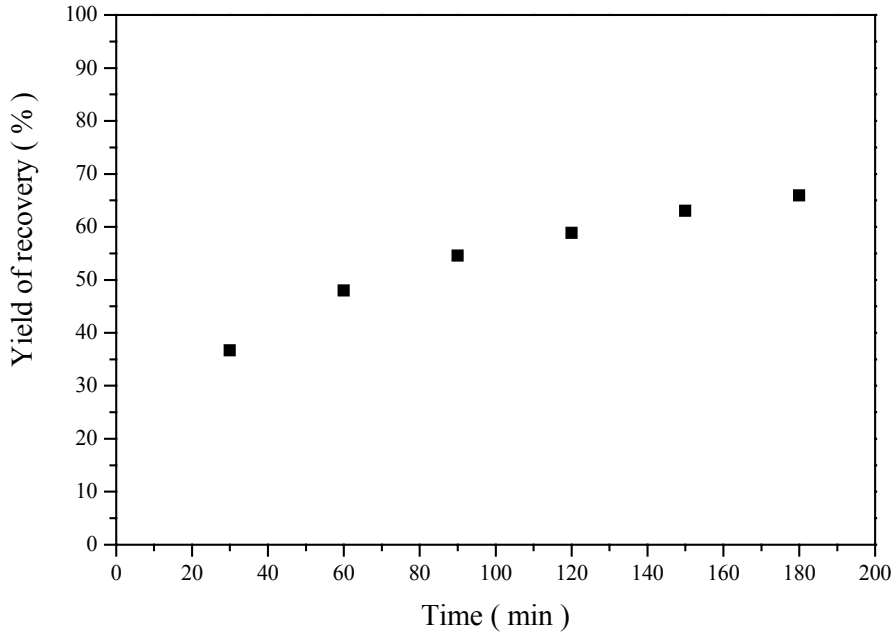

Figure 10: Dependence of the yield of recovery on the time of operation of the EIF; 5.4 x 10^{-7} mol/l Sm^{3+}; 1 mg/l HA; pH 5; 1 x 10^{-3} mol/l $NaClO_4$.

The time dependent distribution of the anionic and cationic species is shown in Figure 11. The relative amount of SmHA becomes constant after 120 min when the surfaces at the anionic part of the chamber are obviously saturated. The relative amount of the free cation was further increasing with time.

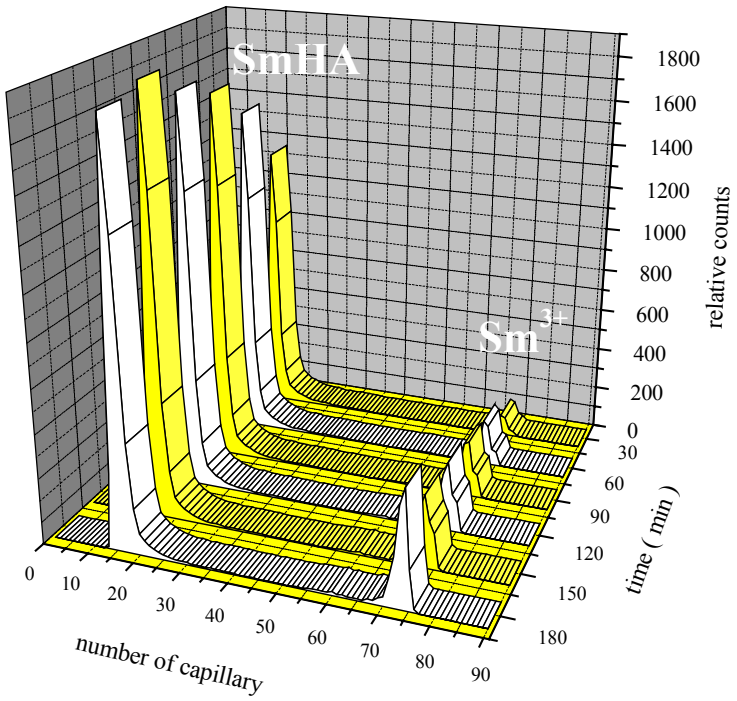

Figure 11: Distribution of SmHA and Sm^{3+} as a function of time of operation of the EIF; surfaces glass and acrylic glass; 1 mg/l HA, 5.4 x 10^{-7} mol/l Sm^{3+} ; pH 5; 1 x 10^{-3} mol/l $NaClO_4$.

Adsorption experiments with solutions containing 0 mg/l, 1 mg/l and 64 mg/l HA and 5.4 x 10^{-7} mol/l Sm^{3+} with several materials gave the lowest adsorption rates for teflon and polychlorotrifluorethylene (PCTFE) whereas glass, silicon, acrylic glass, polyvinylchloride (PVC), and polyethylene (PE) show higher values. Therefore, the electrophoretic chamber was modified. Glass and the capillaries (silicon and PE) were replaced by teflon and acrylic glass by transparent PCTFE. A cross section of the modified apparatus is given in Figure 12.

The adsorption experiments were repeated with the modified apparatus. The chamber was operated for one hour with 5 x 10^{-7} mol/l Sm^{3+} and variable Aldrich-HA concentrations at

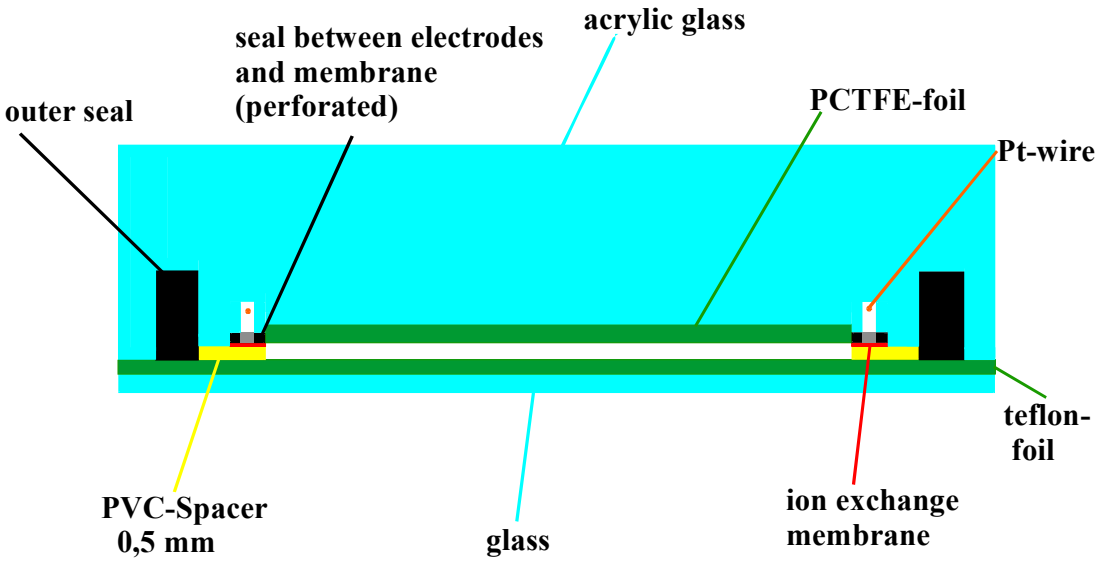

Figure 12: Cross section of the modified electrophoretic apparatus.

pH 5. Without HA, nearly 100 % of the introduced Sm^{3+} were found in the collected fractions, as is seen in Figure 13. At very low HA concentrations about 25% of the Sm is adsorbed. The adsorption is negligible at HA concentrations higher than 5 mg/l which corresponds to the natural conditions.

Experiments at pH 5.0, 6.0 and 7.0 were performed with variable HA concentrations and a

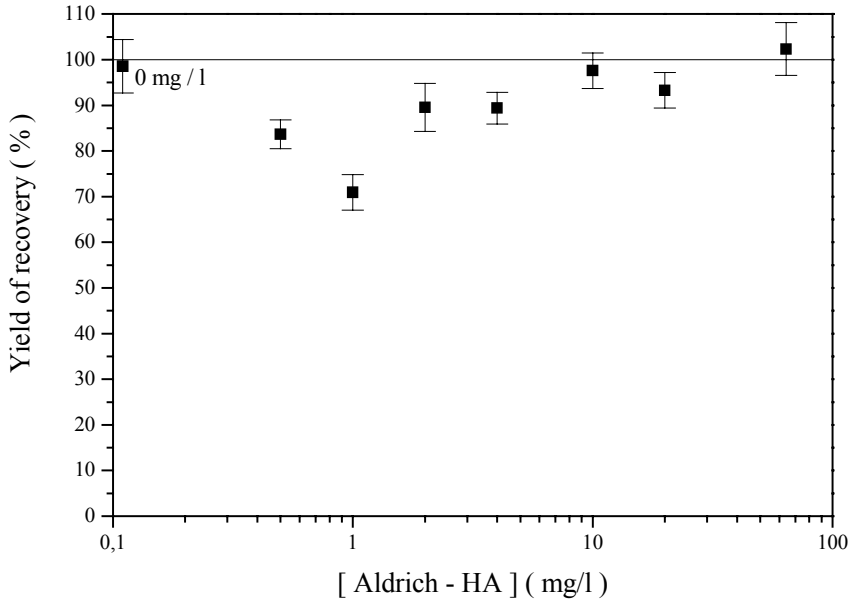

Figure 13: Dependence of the yield of recovery on the total HA concentration for the modified apparatus; 5 x 10^{-7} mol/l Sm^{3+}; pH 5.

constant metal-ion concentration, see Figure 14. The calculated log β_{LC}-values are 7.99 ± 0.16 (pH 5), 9.04 ± 0.11 (pH 6), and 9.69 ± 0.06 (pH 7); i.e. they are pH-dependent and much higher than the values in the literature [Kim89], [Kim93], [Kim96] .

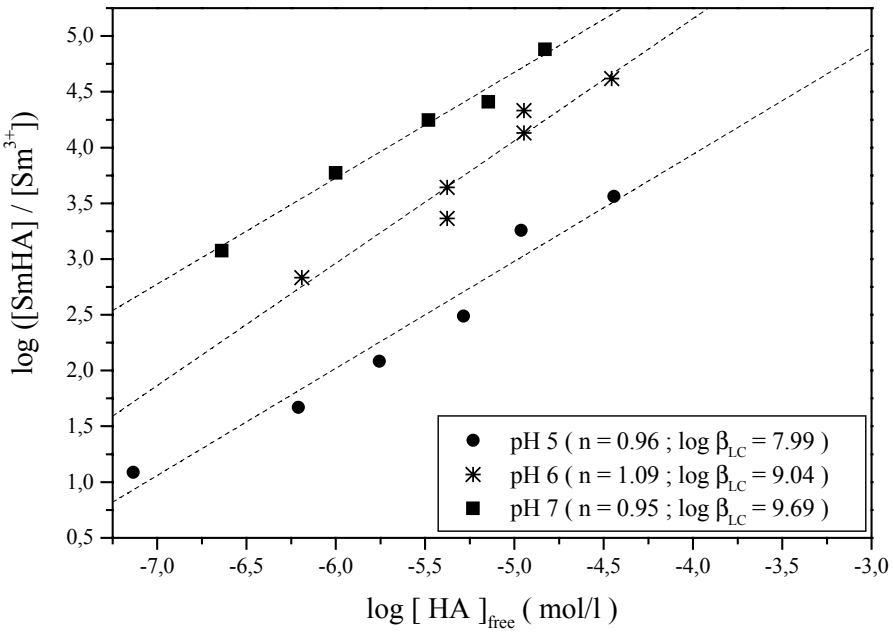

Figure 14: Dependence of log ([SmHA] / [Sm^{3+}]) on log [HA] and pH; 5.4 x 10^{-7} mol/l Sm^{3+}; Aldrich HA; 1 x 10^{-3} mol/l $NaClO_4$; modified electrophoretic apparatus, n = stoichiometric coefficient.

The loading capacities for trivalent ions and Aldrich HA in Table 4 were determined as described by Czerwinski et al. [Cze96] and are summarized for Aldrich humic acid. The pH dependence is in contradiction with the metal-ion charge neutralization model which delivers log β_{LC}-values independent of pH.

Table 4: Loading capacities of Sm^{3+} at pH 5.0, 6.0 and 7.0 and log β_{LC}-values as obtained with the modified electrophoretic apparatus together with literature data; 10^{-3} mol/l $NaClO_4$.

pH	LC this work	LC literature [Kim93] [Kim96] [Kim89]	log β_{LC} this work	log β_{LC} literature [Kim93] [Kim96]
5.0	0.374 ± 0.007	0.476 ± 0.007	7.99 ± 0.16	6.40 ± 0.20
6.0	0.772 ± 0.194	0.679 ± 0.014	9.04 ± 0.11	6.50 ± 0.10
7.0	1.003 ± 0.134	1.000 (pH > 6.8)	9.69 ± 0.06	

The yields of recovery are scattering around 95 %. Because nearly 99.9 % of the cation is complexed, a possible adsorption of the anionic complex on the 5 % level can be ignored. An analogous solution was measured by TRLFS to exclude other anionic species which could increase the measured anionic amount and thereby the log β_{LC}-values. If there is complexation with HA the free cation concentration is decreased to nearly 10^{-9} – 10^{-10} mol/l. Results of adsorption experiments at this low metal-ion concentrations in the absence of HA are shown in Figure 15. The yields of recovery are dependent on the total metal-ion concentration and pH.

Below 10^{-6} mol/l, the yield of Sm^{3+} recovered decreases dramatically and reaches a value of only ~ 20 % at 5 x 10^{-10} mol/l. It is interesting to note that, at 5 x 10^{-10} mol/l where the yield of recovery is minimal, the recovered Sm is to a large extent anionic and neutral. The respective species could be products of hydrolysis or complexation with CO_3^{2-}. The increase of the yield of recovery between 5 x 10^{-8} and 5 x 10^{-10} mol/l at pH 7 might be correlated with the formation of species other than cations.

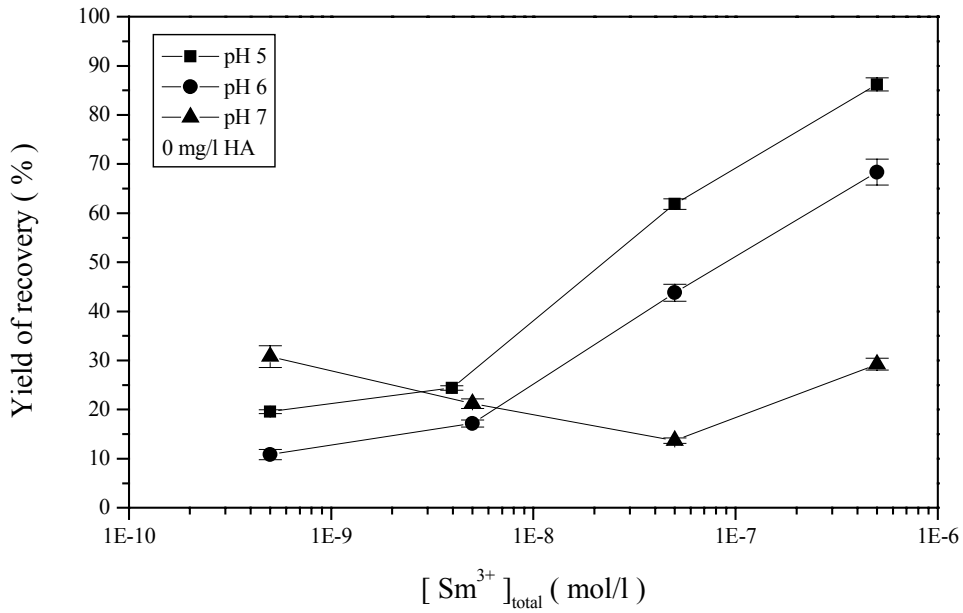

Figure 15: Dependence of the yield of recovery on the total Sm^{3+} concentration and pH for the modified apparatus in the absence of HA.

In the case of HA complexation where, as mentioned above, the free cation concentration is reduced to 10^{-9} - 10^{-10} mol/l, Figure 15 shows for such concentrations that the recovery of the

free cations is grossly supressed resulting in systematically too high log β_{LC}-values. There is also an obvious correlation between Figure 14 and Figure 15: the dependence of the values of log ([SmHA] / [Sm^{3+}]) on pH is at least qualitatively related to the increasing loss of free Sm^{3+} ions with increasing pH in the electrophoretic apparatus. Thus, the EIF technique is not suitable for free trivalent cation concentrations below 10^{-6} mol/l.

Time Resolved Laser Induced Fluorescence Spectroscopy (TRLFS)

Complexation studies of ^{248}Cm(III) with Aldrich humic acid have been performed at pH 5 and 6 for an ionic strength of 1 x 10^{-3} mol/l and a metal-ion concentration of 1 x 10^{-7} mol/l. The Aldrich-HA concentration was kept at 5 mg/l in all experiments. The solutions were buffered with MES. Carrierfree ^{140}La (7 x 10^{-13} mol/l) was used as radiotracer for yield determination.

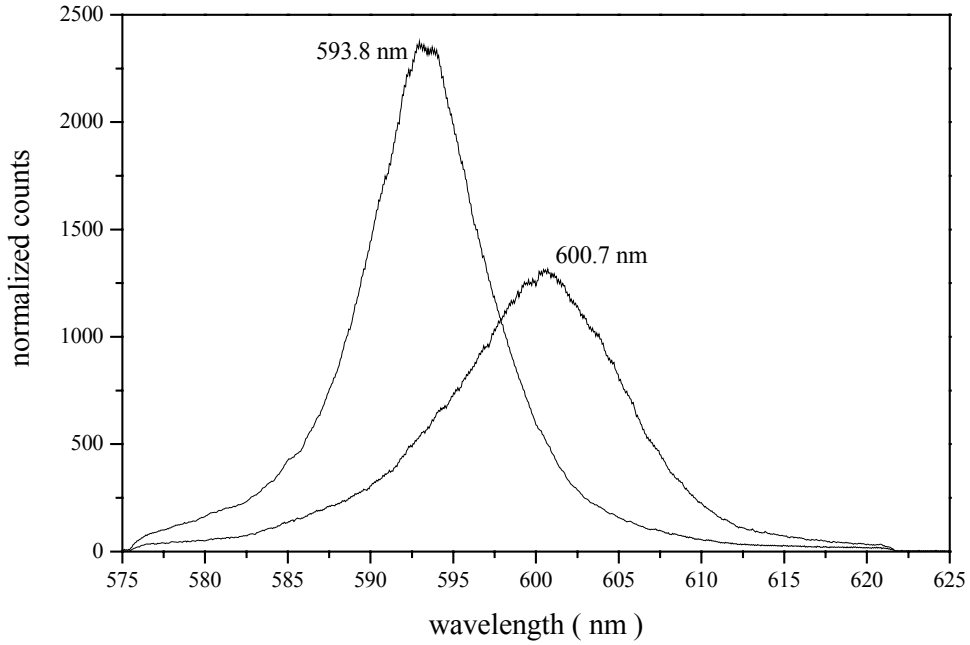

Figure 16: Fluorescence emission spectra of Cm-Aldrich-HA (600.7 nm) and Cm^{3+} (593.8 nm) in a perchlorate solution.

The studies are based on a direct (TRLFS) and an indirect (EIF) speciation method [Kle91] [Mar96]. All solutions were analyzed with TRLFS before and after the electrophoretic separation. The relative fluorescence intensity of the Cm-Aldrich humate, normalized to that of the free Cm^{3+} aquoion, is 0.49 (Gorleben groundwater GoHy-573: 1.47) [Pan96]. The fluorescence decay can be fitted by a monoexponential decay law with a life time of τ = 84 µs

(GoHy-573: τ_1 = 75 µs (82%) and τ_2 = 145 µs (18%)). The emission maximum for the Cm-Aldrich humate is at 600.7 nm (GoHy-573: 601.0 nm), see Figure 16.

The log β_{LC}-values determined before the electrophoretic separation are 6.54 ± 0.10 (pH 5) and 6.52 ± 0.10 (pH 6). After the electrophoretic separation, no free Cm^{3+} was detectable with TRLFS, indicating that adsorption of the free Cm^{3+} occurred in the EIF apparatus. The free Cm^{3+} should be detectable, because the concentration compared to the analyte solution is increased due to the focusing at the conductivity jump.

3.2 Neptunium(V)

Continuous Electrophoretic Ion Focusing

Experiments with the electrophoretic method described above (chapter 2) were carried out with Np(V) and Aldrich humic acid at varying concentrations of humic acid, neptunium and at different pH values. In addition to this, several experiments with synthetic humic acids were performed using the EIF technique.

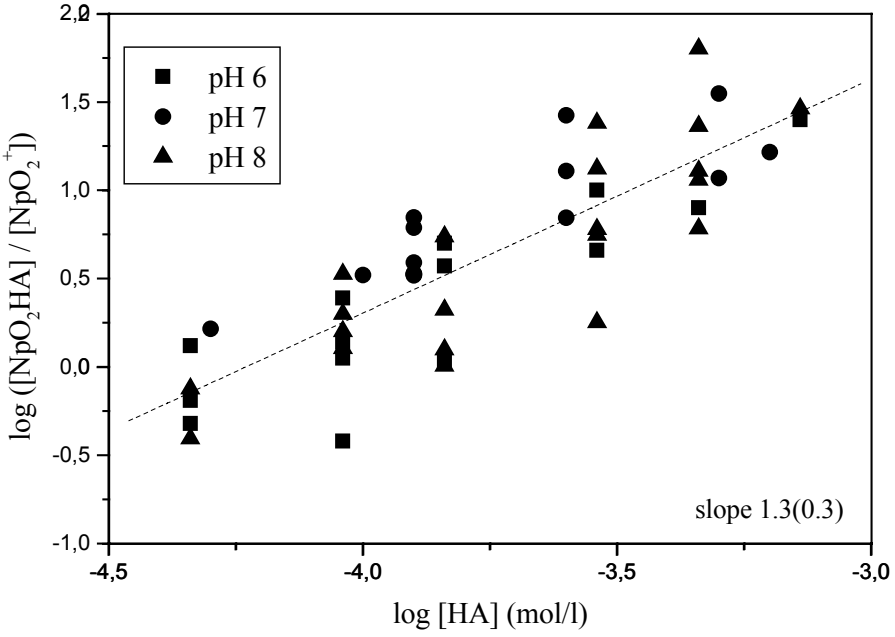

Figure 17: Dependence of log ([NpO_2HA] / [NpO_2^+]) on log [HA]; 1 x 10^{-13} mol/l NpO_2^+, pH 6, 7, and 8; 1 x 10^{-3} mol/l $NaClO_4$.

For the neptunium experiments, the optimal conditions were determined to be: a voltage of 700 V, a residence time in the chamber of ~ 4 min and feeding of the analyte solution through one capillary. Under these conditions, the recovery of the neptunium is higher than 90 %.
By varying the humic acid concentration between 10 and 150 mg/l and keeping the neptunium concentration at 1 x 10^{-13} mol/l a stoichiometric coefficient for the complexation of humic acid with Np(V) can be determined plotting log ([NpO_2HA] / [NpO_2^+]) versus log [HA]. In Figure 17, this is shown for various pH values.

In all cases, the slope is 1.3 ± 0.3 showing that predominantly a 1:1-complex is formed between NpO_2^+ and the complexing groups of the humic acid. The complex stability constants calculated with these data are summarized in Table 5 where the values for log K, log β_α and log β_{LC} are given, too. The loading capacities are taken from [Mar98] as determined for Gorleben humic acid.

Table 5: Comparison of log K, log β_α and log β_{LC} for 1 x 10^{-13} mol/l neptunium at different pH.

	log K	log β_α	LC_{GoHy}[Mar98]	log β_{LC}
pH 6	4.1 ± 0.2	4.3 ± 0.2	0.07	5.3 ± 0.2
pH 7	4.4 ± 0.2	4.5 ± 0.2	0.13	5.3 ± 0.2
pH 8	4.7 ± 0.4	4.7 ± 0.4	0.22	5.4 ± 0.4

Table 6: Comparison of the log β_α of the synthetic humic acids M1 and M1b as well as log $\beta_{\alpha,Aldrich}$ for 1 x 10^{-13} mol/l neptunium at different pH-values.

	log $\beta_{\alpha,M1}$	log $\beta_{\alpha,M1b}$	log $\beta_{\alpha,Aldrich}$
pH 6	3.9 ± 0.1	-	4.3 ± 0.2
pH 7	4.0 ± 0.1	-	4.5 ± 0.2
pH 8	4.3 ± 0.1	4.7 ± 0.1	4.7 ± 0.4

As can be seen, only the log β_{LC}-values are independent of pH. The small deviation at pH 8 may be due to the influence of carbonate, because the experiments were carried out under atmospheric conditions.

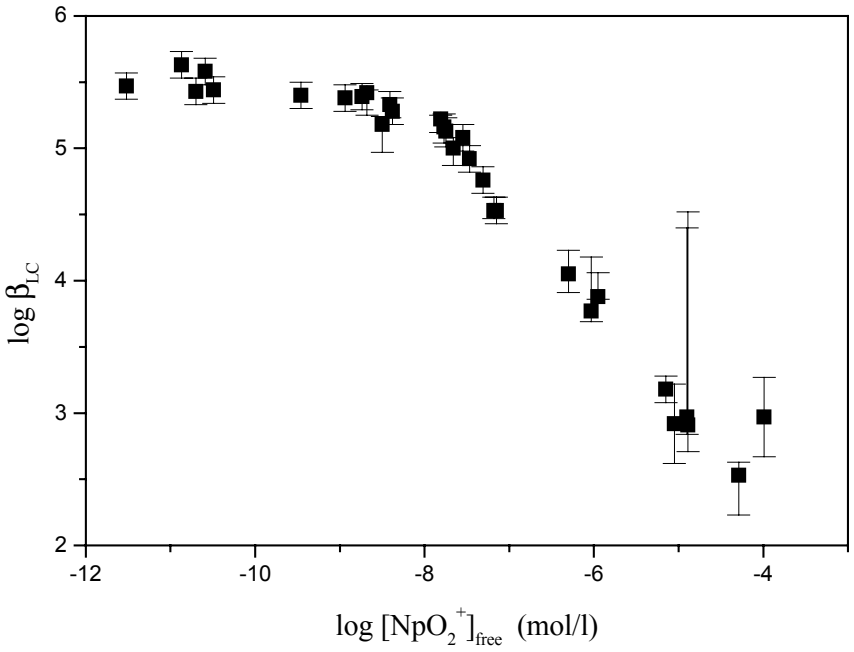

Figure 18: Dependence of log β_{LC} on the free metal-ion concentration as obtained in electrophoretic experiments at pH 6 and 7 with 30 mg/l Aldrich humic acid. The great uncertainties of some data are due to problems with the recovery yield.

In the same way, experiments with the synthetic humic acids M1 and M1b from Rossendorf were performed. As can be seen from Table 6, the log β_α-values are slightly lower than those with Aldrich humic acid.

Nevertheless, compared with data from literature [Mar98, Rao95, Sek91] the log $\beta_{Aldrich}$-values are too high. Because nearly the complete published data are obtained with higher neptunium concentrations in the range 10^{-6} to 10^{-4} mol/l, in our experiments as a next step the neptunium concentration was varied and the humic acid concentration was kept constant at 30 mg/l. The log β_{LC}-values obtained throughout this set of experiments are plotted versus the logarithm of the free NpO_2^+-concentration in Figure 18.

The log β_{LC} varies with the concentration of the metal-ion over a range of nearly 3 orders of magnitude. To confirm these results, experiments were performed in collaboration with the INE, FZ Karlsruhe. Several analyte solutions were investigated using EIF in combination with radiometric methods and ICP-MS and directly with UV-VIS-spectroscopy. The results are depicted in Figure 19.

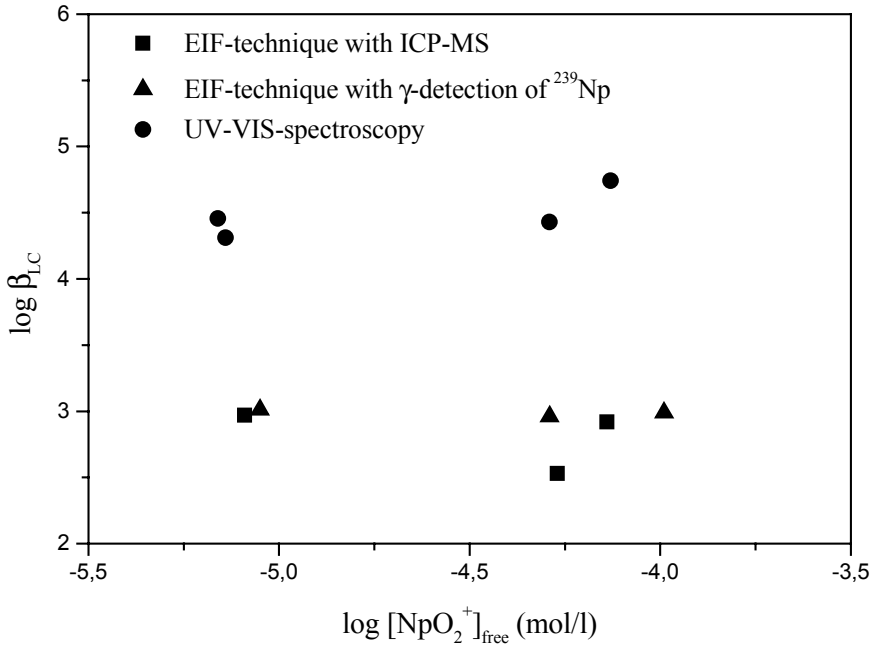

Figure 19: Comparison of log β_{LC}-values for Aldrich humic acid and neptunium obtained with EIF-technique (two different detection methods for the separated species) and UV-VIS-Spectrometry.

Obviously, the log β_{LC}-values determined with EIF are lower than the UV-VIS-data. At this time there is no plausible explanation for the deviation between UV-VIS and EIF; one may speculate whether there is an influence of the electric field on the dissociation of the humate complex at higher neptunium concentrations.

The UV-VIS-data leed to higher log β_{LC}-values than those for GoHy-573 in the literature [Sek91, Mar98]. Therefore, the LC for Aldrich humic acid needs to be determined in forthcoming experiments.

To confirm the EIF-data for low metal-ion concentrations, other experimental techniques were used for the separation of the free NpO_2^+ and its humate complex (see the following sections).

Anion Exchange

By using the batch technique with Sephadex DEAE A-25 resin at pH 6, 7, and 8, different metal-ion concentrations and a humic acid concentration of 10 or 30 mg/l, respectively, the results shown in Figure 20 were obtained.

The experiments are limited to metal-ion concentrations lower than 10^{-6} mol/l, because at higher metal-ion concentrations the negatively charged complex is not completely loaded on the exchange resin. In the metal-ion concentration range (10^{-14} - 10^{-6} mol/l) the results seem to

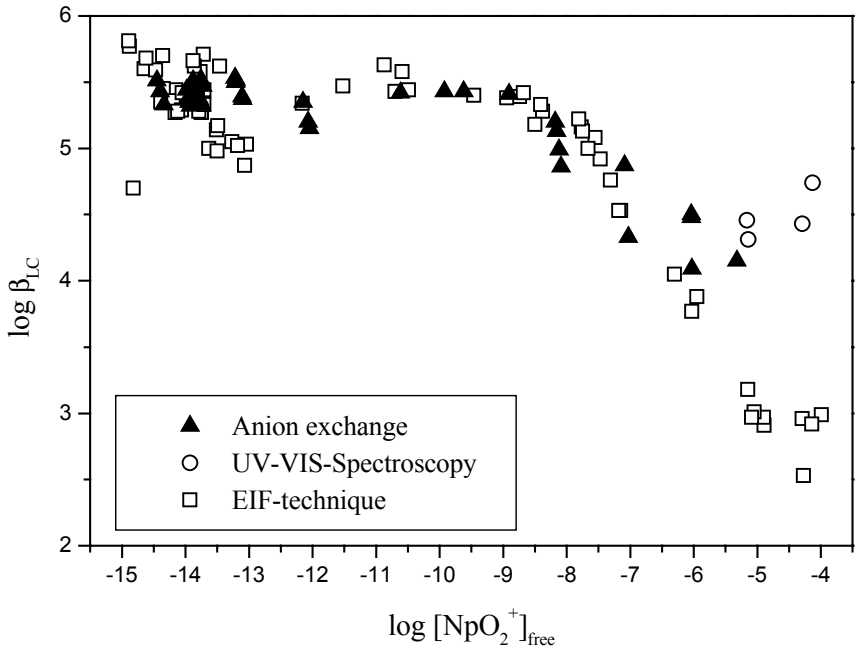

Figure 20: Anion exchange with Sephadex DEAE A-25. The data set was obtained in batch experiments with varying neptunium concentrations; the open symbols represent the EIF-data and UV-VIS-data from previous experiments. The statistical errors from γ-counting do not exceed the size of the symbols.

be in agreement with the EIF-data. The decrease of the log β_{LC}-values from 5.4 to about 4.4 between 10^{-9} and 10^{-6} mol/l, in particular, as shown by the EIF data is reproduced by the AIX experiments.

Ultrafiltration

As another independent experimental approach, ultrafiltration was used for the separation of the humate complex from the free cation. For concentrations above 10^{-6} mol/l neptunium the log β_{LC} is around 4.6 and increases to 5.4 at lower concentrations (see Figure 21), in agreement with the EIF and AIX data.

Discrepancies between the EIF data and the UV-VIS data, the AIX data, and the ultrafiltration data persist for $[NpO_2^+]_{free} > 10^{-6}$ mol/l. As mentioned above, at this time we are unable to give an explanation for this.

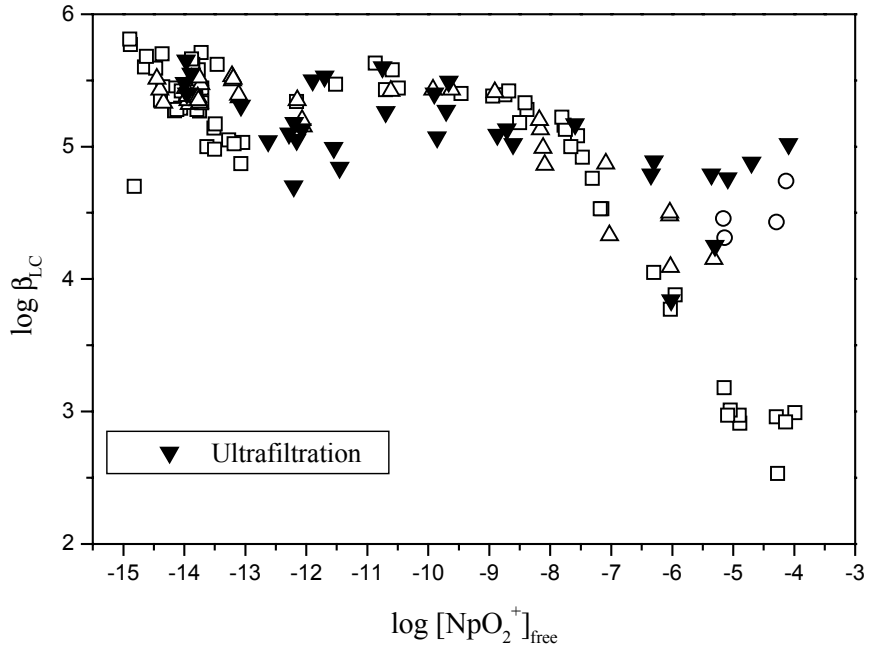

Figure 21: Ultrafiltration data obtained with varying neptunium concentrations for Aldrich humic acid; the open symbols represent the EIF-data, UV-VIS-data and anion exchange data from the previous experiments.

Batch Experiments with Np(V), GoHy-532 and Gorleben sand

The time dependent sorption behaviour of Np on a sandy sediment from the Gorleben area is shown in Figure 22. The liquid phase was the groundwater GoHy-532 from a borehole in Gorleben. Experiments without sand proved that there is no adsorption of the neptunium on the walls of the vessels.

Because the short-lived ^{239}Np was used in these experiments the equilibrium time could not be extented over two weeks. During this period, about 40 % of the added neptunium was sorbed on the solid phase.

Besides the adsorption effect, there is a reduction of the originally added Np(V) to Np(IV) in the groundwater. This behaviour was also observed during the column experiments (see next section). The percentage of Np(IV) in the concentration range between 10^{-12} to 10^{-7} mol/l was determined by liquid-liquid-extraction with trifluorothenoylacetone (TTA) or dibenzoylmethane (DBM). With increasing reduction, the total recovery of neptunium in the extraction experiments decreases. Several experiments point to the fact that the neptunium which is not recovered builds up a third phase between the organic and aqueous phase that could not be separated from these. So the liquid-liquid-extraction data is associated with higher error limits than the UV-VIS data.

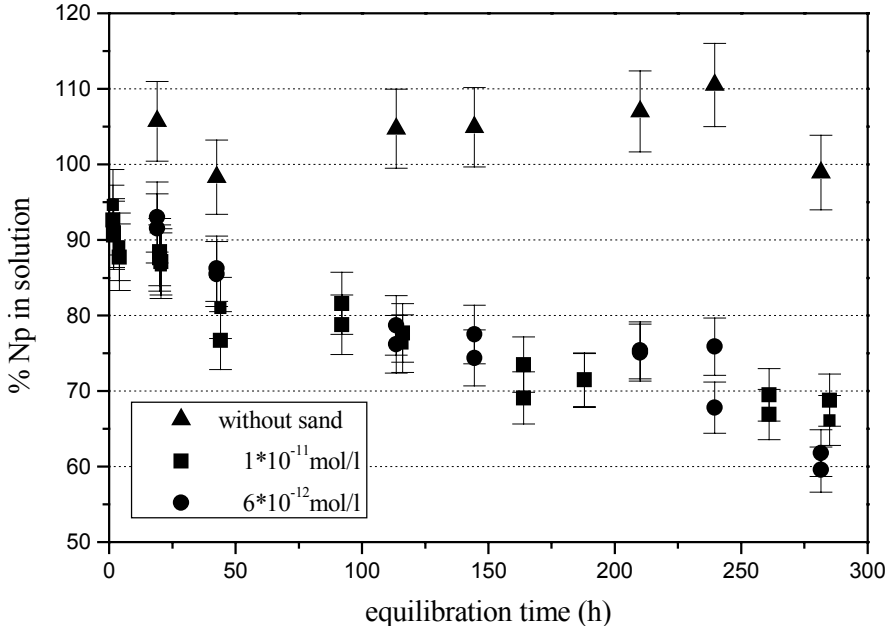

Figure 22: Sorption of neptunium on pretreated sand at low metal-ion concentrations with the groundwater GoHy-532 as liquid phase.

A similar reduction was found in other studies [MarPers.Com.] and seems to be related to the iron contents of the groundwater besides the quinone/hydroquinone equilibrium postulated for the reduction ability of humic substances [Zie80]. Experiments with purified Aldrich-humic acid and neptunium (under atmospheric conditions) show that there is no significant reduction to Np(IV); to a small extent, reduction occurs under anaerobic conditions even with the purified humic acid.

Column Experiments with Np(V), GoHy-532 and Gorleben sand

With the set-up described above (chapter 2) migration experiments with varying neptunium concentrations and equilibration times were carried out. The details of the experiments are summarized in Table 7.

The aquatic transport of metal-ions through a sediment matrix may be retarded by various sorption reactions like ion exchange, surface complexation or diffusion into micro pores of the sediment. The migration behavior is expressed by the retardation factor $R_f = v_{groundwater}/v_{colloid}$, where $v_{groundwater}$ is the mean flow velocity of the groundwater measured by the tracer HTO and $v_{colloid}$ the mean flow velocity of the colloid bound neptunium ion. In addition to the retardation factor, the total recovery of the injected metal-ion is an important dynamic sorption parameter.

The migration characteristic of Np(V) is depicted in Figure 23 together with the break-through curve of the HTO tracer; the neptunium activity in the eluate is normalized to the

injected activity (after correction for the half-life of the ^{239}Np) and plotted as a function of the ratio of the eluted groundwater volume V to the free pore volume of the column, V_p.

The HTO tracer was injected directly after the neptunium/groundwater solution. The retardation factors R_f for the various experiments are listed in Table 7 together with the total recovery of the neptunium.

The mean retardation factor is < 1, which means that the mobile Np-species migrates slightly faster than water. This can be explained by the fact that the mobile neptunium species are humic colloids to which the neptunium is bound. Due to size exclusion effects, their mean longitudinal velocity is larger in the column than that of water.

Table 7: Details of the column experiments with $^{237/239}$Np, GoHy-532 groundwater and pre-equilibrated Gorleben sand; hydraulic properties (the retardation factor and the longitudinal dispersion coefficient) of the column were determined with HTO.

Groundwater/ experiment-no.	Pore water flow velocity (10^{-4} cm/s)	Np-conc. (mol/l)	Effect. porosity (%)	Longitudinal dispersion coefficient (10^{-5} cm^2/s)	Equili-bration time (d)	pH	Recovery (%)	R_f
GoHy-532/1	3.8	2 x 10^{-10}	32.4	5.26	0.04	7.2	8.4	0.96
GoHy-532/2	3.7	4 x 10^{-8}	32.3	6.19	0.04	2.9	10.4	0.97
GoHy-532/3	3.5	3 x 10^{-4}	32.4	6.47	0.04	7.5	2.0	1.01
GoHy-532/4	3.5	2 x 10^{-7}	32.2	6.05	0.04	7.6	3.2	0.99
GoHy-532/5	3.3	9 x 10^{-9}	32.8	2.97	0.04	7.2	2.9	0.98
GoHy-532/5b	3.3	9 x 10^{-9}	32.8	3.41	2		20.5	0.97
GoHy-532/6	3.3	1 x 10^{-5}	32.8	3.08	0,04		8.5	0.95
GoHy-532/6b	3.4	1 x 10^{-5}	33.0	3.44	2	7.2	37.5	0.95
GoHy-532/6c	3.3	1 x 10^{-5}	32.9	3.38	8		85	0.95

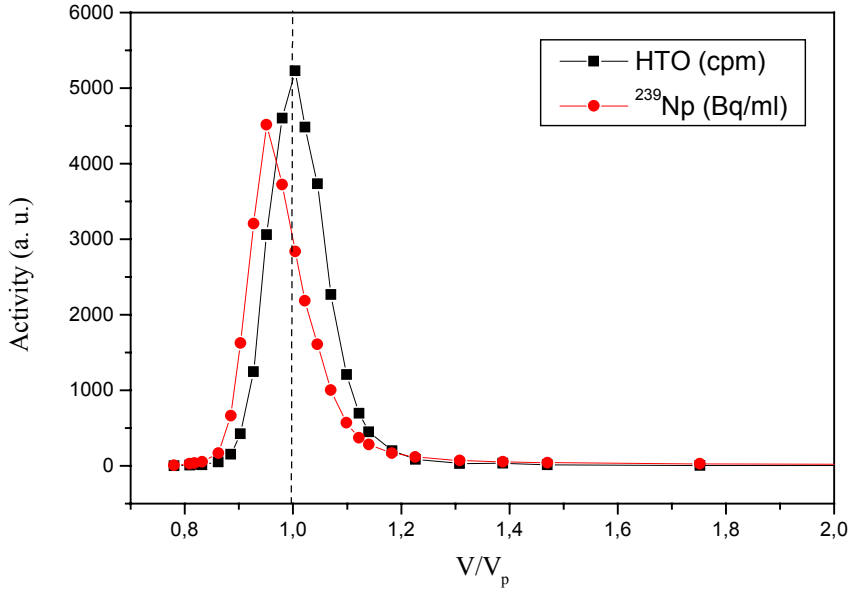

Figure 23: Example of break-through curves for neptunium on GoHy-532/sand-system and the HTO-tracer.

This is supported by ultrafiltration experiments of the eluates and of the input solution. Several eluate fractions show a size distribution similar to that of the groundwater-DOC [ArtPers.Com.] (see Figure 24). In the case of this groundwater, about 10 % of the dissolved organic carbon content is found in the eluate from the 1 K membranes. This can be explained

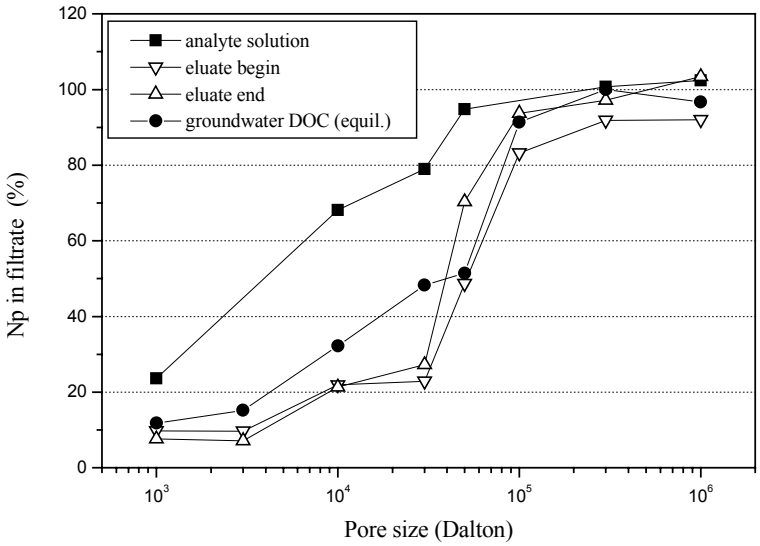

Figure 24: Ultrafiltration of analyte solution, of two eluate fractions (the ^{239}Np activity was measured) and of pre-equilibrated groundwater GoHy-532 (the DOC content was measured).

by an admixture of very small and hydrophilic molecules of humic acid that could pass through the membrane. In the case of the Aldrich humic acid such molecules may be removed in the purification process.

The size distribution of the analyte solution varies with the equilibration time and therefore with the degree of reduction of Np(V). This is depicted in Figure 25. The nearly complete reduction to Np(IV) is accompanied by an increase in molecular size of the colloids that contain neptunium.

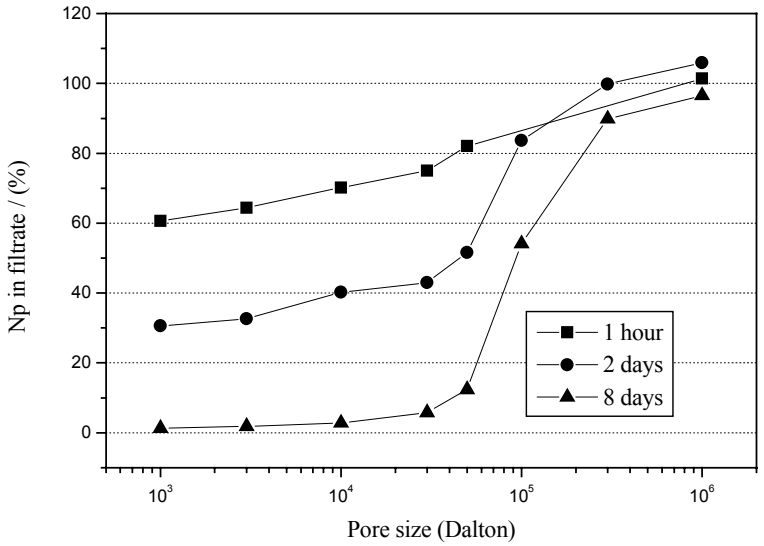

Figure 25: Ultrafiltrations of the analyte solution of experiment 6, in which the equilibration time between Np(V) and the groundwater was varied between 1 hour and 8 days; $[Np]_t$ = 1.3 x 10^{-5} mol/l.

Figure 26 shows that there is no significant influence of the neptunium concentration on the total recovery. With an equilibration time of two hours before the injection onto the column the recovery over the concentration range between 2 x 10^{-10} and 3 x 10^{-4} mol/l is below 10 %. With increased equilibration time, the recovery increases. This indicates that, with increasing reaction time, more Np(V) is reduced to the tetravalent oxidation state which is stronger bound to the humic colloids than Np(V). The reduction was observed in experiment 6 with an initial Np(V)-concentration of 1,3 x 10^{-5} mol/l by UV-VIS-spectroscopy (see Figure 27) and with liquid/liquid extraction with TTA and DBM.

As can be seen from Figure 27, the Np(V)-concentration, the concentration of the free NpO_2^+ cation as well as that of the Np(V) complex species, decreases with the contact time.

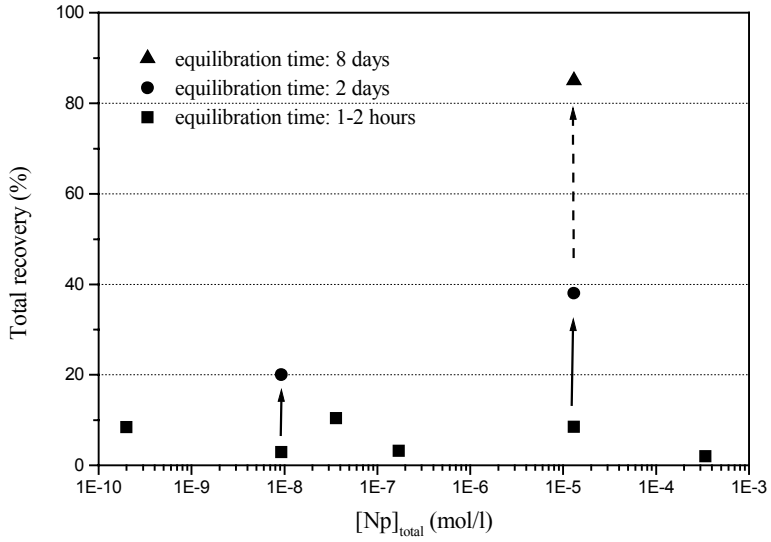

Figure 26: Total recovery of neptunium from a GoHy-532/sand column as a function of the neptunium concentration and the equilibration time prior to the feeding of the activity onto the column.

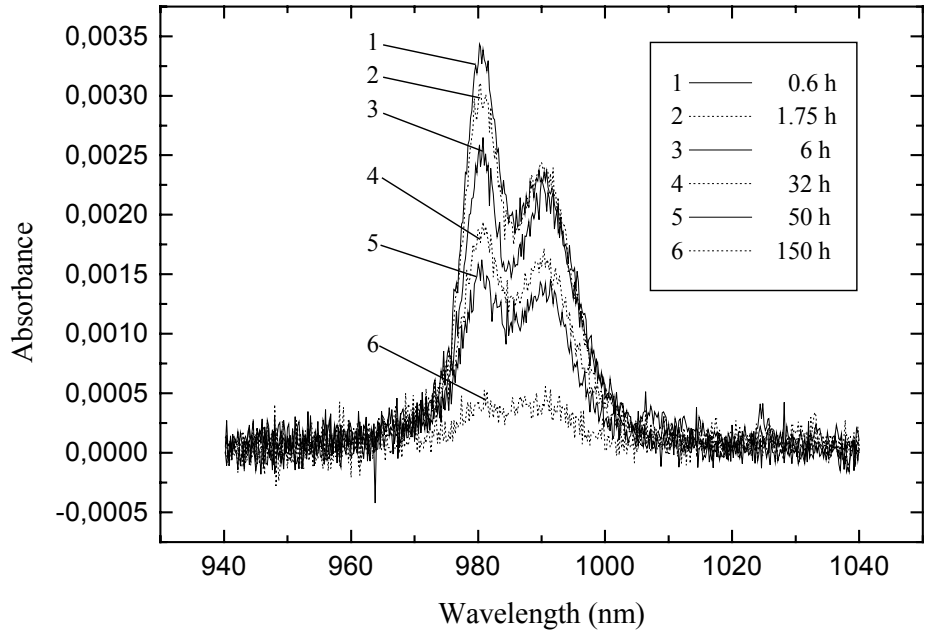

Figure 27: UV-VIS-spectra of the input solution 6 as a function of the equilibration time; 980 nm NpO_2^+, 989 nm Np(V)-carbonate and -humate species.

3.3 Uranium(VI)

In order to determine the best conditions to study the system Pu(VI)/HA as well as to test the experimental methods used for speciation at low metal-ion concentrations, experiments have been carried with the oxidation state analog U(VI), as a surrogate for Pu(VI).

Anion exchange

The complexation of U(VI) by HA has been investigated at pH 4 and 5 with the ionic strength I ranging from 0.004 mol/l to 0.1 mol/l, uranium concentrations from 2 x 10^{-8} mol/l to 5 x 10^{-6} mol/l and humic acid concentrations from 1 to 2.5 mg/l. In a first step, experiments have been carried out without HA in order to estimate the quantity of free U(VI) adsorbed on the exchange resin under the experimental conditions of this work.

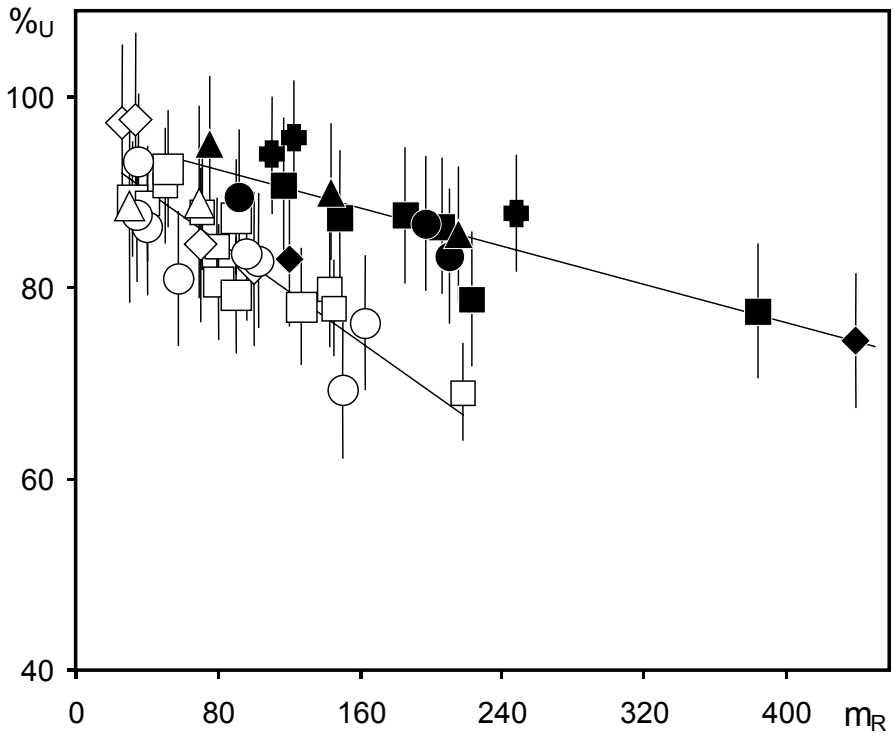

Figure 28: Percentage of free U(VI) in solution (without HA) after mixing with various amounts of resin (in mg) at pH 5 in 0.1 (open symbols) and 4 x 10^{-3} mol/l (full symbols) $NaClO_4$. $C_{U(VI)}$ = 3.2 (cross), 2.8 (open square), 1.5 (full square), 1 (open diamond), 0.11 (full triangle), 0.05 (full circle), 0.04 (open circle), 0.03 (full diamond), and 0.015 µmol/l (open triangle).

At pH 4, adsorption of U(VI) can be neglected for amounts of exchanger material below 150 mg. On the other hand, at pH 5, the adsorption must be taken into accounts illustrated in Figure 28: while it is weak for $m_{Resin} < 40$ mg, with nearly 100 % of U(VI) in solution, it increases with the mass of the resin to reach, for $m_{Resin} = 200$ mg, values of nearly 30 % and 20 % for I = 0.1 and 0.004 mol/l, respectively.

According to the literature, this adsorption can be explained by the presence of impurities on the exchange resin which behave as cationic exchanger sites [Hir89]. In order to saturate these, the resin has been treated before use with Hf^{4+} ranging from 1 to 100 µmol/l. The results show no significant difference with respect to the data obtained with the non-treated exchange resin, indicating that this explanation is not valid in this system. Most probably, this adsorption is related to the presence of hydrolysis species, more important at pH 5 than at pH 4, which are known to sorb on inactive organic material.

It is also observed that the decrease of U(VI) in solution varies linearly with the amount of resin m_R and that it is nearly independent of the U(VI) concentration. Based on these observations, the effect can be described, in the range of U(VI) concentration and mass of resin investigated, by linear relationships (solid lines in Figure 28). These relations have been used for the correction of complexation data for adsorption, as described in the following.

The experimental data are described by linear relationships of the general form $\%_{U(VI)} = a \cdot m_{Resin} + b$, with $a = -0.130 \pm 0.002$ and $b = 95 \pm 3$ for I = 0.1 mol/l and $a = -0.051 \pm 0.009$ and $b = 96 \pm 3$ for $I = 4 \times 10^{-3}$ mol/l.

The results obtained at pH 4 are presented in Figure 29. The K_d values are not significantly affected by the change of ionic strength, indicating a low ionic strength effect on the equilibrium U(VI)/HA.

At pH 5, the K_d values can be corrected for the adsorption of the free cation on the resin by the following expressions:

$$[UHA] = [U(VI)]_R - [U(VI)]_{ads}$$

$$[U(VI)] = [U(VI)]_s + [U(VI)]_{ads},$$

with $[U(VI)]_R$, $[U(VI)]_s$, and $[U(V)]_{ads}$ corresponding to the amount of U(VI) fixed on the resin, measured in solution and adsorbed on the resin, respectively. The two first concentrations are determined experimentally, whereas the last one is calculated according to

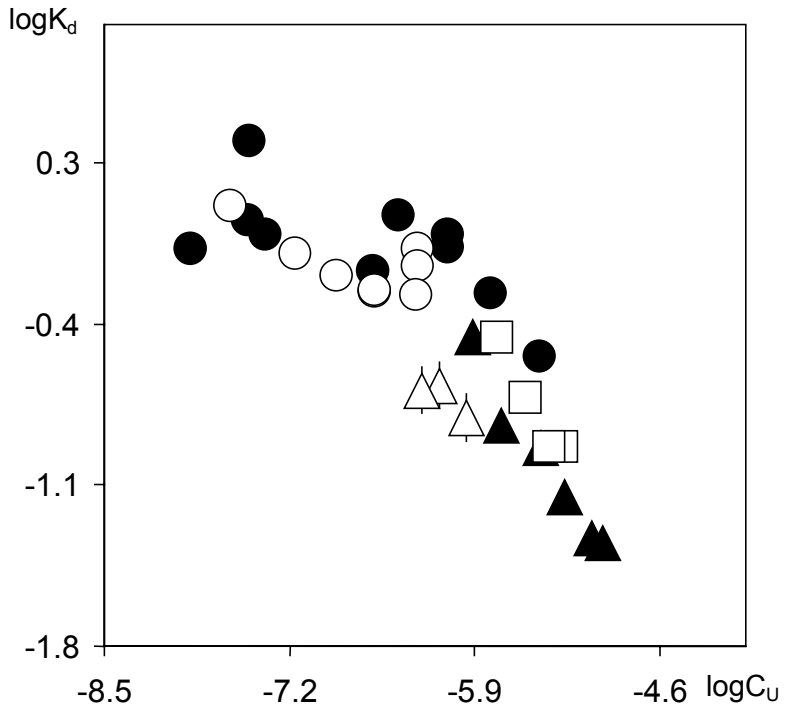

Figure 29: Humate complexation of U(VI) studied by AIX at pH 4 in 0.1 mol/l (full symbols) and 0.004 mol/l $NaClO_4$ (open symbols) with [HA] = 2.5 (circles), 1.5 (squares) and 1 mg/l (triangles). Effect of metal-ion concentration on K_d values.

the relation derived from adsorption experiments (see Figure 28). Note that this correction is valid only if the composition of the free U(VI) in solution (UO_2^{2+} and hydrolysis species) in the presence of HA is not significantly affected as compared to that for a similar uranium solution (same pH and free U(VI) concentration) without complexing agent. Calculations, using the data derived from the charge neutralization model (see below), show that this is true under the experimental conditions of this work.

The K_d values corrected in this way have to be independent of the U(VI) adsorption, and thus of the amount of resin used for the experiment.

This experiment has been repeated for other U(VI) concentrations from which mean K_d values were deduced. They are displayed in Figure 30 as a function of the nominal U(VI) concentration, the errors correspond to the standard deviations.

The experimental data at I = 0.004 mol/l are measured in the presence of 0.05 mol/l MES to reproduce the EIF experimental conditions (see experimental section). The good agreement between these values and those obtained at I = 0.1 mol/l without MES shows that neither ionic strength nor the buffer affects significantly the equilibrium U(VI)/HA. Moreover, it is observed that the K_d values are close to those measured at pH 4 (circles in dotted line)

whereas the complexation ability of HA towards metal-ions is known to increase with the deprotonation of HA binding sites and thus with the pH [Cho85], [Cho88]. This can be explained by a weak competition between the formation of the hydrolysis species and the humate complex which increases when the pH increases.

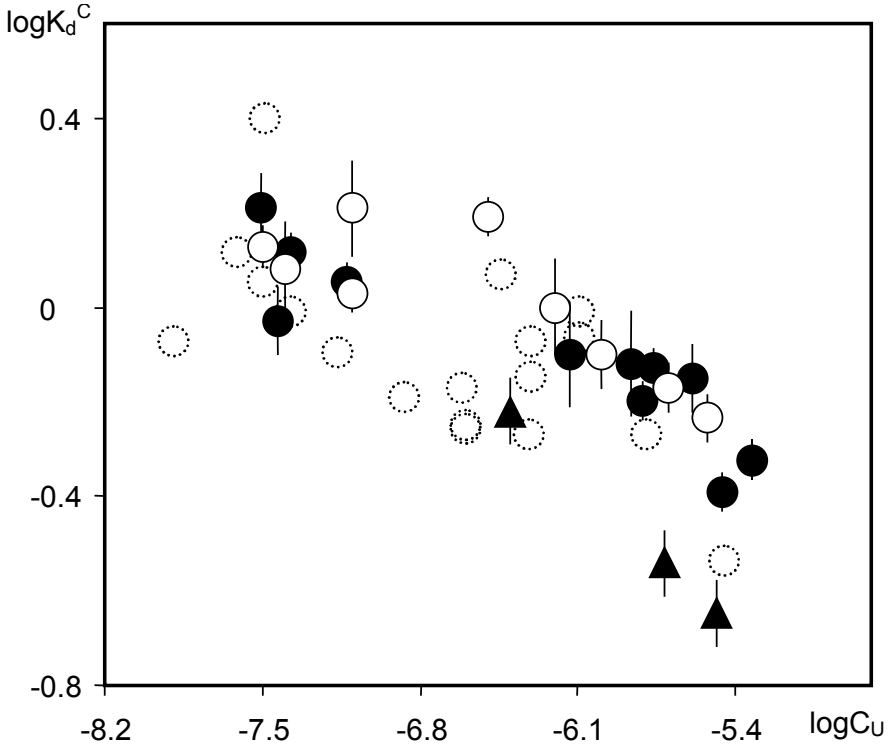

Figure 30: Humate complexation of U(VI) measured by AIX at pH 5 for 0.1 mol/l $NaClO_4$ (full symbols) and 0.004 mol/l $NaClO_4$ (open symbols) with [HA] = 2.5 (circles) and 1.25 mg/l (triangles). Effect of metal-ion concentration on K_d values and comparison with data obtained at pH 4 for [HA] = 2.5 mg/l (circles in dotted line).

Continuous Electrophoretic Ion Focusing

In order to compare this separation technique with the AIX experiments, experiments have been performed at pH 5 in the same range of U(VI) concentrations as that explored by AIX. The K_d values obtained are shown in Figure 31 (open symbols) together with those measured by AIX (full symbols).

While there is a good agreement between both separation methods for U(VI) concentrations above 10^{-6} mol/l, this is no longer the case when the concentration decreases. Indeed, below 10^{-6} mol/l, the apparent K_d values measured by EIF increase with respect to those measured by AIX to become nearly 40 times higher for the lowest U(VI) concentrations studied.

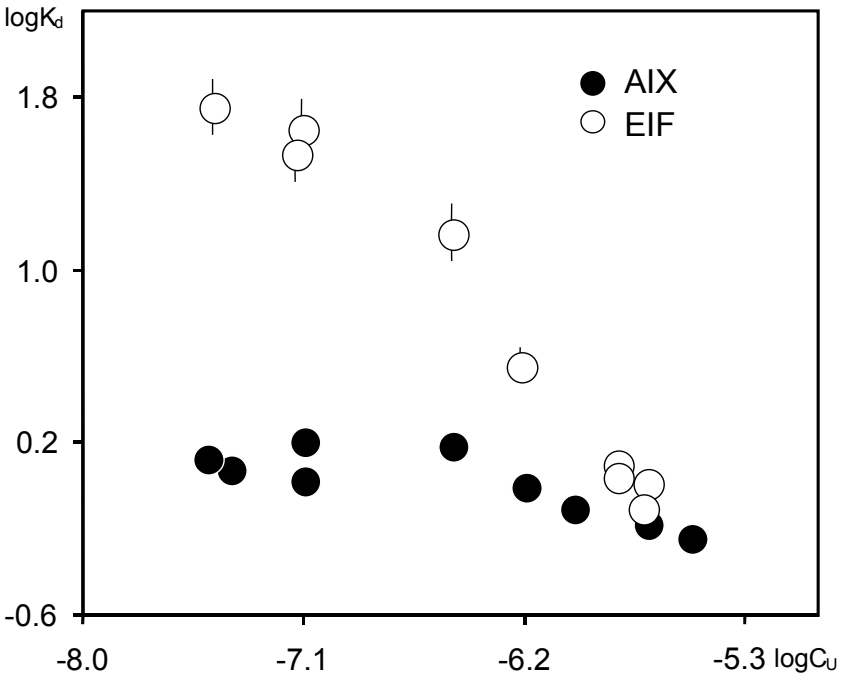

Figure 31: Humate complexation of U(VI) studied by EIF (open circle) and AIX (full circle) at pH 5 in 0.001 mol/l $NaClO_4$ and 0.05 mol/l MES with [HA] = 2.5 mg/l. Effect of metal-ion concentration on K_d values.

Experiments carried out in the absence of HA showed that all U(VI) was recovered at the cathode. This indicates that an additional interaction U(VI):HA, in addition to the complexation evidenced by batch experiments, occurs in the separation chamber.

In order to confirm this, an experiment was carried out by introducing into the chamber, instead of a mixed solution U(VI)/HA, two solutions of free HA and free U(VI) through capillaries 7 and 6, respectively. In this system, the complexation is expected to be negligible since (i) the time of contact between both species in the upper part of the chamber is very short (below 2 min) and (ii) the mixing between U(VI) and HA, based on the migration of both species, is poor. In any case, the fraction of U(VI) complexed, according to the known K_d values obtained by AIX, was expected not exceed about 30 %.

However, the results obtained showed that 81 % and 67 % of U(VI) was complexed for nominal metal-ion concentrations of 6 x 10^{-8} and 10^{-6} mol/l, respectively, and thus confirm the occurrence of an interfering interaction U(VI)/HA in the electrophoresis chamber in the course of the separation of both species. The effect expected not to be significant for $C_U \geq 10^{-6}$ mol/l, according to the results of Figure 31, appears important. This indicates that the efficiency of this additional interaction increases when the contact time between U(VI) and HA increases in the separation chamber; the analyte solution in the first experiments was introduced through 1 capillary whereas in the second experiment, two capillaries were used.

To confirm this contact-time dependence, a third experiment was carried out for $C_U = 2.10^{-6}$ mol/l in the system 2(E):2(A):3(M):2(A):2(E), for which 3 capillaries were used to feed the mixed solution. In agreement with the assumption made above, a K_d value three times higher than that measured in the system 3(E):2(A):1(M):2(A):3(E) was determined.

In conclusion, the evidence for this interference makes the EIF technique not well suited for investigations of the system U(VI)/HA below 10^{-6} mol/l U(VI).

Quantitative Treatment of the Experimental Data

When $[UO_2^{2+}]_{free}$ is known and varied, LC is conventionally determined graphically by a slope analysis of the experimental data [Kim96]. In this study, hydrolysis species are present and only the total concentration of the free U(VI) is known. Therefore, this method cannot be applied and a new approach for the evaluation of LC values has been examined requiring a series of experimental data i, represented by the K_d^i values, measured at fixed pH and ionic strength for various nominal U(VI) concentrations, C_u^i.

In a first step, the stability constant β is fixed arbitrarily and the LC^i values are calculated and plotted as a function of log C_U^i. The curve obtained is fitted by a straight line and its slope $a(\beta)$ is associated with the couple of values β and $LC(\beta)$; $LC(\beta)$ corresponding to the mean LC value calculated from LC^i. What we know, is that the LC values are independent of the U(VI) concentration under the experimental conditions of this study, C_U^i being much lower than the ionic strength. Therefore, in a second step, β is varied and the value of $LC(\beta)$ retained is that for which $a(\beta)$ tends to 0.

The method has been first applied to complexation data measured with Np(V) at pH 7 and 8, for which no hydrolysis species are expected in solution [Mar98]. The LC values determined in this way correspond within the errors to those obtained by the common graphical method, indicating the validity of the approach. A good agreement between both methods is also observed with data obtained for U(VI) at pH 4, where the hydrolysis species can be neglected [Cze94]. The method has been finally applied to the U(VI) complexation data at pH 5, leading to LC values nearly 1.7 higher than those estimated at pH 4. All the results of the calculation are presented in Table 8.

The LC values obtained at pH 4 and 5 appear to be nearly independent of the ionic strength. There are indications of a slight decrease of the amount of available sites for U(VI) complexation when ionic strength decreases. This variation is not consistent with that currently observed with soluble polyelectrolytes; due to HA configuration change, the surface

binding on the polyanion at fixed pH is expected to be more important when the ionic strength decreases [Kre97], [Cze96]. For instance, Czerwinski et al. [Cze96] have shown that measured LC of Am^{3+} with GoHy-573 humic acid at pH 6 varied with ionic strength according to the equation $LC = -0.126\sqrt{I} + 0.683$. It remains however for U(VI) as well as for Am(III), that the ionic strength effect remains weak in the range studied here and does not affect significantly the values of the stability constants.

Table 8: Determination of the loading capacities of Np(V) and U(VI) under the experimental conditions of this work and comparison of LC values estimated with the "new" approach and that currently used with complexation data of the system Np(V)/HA [Mar98].

	pH - I	LC (β)	LC
Np(V)	7 - 0.1	0.13 ± 0.02 (3.51-3.53)	0.13 ± 0.01
	8 - 0.1	0.21 ± 0.05 (3.65-6.66)	0.22 ± 0.015
U(VI)	4 - 0.1	0.20 ± 0.05 (6.06-6.10)	0.19 ± 0.01
	4 - 0.004	0.17 ± 0.04 (5.95-5.99)	0.18 ± 0.02
	5 - 0.1	0.34 ± 0.05 (6.04-6.05)	_
	5 - 0.004	0.31 ± 0.04 (6.15-6.17)	_

The latter, calculated for each experimental point i, are displayed in Figure 32. The resulting complexation constant log β_{LC} = 6.08 ± 0.15 is in very good agreement with that determined by other speciation methods [Cze94], [Pom98] and appears to be invariant of the experimental conditions and in particular of the uranyl concentration. Furthermore, this result shows that the formation of hydrolysis species, as reported by Zeh et al. [Zeh97], is not significant under these experimental conditions.

It is believed that the experimental method explored here for the measurement of log β_{LC} for the humate complexation of U(VI) could be equally applied to the oxidation state analog Pu(VI).

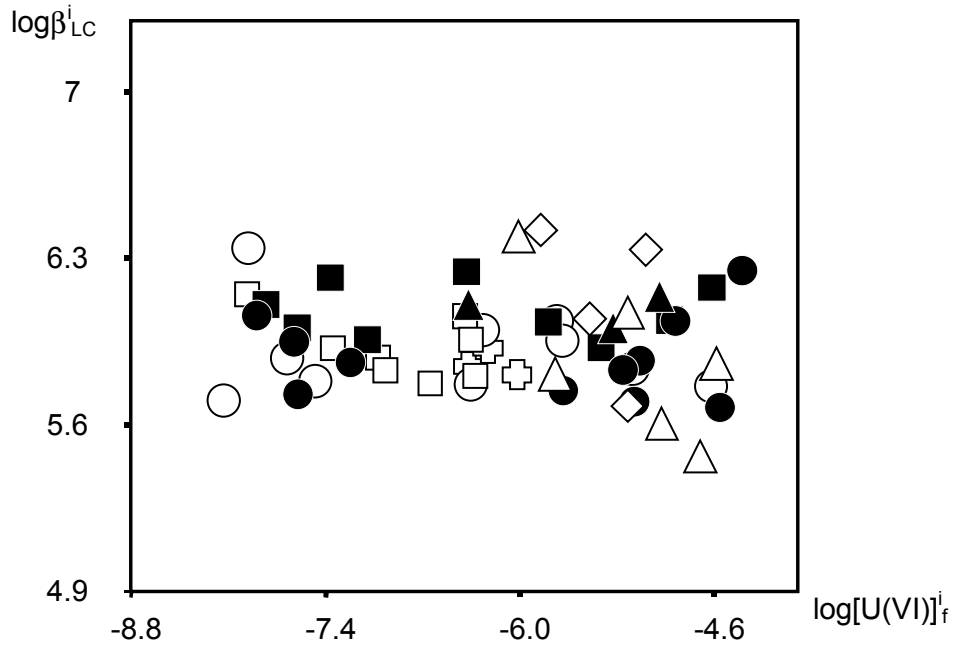

Figure 32: Humate complexation (Aldrich humic acid) of U(VI) studied by AIX. log β_{LC} values calculated and plotted as a function of the logarithm of the free U(VI) concentration in solution. pH 4 (open symbols); I = 0.1 mol/l: [HA] = 2.5 (circles) and 1 mg/l (triangles). I = 0.004 mol/l: [HA] = 2.5 (squares), 1.5 (diamonds) and 1 mg/L (crosses). pH 5 (full symbols); I = 0.1 mol/l: [HA] = 2.5 (circles) and 1.25 mg/l (triangles). I = 0.004 mol/l: [HA] = 2.5 mg/l (squares).

3.4 Plutonium(VI)

The experiments carried out with U(VI) concern the evaluation of the best experimental conditions for the investigation of the system Pu(VI)/HA. In analogy to U(VI), the complexation of Pu(VI) with humic acid should be studied with anion exchange. Therefore, a stock solution of Pu(VI) which contains no other oxidation states is required. The standard potentials are shown in Figure 33.

The hexavalent oxidation state of Pu has to be stabilized in the presence of humic acid by an oxidizing agent because plutonium may occur in different oxidation states (III, IV, V, VI). For this purpose, Ag^{2+} has been chosen since it is a strong oxidizing agent and it is expected that a divalent ion does not interact strongly with humic substances and thus would not interfere with the reaction Pu(VI)/HA. This could be confirmed in experiments with the system U(VI)/ HA and is illustrated in Figure 34. The presence of Ag^{2+}, up to concentrations of 10^{-3} mol/l, does not affect significantly the complexation equilibrium U(VI)/HA at pH 4 in 0.1 mol/l $NaClO_4$. Another possibility, which could prevent the reduction of Pu(VI) in humic acid solution, is to limit the contact time between Pu(VI) and HA. A kinetic experiment performed with U(VI) showed that the complexation equilibrium was reached within less than 30 min.

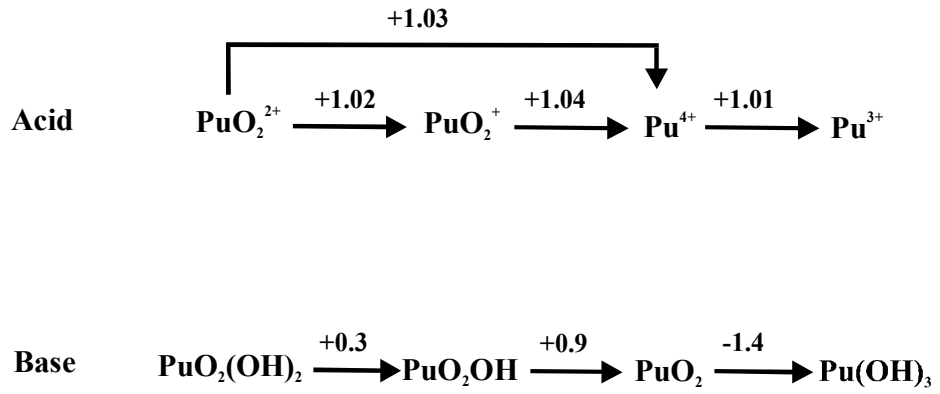

Figure 33: Standard reduction potentials (volts vs. standard hydrogen electrode) of plutonium in acidic (pH 0) and basic (pH 14) aqueous solution [Kat86].

Based on the results, the time of contact between Pu(VI) and HA will be first of all fixed to 30 min.

The preparation of Pu(VI) by fuming the stock solution (containing plutonium polymers) several times with $HClO_4$ has failed. But the preparation is possible by an electrochemical method. After fuming the stock solution with H_2SO_4 which destroys the polymer species, the plutonium was dissolved in 1 mol/l $HClO_4$ and anodically oxidized at 1.50 V over twelve hours [Geh86], [Coh61], [Neb61]. The oxidation state is checked by liquid/liquid extraction with TTA [Ber82].

The determination of plutonium is done by beta-delayed neutron-counting (BDNC) after neutron-induced fission of the isotope ^{239}Pu [Rud77] or liquid-scintillation-counting (LSC). The BDNC has a detection limit of 6×10^{11} atoms (3σ) and is independent on the matrix. The plutonium was irradiated at the Mainz TRIGA-Reactor at a flux of 1.7×10^{12} n /s cm^2 for two minutes and the counting time was one minute. Twelve concentrically arranged ^3He-tubes embedded in paraffin were used as neutron detector.

The detection limit of LSC is 4×10^9 atoms (3σ) for a counting time of 24 hours for ^{239}Pu. The LSC is dependent on the matrix, especially colour quenching by humic acid must be considered.

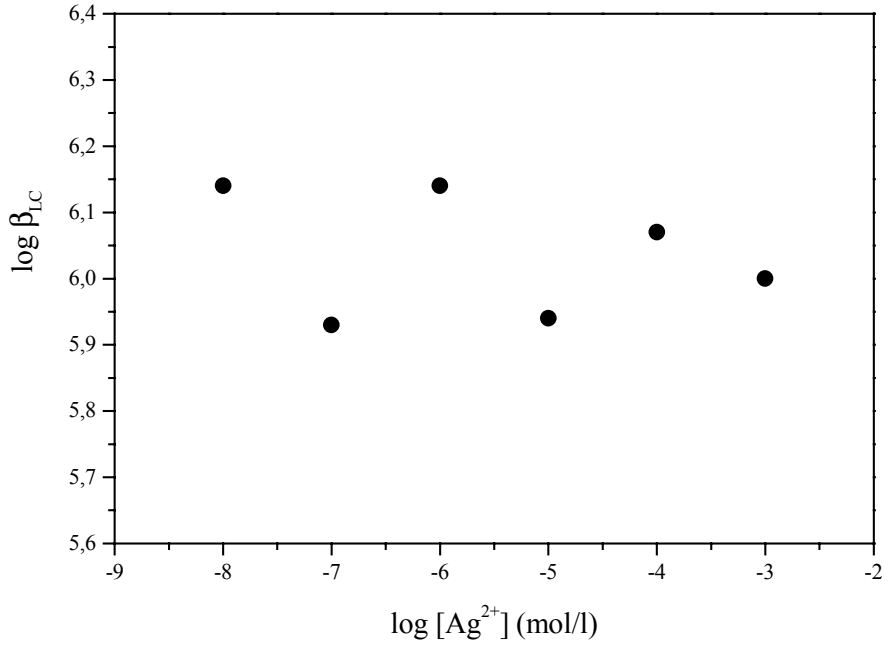

Figure 34: Humate complexation of U(VI) by AIX at pH 4 and ionic strength of 0.1 mol/l in the presence of Ag^{2+} at various concentrations.

4. Conclusions

Trivalent Actinides and Lanthanides

The log β_{LC}-value for trivalent metal-ions and Aldrich humic acid determined with cation exchange is too low (2.73 ± 0.44) because the cation exchange resin intervenes in the metal-ion humic acid complexation equilibrium. Small amounts of the free cation are adsorbed on an anion exchange resin and the log $\beta_{LC,Sm}$-value is 6.40 ± 0.30.

The original electrophoretic chamber showed strong adsorption of the humic acid complex and the free cation on different surfaces. The log β_{α}-value was determined to 7.21 ± 0.58. The artificial humic acid M1 has a similar complexation behaviour under these conditions. After a modification of the electropheric apparatus the adsorption was minimized and the yields of recovery were around 100 %. In spite of pH-correction the log $\beta_{LC,An(III)}$-values depend on pH (7.99 ± 0.16 at pH 5, 9.04 ± 0.11 at pH 6, 9.69 ± 0.06 at pH 7). The yields of recovery at very low metal-ion concentrations and in the absence of humic acid are only about 20 % and are dependent on pH. This explains qualitatively the too high pH dependent log β_{LC}-values. Thus, continuous electrophoretic ion focusing is not suitable for trivalent cations at metal-ion concentrations below 10^{-6} mol/l.

Direct speciation measurements with the TRLFS give log β_{LC}-values of 6.54 ± 0.10 (pH 5) and 6.52 ± 0.10 (pH 6) for Aldrich humic acid and Cm^{3+}.

Neptunium(V)

For the NpO_2^+-ion, an adsorption, as observed for the trivalent actinides in the electophoretic chamber, is negligible. The calculated log β_{LC}-values are independent of the pH but vary with the metal-ion concentration. The examination of this dependency with UV-VIS-spectroscopy in the concentration range between 10^{-5} and 10^{-4} mol/l $[NpO_2^+]_{total}$ and the use of the electrophoretic technique shows that there is a discrepancy between the results obtained with the two different methods. The data obtained with UV-VIS-spectroscopy leed to log β_{LC}-values of 4.4(3) (EIF: log β_{LC} = 3.0(2)) which are confirmed by anion exchange and ultrafiltration experiments. The change of the log β_{LC} = 4.4 at 10^{-5} to 10^{-4} mol/l $[NpO_2^+]_{total}$ to log β_{LC} > 5 below 10^{-8} mol/l is unexplained at this time.

On the other hand, below 10^{-8} mol/l, similar experiments (EIF, AIX and UF) give consistent log β_{LC}-values > 5 for the very low neptunium concentrations.

In column experiments with NpO_2^+ under the natural conditions of the Gorleben aquifer, a mean retardation factor R_f < 1 is obtained, which implements that the eluted neptunium migrates faster than water (HTO). Analysis of the input solutions and the eluates by ultrafiltration shows that in the eluate, the recovered neptunium is bound to the humic colloids. So the migrating species is the colloid bound neptunium which moves faster than water because of size exclusion effects. The experiments also show that there is no significant dependence of the total recovery of the neptunium on the neptunium concentration. However, the total recovery is strongly dependent on the reaction time. With increasing reaction time before the injection of the analyte solution onto the column (1 or 2 hours to 8 days) the recovery increases from 10 % to 85 %. This is due to a reduction of Np(V) to Np(IV) that could be observed by UV-VIS-spectroscopy and by separation of the oxidation states with liquid-liquid-extraction combined with radiometry.

Uranium(VI)

Batch experiments with U(VI) and an anion exchange resin were performed at pH 4 and 5. Some uranium is adsorbed on the resin in the absence of humic acid at pH 5. The decrease of U(VI) in solution varies linearly with the amount of resin and is nearly independent of the U(VI) concentration. This relation was used for the correction of the complexation data. The K_d- values are not significantly affected by the ionic strength. EIF-experiments carried out in the absence of humic acid showed that there is no adsorption of the uranium in the electrophoretic chamber. With humic acid, there is a good agreement between both separation

methods (AIX and EIF) for uranium concentrations above 10^{-6} mol/l but with decreasing uranium concentration the log K_d –values from EIF are increasing with respect to those measured by AIX. There is evidence of an interference of the electric field in the electrophoresis chamber on the interaction of uranium and humic acid which makes the EIF-technique unsuitable for investigations of this system at low metal-ion concentrations. The loading capacity can be determined graphically when $[UO_2^{2+}]_{free}$ is known. In our AIX-experiments hydrolysis species may be present and only the total concentration of uranium in solution was measured. The validity of a new approach for the evaluation of LC-values was shown. The method was applied to the uranium complexation data for pH 5 leading to LC-values of 0.34 (I = 0.1 mol/l) and 0.31 (I = 0.004 mol/l). With these loading capacities, the log β_{LC}-value was determined as 6.08 ± 0.15 which is in good agreement with literature data.

Plutonium(VI)

Concerning Pu, experimental conditions to study the System Pu(VI)/HA have been deduced from the results obtained with U(VI). However, due to problems encountered with the preparation of Pu(VI), no complexation data could be obtained thus far for low metal-ion concentrations by indirect speciation methods.

For ultratrace analysis of plutonium, a pulsed laser system in combination with a time-of-flight (TOF) mass spectrometer was installed. A commercially available Nd:YAG laser (Clark-MXR ORC-1000) is used to simultaneously pump three titanium-sapphire (Ti:Sa) lasers. Starting from a sample containing 3.25 x 10^{11} atoms of ^{239}Pu, a total number of 2.6 x 10^6 ions of $^{239}Pu^+$ have been detected during a measuring time of 2.5 hours. Thus, an overall efficiency of ε = 8.0 x 10^{-6} is obtained. Taking the background into account, a detection limit of approximately 1 x 10^7 atoms of plutonium was obtained at a confidence level of 99.7 % (3σ).

5. Literature

Art98 R. Artinger, B. Kienzler, W. Schüßler, J.I. Kim, J. Contam. Hydrol. **35**(1-3): 261 – 275 (1998)

ArtPers.Com. R. Artinger, personal communication, 1999

Ber82 P.A. Bertrand, G.R. Choppin, Radiochim. Acta **31**, 135-137 (1982)

Cho85 G.R. Choppin, Complexes of Actinides with Naturally Occurring Organic Compounds, in: *Handbook of the Physics and Chemistry of the Actinides*, Vol. 3, eds. A.J. Freeman and C. Keller, Elsevier Sci. Publ. Chap. 11 (1985)

Cho88 G.R. Choppin, Radiochim. Acta **44/45**, 23 (1988)

Coh61 D. Cohen, J. Inorg. Nucl. Chem., Vol. **18**, 207-210, 1961

Cze94 K.R. Czerwinski, G. Buckau, J.I. Kim, Radiochim. Acta **65**, 111 (1994)

Cze96 K.R. Czerwinski, J.I. Kim, D.S. Rhee, G. Buckau, Radiochim. Acta **72**, 179-187 (1996)

End38 C. Enders, K. Theis, Die Melanoidine und ihre Beziehung zu den Huminstoffen, Brennstoff-Chemie **19**, 360 (1938)

Fra97 C. Franz, G. Herrmann, N. Trautmann, Radiochim. Acta **77**, 177-181 (1997)

Geh86 H. Gehmecker, G. Herrmann, N. Trautmann, Radiochim. Acta **40**, 81-86 (1986)

Hir89 M. Hiraide, Kontakte (Darmstadt) **3**, 37 (1989)

Kat86 J.J. Katz, G.T. Seaborg, L.R. Morss, The Chemistry of the Actinide Elements, 2nd ed., Vol. 2, Chapman and Hall, New York 1986, 1133-1146

Kim88 J.I. Kim, G. Buckau, Report RCM 02188, Institut für Radiochemie der TU München, 1988

Kim89 J.I. Kim, G. Buckau, E. Bryant, R. Klenze, Radiochim. Acta **48**, 135-143 (1989)

Kim91 J.I. Kim, H. Wimmer, R. Klenze, Radiochim. Acta **54**, 35-41 (1991)

Kim93 J.I. Kim, D.S. Rhee, H. Wimmer, G. Buckau, R. Klenze, Radiochim. Acta **62**, 35-43 (1993)

Kim96 J.I. Kim, K.R. Czerwinski, Radiochim. Acta **73**, 5-10 (1996)

Kle91 R. Klenze, J.I. Kim, H. Wimmer, Radiochim. Acta **52/53**, 97-103 (1991)

Kre97 R. Kretzschmar, D. Hesterberg, H. Sticher, Soil. Sci. Soc. Am. J. **61**, 101 (1997)

Mar96 C. Marquardt, G. Herrmann, N. Trautmann, Radiochim. Acta **73**, 119-125 (1996)

Mar98 C. Marquardt, J.I. Kim, Radiochim. Acta **80**, 129-137 (1998)

MarPers.Com. C. Marquardt, personal communication, 1998, to be published

Mou92 V. Moulin, J. Tits, Radiochim. Acta **58/59**, 121-128 (1992)

Neb61 D. Nebel, E. Nebel, Kernenergie, 4. Jahrgang, Heft **1/61**, 15-18, 1961

Pan96 P. Panak, R. Klenze, J.I. Kim,Radiochim. Acta **74**, 141-146 (1996)

Pom96 S. Pompe, M. Bubner, M.A. Denecke, T. Reich, A. Brachmann, G. Geipel, R. Nicolai, K.H. Heise, H. Nitsche, Radiochim. Acta **74**, 135-140 (1996)

Pom98 S. Pompe, A. Brachmann, M. Bubner, G. Geipel, K.H. Heise, G. Bernhard, H. Nitsche, Radiochim. Acta **82**, 89 (1998)

PomPers.Com. S. Pompe, personal communication, 1996

Rao95 L. Rao, G.R Choppin, Radiochim. Acta **69**, 87 (1984)

Rud77 W. Rudolph, K.L. Kratz, G. Herrmann, J. Inorg. Nucl. Chem. **39**, 753 (1977)

Sek91 J.I. Kim, T. Sekine, Radiochim. Acta **55**, 187 (1991)

Tor84 R.A. Torres, G.R. Choppin, Radiochim. Acta **35**, 143-148 (1984)

Wag89 H. Wagner, R. Kuhn, S. Hoffstetter, Praxis der präparativen Free-Flow-Elektrophorese, in: *Praxis der elektrophoretischen Trennmethoden*, 223 - 285, H. Wagner, E. Blasius (Editors), Springer Verlag, 1989

Zeh97 P. Zeh, K.R. Czerwinski, J.I. Kim, Radiochim. Acta **76**, 37 (1997)

Zie80 H. Ziechmann, *Huminstoffe*, Verlag Chemie, Weinheim, 1980

Appendix 2

Characterization and Fractionation of Humic Acid and Determination of Complex-Formation Constants with Toxic Heavy Metals

H.P. Beck, U. Keuth, H. Schank, H. Wagner

Institut für anorganische und analytische Chemie und Radiochemie,
Universität des Saarlandes, Saarbrücken

Content

Abstract

The humic acid applied was characterized using chromatographic and electrophoretic methods. Size exclusion chromatography (SEC) allowed a size distribution to be obtained for the Aldrich humic acid. In the chromatogram, two components could be noticed, a higher-molecular humic acid fraction with molecule sizes of about 150000 D and the main fraction with molecule sizes of about 3000 D. Capillary zone electrophoresis (CZE) yielded a mass/charge distribution using conventional basic electrolytes. By means of a borate buffer and the addition of hydroxycarboxylic acids, a differentiated separation was obtained. The reason was assumed to be the esterification of individual humic acid constituents. Characterization of metal humate complexes by CZE showed that loading with metal cations had significant effects on the mobility distribution of the humates. Differentiation into strongly and less strongly charged species took place. By micellar electrokinetic chromatography (MEKC), the influence of the metal ion load on the hydrophily of the humic acid constituents was illustrated. A coordination of the heavy metal cations by the different functional groups of the humic acid caused the hydrophily to decrease.

Fractionation of Aldrich humic acid by free flow electrophoresis and ultrafiltration allowed to obtain individual components for further investigations. From these studies, additional findings were obtained with regard to the composition and properties of the humic acid. When transferring the capillary electrophoresis (CE) of humic acid to free flow electrophoresis (FFE) by adding hydroxycarboxylic acids, both main fractions could be isolated. While studying the stability of the fractions, the dynamic character of the humic acid in alkaline solution could be noticed. Each fraction was separated into two signals again by means of CE. However, both signal pairs differed considerably in terms of migration time. After a residence time of 24 h, the migration times were the same again. Obviously, the molecules in the solution had been in an equilibrium state. Following fractionation, they tried to reach this state again, which was eventually achieved by molecular reorientation.

Aldrich humic acid was fractionated by means of ultrafiltration with various filter pore sizes being used. As the individual ultrafiltrates had about the same UV-Vis spectra, the humic acid concentration in the individual ultrafiltrates could be determined quantitatively. The size distribution obtained could be compared with the SEC results. Time-dependent investigation of the individual ultrafiltrates by SEC indicated a variation in the size of the fractions after

20 h. This suggested a dynamic character of the humic acids, as did the FFE. By free flow isotachophoresis (FF-ITP), metal humate complexes were subjected to fractionation. Determination of the metal contained in the individual fractions demonstrated that all fractions of the humic acid were able to coordinate metal cations. At pH 9, lead humate complexes of 1:1 in stoichiometry were observed. Mixed complexes of humic acid and other complexing agents, such as hydroxo ligands, might exist.

Using various analytical methods, the formation constants were determined on the basis of the charge neutrality model. In addition to ultrafiltration, field surge electrophoresis (FSE) and anodic stripping voltammetry were applied. The complex-formation constants (cf. Tab. A, Tab. B) obtained by ultrafiltration were higher by nearly an order of magnitude. This was explained by adsorption effects of heavy metal ions on separated humate complexes or humic acid on a membrane.

Tab. A: Comparison of the formation constants for lead-humate complexes at pH 5 and 6; I < 0.01 mol/l and I = 0.1 mol/l

	pH 5	**pH 6**
FSE	5.2 ± 0.1	5.6 ± 0.1
ASV	5.6 ± 0.1	-
UF **(I = 0.1)**	6.4 ± 0.2 (5.4 ± 0.1)	6.1 ± 0.2 (5.9 ± 0.2)

Tab. B: Comparison of the formation constants for cadmium-humate complexes at pH 5 and 6; I < 0.01 mol/l

	pH 5	**pH 6**
FSE	4.0 ± 0.1	4.1 ± 0.1
ASV	4.3 ± 0.1	-
UF	5.0 ± 0.1	5.6 ± 0.1

Tab. C: Formation constants for zinc-humate complexes at pH 5 and 6.

	pH 5	**pH 6**
FSE	3.9 ± 0.1	4.2 ± 0.1

With different metal cations being available at the same time, those cations which form complexes of highest thermodynamic stability with the humic acid ligands are preferred. Complexed cadmium ions are not exchanged completely even at a high alkaline-earth ion concentration. But also in humic acids loaded with calcium ions, not all calcium ions are replaced by the added cadmium ions. Only magnesium ions are completely exchanged for cadmium ions. Formation of pseudomicelles with part of the bound cations existing inside the agglomerate and, hence, escaping an exchange may be a possible explanation of these results.

For investigating defined solid phases, batch and column experiments were performed. In the selected concentration range, lead and cadmium ions exhibited the same adsorption behavior on sea-shore sand as the solid phase. Addition of humic acid resulted in less heavy metal ions being adsorbed on the sand. This effect was found to be stronger for lead ions than for cadmium, which was attributed to the varying complex-formation constants. A quantitative evaluation suggests that complexed heavy metal ions are adsorbed in addition to non-complexed ions. Taking into account the colloidal character of the humic acid, adsorption as a colloid on the sand surface is supposed to take place. In column experiments the eluted amount of heavy metals was found to increase with an increasing equilibration time of the heavy metal-humate solutions applied. Here, it is referred to complexed heavy metal ions which only make up a certain fraction of the entire amount of heavy metals. The dependence of the amount of eluted heavy metal on the equilibration time can be explained by the formation of pseudomicelles due to a changed configuration of the humic acid molecules, which is caused by complex formation. Furthermore, more lead than cadmium is observed to be subject to elution, which is explained by the variable complex-formation constants.

Under the given conditions, batch and column experiments with technetium having an oxidation degree of +7 on Gorleben sand using Gohy water (Gohy-532) did not reveal any significant adsorption on the solid phase, as was expected.

1. Introduction

The project performed focused on the characterization of humic acid and its separation into individual components. Particular attention was devoted to the dynamics of the humic acid system. The isolation of individual fractions of the humic acid was to provide information on larger components of the heterogeneous humic acid compound. Stability constants were determined for metal-humate complexes of Aldrich humic acid and the toxic heavy metals of lead and cadmium. In addition, the influence of humic acid on the adsorption of metal ions by defined solid phases was studied in batch and column experiments.

For the investigations, chromatographic, electrophoretic, and voltammetric methods were applied. By means of size exclusion chromatography (SEC), the size distributions of the humic acid macromolecules can be determined. In addition, ultrafiltration (UF) is applied for the fractionation of components of variable size. The fractions thus obtained are characterized by means of SEC. Capillary zone electrophoresis (CZE) is a method of high resolution and separation capacity. It allows to characterize the distribution of electrophoretic mobilities of humic acid. The conditions of CZE separations may be transferred to free flow electrophoresis (FFE), which allows a preparative isolation of individual constituents. Both methods are also employed to study the influence of metal cation complexation on the electrophoretic mobility of the humic acid. The formation constants are determined by voltammetric stripping processes, continuous ion focussing by FFE, and ultrafiltration.

The results serve to extend the data base required for modeling the transport processes of mobilized pollutants in certain geological formations. Modeling of humate complexation and transport processes allows predictions to be made with regard to possible environmental hazards caused by the release of pollutants. In this respect, information is needed on the reaction behavior between heavy metal ions and humic acid. For modeling, the complex stability constants of the metal-humate complexes are required.

2. Experimental

Chemicals and Radionuclides

For the experiments in the trace element range, suprapure chemicals produced by the Merck company were applied. All other experiments were performed using chemicals of analytical purity. In trace analysis, CE, and HPLC, water from a millli-Q plant was applied. In other cases, demineralized water was used.

Technetium-99: A stock solution of ammonium pertechnate was applied.

Humic Acid

Commercially available humic acid (sodium salt) was cleaned according to the instructions given by [Kim2]. In electrophoretic experiments, cleaned humic acid manufactured by the Fluka company was applied in addition to Aldrich humic acid. By means of potentiometry, the cleaned Aldrich humic acid was found to have a proton exchange capacity of 3.88 meq/g.

Size Exclusion Chromatography

Size exclusion chromatography (SEC) is a chromatographic method, by means of which the analyte molecules are separated as a function of their size. The elution volume depends on the pore size distribution in the stationary phase and on the molecular size of the molecules to be separated. Very large molecules may not be able to enter the pores and, hence, are eluted first. In contrast to this, very small molecules are eluted later, as they are able to penetrate into the pores.

A HPLC system supplied by the Beckman company (Beckman System GOLD), consisting of the Beckman autosampler 507, the Beckman programmable solvent module 126, the Beckman diode array detector module 168, and the software GOLD version v601 SCC 2.000, was applied. For size determination, a polymer-based SEC column provided by the Alltech company (Jordi-Gel DVB 10000 Å GBR, length 300 mm, i.d. 7.8 mm) was used. The standards employed for size determination consisted in polystyrene sulfonic acids (sodium salts) of variable sizes (3800 D, 16900 D, 46400 D, 123000 D, 356000 D, 800000 D) and were supplied by the Polymer Standards Service company (Mainz).

Capillary Electrophoresis

Capillary electrophoresis represents an analytical method, by means of which sample components are separated in an electric field. In the capillary zone electrophoresis (CZE) method used here, separation is based on the variable mobilities of the sample components. The setup of a capillary electrophoresis system is shown schematically in Fig. A.

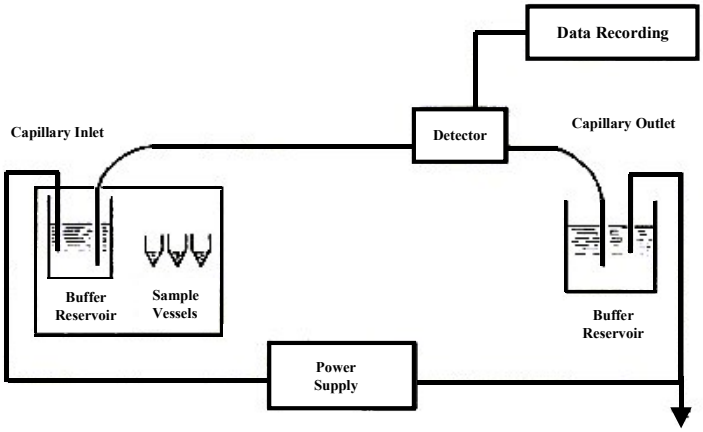

Fig. A: Schematic setup of the capillary electrophoresis system [Eng]

A quartz capillary (fused silica) with an internal diameter of 25 - 100 µm and a length of 20 - 100 cm is filled with a basic electrolyte and immersed into the buffer reservoirs at both ends. Between them, a voltage of up to about 30000 V is applied. The sample is injected hydrodynamically, i.e. by a pressure difference. The sample volume is in the nanoliter range. Detection is accomplished by means of a diode array detector. The advantages of CE consist in its high sharpness and efficiency of separation. This is caused by a plug-shaped flow profile in the capillary. Band broadening by a parabolic flow profile does not occur. The plug flow results from the electro-osmotic flow (EOF). The EOF is caused by the use of quartz capillaries. The silanol groups of the untreated quartz capillaries are deprotonated over wide pH ranges. Their negative charge is partially compensated by cations from the buffer solution. A diffuse layer with an excess of cations follows. The zeta potential is slowly reduced. The liquid column is charged positively towards the capillary wall and moved towards the cathode when a strong field is applied. Therefore, detection takes place near the cathodic end of the capillary. All uncharged constituents of the solution also move towards the cathode at the

speed of the EOF. Cations are accelerated, as the EOF adds up to their own migration speed. Slow anions are also transported to the cathode and led past the detector window. Their own migration towards the anode is overcompensated by the EOF. Only fast anions are able to move in opposite direction of the EOF. They move towards the anode at slow speed and, hence, escape cathodic detection. When analyzing fast anions, a pole reversal is required. Detection is then accomplished anodically. In addition, the EOF may be reversed. For this purpose, the silanol groups are loaded by cationic detergents. Thus, the liquid column in the capillary is charged negatively on the outer surface and moved towards the anode. Acceleration of the sample anions allows a more rapid analysis to be made.

The SZE separations were performed using a HP 3D CE station by Hewlett Packard GmbH, Waldbronn. Evaluation was accomplished using the pertinent software HP 3D CE Rev. A. 01.02 (version 1995).

Free Flow Electrophoresis

Free flow electrophoresis (FFE) is suited for electrophoretic separations on the preparative scale. The central unit consists of two plane-parallel plates. Between them, a thin liquid film is pumped (Fig. B). At the edges, two electrodes are inserted. The separated sample zones can be fractionated at the end of the separation gap. Hence, free flow electrophoresis can be used for all separations on the preparative scale. Depending on the separation problem, various processes may be implemented in the free flow setup. Their principles are already known from other electrophoresis setups. Analytical separations may be transferred from CE to FFE. The sample and the basic electrolyte have to be diluted accordingly in order to prevent high currents. Separation problems may hence be solved analytically by automated CE and handled on the preparative scale by FFE.

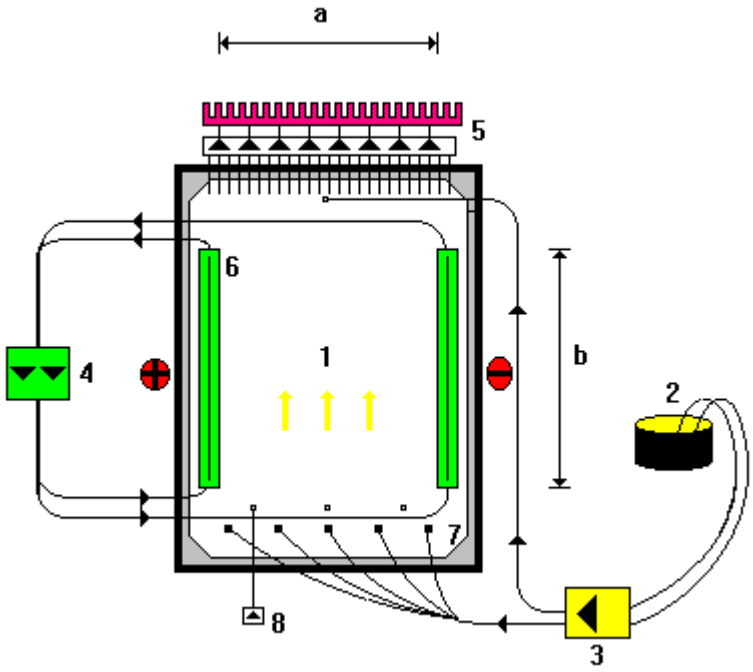

1: Separation gap, 2: Buffer reservoir, 3: Pump, 4: Electrode gap pump, 5: Fraction collector, 6: Electrode gap, 7: Spacer, 8: Sample pump

Fig. B: Schematic setup of the free flow electrophoresis system

It must be noted that the EOF does not play any major role in FFE as it does in the capillary. In contrast to the capillary, FFE represents a closed separation system. The EOF is not directed, but led in a cycle which does not contribute to the transport of the sample ions. Depending on the separation problem, various methods may be applied. Their principles are already known from other electrophoresis setups [Wag1].

The “Octopus” separation chamber by Dr. Weber GmbH, Munich, was applied.

Electrochemical Stripping Analysis

Electrochemical stripping analysis allows to determine heavy metals in the trace range (ng/l). The measuring cell consists of a PFE vessel, into which the solution to be analyzed is filled. A HMDE is used as the collector. Together with a platinum counter electrode and a silver/silver chloride electrode, it is integrated in an electrochemical measurement station designed by

EG&G Princeton Applied Research (SMDE model 303A). As potentiostat, the potentiostat/galvanostat M263A was available. The measurement system was controlled by a PC using the pertinent M270/250 research electrochemistry software, version 4.30 (1996), via an IEEE-488 interface.

Ultrafiltration

By means of ultrafiltration, the constituents of a solution can be separated due to their particle size. Molecules or ions which are smaller than the cut-off of the ultrafiltration membrane pass the latter and may, hence, be enriched in the ultrafiltrate. Ultrafiltration units for use in a centrifuge were supplied by the Pall Filtron company. Prior to use, the ultrafilters were rinsed several times with milli-Q water in order to remove the glycerol used by the manufacturer to prevent the membrane from drying out. For the characterization of Aldrich humic acid, ultrafilters with a cut-off ranging from 1000 D to 1000 kD were used. When determining complex-formation constants by ultrafiltration, ultrafilters with a cut-off of 1000 D were applied. This resulted in the humic acid molecules being retained nearly completely. Non-complexed metal ions, however, enter the ultrafiltrate.

Batch and Column Experiments

The solid phase used for the batch and column experiments with lead and cadmium was cleaned sea-shore sand supplied by the Merck company. For experiments with Tc-99, sand from Gorleben and water (Gohy 532) supplied by the INE, Karlsruhe Research Center, were available. In the batch experiments, a ratio of 10 ml liquid to 2.5 g sand was chosen. The filled PE vessels were shaken in a shaking machine for 24 h prior to each measurement. In the column experiments with lead and cadmium, a glass column (length 25 cm, i.d. 1 cm) was filled with cleaned sea-shore sand (Merck). For the technetium experiments, a column (length 25 cm, diameter 5 cm) constructed according to plans of the INE, Karlsruhe Research Center, was employed. Prior to the experiment, the columns had been subjected to conditioning with the eluent for several days. The setup used for the column experiments is shown in Fig. C. The eluent is pumped into a column filled with sea-shore sand using a hose pump. The solution is injected via an injection valve. The concentration of the eluted heavy metal and the bromide concentration are determined by direct coupling of the column outlet to an ICP-MS.

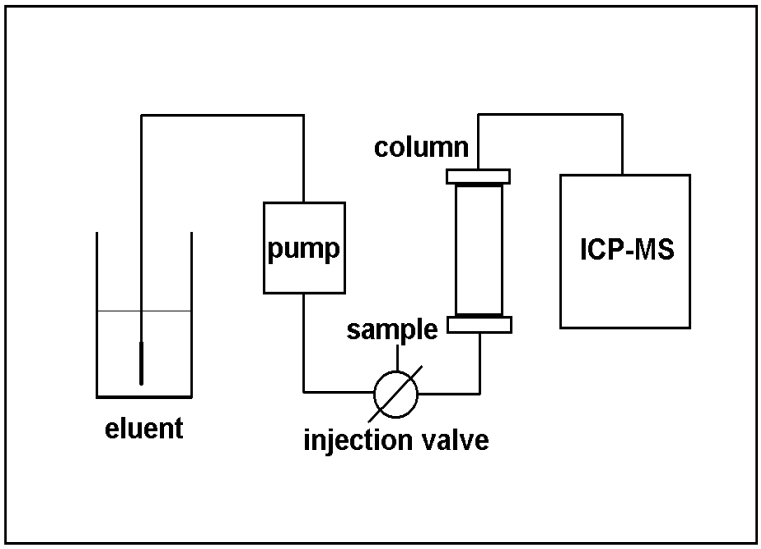

Fig. C: Experimental setup for the column experiments with Pb and Cd. Determination of Pb and Cd by ICP-MS at the column outlet

For the column experiments with technetium, an automatic fraction collector was applied downstream of the column instead of the ICP-MS. The individual fractions were analyzed using a liquid scintillation counter manufactured by Beckman (Beckmann scintillation system LS 6500).

Other Analytical Methods

In addition, other well-established analytical methods were applied, such as inductively coupled plasma emission spectroscopy (ICP-OES), graphite tube-atomic adsorption spectroscopy (GF-AAS) as well as flame-atomic adsorption spectroscopy (flame AAS).

3. Results and Discussion

3.1 Characterization of Humic Acids

A number of analytical methods are used for the characterization of humic acids (Fig. 1). The different properties of the humic acids represent various starting points for an investigation. The methods applied within the framework of this project are set off in Fig. 1.

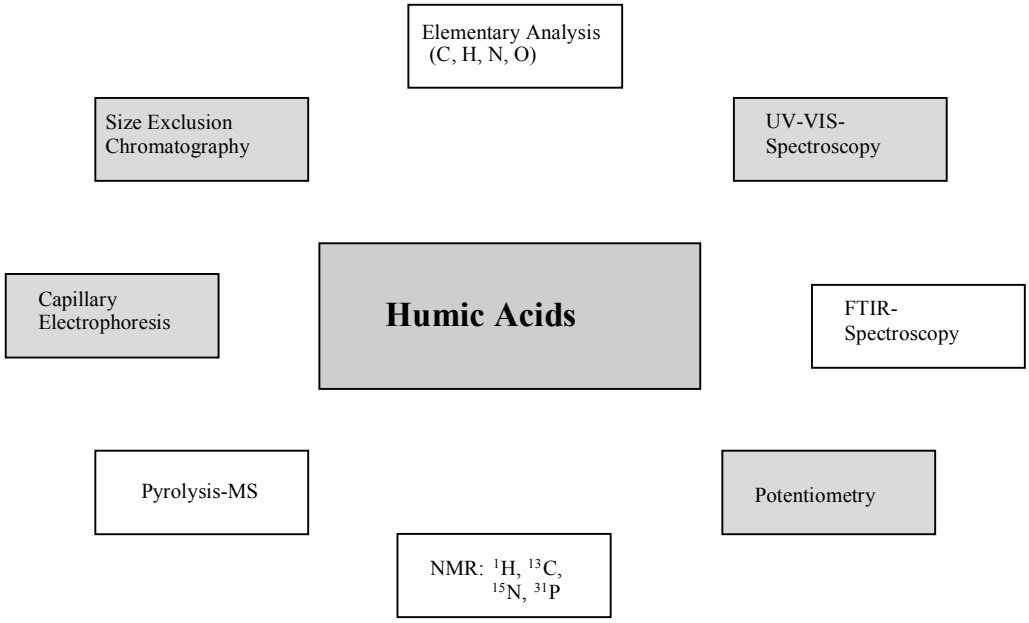

Fig. 1: Analytical methods for the characterization of humic acids

The complexing properties and the solution behavior of humic acids are influenced decisively by the particle size and charge distribution. Our investigations were mainly accomplished by size exclusion chromatography (SEC) and capillary electrophoresis (CE).

3.1.1 Size Exclusion Chromatography

When investigating humic acid, a size distribution is obtained. Within the framework of the project, all investigations have been performed with cleaned Aldrich humic acid. In the chromatogram, two peaks can be distinguished. One peak indicates higher-molecular humic acid fractions with molecule sizes of about 150000 D at the peak maximum. The second peak at a longer retention time refers to smaller molecule sizes of about 3000 D ± 500 D at the peak maximum (main component). The divinyl benzene-based SEC column was calibrated using polystyrene sulfonic acid standards with a size ranging from 3800 D to 800000 D.

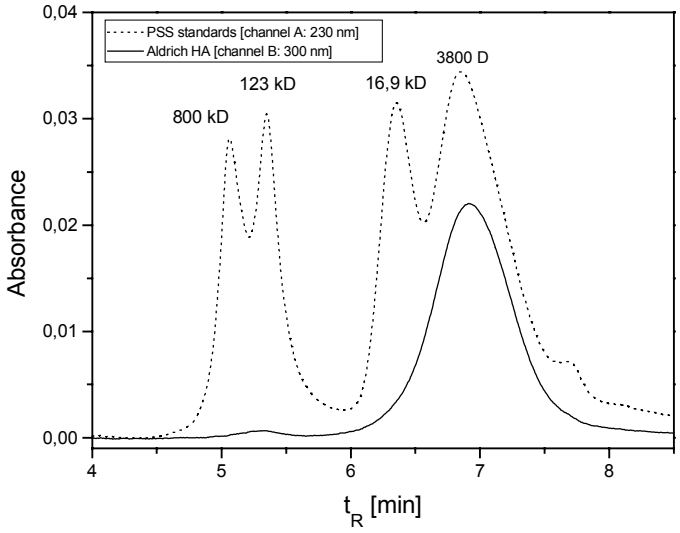

Fig. 2: SEC chromatogram of cleaned Aldrich HA and PSS standards; column: Jordi Gel DVB 10000 Å; eluent: 0.05 M NaOH

3.1.2 Capillary Electrophoresis

Capillary zone electrophoresis (CZE) allows to separate the humic acid constituents in accordance with their mass-charge ratios. Similar to size exclusion, CZE normally yields a sum peak for humic acids, which reflects the broad distribution of electrophoretic mobilities [Rig, Sch]. Humic acids of various origins differ in details of their pherogram, such that it is referred to humic acid finger prints [Bur, Dun, Pom].

By adding hydroxycarboxylic acids, e.g. tartaric acid, malic acid or citric acid, to the humic acid sample, base line separations into two or three zones may be obtained (Fig. 3). The usually applied borate buffer is still used as basic electrolyte. The migration times of the zones of Aldrich and Fluka humic acid differ noticeably such that these humic acids can be identified (Fig. 3, Fig. 4).

The separation result is to be attributed to an interaction between the humic acids and the added hydroxycarboxylic acids. An esterification of the hydroxyl groups of the hydroxycarboxylic acids with the carboxyl functions of the humic acids may be possible. The constituents with an increased carboxyl group density exhibit a higher degree of esterification and, hence, differ considerably from the other humic acid constituents in terms of mobility.

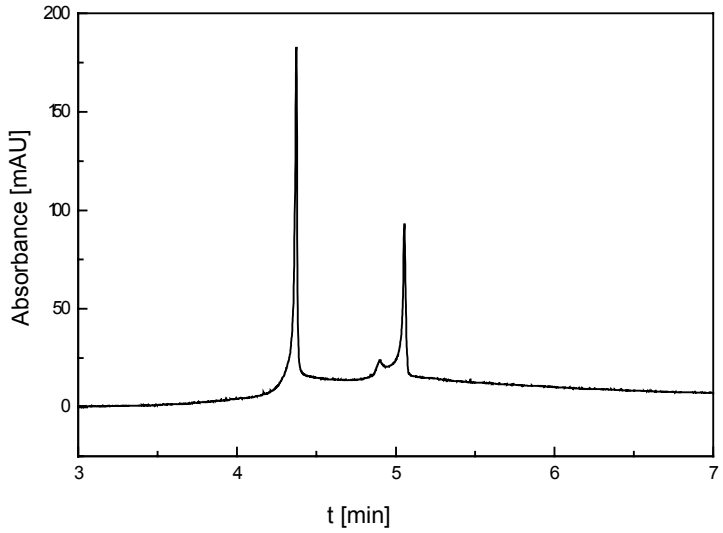

Fig. 3: CZE of cleaned Aldrich humic acid (500 mg/l)
Sample buffer: Borate (50 mM), citrate (25 mM), pH 8.6
Basic electrolyte: Borate (50 mM), pH 8.6
Separation conditions: 20 kV, 19 μA, 250 mbar s, 50 cm, 75 μm i.d.
Detection: DAD 200, 16 nm, cathodic

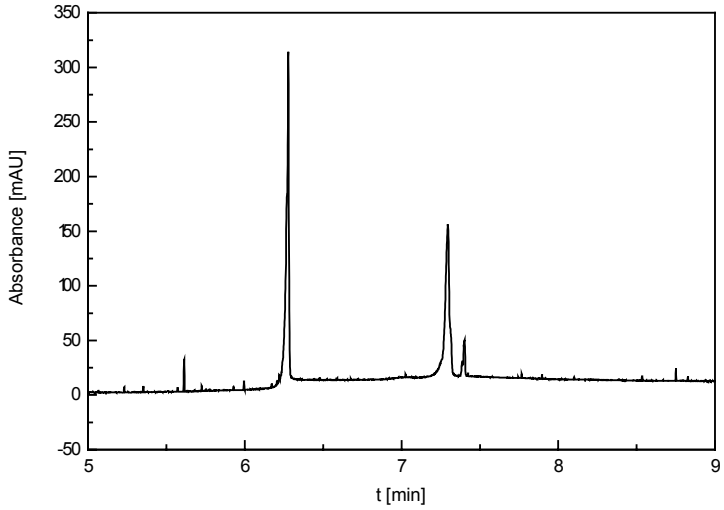

Fig. 4: CZE of cleaned Fluka humic acid (500 mg/l)
Sample buffer: Borate (50 mM), citrate (25 mM), pH 8.6
Basic electrolyte: Borate (50 mM), pH 8.6
Separation conditions: 20 kV, 19 μA, 250 mbar s, 50 cm, 75 μm i.d.
Detection: DAD 200, 16 nm, cathodic

Thus, a base line separation is achieved. This assumption is supported by the observation that dicarboxylic acids without hydroxyl functions do not yield a comparable separation when added to the buffer.

3.1.3 Characterization of Metal Humate Complexes

Capillary electrophoresis may also be applied to study the influence of complexation of metal cations on the mobility of the humic acids. The humic acid peak is shifted to shorter migration times with increasing metal addition. Although loaded with cations, all humates remain negatively charged and are transported towards the cathode by the EOF. At an increased metal concentration, the broad humic acid peak is followed by a narrow signal at a longer migration time (Fig. 5).

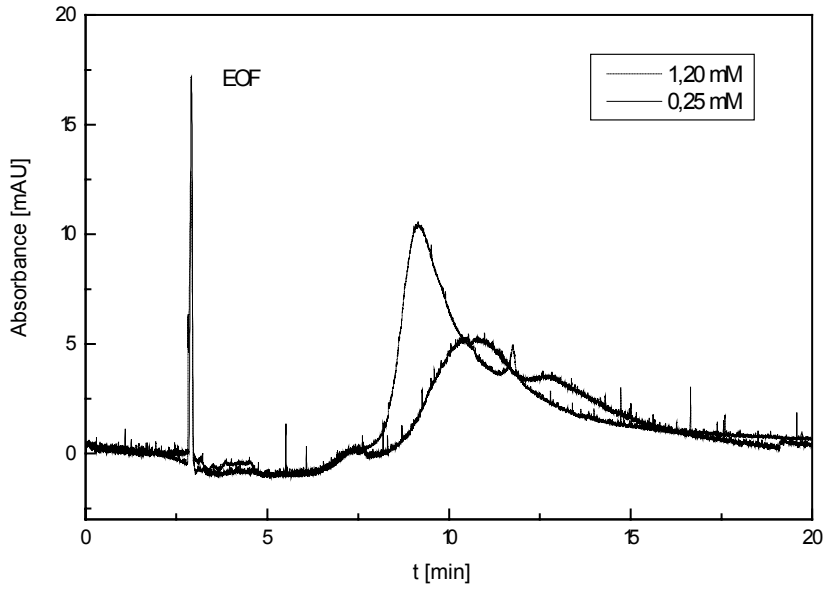

Fig. 5: CZE of cleaned Aldrich humic acid (500 mg/l) with the addition of lead ions
Buffer: Borate (50 mM), pH 8.6
Separation conditions: 20 kV, 10 µA, 250 mbar s, 50 cm, 75 µm i.d.

This result can be explained by the variable complexation tendency of the humates. The metal cations are first bound to components with a high coordination tendency. Other ranges are less loaded with cations and keep their negative charge centers. As a result, the signal is differentiated into ranges of clearly varying mobility. The strongly complexing constituents lose major fractions of their negative charge and, hence, of their anionic mobility. They can set less migration speed against the EOF and are led past the detective window at an earlier point of time.

By means of micellar electrokinetic chromatography (MEKC), also uncharged particles can be separated by capillary electrophoresis [Ter]. Here, a surfactant is added to the basic electrolyte. Above the critical micellar concentration, micelles are formed. The substances are separated in accordance with their variable tendency to stay in both phases.

The influence of metal cation loading on the ionic properties of the humic acid is also revealed by this separation method. The signal loses width with increasing metal concentration (Fig. 6). At the same time, the peak maximum shifts towards shorter migration times.

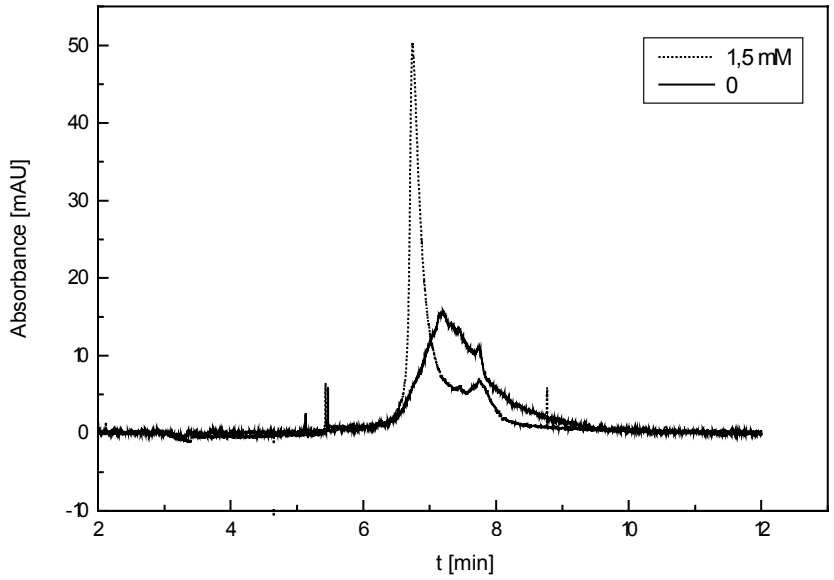

Fig. 6: MEKC of cleaned Aldrich humic acid (500 mg/l) with the addition of lead ions
Buffer: Borate (50 mM), SDS (15 mM), pH 8.6
Separation conditions: 20 kV, 25 µA, 250 mbar s, 50 cm, 75 µm i.d.

Coordination of cations by the different functional groups of the humic acid results in a reduced hydrophily. The larger fraction of humic acid constituents preferably stays in the micelles at a high metal load. The smaller peak at a later migration time may be assigned to humic acid constituents having an increased number of anionic groups. These constituents are more hydrophilic and stay in the micelles with less probability.

3.2 Fractionation of Humic Acids

Fractionation of humic acids is aimed at producing the individual components. The studies described below have provided information on the composition of the humic acid and the properties of its constituents. Free flow electrophoresis (FFE) and ultrafiltration are applied for fractionation.

3.2.1 Free Flow Electrophoresis

Analytical separation of humic acids in a borate buffer modified by the addition of hydroxycarboxylic acids may also be performed preparatively. For this, the separation conditions of analytical separation are transferred to the FFE system. Following separation, humic acid fractions of variable mobility can be isolated in solid form by freeze drying and investigated using various analytical methods.

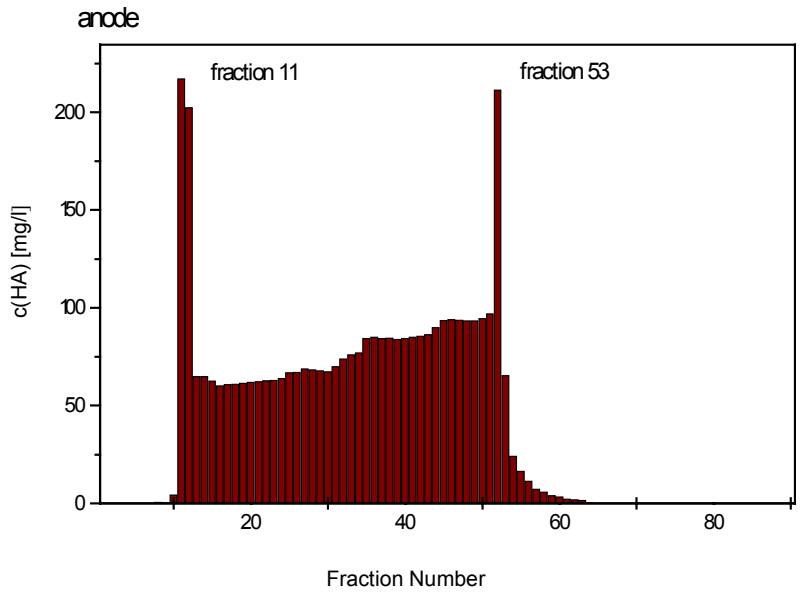

Fig. 7: FFE separation of cleaned Aldrich humic acid (60 mg/l)
Buffer: Borate (50 mM), tartrate (20 mM), pH 8.6
Contact solutions: Borate (10 mM), anode: Chlorite, cathode: Acetate
Separation conditions: 500 V, 90 mA, 4 min residence time

Characterization of the fractions by IR and UV-Vis spectroscopy as well as by CHN analysis does not reveal any striking differences between both fractions and the cleaned Aldrich humic acid. From this, it may be concluded that both fractions are made up of the same constituents. The molecular weights of both fractions can be determined by the flow-field flow

fractionation method. It was first described by Giddings and Beckett [Bec, Gid]. This method represents an alternative to gel permeation chromatography. The analytes are separated according to their hydrodynamic radius. The molecular weights of both FFE fractions were determined at the Institut für Nukleare Entsorgungstechnik (INE, Institute of Nuclear Waste Management) of the Karlsruhe Research Center. The fractograms obtained exhibit two peak maximums each. Due to calibration problems, the molecular weights of both fractions cannot be given in absolute values, but differ significantly. The smaller molecular weight is assigned to fraction 11, which may explain its higher electrophoretic mobility. To investigate the stability of the fractions in the solution, the precipitated humic acids are dissolved again in the borate-tartrate buffer and injected into the CE. The separation conditions are the same as in the original CE experiment. The electropherogram shows the separation of both fractions into two signals each (Fig. 8).

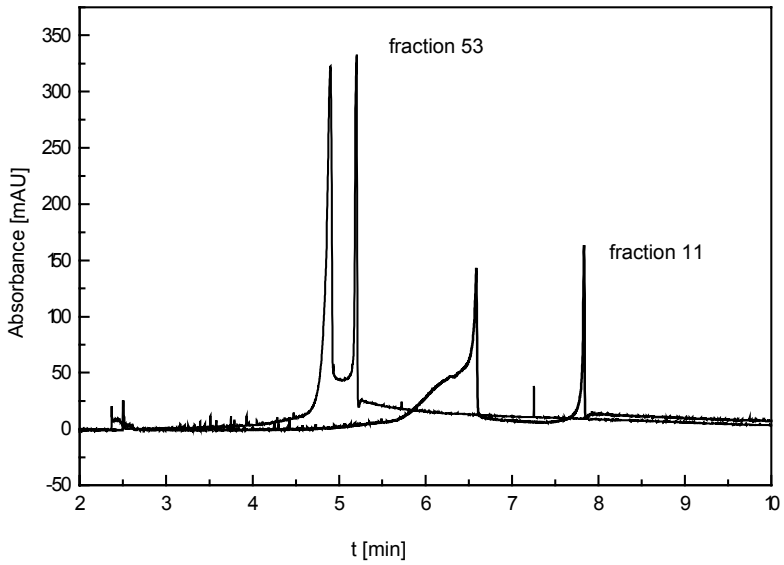

Fig. 8: Characterization of the solid FFE fractions using CZE
Buffer: Borate (50 mM), tartrate (25 mM), pH 8.6
Separation conditions: 20 kV, 17.5 μA, 250 mbar s, 50 cm, 75 μm i.d.

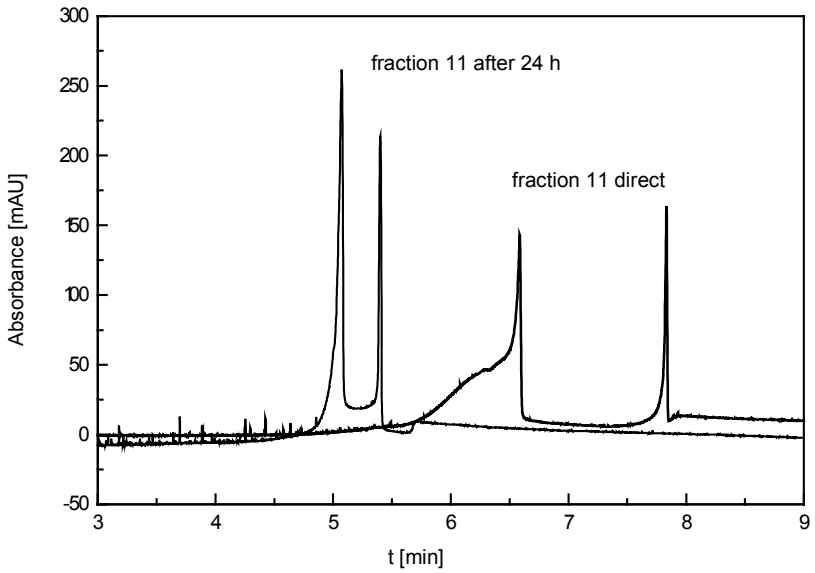

Fig. 9: Characterization of FFE fraction 11 directly and after 24 h
Buffer: Borate (50 mM), tartrate (25 mM), pH 8.6
Separation conditions: 20 kV, 17.5 μA, 250 mbar s, 50 cm, 75 μm i.d.

For stable components, one peak is to be expected. This is not only attributed to an incomplete separation in the FFE, as at least one of the species must have been enriched in an FFE fraction. Moreover, the signal pairs differ considerably in terms of migration time. The signal pair of FFE fraction 11 appears at later migration times, as the humic acids of this fraction set more anionic mobility against the EOF.

The dynamic character of the secondary structure of the humic acid in alkaline solution becomes obvious from the time-dependent experiment. The solutions of both humic acid fractions in the borate-tartrate buffer are injected after a residence time of 24 h.

While the electrophoretic mobility of the signal pair of fraction 53 remains constant, the migration times of both peaks of fraction 11 are shifted (Fig. 9). The humic acids lose a part of their effective negative charge and are transported more rapidly than before to the detector by the EOF. They then become equal to fraction 53 in terms of mobility.

According to the results of these experiments, humic acid is subject to an equilibrium in the aqueous solution. Spatial orientation of charged groups towards each other and, hence, folding of the humic acid molecules tend to reach an energetic minimum in alkaline solution.

Fractionation of humic acid or of the reaction products of humate and hydroxy carboxylate yields humic acid constituents which are able to reach the original equilibrium state in the solution again.

3.2.2 Ultrafiltration

Investigation of the Aldrich humic acid used by means of SEC yields a size distribution of the humic acid molecules. By means of ultrafiltration (UF), fractions of a certain size range can be obtained. The separation into various sizes takes place by means of membranes with various cut-offs (1000 D - 1000 kD).

The humic acid content of the individual ultrafiltrates is quantified photometrically. As a prerequisite, the absorption coefficients of the individual fractions have to agree at the wavelength relevant for the measurement. For this, the UV-Vis spectra of the individual fractions are recorded. Following their normalization, the spectra can be compared directly.

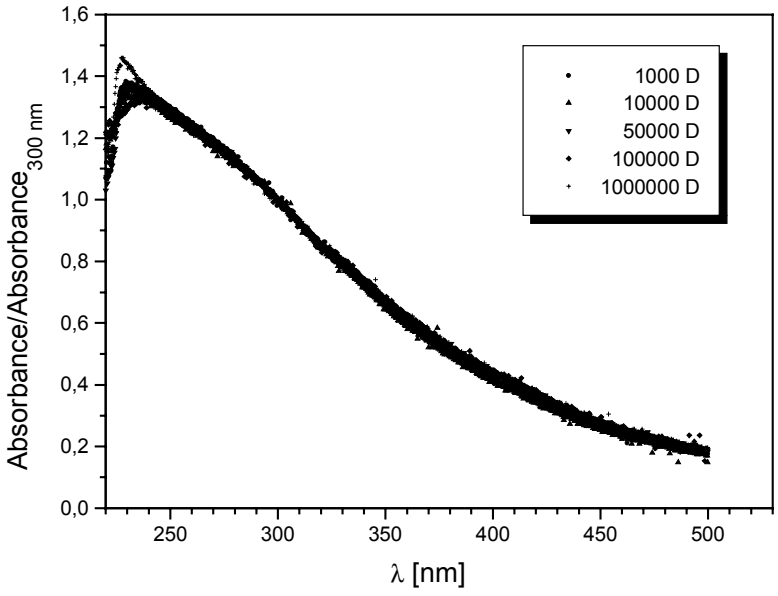

Fig. 10: Normalized UV-Vis spectra of the ultrafiltrates

A maximum of absorption at 230 - 240 nm and a continuous decrease in absorption with increasing wavelength can be observed. The normalized UV-Vis spectra of the individual fractions do not differ within the limits of measurement accuracy. Hence, the humic acid content of the individual fractions can be determined quantitatively.

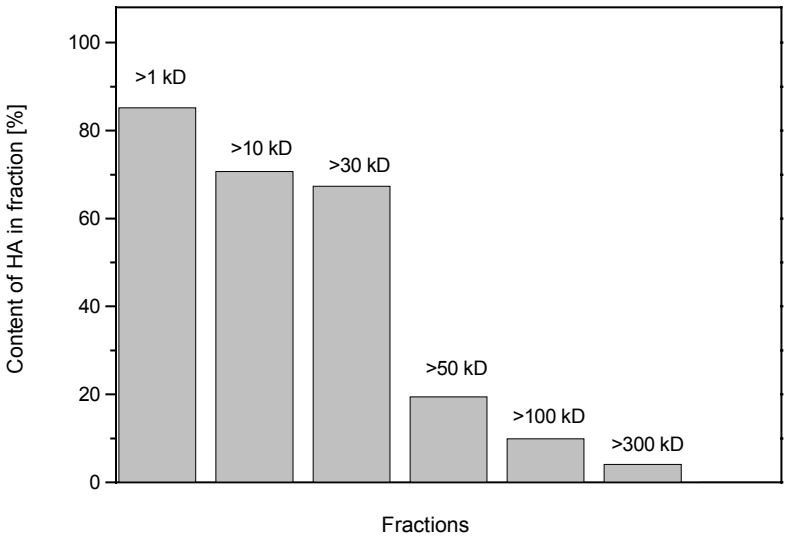

Fig. 11: Humic acid contents of the individual ultrafiltrates

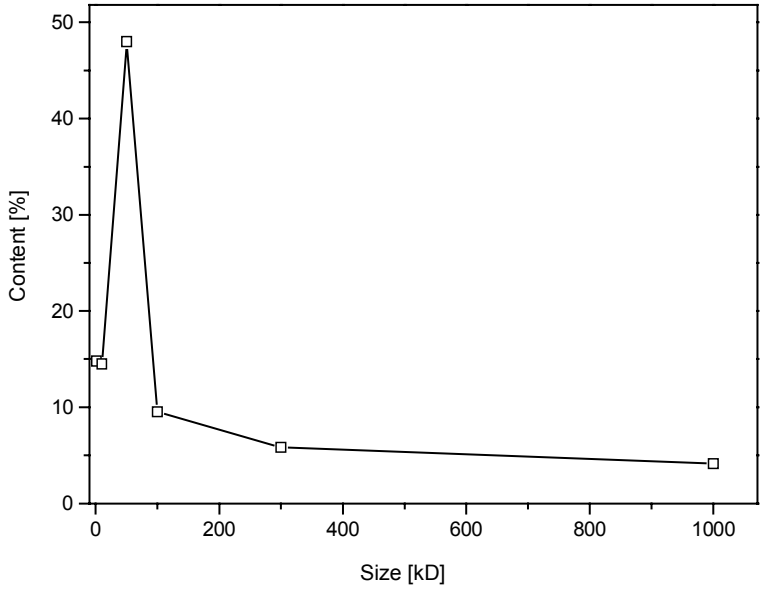

Fig. 12: Size distribution calculated from the humic acid contents of the individual fractions

The size distribution obtained by ultrafiltration may be compared with the SEC results. The main fraction of the humic acids consists of smaller molecules (< 50 kD). No detailed statement can be made with regard to the size distribution of the applied HA in UF due to the limited number of ultrafilter sizes and the thus limited resolution.

As compared to SEC, increased molecular sizes are obtained, as larger molecules block the pores during the UF and, hence, prevent molecules that are smaller than the cut-off of the membrane from passing it. Ultrafiltration represents a method, by means of which specific size fractions of humic acids may be obtained on a preparative scale.

Using electrophoretic methods, a change of the mass-charge distribution of humic acid fractions over time can be determined. Now what about a possible size variation? For this, fractions of the cleaned Aldrich humic acid were studied as a function of time. After 20 hours, shifting of the retention times of the individual fractions was observed (Fig. 13).

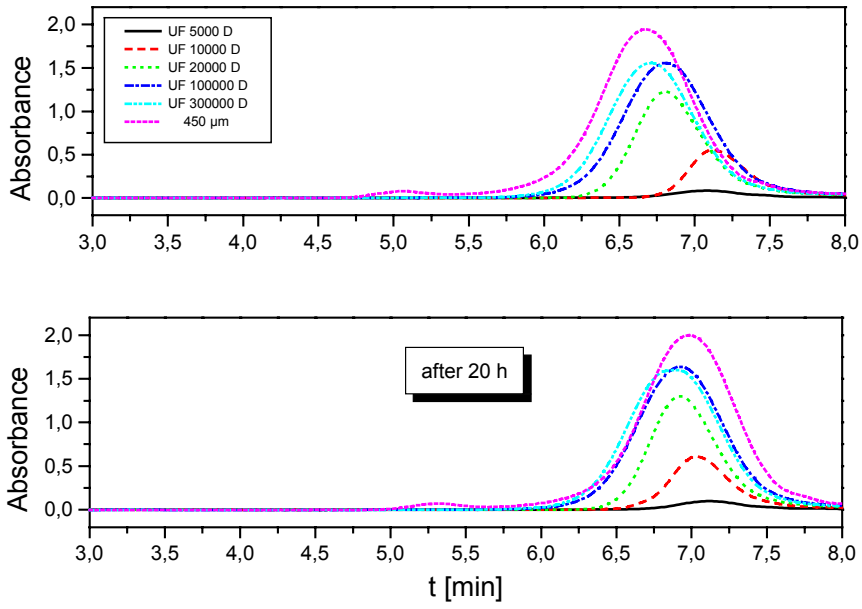

Fig. 13: Shifting of the retention times of the individual ultrafiltrate fractions after 20 hours in the SEC chromatograms; column: Jordi Gel DVB 10000 Å; eluent: 0.05 M NaOH

This result indicates an equilibrium state of the humic acid molecules in terms of their size. It must be taken into account, however, that for the size calibration curve studied here a small shift of retention time is sufficient already to cause a larger change of the molecule size. For this reason, another test series was performed using an SEC column with a smaller pore diameter. Within the standard deviations of the retention times, however, no reliable statement can be made with regard to the variation of the molecule size.

3.2.3 Fractionation of Metal Humate Complexes

Capillary electrophoretic separation of metal humate complexes has the drawback of not providing any information on the metal content of the individual fractions. Free flow electrophoresis (FFE) as a preparative method, however, allows an investigation of the individual fractions using various analytical methods. Due to its higher sharpness of separation, free-flow isotachophoresis (FF-ITP) is applied.

Addition of lead ions causes considerable changes in the distribution of the humic acid concentration. Compared to the distribution of humic acid without the addition of lead ions (cf. Fig. 14), a second maximum occurs (Fig. 15).

Two major results are obtained: All fractions that contain the humic acid also contain lead. Distribution of the humates is broadened considerably by the addition of lead ions. From this, it follows that all humic acid constituents are able to coordinate metal cations. Furthermore, complexation causes a stronger differentiation of the electrophoretic mobilities of humic acid constituents.
Plotting of the molar ratios of complexed lead ions and deprotonatible functional groups of the humic acid yields the stoichiometric composition of the individual complexes.

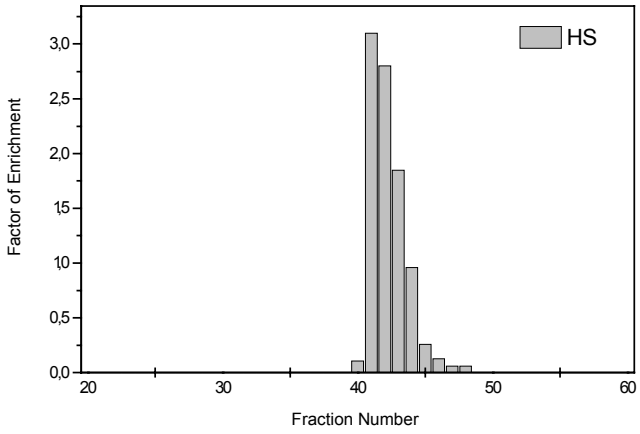

Fig. 14: FF-ITP of cleaned Aldrich humic acid (100 mg/l) at pH 6
Counterion: MES (1 mM), L: Chloride, T: Acetate
Separation conditions: 200 V, 5 mA, 3 min residence time

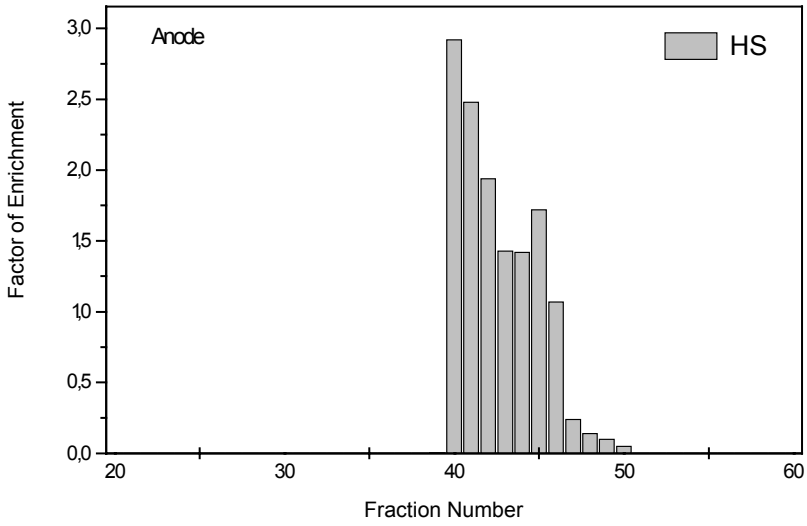

Fig. 15: FF-ITP of cleaned Aldrich humic acid (100 mg/l), c (Pb^{2+}): 25 mg/l
Counterion: MES (1 mM), L: Chloride, T: Acetate, pH 6
Separation conditions: 200 V, 5 mA, 3 min residence time

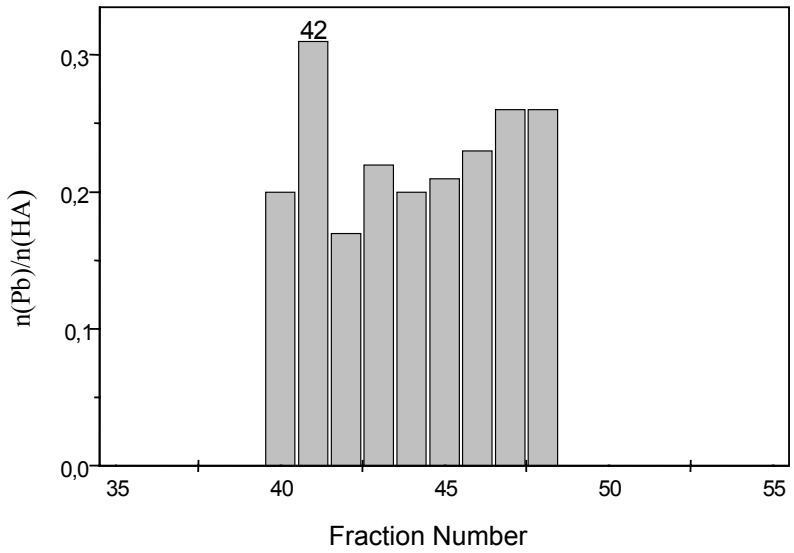

Fig. 16: Molar ratios of lead ions and deprotonatible functional groups
FF-ITP of cleaned Aldrich humic acid (100 mg/l), c (Pb^{2+}): 25 mg/l
Counterion: MES (1 mM), L: Chloride, T: Acetate, pH 6
Separation conditions: 200 V, 5 mA, 3 min residence time

At pH 6, a heterogeneous distribution of the molar ratios of the humic acid fractions is obtained (Fig. 16). At this pH value, nearly only carboxyl groups are responsible for complexation. As a consequence, separation of the humate constituents is due to the varying number of carboxyl groups that are not loaded with cations. It is shown by the high mobility of fraction 42 in FF-ITP (Fig. 16) that a high cation load does not automatically cause a considerable reduction of mobility. In spite of their strong complexation, humic acid constituents may still possess a high anionic charge. These may be pseudomicelles with a high external charge and the charge centers being turned towards the interior of the agglomerate.

At pH 9, changes in the mobility distribution of the humic acid constituents become visible at metal concentrations which are smaller than at pH 6. Again, all fractions containing humic acids also contain lead. A lead concentration of 25 mg/l (0.1 mM) yields two discrete humate bands that may be interpreted as fractions of considerably varying mobility (Fig. 17). Between them, a broad area with lead humates of medium mobility is located.

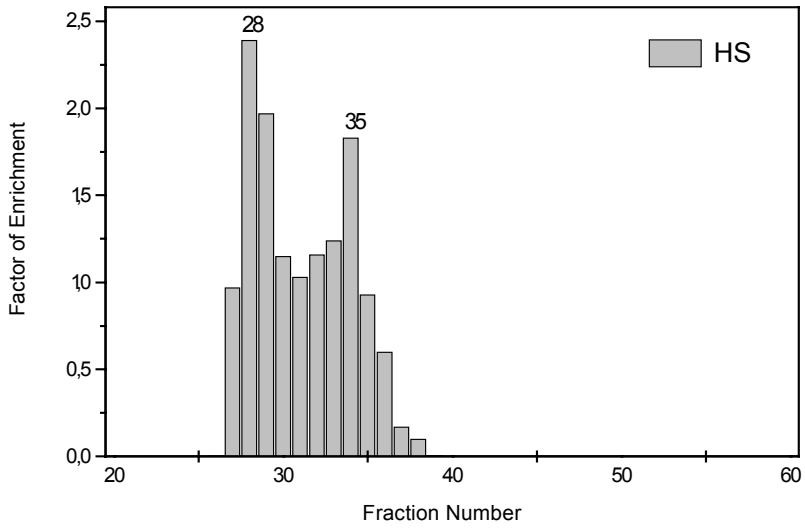

Fig. 17: FF-ITP of cleaned Aldrich humic acid (100 mg/l), c (Pb^{2+}): 25 mg/l
Counterion: TRIS (1 mM), L: Chloride, T: Acetate, pH 9
Separation conditions: 200 V, 6 mA, 3 min residence time

The molar ratio of the lead ions and the deprotonatible humic acid ligands provides information on the stoichiometry of the lead complexes of the different humic acid constituents.

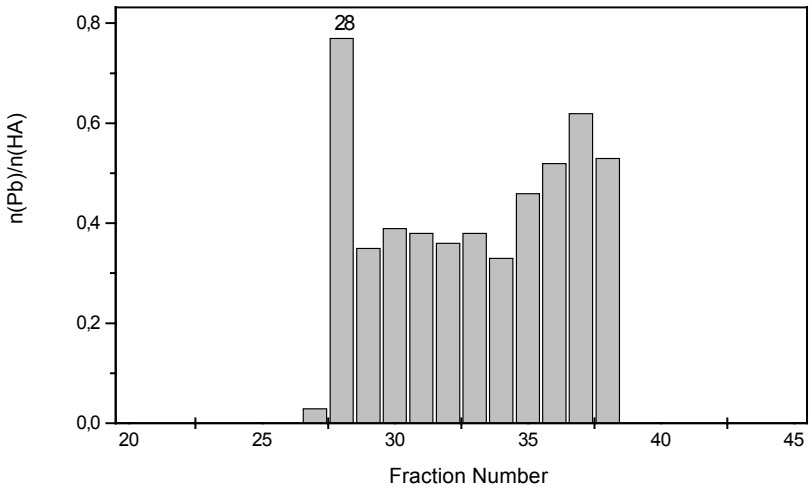

Fig. 18: Molar ratios of lead ions and deprotonatible functional groups
FF-ITP of cleaned Aldrich humic acid (100 mg/l), c (Pb^{2+}): 25 mg/l

At pH 9, differentiation is stronger than at pH 6 (Fig. 18). In most fractions, the ratios are below 0.5 even at high metal loads. This means that most constituents of the humic acid use at least two coordination positions for binding the metal cations. For fraction 28, however, a ratio of 0.8 is obtained. Here, a 1:1 complexation is nearly reached. These may be strongly binding Lewis bases which do not possess any direct neighboring donors such that no bidental coordination may develop. Humic acid constituents with mass ratios above 0.5 can also be found at the end of the mobility distribution. These may be mixed complexes with the metal cations being complexed by coordination positions of both the humic acid and other complexing agents, i.e. hydroxo ligands.

3.3 Complexation

Knowledge of the formation constants of metal-humate complexes allows to estimate mobilization of metal cations in soil and groundwater. The constants serve as the base data for modeling scenarios, in which pollutants pass the biological barriers of dumps or underground repositories and enter the hydrosphere. In this connection, not only radionuclides, but also cations of toxic heavy metals are of ecological relevance [Nie].

3.3.1 Formation Constants of Heavy Metal-Humate Complexes

The formation constants of humate complexes of the heavy metals of lead, cadmium, and zinc have been determined by means of continuous ion focussing (field surge electrophoresis (FSE), ultrafiltration (UF), and anodic stripping voltammetry (ASV).

Determination of a complex-formation constant for metal complexes of the humic acid requires knowledge on the individual species concentrations in the equilibrium. If no species analysis is available, the complexed metal cations have to be separated from the free ones. Preparative field surge electrophoresis allows to separate the negatively charged metal humates from the free cations. In the analysis range of the electrophoresis chamber, the ions move rather rapidly, as here a high field prevails at low conductivity. As soon as they hit the interface with the edge buffer area of high conductivity, they are decelerated and enriched in the respective fractions. Accordingly, the metal humate complexes are focused on the anodic side at the boundary edge buffer [Wag 2-3].

Due to their sensitivity, electrochemical stripping methods are well suited for the determination of heavy metals in the trace range (ng/l) [Haa], [Wan]. They are used for determining complex-formation constants [Bha], [Pin], as they allow a species analysis of the free metal ions to be performed. In this case, the non-complexed metal ions can be determined without a prior separation. Thus, adsorption effects and equilibrium shifts are avoided.

Another method for the separation of metal humate complexes and free cations is ultrafiltration. Here, the heavy metal humate and free humic acid are separated from the non-complexed heavy metal. Calculation of the formation constants from the thus obtained values was carried out on the basis of the charge neutrality model [Kim 1].

Tab. 1: Comparison of the formation constants of lead humate complexes at pH 5 and pH 6 and I < 0.01 mol/l and I = 0.1 mol/l

	pH 5	pH 6
FSE	5.2 ± 0.1	5.6 ± 0.1
ASV	5.6 ± 0.1	-
UF (I = 0.1)	6.4 ± 0.2 (5.4 ± 0.1)	6.1 ± 0.2 (5.9 ± 0.2)

Tab. 2: Comparison of formation constants for cadmium humate complexes at pH 5 and 6 and I < 0.01 mol/l

	pH 5	**pH 6**
FSE	4.0 ± 0.1	4.1 ± 0.1
ASV	4.3 ± 0.1	-
UF	5.0 ± 0.1	5.6 ± 0.1

Tab. 3: Formation constants for zinc humate complexes at pH 5 and 6

	pH 5	pH 6
FSE	3.9 ± 0.1	4.2 ± 0.1

Depending on the measurement method, the log β values of the lead humates vary by up to an order of magnitude (cf. Tabs. 1 and 2). At high ionic strengths (I = 0.1 mol/l), the log β values are smaller than at small ionic strengths (I < 0.01 mol/l). A possible reason for the strong differences of the log β values obtained with different methods is that ultrafiltration may result in an equilibrium shift due to concentration changes during the filtration process. In addition, adsorption effects may occur. The separated humate complexes partially deposit on the filter material. In addition to complex formation as a solution equilibrium reaction, metal cations may be adsorbed on the solid phase formed during further filtration. As a consequence, too high formation constants will be obtained.

Another possible reason is the interference with the solution equilibrium: In FSE, the humate complexes meet with a solution of high ionic strength (I = 0.05 mol/l) at the conductivity boundary. Kinetically unstable complexes may be disintegrated there and, as a consequence, the formation constant may be reduced. In stripping voltammetry, a very small fraction as compared to the total amount of heavy metal used is converted at the collector. Therefore, an equilibrium shift due to a reduced amount of free heavy metal ions can be neglected. An adsorption of humic acid at the collector may cause a reduction of the measured value. This effect may be counteracted by selecting a short deposition time and small humic acid concentrations.

Summing up the results obtained with regard to the formation constants, it must be noticed that of all cations selected lead ions form the thermodynamically most stable humate complexes under identical conditions.

3.3.2 Investigation of Competing Complexations on Humic Acid

In soils and natural water bodies, humic substances are loaded with those cations that enter the solution by weathering of the adjacent rock. In high-lime areas, these are calcium and magnesium ions. They compete with the anthropogenic heavy metal ions for the coordination positions of the humic acids. The exchange reaction between cadmium ions and alkaline-earth ions on humic acid was studied as an example. Cadmium forms complexes with humic acid ligands. These complexes have a higher thermodynamic stability than the humate complexes of calcium and magnesium [Ste]. Sometimes, however, considerable concentrations of alkaline-earth ions are found in nature. As a result, the complex-formation equilibrium may be shifted.

CZE with an indirect UV detection allows to simultaneously detect and quantify all cations involved in the exchange processes upon prior separation by ultrafiltration. It is applied for cation determination in various matrices and characterized by a sufficient sensitivity and good reproducibility [Bar, Lee].

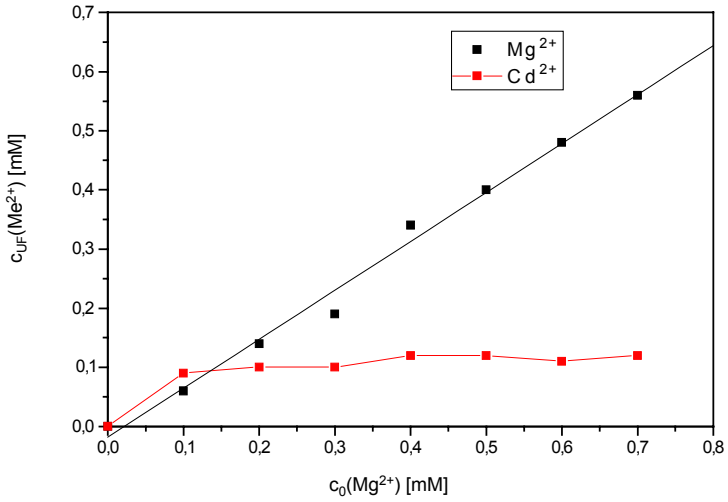

Fig. 19: Displacement of cadmium ions (0.2 mM) from humate complexes by Mg^{2+} at pH 7, concentrations of free cadmiums in the ultrafiltrate

By the addition of magnesium ions, cadmium ions are displaced from their coordination positions. However, this exchange remains incomplete. Part of the cadmium ions remains complexed even at a high magnesium concentration (Fig. 19). Also when adding calcium ions as competing ions, only about half of the complexed heavy metal is displaced. In case of alkaline-earth humates and the addition of cadmium as a competing ion, also calcium is displaced from its complexes to an incomplete extent only. In contrast to this, magnesium is completely exchanged for the added cadmium.

These observations may be interpreted by the colloidal character of the humic acid. Addition of bivalent cations causes a change of the secondary structure of the humic acid in the aqueous solution [Cho, Wan]. Electrostatic repulsion between the negative charge centers is decreased by the binding of cations. The macromolecule is subject to stronger coiling. The cations added after the development of the equilibrium may only replace the cations bound on the outer surface of the agglomerate. They cannot penetrate into the hydrophobic interior of the micelles with their extended hydrate shell. The cadmium or calcium bound there cannot be displaced.

For the magnesium ion with its extended hydrate shell, this influence on the secondary structure of the humic acid colloids is less marked. The magnesium cations only form weak bonds with the humate ligands. Thus, the humic acid largely keeps its folded structure and remains accessible to metal cations that approach from the solution. Cations strongly differ in their structure-modifying effect on humic acid polyelectrolytes. These differences affect ion exchange processes in the soil and in natural water bodies. The properties and concentrations of the various cations decide on which cations are bound to the humic acid. This results in a direct influence on the mobilization of toxic heavy metal cations in nature.

Further experiments were carried out to study whether certain cations are preferred in complexation or whether or not mixed complexes form. In the experiment, the heavy metal cations of zinc and cadmium as well as the alkaline-earth ions of calcium and magnesium existed side by side. In another test series, the magnesium, cadmium, and zinc ions competed with the lead ions.

The concentration of free zinc and cadmium ions decreases with increasing humic acid concentration. Only after advanced complexation of the heavy metal ions are the alkaline-

earth ions subject to increasing binding. As compared to their competitors, lead ions are preferred in complexation. In the analytical solution, a strong decrease of the concentration of free lead with increasing humic acid concentrations can be noticed (Fig. 20).

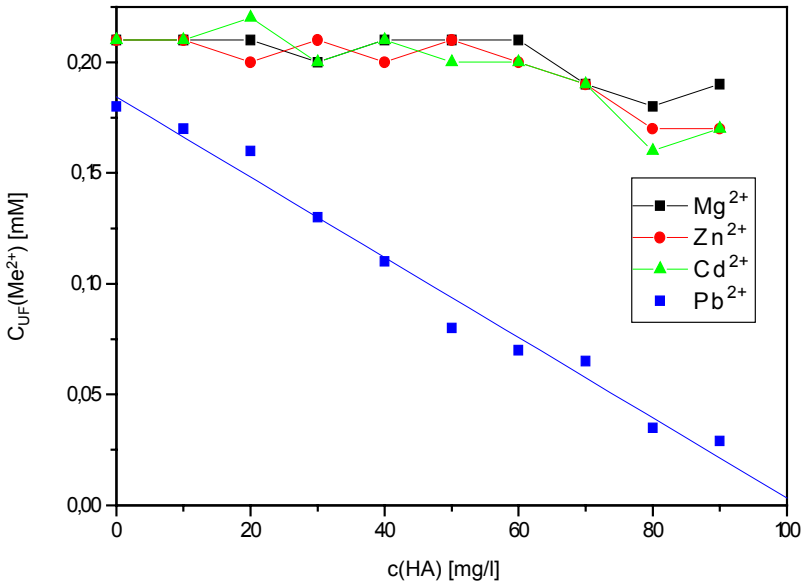

Fig. 20: Complexation of Cd, Mg, Pb, and Zn (all 0.1 mM) by cleaned Aldrich humic acid, pH 6 - 7, concentrations of free cations in the ultrafiltrate

Of all cations studied lead forms the most stable humate complexes. According to our results, its formation constant exceeds that of zinc and cadmium humate by an order of magnitude. The cations are complexed by humic acid in the order of their complex stability.

3.4 Investigations on Defined Solid Phases

Laboratory experiments on the three-substance system of heavy metal/humic acid/solid phase may provide information on the interaction of the heavy metal/humic acid complexation and heavy metal sorption on a stationary phase. Batch and column experiments are distinguished. In batch experiments, a static equilibrium between the mobile phase and the solid phase is waited for. In column experiments, a flow equilibrium is obtained. In an ideal case, the solid phase used for the laboratory experiments has been removed from the geological system in an undisturbed manner and, hence, precisely reflects the geological conditions. In addition, use of the respective geogenic groundwater contributes to simulating the natural conditions as closely to nature as possible.

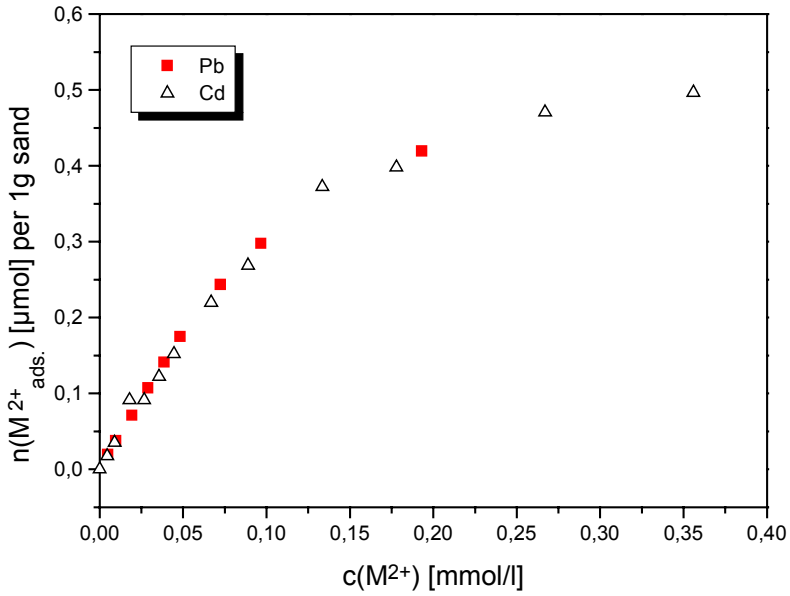

Fig. 21: Adsorption isotherms of Pb^{2+} and Cd^{2+} on sand; preparation: 2.5 g Merck sand in 10 ml sodium acetate/acetic acid buffer solution 2 mM, pH = 5, after 24 h

3.4.1 Batch Experiments with Lead and Cadmium

For preliminary investigations of the heavy metal complexation with humic acid and of sorption, the heavy metals of lead and cadmium and the solid phase of cleaned sea-shore sand (Merck) were applied. To minimize complex formation of the heavy metal ions with the used buffer, an acetic acid/acetate buffer of pH = 4.9 ($c_{(acetate)}$ = 0.002 M) was applied when studying the adsorption of cadmium and lead ions on sea-shore sand. The heavy metal concentration was varied. Following centrifugation, the concentration of cadmium and lead in the solution was determined by means of ICP-OES. From the difference to the originally applied concentration, the amount of adsorbed heavy metal, for 1 g of sand, was calculated (Fig. 21).

The adsorption isotherms (Fig. 21) agree with the behavior according to Langmuir in good approximation. Both heavy metal ions behave nearly identically as far as their adsorption on sand in the concentration range studied is concerned.

To investigate the influence of humic acid on the complexation behavior in more detail, batch experiments were performed where the concentration of humic acid was varied between 0 and 100 mg/l (Figs. 22, 23). The lead or cadmium concentration was kept constant.

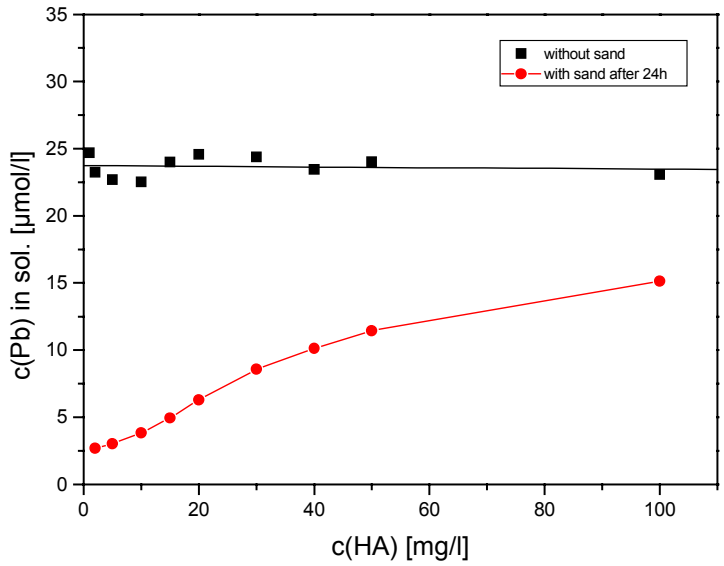

Fig. 22: Influence of humic acid on the adsorption of PB^{2+} on sand; c(Pb^{2+}) in the solution is plotted after 24 h. Preparation: 2.5 g Merck sand in 10 ml sodium acetate/acetic acid buffer solution 2 mM, pH = 5, $c_0(Pb^{2+})$ = 5 mg/l

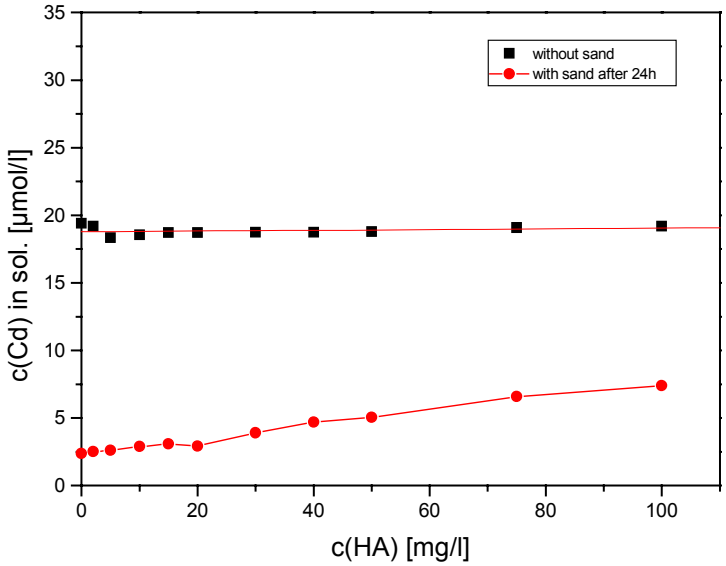

Fig. 23: Influence of humic acid on the adsorption of Cd^{2+} on sand; c(Cd^{2+}) in the solution after 24 h is plotted. Preparation: 2.5 g Merck sand in 10 ml sodium acetate/ acetic acid buffer solution 2 mM, pH = 5, $c_0(Cd^{2+})$ = 2 mg/l

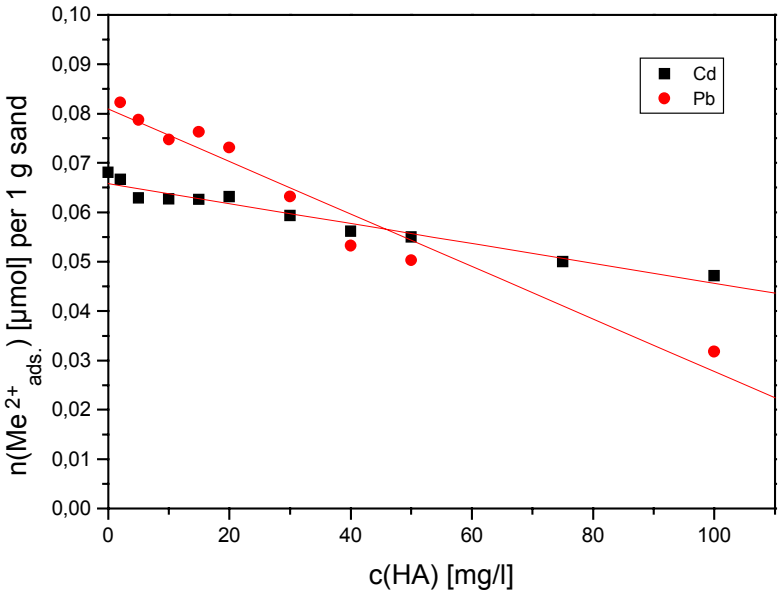

Fig. 24: Comparison of the adsorbed heavy metal amounts of Pb^{2+} and Cd^{2+} on 1 g sand after 24 h as a function of the humic acid concentration. Preparation: 2.5 g Merck sand in 10 ml sodium acetate/ acetic acid buffer solution 2 mM, pH = 5, $c_0(Pb^{2+})$ = 5 mg/l, $c_0(Cd^{2+})$ = 2 mg/l

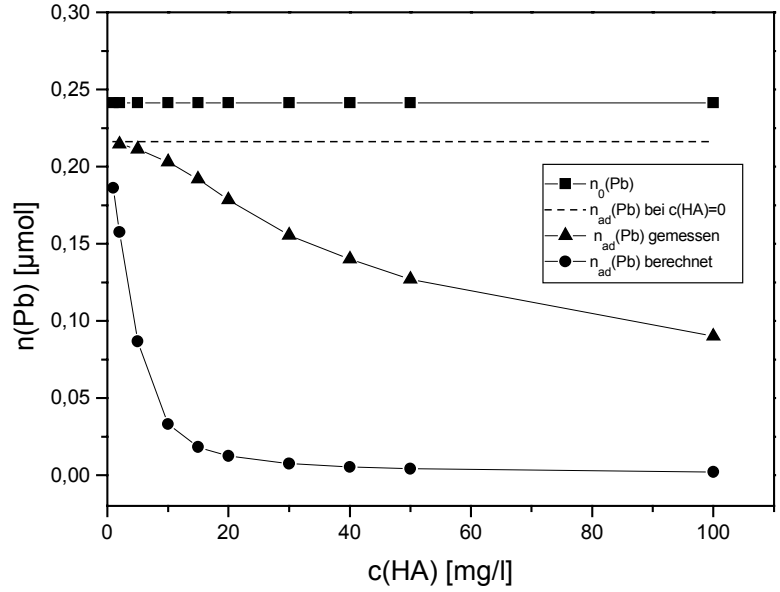

Fig. 25: Comparison between the theoretically calculated (n_{ad}(Pb) calculated) and actually determined amount of adsorbed Pb^{2+} (n_{ad}(Pb) measured); n_0 (Pb): Total amount of Pb^{2+}; n_{ad} (Pb) at c(HA) = 0: Calculated adsorbed amount of Pb^{2+} on 2.5 g sand in the absence of humic acid

For the adsorption of both cadmium and lead, the concentration of the heavy metal ions in the solution is observed to increase with increasing humic acid concentration. When comparing the amounts of adsorbed cadmium and lead calculated on this basis (Fig. 24), it is found out that the amount of adsorbed lead is subject to a stronger decrease with increasing humic acid concentration than that of cadmium.
To explain the influence of humic acid on the adsorption of the heavy metal ions on sand, a theoretical study was carried out first. Here, the adsorbed amount of lead on sand was calculated (Fig. 25). Calculation was accomplished taking into account the complex-formation constant determined (cf. Section 3.3.1) and assuming that free lead ions only were adsorbed on sand.

When comparing the calculated amounts of adsorbed lead, it can be noticed that they are far below the actually measured values. This indicates that not only non-complexed, but also complexed heavy metal ions are adsorbed on the sand surface. This effect which is encountered in spite of Coulomb's repulsion between the sand surface and the negatively charged humic acid may be explained by the colloidal properties of the humic acid. Like all colloids, humic acid may be adsorbed on surfaces. Obviously, also humic acid molecules loaded with heavy metal ions are adsorbed. By subtracting the calculated values from the measured ones, the curve shown in Fig. 26 is obtained.

The difference shown (Fig. 26) represents the amount of lead ions, which is adsorbed on the sand surface in the form of lead humate. With increasing humic acid concentrations in the solution, the amount of adsorbed lead humate increases. As of a certain humic acid concentration, however, the adsorbed amount of lead humate decreases again. This may be explained by the fact that free humic acid molecules are adsorbed on the sand surface as colloids at a high humic acid concentration. They thus prevent other heavy metal-loaded humic acid molecules from accessing.

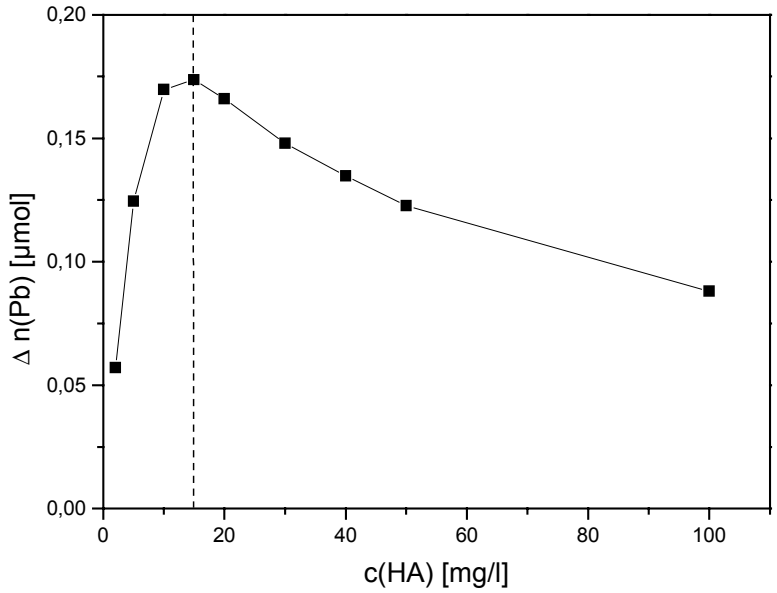

Fig. 26: Subtraction of the calculated amount of adsorbed Pb^{2+} from the measured one given in Fig. 25

3.4.2 Batch Experiments with Technetium

One of the long-lived radionuclides existing in the environment is technetium (Tc-99; $t_{1/2}$ = 2.1 x 10^5 years). With respect to the nuclear repository storage of radioactive wastes, it is important to study the properties of this element.

For the experiments with Tc-99, water (Gohy-532), and sand from Gorleben were used. As the humic acid concentration in the Gorleben water was given, the concentration of technetium was varied in comparison with the batch experiments performed with lead and cadmium (Fig. 27). To determine the influence of humic acid, experiments with synthetic water were performed. Its ionic strength and pH value corresponded to those of the Gohy water. The Tc-99 concentration was determined by means of a liquid scintillation counter.

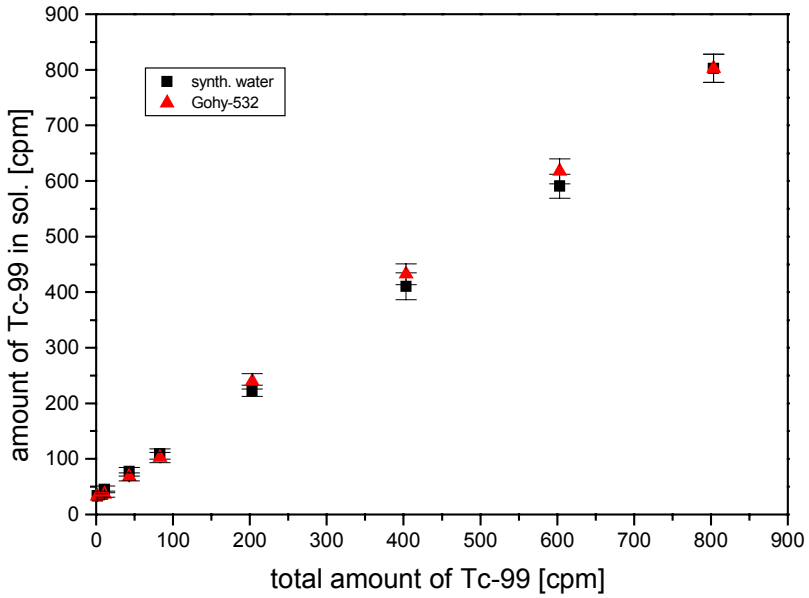

Fig. 27: Batch experiments in the system Tc-99/Gohy-532/Gorleben sand
Preparation: 2.5 g Gorleben sand; 10 ml solution (pH = 8.6)
Graphics: [cpm] in 0.5 ml solution

It was found out in the experiments that no significant adsorption of technetium on sand takes place under the conditions selected (Fig. 27). Nore was the humic acid found to influence the adsorption behavior.

In the experiments, pertechnate was used, as here technetium exists with the stable oxidation degree of +7. Due to its negative charge, a Coulomb's repulsion occurred on the sand surface which is charged negatively by the deprotonated silanol groups. For this reason, a complexation of technetium in its anionic form by negatively charged humate molecules appears improbable. The test results are in agreement with those of [Pal], [Beh], [Bal].

3.4.3 Column Experiments with Lead and Cadmium

When transferring the results of the laboratory experiments to natural conditions, it must be taken into account that the solid phase, on the surface of which an adsorption takes place, is not always in contact with a heavy metal-containing solution as in the batch experiments, but that a constant migration through soil layers takes place. To model these natural conditions as closely as possible, column experiments were performed. An eluent containing the humic acid was pumped through a column filled with sea-shore sand. The solution of 1 mg/l Cd or 1 mg/

l Pb was injected into the humic acid-containing eluent (50 mg/l). Potassium bromide was applied as the reference substance for the determination of the dead time. Coupling with ICP-MS has the advantage of the concentrations of bromide and the heavy metal being recorded in parallel by a single measurement. Hence, system fluctuations over time can be compensated. For determining the metal concentration, the isotope 208 (relative occurrence 52.4%) was selected for lead. The isotope 114 (relative occurrence 28.7%) and the isotope 79 (relative occurrence 50.7%) were chosen for cadmium and bromine, respectively.

In both the column experiments for lead (Fig. 28) and the experiments for cadmium (Fig. 29), the eluted heavy metal occurred as a peak before the inert peak. For cadmium and lead, the peak exhibited a slight tailing. The peak height depended on the equilibration time of the heavy metal humate solution used. In addition, the peak height was found to be dependent on the equilibration time, i.e. the time difference between the preparation of the sample solution to be injected and its injection into the column. Within increasing age of the injected solution, the amount of eluted heavy metal increases. This can be observed for both cadmium and lead.

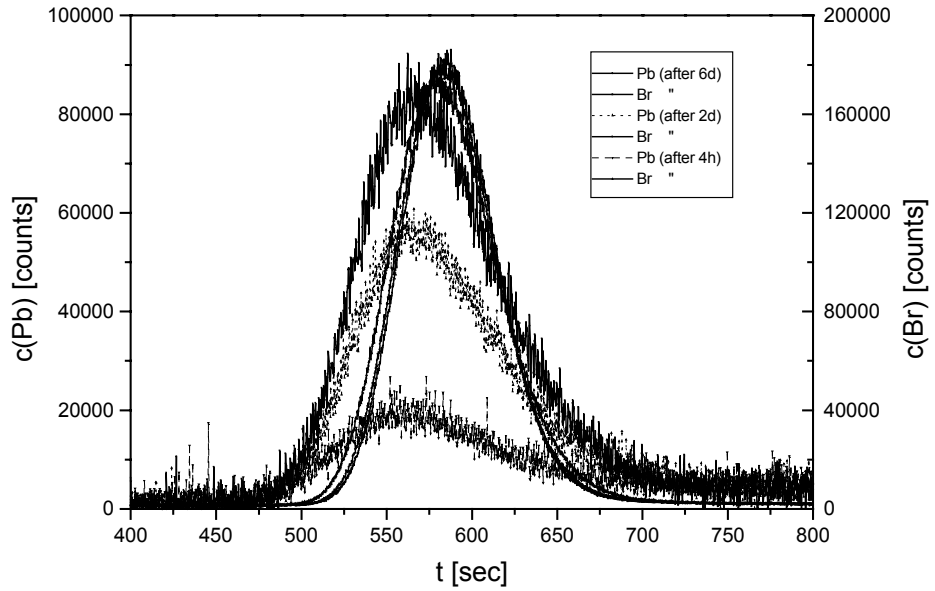

Fig. 28: Column experiments with Pb. Column packed with Merck sand (25 cm, ∅= 1cm)
Flow: 0.83 ml/min
Detection: ICP-MS [Br, Pb] (simultaneously)
Eluent: c(HA) = 50 ppm; pH = 5.3 MES (1 mM); $NaClO_4$ (2 mM)
Injection: 0.5 ml Pb (1 ppm) (prepared in the eluent)

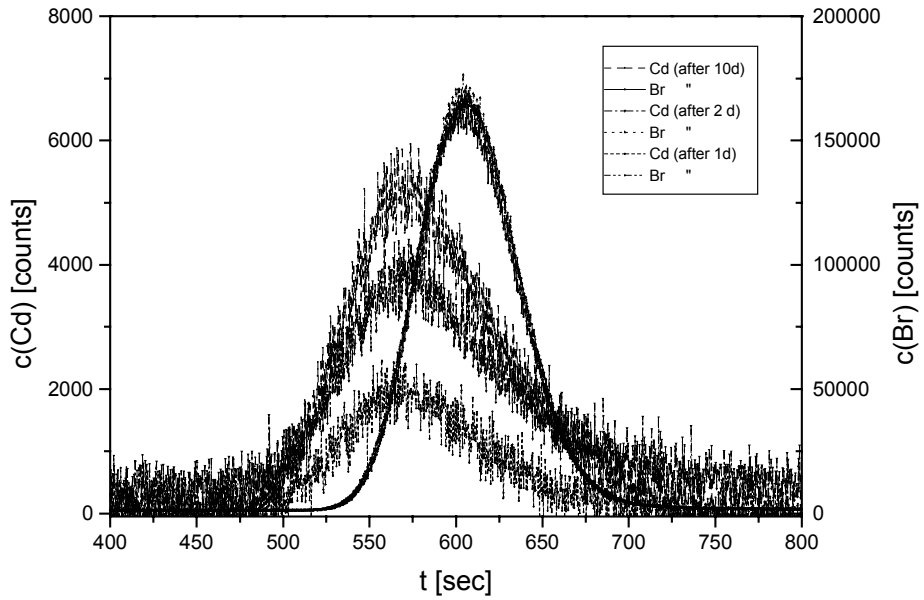

Fig. 29: Column experiments with Cd. Column packed with Merck sand (25 cm, ∅ = 1cm)
Flow: 0.83 ml/min
Detection: ICP-MS [Br, Cd] (simultaneously)
Eluent: c(HA) = 50 ppm; pH = 5.3 MES (1 mM); $NaClO_4$ (2 mM)
Injection: 0.5 ml Cd (1 ppm) (prepared in the eluent)

Due to the adsorption equilibrium on the sand surface, the major fraction of heavy metal ions is retained and desorbed after a longer period of time only. The peak observed for lead or cadmium thus represents only part of the entire heavy metal amount used. It is demonstrated by the experiments that more lead than cadmium is eluted at the same humic acid concentration. This finding may be explained by the complex-formation constants obtained for lead and cadmium humate. Lead has a complex-formation constant which is higher by an order of magnitude. Hence, more lead than cadmium is complexed by the humic acid.

Consequently, the heavy metal species detected represents a heavy metal humate. By complexation, the configuration of the humic acid molecules is changed. Instead of the long-chained configuration of the humic acid molecules due to repulsion under the given conditions, the addition of heavy metal ions results in the formation of pseudomicelles [Wan]. Due to the relatively small polarity of the pseudomicelles, they are eluted in a quasi-inert manner. Obviously, the kinetics of pseudomicelles formation influence the amount of heavy metal eluted at the inert time. The consequence is the increase in the peak height observed for

cadmium and lead with increasing equilibration time of the injected heavy metal/humate solution.

3.4.4 Column Experiments with Technetium

For the column experiments with technetium, the same experimental setup was applied except for the detection with ICP-MS. Now, a column constructed according to plans of the INE, Karlsruhe Research Center, was employed.

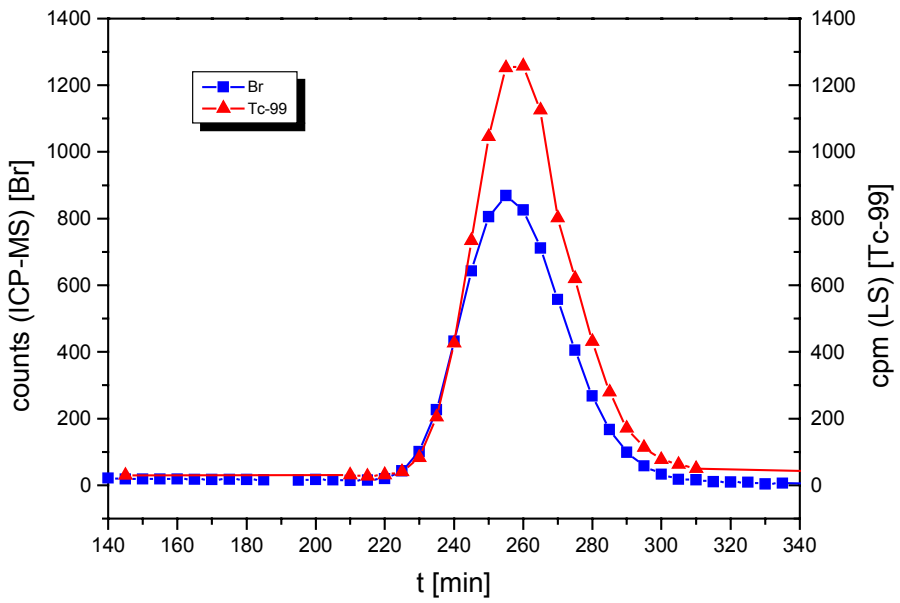

Fig. 30: Column experiment Tc-99. Column packed with Gorleben sand (25 cm, ∅ = 5 cm)
Flow: 0.83 ml/min
Detection: ICP-MS [Br] or LS [Tc]
Eluent: Gohy water 532
Injection: 0.8 ml NH_4TcO_4 solution (2.1 E-5 mol/l)

The inert peak obtained by the injection of a potassium bromide solution with the subsequent determination of the bromide content of the individual fractions occurs at about the same time than the technetium peak (Fig. 30). Technetium migrates through the column in an inert manner. No interaction between humic acid and Tc in the form of pertechnate was noticed. As the experiment was not performed under oxygen exclusion (e.g. argon atmosphere), redox processes were not found. Under reducing anaerobic conditions, a reduction of Tc(VII) to Tc(IV) takes place. During this, Tc is adsorbed on mineral solid phases [Kum]. In nature, the

reduction of Tc (VII) may be caused by surfaces containing Fe(II) (e.g. magnetite). With reduced technetium species, complexation with humic acid may take place [Sek].

4. Outlook

Within the framework of the project, a number of investigations were performed with regard to the characterization and fractionation of humic substances.

Size exclusion chromatography (SEC) of Aldrich humic acid yields a size distribution. Two components can be noticed in the chromatogram: A higher-molecular humic acid fraction with molecule sizes of about 150000 D and the major fraction with molecule sizes of about 3000 D. Capillary zone electrophoresis (CZE) also yields a distribution. By the use of a borate buffer and the addition of hydroxycarboxylic acids, a differentiated separation from Aldrich humic acid is obtained. Here, it is assumed to be caused by an esterification of the individual humic acid constituents. Characterization of metal humate complexes by CZE shows that loading with metal cations has considerable effects on the mobility distribution of the humates. Differentiation into strongly and less strongly loaded species takes place. Micellar electrokinetic chromatography (MEKC) illustrates the influence of metal ion loading on the hydrophily of the humic acid constituents. Coordination of heavy metal cations by the different functional groups of the humic acid leads to a decreasing hydrophily.

The dynamic character of the humic acids, which becomes obvious when interfering with the equilibrium by fractionation or electrophoretic methods, is of crucial importance to the understanding of humic acid chemistry. It also influences the complexation behavior with regard to heavy metal ions, which was shown in the column experiments with lead and cadmium. Hence, more detailed studies of the kinetics of complexation are required. The influence of competing ions under natural conditions shall then be taken into account. Also redox effects (e.g. of iron species) have to be investigated in more detail. Interactions with naturally occurring anions are significant with regard to the ligand exchange processes. It therefore appears to be necessary to study the influence of anionic components that may be suited as ligands in natural systems on the complexation behavior of humic acids.

The approaches of characterizing humic acid by means of CZE using a modified borate buffer and the separation into several components achieved show the influence of various functional

groups, which plays a crucial role in the complexation of heavy metals. In this respect, carboxyl and hydroxyl groups have to be mentioned above all. The influence of functional groups on the complexation may be determined by specific blocking of certain functional groups. Besides naturally occurring humic acids, a chemically modified synthetic humic acid produced by the Institut für Radiochemie (Institute of Radiochemistry) of the Rossendorf Research Center may be applied as model substance.

During the batch and column experiments with technetium of the oxidation state of +7, no interactions with the solid phase were observed. The influence of humic acids on sorption could also be neglected under the given conditions. In natural systems, however, a reduction of Tc(VII) to Tc(IV) may take place under reducing anaerobic conditions. Further experiments under other conditions are required.

5. References

[Bal] Balogh J.C., Gridal D.F., *Soil Sci.*, 1980, 130, 278

[Bar] Barger W.R., Mowery R.L., Wyatt J.R., *J. Chromatogr*., 1994, 680, 659-665

[Bec] Beckett R., Zhang J., Giddings J.C., *Environ. Sci. Technol*., 1987, 21, 289-295

[Beh] Behrens H., Klotz D., Lang H., et al., *Mater. Res. Soc. Symp. Proc*., 1982, 11, 783

[Bha] Bhat G.A., *Anal.Chem*., 1981, 53, 2275-2280

[Bur] Burba P., *Nachr. Chem. Tech. Lab*., 1998, 46 (4), 426-430

[Cho] Choppin G.R., *Radiochim. Acta*, 1988, 44/45, 23-28

[Dun] Dunkelog R., Rüttinger H.H., Peisker K., *J.Chromatogr*., 1997, *777*, 355-362

[Eng] Engelhard H., Beck W., Kohr J., Schmitt Th., *Angew. Chem.,* 1993, 105, 659-680

[Gid] Giddings J.C., *C & E News*, 1988, 66, 34-45

[Haa] Haase H.J., *Elektrochemische Stripping-Analyse*, Verlag Chemie, Weinheim 1996

[Kim1] Kim J.I., Czerwinski K.R., *Radiochim. Acta*, 1996, *73*, 5-10

[Kim2] Kim J.I., Buckau G., *Report RCM 02188*, 1988, Institut für Radiochemie, TU München

[Kum] Kumata M., Vandergraaf T.T., *Radiochemistry*, 39 (4), 313

[Lee] Lee Y.H., Lin T.I., *J. Chromatogr*., 1994, 675, 227-236

[Nie] Nießner R., *Nachr. Chem. Tech. Lab*., 1998, 46 (3), 302-314

[Ost] Osteryoung, J.G., Osteryoung R.A., *Anal. Chem.*, 1985, *57*, 101A

[Pal] Palmer D.A., Meyer R.E., *J. Inorg. Nucl. Chem*., 1981, 43, 2979

[Pin] Pinheiro J.P., *Anal. Chim. Acta*, 1994, 284, 525-537

[Pom] Pompe S., Heise K.H., Nitsche H., *J. Chromatogr*., 1996, *723*,215-218

[Rig] Rigol A., Lopez-Sanchez J.F., Rauret G., *J. Chromatogr*., 1994, *664*, 301-305

[Sch] Schmitt P., Kettrup A., Freitag D., Garrison A.W., *Fresenius J. Anal. Chem*., 1996, *354*, 915-920

[Sek] Sekine T., Watanabe A., Yoshihara K., Kim J.I., *Radiochim. Acta*, 1993, *63*, 87-90

[Ste] Stevenson F.J., *Humus chemistry*, J. Wiley & Sons, New York 1982, pp 337-354

[Ter] Terabe S., Otsuka K., Ichikawa A., Ando T., *Anal. Chem*., 1984, 56, 111

[Wag1] Wagner H., Blasius E*., Praxis der elektrophoretischen Trennmethoden*, Springer Verlag, Berlin / Heidelberg, 1989, pp 223-261

[Wag2] Wagner H., Neupert D., *J. Chromatogr*., 1978, 156, 219-224

[Wag3] Wagner H., Neupert D., *J. Chromatogr*., 1978, 147, 281-289

[Wan] von Wandruzka R., Ragle C., Engebretsen R., *Talanta*,1997, 44, 805-809

[Wang] Wang, J., *Stripping Analysis*, Verlag Chemie, Weinheim 1985

Appendix 3

Synthesis, radiometric determination of functional groups, complexation

S. Pompe, M. Bubner, K. Schmeide, K. H. Heise,
G. Bernhard, H. Nitsche

Institut für Radiochemie, Forschungszentrum Rossendorf e.V.

Abstract

The interaction behavior of humic acids with uranium(VI) and the influence of humic substances on the migration behavior of uranium was investigated. A main focus of this work was the synthesis of four different humic acid model substances and their characterization and comparison to the natural humic acid from Aldrich. A radiometric method for the determination of humic acid functional groups was applied in addition to conventional methods for the determination of the functionality of humic acids. The humic acid model substances show functional and structural properties comparable to natural humic acids. Modified humic acids with blocked phenolic OH were synthesized to determine the influence of phenolic OH groups on the complexation behavior of humic acids. A synthesis method for ^{14}C-labeled humic acids with high specific activity was developed.

The complexation behavior of synthetic and natural humic acids with uranium(VI) was investigated by X-ray absorption spectroscopy, laser-induced fluorescence spectroscopy and FTIR spectroscopy. The synthetic model substances show an interaction behavior with uranium(VI) that is comparable to natural humic acids. This points to the fact that the synthetic humic acids simulate the functionality of their natural analogues very well. For the first time the influence of phenolic OH groups on the complexation behavior of humic acids was investigated by applying a modified humic acid with blocked phenolic OH groups. The formation of a uranyl hydroxy humate complex was identified by laserspectroscopic investigations of the complexation of Aldrich humic acid with uranium(VI) at pH 7.

The migration behavior of uranium in a sandy aquifer system rich in humic substances was investigated in column experiments. A part of uranium migrates non-retarded through the sediment, bound to humic colloids. The uranium migration behavior is strongly influenced by the kinetically controlled interaction processes of uranium with the humic colloids.

The influence of humic acids on the sorption of uranium(VI) onto phyllite was investigated in batch experiments using two different humic acids. The uranium(VI) sorption onto the phyllite is influenced by the pH-dependent sorption behavior of the humic acids.

Zusammenfassung

Im Rahmen des Forschungsvorhabens wurde das Wechselwirkungsverhalten von Huminsäuren mit Uran(VI) sowie der Einfluß von Huminstoffen auf das Migrationsverhalten von Uran untersucht. Einen Schwerpunkt der Arbeiten bildete die Synthese von vier verschiedenartigen Huminsäuremodellsubstanzen sowie deren Charakterisierung im Vergleich zur natürlichen Huminsäure von Aldrich. Eine radiometrische Methode zur Bestimmung funktioneller Gruppen wurde neben herkömmlichen Methoden zur Bestimmung der Huminsäurefunktionalität eingesetzt. Die Modellhuminsäuren zeigen mit natürlichen Huminsäuren vergleichbare funktionelle und strukturelle Eigenschaften. Zur Bestimmung des Einflusses phenolischer OH-Gruppen auf das Komplexbildungsverhalten von Huminsäuren wurden modifizierte Huminsäuren mit blockierten phenolischen OH-Gruppen synthetisiert. Ein Syntheseverfahren für ^{14}C-markierte Huminsäuremodellsubstanzen mit hoher spezifischer Aktivität wurden entwickelt.

Das Komplexbildungsverhalten synthetischer und natürlicher Huminsäuren mit Uran(VI) wurde mittels Röntgenabsorptionsspektroskopie, laserinduzierter Fluoreszenzspektroskopie und FTIR-Spektroskopie untersucht. Es wurde nachgewiesen, daß die synthetischen Huminsäuremodellsubstanzen ein mit natürlichen Huminsäuren vergleichbares Wechselwirkungsverhalten gegenüber Uran(VI) zeigen und somit die Funktionalität der natürlichen Analoga gut simulieren. Erstmals wurde unter Verwendung einer modifizierten Huminsäure der Einfluß phenolischer OH-Gruppen auf das Komplexbildungsverhalten von Huminsäuren untersucht. Im Rahmen von laserspektroskopischen Untersuchungen zur Komplexierung von Aldrich Huminsäure mit Uran(VI) bei pH 7 wurde die Bildung eines Uranylhydroxyhumat-Komplexes nachgewiesen.

Das Migrationsverhalten von Uran in einem sandigen huminstoffreichen Grundwasserleiter wurde in Säulenexperimenten untersucht. Ein Teil des Urans wird ungehindert, huminstoffgebunden durch das Sediment transportiert. Das Migrationsverhalten von Uran wird stark durch kinetisch kontrollierte Wechselwirkungs-prozesse mit den Huminstoffkolloiden beeinflußt.

Der Einfluß von Huminsäuren auf die Sorption von Uran an Phyllit wurde in Batchexperimenten mit zwei verschiedenen Huminsäuren untersucht. Die Sorption von Uran an Phyllit wird durch das vom pH-Wert abhängige Sorptionsverhalten der Huminsäuren beeinflußt.

Content

1 Introduction

The study of the migration behavior of radioactive and toxic metal ions in the environment is important for long-term risk assessment of potential nuclear waste repositories, of facilities of the former uranium mining and milling in Saxony and Thuringia, and of subsurface dumps and sites with radioactive and/or heavy metal-containing inventory. The behavior of such pollutants is strongly influenced by humic substances.

Humic substances are ubiquitous, polyelectrolytic organic macromolecules. They are formed by the decomposition of biomass. Because of the multitude on precursor substances the formation process of humic substances can not be described by simple chemical or biochemical reactions. Depending on their origin humic substances show different structural and functional properties. This leads to the fact that humic substances show a great structural and functional heterogeneity which causes difficulties in the description of their chemical properties. Humic substances can be divided by an operational definition into three fractions [1]. Humin represents the fraction of humic substances which is insoluble at all pH values, whereas the humic acid fraction is soluble at pH values greater than pH 3.5 and the fulvic acid fraction is soluble at all pH values.

Humic acids play a decisive role within natural interaction processes because of their good solubility in the pH range of natural waters and because of their high complexing capacity. For instance, due to their high complexing capacity, humic acids influence the speciation of metal ions, e.g., actinides, and therefore, the migration and/or immobilization of this pollutants in the environment. Due to their complicated and heterogeneous nature, a thermodynamically based description of the complex formation of humic acids with metal ions is difficult but nevertheless important. There are different thermodynamic models describing the complexation behavior of humic acids. However, these models differ from each other in the definition of the complexation reaction and of the humic acid ligand concentration. Moreover, the existing database for the interaction between metal ions and humic acids is incomplete, especially for actinides in the pH and concentration range of natural systems.

It was the scope of this project to improve the knowledge about the interaction of metal ions with humic acids under natural conditions. For this purpose model substances for humic acids were developed to investigate the humic acid complexation with well-defined substances. Applying natural and synthetic humic acids, studies concerning the interaction process metal

ion - humic acid were performed and thermodynamic data were determined. In addition, migration and sorption studies under conditions close to the nature were carried out. Such information are essential to allow more precise geochemical modeling for the migration of radioactive and toxic metal ions in the environment in the presence of humic acids.

Within the framework of this project the research program of the Institute of Radiochemistry of the Forschungszentrum Rossendorf included the following main topics:

1. The development of synthesis procedures for the preparation of humic acids with defined properties and their labelling with ^{13}C or ^{14}C. Synthetic humic acids were to be provided to the project partners.
2. The radiometric determination of functional groups of synthetic and natural humic acids and their selective blocking by methylation and/or acetylation. Functional groups should be blocked by selective chemical reactions to determine their contribution to the complexation behavior of humic acids with metal ions.
3. The investigation of the complexation behavior of uranium in humic acid-containing solutions above pH 4.
4. First studies regarding the sorption of uranium - humic acid - complexes onto relevant sediment materials.

This research project was performed in cooperation with a R&D-project of the Universities of Mainz and Saarbrücken funded by BMBF (contract number: 02 E 8795 8).

2 Model substances for humic acids

To gain a more basic knowledge about the influence of humic acids on the speciation of metal ions in the environment, especially about the interaction process between humic acid and radionuclides, it is necessary to perform model investigations with well-defined humic acid model substances [2]. Compared to natural humic acids such model substances should be characterized by comparable chemical and operational properties. However, they should show a higher homogeneity, a simpler overall structure and a well defined functionality compared to their natural analogues. The synthesis of such model substances should be easy and reproducible. Furthermore, the model substances should offer the possibility for well-defined variations in their functionality and for a defined isotopic labelling (^{13}C, ^{14}C). Model

substances for the investigation of the interaction between humic acids and metal ions should be characterized by a functionality comparable to natural humic acids [3].

Low-molecular organic substances, e.g., salicylic acid and malonic acid, which were identified as structural elements of natural humic acids are potential functional models for humic acids. These substances are useful to investigate elementary processes of the humic acid behavior, e.g., the interaction of such structural elements with metal ions. However, these monomeric substances are not sufficient to precisely describe the overall behavior of the polymeric humic acids because they are highly ordered in contrast to natural humic acids.

Furthermore, synthetic humic acid-like polymers, e.g., humic acid-like melanoidin fractions [3] or condensation products of phenolic compounds [4] can be used as humic acid model substances. Within the scope of this project, we synthesized humic acid-like melanoidins, condensation products of reducing sugars and α-amino acids, as functional models for humic acids.

2.1 Melanoidins as humic acid model substances with defined properties

Melanoidins are formed by condensation of reducing sugars and amino acids, peptides or proteins [5-8]. They play a special role in many natural processes. Their formation is considered as one possible way for the formation of humic substances in the environment [9].

Melanoidins represent a mixture of different polymers that can be operational separated into a humin-like, humic acid- and fulvic acid-like fraction because of their different solubility at different pH values. It was shown [3,10] that humic acid-like melanoidin fractions, which were obtained from the whole melanoidin by alkaline dissolution and acid precipitation, show chemical properties comparable to natural humic acids.

Melanoidins are especially suitable as functionality models for humic acids because they show both structural and also functional similarities with natural humic acids. In contrast to the condensation products of phenolic compounds they contain aliphatic nitrogen and they offer many possibilities to vary their structural and functional properties by selective variations of their precursor substances [3]. For instance, it is possible to increase the number of carboxylic groups by using amino dicarboxylic acids as precursor substance or to change the amount of aromatic or aliphatic structural elements by using aromatic or aliphatic amino acids. In addition, it is possible to change the elemental composition of the synthetic humic acids [3]. All of that offer the possibility to investigate the influence of different functional groups or structural elements on the chemical behavior of humic acids, for instance the

complexation behavior with metal ions. Furthermore, the synthesis of melanoidins starting from isotopically labelled precursor substances enables us to synthesize stable isotopically labelled humic acids with high specific activity.

3 General description of the synthesis of humic acid-like melanoidins

The synthesis of humic acid model substances is based on the preparation of a "standard melanoidin" by Enders and Theis [6]. The synthesis of humic acid-like melanoidins is carried out starting from a mixture of α-amino acid, sugar and water. This mixture is heated temperature- and time-controlled under reflux in a nitrogen stream. During the reaction a solid, dark brown, polymeric substance is formed. This solid is separated from the solution by centrifugation. From the solid phase the humic acid-like fraction is extracted with NaOH and then precipitated with HCl (pH < 3). The humic acid precipitate is centrifuged, washed, dialyzed against purified water using dialysis tubes (Thomapor®, exclusion limit MWCO < 1000, Reichelt Chemietechnik, Heidelberg, Germany), and then lyophilized.

Within this project four different types of synthetic humic acid were developed. The precursor substances, i.e., α-amino acids and sugars, as well as their quantitative proportions were varied depending on the aspired humic acid functionality. The used precursors, their proportions and special requirements of the synthesis are summarized in the paragraphs which deal with the synthesis and characterization of the specific humic acid type.

4 Purification of natural humic acid reference materials

The commercially available natural humic acid from Aldrich (Aldrich, Steinheim, Germany) was used as reference material. It was purchased in its sodium humate form (charge H1, 675-2).

The natural humic acid was purified according to the purification method described by Kim and Buckau [11]. The sodium humate was dissolved in 0.1 M NaOH + 0.01 M NaF and stirred over night under nitrogen atmosphere. Then, the solution was centrifuged. The supernatant was acidified with HCl to pH 1. The humic acid precipitate was washed several

times with 0.1 M HCl. The whole procedure was repeated three times. The precipitate was then lyophilized.

Furthermore, the commercially available natural humic acid from Fluka (Fluka, Neu-Ulm, Germany) was used as reference material for some investigations. The purification method of Fluka humic acid, based on alkaline dissolution and acid precipitation with HCl, is described in detail elsewhere [10].

5 Radiometric determination of functional groups by derivatization with [^{14}C]diazomethane

The radiometric determination of functional groups [12] is an alternative method for the characterization of humic acids regarding their functional group content. This method bases on the derivatization of carboxylic and phenolic OH groups with [^{14}C]diazomethane by esterification and etherification, respectively. The number of methylated functional groups of the humic acid can be determined precisely by measuring the specific activity of the reaction product and comparison with the specific activity of the [^{14}C]diazomethane. The differentiation between carboxylic and phenolic OH groups is accomplished by the alkaline saponification of methyl esters, whereby the phenolic ethers remain blocked as methyl ethers.

The advantage of this method is the possibility to distinguish between phenolic OH groups and carboxylic groups because of the different behavior of ethers and esters in alkaline solutions. In contrast to potentiometric methods this method represents a procedure for the characterization of the humic acid functionality which is independent of the pKa values of the functional groups.

Fig. 5.1 shows the reaction scheme for the radiometric determination of carboxylic, phenolic OH and ester groups.

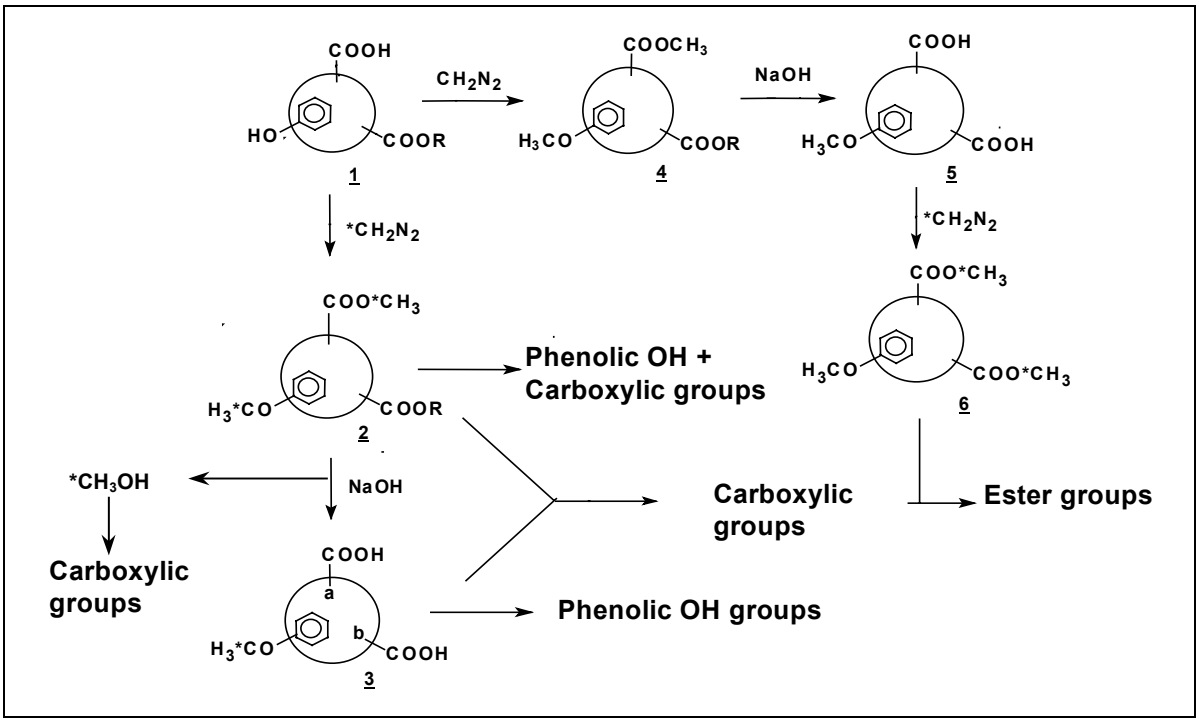

Figure 5.1: Radiometric determination of humic acid functional groups (*C = ^{14}C) [12].

During the first reaction step phenolic OH and carboxylic groups are methylated simultaneously with [^{14}C]diazomethane (cf. Fig. 5.1, (2)). The total number of methylated groups, i.e., carboxylic and phenolic OH groups, in the humic substance is derivable from the specific activity of the reaction product (2) in connection with the specific molar activity of the radioactive reagent. In the next reaction step the carbonic methyl esters of the carboxylic groups are hydrolyzed by alkaline saponification of the methylation product. The phenolic OH groups remain blocked as methyl ethers (3). The resulting specific activity of the humic acid (3) represents the amount of phenolic OH groups of the humic acid. The number of carboxylic groups can be calculated from the total activity of [^{14}C]methanol that is released during the saponification process ($^{14}CH_3OH$) and the specific activity of the used radioactive reagent ([^{14}C]diazomethane). The specific activity of the released methanol is equivalent to the number of hydrolyzed [^{14}C]methyl ester groups. In addition, the number of carboxylic groups can be determined by subtracting the number of phenolic OH groups (3) from the total number on methylated groups (2).

The original ester groups of the humic acid are hydrolyzed simultaneously during the saponification of the methyl esters. This effect can be used for the determination of the ester groups in the original humic acid. For this determination the humic acid is methylated with inactive diazomethane in the first derivatization step and than saponified with NaOH,

resulting in a blocking of the phenolic OH groups and a hydrolysis of the original ester groups of the humic acid (4,5). Following, the humic acid is methylated with [^{14}C]diazomethane. The specific activity of the reaction product (6) represents the sum of all carboxylic groups of the humic acid, i.e., the initial carboxylic groups as well as the hydrolyzed original ester groups. The difference between this amount and the number of carboxylic groups represents the number of ester groups in the original humic acid.

However, acidic hydroxyl groups which are substituted to five-membered heterocycles or other H-acidic hydroxyl groups, may also be methylated by [^{14}C]diazomethane beside phenolic OH groups. The resulting [^{14}C]methyl ether groups are also not hydrolyzable. Hence it follows, that these acid hydroxyl groups are determined together with phenolic OH groups, which leads to an overevaluation of the number of phenolic OH groups.

Disadvantages exist in the occurrence of secondary reactions which may occur during the methylation, e.g., the methylation of aldehyde, keto and amino groups. Such secondary reactions may cause an overestimation of the sum of carboxylic and phenolic OH groups. The determination of carboxylic groups is not influenced by such reactions, if the methanol which is released during the saponification is used for their quantification. Further sources of errors are secondary reactions caused by UV light and metal catalysts as well as the many required operations, especially weightings, during the analytical process. However, the extent of these errors can be minimized.

6 Synthesis and characterization of humic acids

The objective of the synthesis of humic acids was to prepare model substances which show operational properties comparable to natural humic acids, a defined functionality and a higher chemical homogeneity than natural humic acids.

The following paragraphs show the synthesis and characterization of four different humic acids:

- a humic acid with a low content of carboxylic groups and a high amount of aromatic structural elements (Type M1, [10]),
- a humic acid type M1 with an ultra high purity,
- a humic acid with a carboxylic group content comparable to most natural humic acids (Type M42), and
- a nitrogen-free humic acid.

The characterization of the synthetic humic acids was performed in comparison to Aldrich humic acid as reference material.

6.1 Synthesis of humic acid type M1 with a low content of carboxylic groups and a high amount of aromatic structural elements

6.1.1 Synthesis

Synthetic humic acid type M1 (charge R36/95) was synthesized from a mixture of 34 g xylose (Merck, Darmstadt, Germany), 10 g phenylalanine (Merck), 5 g glycine (Merck) and 80 mL water (Fig. 6.1). This mixture was refluxed in a nitrogen stream for 10 hours.

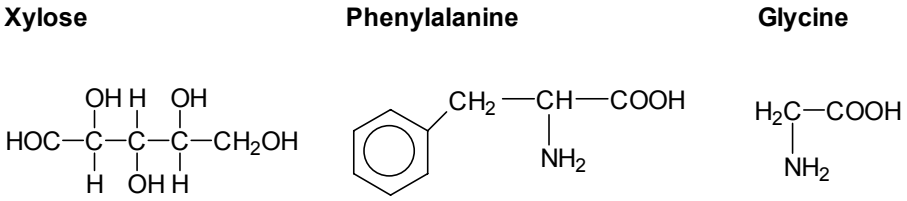

Figure 6.1: Precursor substances of humic acid type M1.

The reaction product was washed and then ground with ethanol (Merck) and ether (Merck). Subsequently, the product was shaken with 2 M NaOH (Merck) for 24 hours under inert gas. After centrifugation the supernatant was acidified with 2 M HCl (Merck) to pH < 3. The resulting humic acid precipitate was washed, dialyzed against purified water using dialysis tubes (Thomapor®, exclusion limit MWCO < 1000), and lyophilized. The synthesis was repeated five times. The total yield of synthetic humic acid amounts to 90 g.

This synthetic humic acid was handed out to all project partners for comparative studies and to establish similar experimental conditions for further investigations.

6.1.2 Characterization

Elemental analysis

The results of the elemental analysis for humic acid type M1 and Aldrich humic acid are summarized in Tab. 6.1. in comparison to literature values. The values were corrected considering the moisture and ash content of both humic acids.

Table 6.1: Elemental composition of synthetic humic acid type M1 in comparison to natural humic acids.

Element / (%)	Synthetic humic acid type M1 (charge R36/95)	Aldrich humic acid (charge A2)	Literature [13]
C	63.92 ± 0.72	54.47 ± 1.42	50 – 60
H[a]	4.75 ± 0.26	3.82 ± 0.14	4 – 6
N	5.34 ± 0.07	0.75 ± 0.04	2 - 6
S	-	3.80 ± 0.10	0 – 2
O[b]	22.51 ± 0.53	29.26 ± 1.53	30 – 35
Ash content / (%)	0.7	3.7	-
Moisture content / (%)	2.8	4.2	-

[a] Corrected for water content of the humic acid. [b] The oxygen content was calculated from the difference to 100 %.

The synthetic product exhibits an elemental composition that is close to literature values for natural humic acids of different origins. Contrary to Aldrich humic acid the synthetic product contains no sulfur due to the use of sulfur-free amino acids. The synthetic product has a higher amount of carbon and nitrogen and a slightly lower oxygen content than Aldrich humic acid.

The elemental composition of the synthetic humic acids, e.g., the nitrogen or sulfur content, could be modified by varying the precursor substances as well as their proportions.

Inorganic constituents

Tab. 6.2 summarizes the amount of inorganic constituents of synthetic humic acid type M1 in comparison to Aldrich humic acid.

Table 6.2: Inorganic main constituents of synthetic humic acid type M1 in comparison to the purified Aldrich humic acid.

Element / (ppm)	Synthetic humic acid type M1	Aldrich humic acid
Na	2451 ± 698	2465 ± 418
Mg	206 ± 104	10 ± 5
Al	204 ± 179	78 ± 9
Si	205 ± 128	372 ± 187
Ca	886 ± 604	126 ± 95
Fe	**< 250**	**3651 ± 224**

As expected, the synthetic humic acid has only a low amount of inorganic impurities. The inorganic impurities that are present in the synthetic product may be caused by the precursor materials applied and by the glassware used. The high sodium content is due to an incomplete sodium elimination by dialysis.

Contrary to the purified Aldrich humic acid and other natural humic acids, which always contain non-removable iron, the synthetic humic acid shows a smaller amount of iron. The iron which is non-removable bound to natural humic acids can compete to other metal ions, e.g., in experiments investigating the complexation behavior of humic acids with metal ions. This might lead to incorrect results. Thus the low iron content of synthetic humic acids represents a great advantage of these products compared to natural humic acids, when they are used for model investigations.

Functional groups

Tab. 6.3 shows the functional group content of synthetic humic acid type M1 and Aldrich humic acid in comparison to literature data [14]. The synthetic humic acid has fewer functional groups than Aldrich humic acid. Particularly the amount of carboxylic groups, which are the most important functional groups for the protolysis and complexation behavior of humic acids, is smaller than in Aldrich humic acid. However, other natural humic acids having low amounts of functional groups and comparable low amounts of carboxylic groups like humic acid type M1 have been reported in the literature [14].

Table 6.3: Functional groups of synthetic humic acid type M1 (charge R36/95) compared to the natural humic acid from Aldrich (charge A2) and to literature data of additional natural humic acids.

Functional groups / (meq/g)	Radiometric determination		Calcium acetate exchange		Barium hydroxide method		Direct titration		Literature [14]
	Type M1	Aldrich	Type M1	Aldrich	Type M1	Aldrich	Type M1	Aldrich	Natural
COOH + phenolic OH	3.6 ± 0.1	6.9 ± 0.7	-	-	3.04 ± 0.93	7.45 ± 0.29	-	-	5.6 – 8.9
COOH	1.3 ± 0.1	4.0 ± 0.4	1.02 ± 0.06	4.74 ± 0.05	-	-	-	-	1.5 – 5.7
phenolic OH	2.3 ± 0.1	3.2 ± 0.7	-	-	2.02 ± 0.99[b]	2.71 ± 0.34[b]	-	-	2.1 – 5.7
PEC [a]	-	-	-	-	-	-	1.36 ± 0.08	5.33 ± 0.12	-

[a] PEC = Proton exchange capacity.
[b] Calculated from the difference between the total acidity determined by the barium hydroxide method and the carboxylic group content determined by the calcium acetate exchange method.

Capillary electrophoresis

Fig. 6.2 depicts the electropherograms of synthetic humic acid type M1 and purified Aldrich humic acid. The electropherograms are different. Aldrich humic acid shows superimposed peaks that were also present in other natural humic acids [15]. We assume that this is due to the presence of several individual humic acid fractions with different charge-to-size-ratios. Synthetic humic acid type M1 shows only one peak in the electropherogram. From this, we conclude that our synthetic product is more homogeneous (smaller charge-to-size-ratio distribution) than the natural humic acid. Furthermore, the synthetic product shows a shorter migration time compared to Aldrich humic acid. This can be explained by a smaller charge-to-size-ratio of humic acid type M1 caused by a larger molecular size and a smaller number of dissociated functional groups, which are the charge carriers of the humic acid. Its relatively smaller number of dissociated functional groups corresponds to its lower total amount of functional groups. The larger molecular size of the synthetic product was determined by size exclusion chromatography.

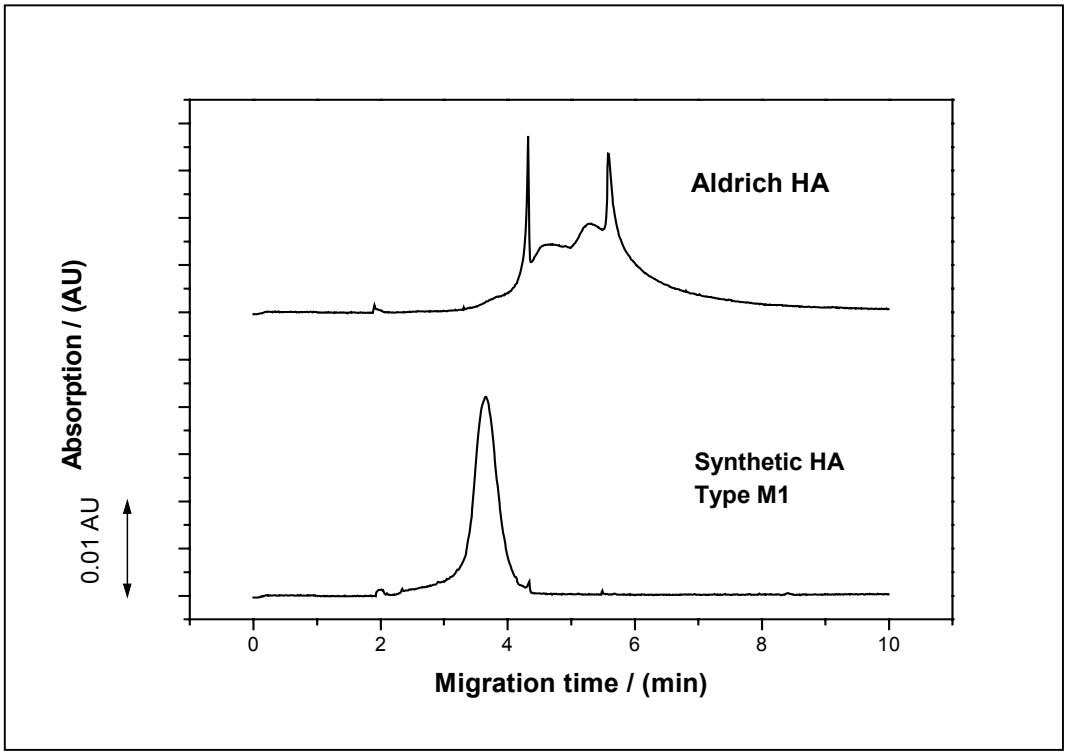

Figure 6.2: Capillary electropherograms of synthetic humic acid (HA) type M1 and purified Aldrich humic acid. Separation conditions: buffer KH_2PO_4 (3 mM) - $Na_2B_4O_7$ (6 mM), pH 8.9; fused silica capillary 75 µm i.d. x 50 cm effective length, 57 cm total length; separation voltage 30 kV; temperature 30 °C; 15 s pressure injection; detection wavelength 214 nm.

FTIR spectroscopy

Fig. 6.3 shows the FTIR spectra of synthetic humic acid type M1 and Aldrich humic acid. In general synthetic humic acid type M1 shows IR absorption bands which are characteristic for natural humic acids [9,16]. Both humic acids differ in their aromatic and aliphatic carbon content. The synthetic product exhibits a greater amount of mono-substituted aromatic carbon structures than Aldrich humic acid, which is indicated by the IR absorption bands at 700 cm^{-1} and 750 cm^{-1}. These structural elements are caused by the use of phenylalanine as precursor substance. Aldrich humic acid possesses a higher content of aliphatic structural elements indicated by the higher intensities of the corresponding absorption bands at 2920 cm^{-1} and 2850 cm^{-1}.

Furthermore, the FTIR spectra point to the higher carboxylic group content of Aldrich humic acid in contrast to synthetic humic acid type M1. The IR absorption band at 1720 cm^{-1} which corresponds to carboxylic groups is stronger pronounced in the spectrum of Aldrich humic acid. This result corresponds to the result of the functional group determination (Tab. 6.3).

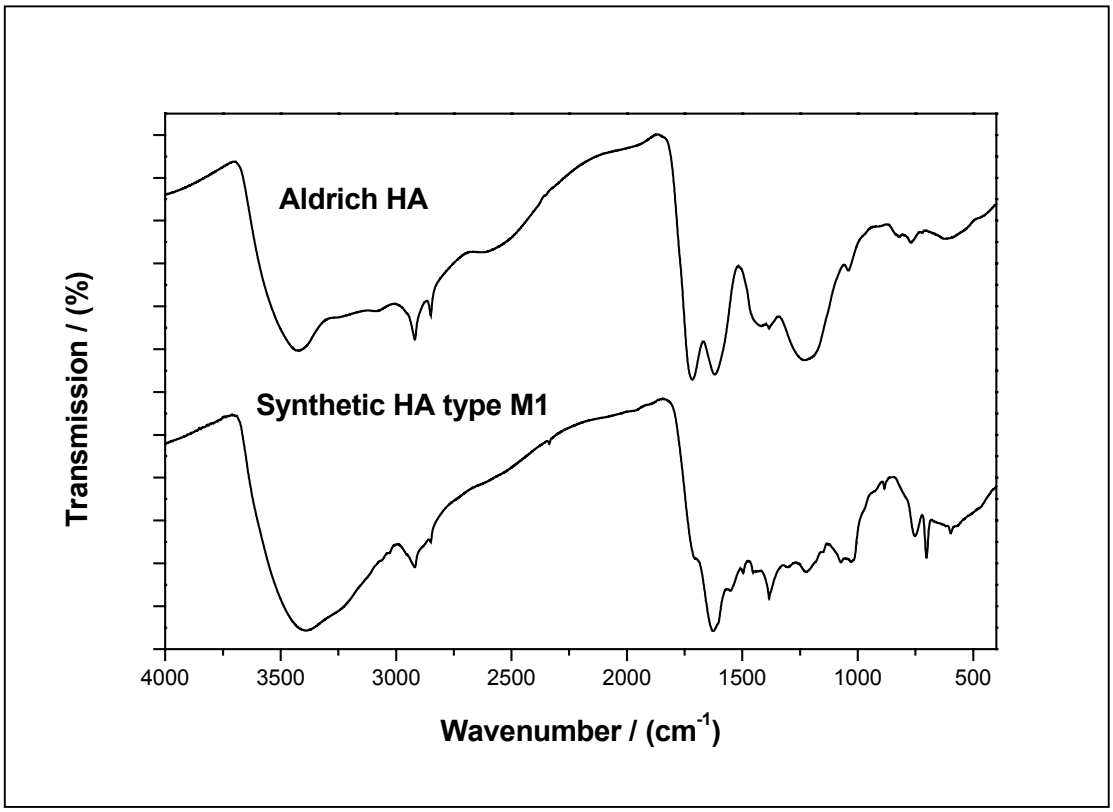

Figure 6.3: FTIR spectra of synthetic humic acid type M1 and Aldrich humic acid.

^{13}C-CP/MAS-NMR-spectroscopy

Fig. 6.4 shows the ^{13}C-CP/MAS-NMR spectrum of synthetic humic acid type M1. The spectrum shows ^{13}C chemical shifts which are characteristic for humic acids [9,17,18]. This result points to structural and functional similarities between the synthetic product and natural humic acids and agrees with the FTIR results.

The spectrum of the synthetic humic acid shows an intensive resonance signal at 129 ppm, corresponding to mono-substituted aromatics due to the use of phenylalanine as precursor substance. The small half-width of this signal indicates similar aromatic structural elements and/or free-movable aromatic end groups. The diffuse, not well-resolved resonance signals can be attributed to aliphatic carbon (20-50 ppm) and aliphatic C-O groups (60-90 ppm). The width of these signals indicates a high heterogeneity and/or a rigid binding of these structural elements. The weak signal at 172 ppm is caused by carboxylic-, ester- and amide groups. A differentiation between these functional groups is not possible with this spectrum. The resonance signals at 110 and 150 ppm indicate the presence of phenolic structural elements.

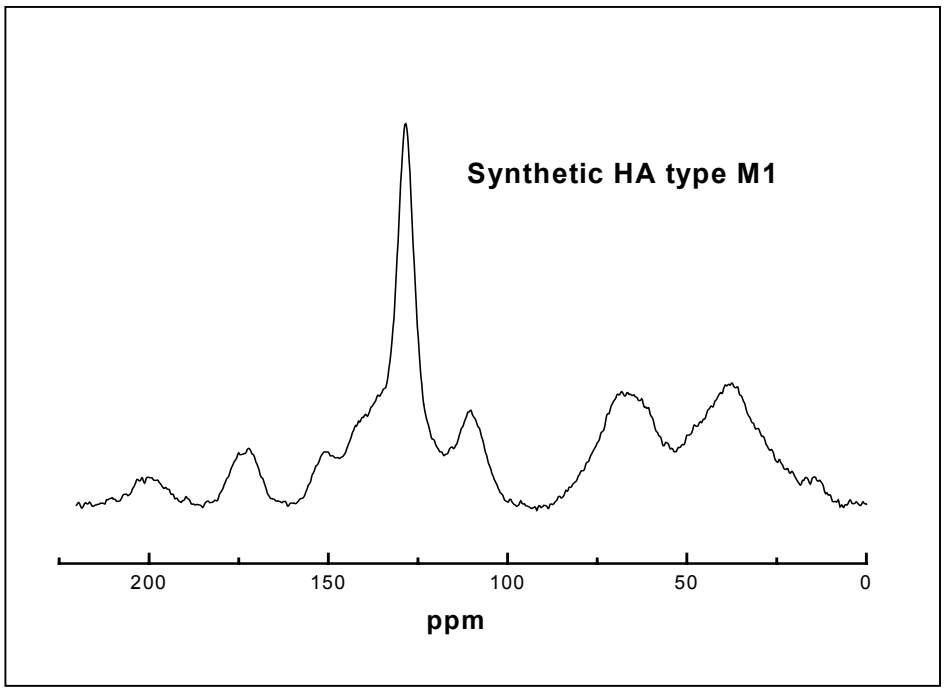

Figure 6.4: ^{13}C-CP/MAS-NMR spectrum of synthetic humic acid type M1.

The ^{13}C-CP/MAS-NMR spectrum of Aldrich humic acid is not shown because this spectrum is hampered by the relatively large concentration of residual iron, which could not be separated during the purification of the humic acid.

Pyrolysis-Gas chromatography/Mass spectrometry (Py-GC/MS)

The pyrolysis gas chromatograms of synthetic humic acid type M1 and Aldrich humic acid are depicted in Fig. 6.5 a and 6.5 b, respectively. The dominant carbon dioxide peaks are due to decarboxylation reactions, mainly of carboxylic groups. The difference in the peak intensities between the synthetic humic acid and Aldrich humic acid corresponds to the analysis of the carboxylic group concentration.

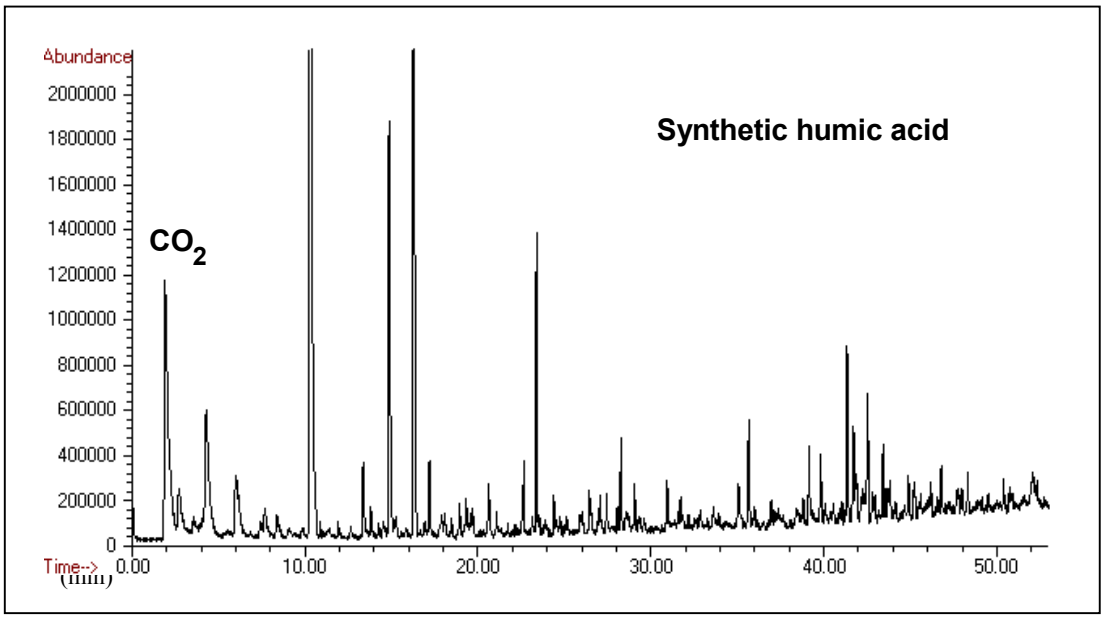

Figure 6.5 a: Pyrogram of synthetic humic acid type M1.

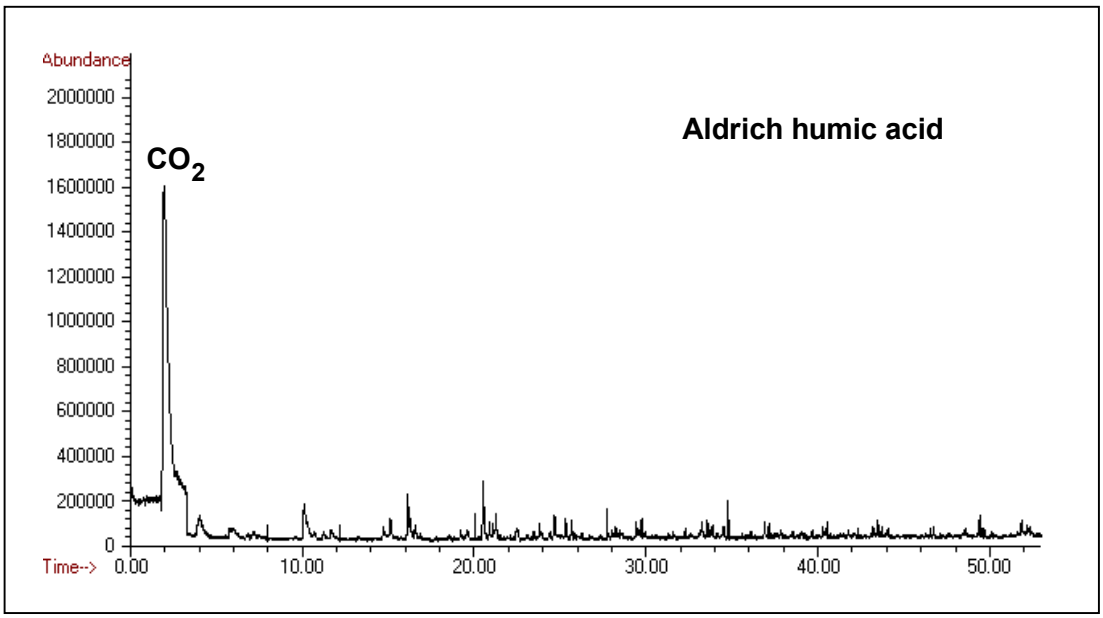

Figure 6.5 b: Pyrogram of the natural humic acid from Aldrich.

The pyrogram of synthetic humic acid type M1 shows intensive peaks in the range between 4 and 12 minutes originating from aromatic fragments such as, for example, benzene, toluene, ethyl benzene, and styrene. These organic structures are due to the use of phenylalanine for the synthesis. Such fragments are also present in the pyrogram of Aldrich humic acid but to a lesser extent. Aldrich humic acid shows a large number of aliphatic pyrolysis fragments, i.e., alkanes and alkenes up to C_{21}, detected between 20 and 50 minutes retention time, which were not detected for the synthetic product type M1.

The pyrolysis fragments of synthetic humic acid type M1 consist of several nitrogen-containing components. Thus, we identified aromatic amines, e.g., 2-aminonaphthalene and N-methyl-N-phenylbenzylamine, as well as substitution products of pyridine, e.g., 3-phenylpyridine and 4-phenyl-N-methylpyridine. Again, this structural elements can be explained by the use of phenylalanine as a synthesis precursor. The pyrogram of Aldrich humic acid did not show any nitrogen-containing product because of its low nitrogen content (0.7 %).

6.2 Synthesis of humic acid type M1 with an ultra high purity

As already mentioned above natural humic acids, e.g., Aldrich humic acid, contain a considerable quantity of non-removable bound inorganic elements, especially iron, which can influence the structure and functionality of humic acids and which can compete to other metal ions during complexation processes. A great advantage of the synthetic humic acids is there low content on inorganic impurities, especially iron. The use of these substances offers the possibility to minimize or to exclude competition reactions during basic studies of the complexation behavior of humic acids with metal ions.

Although synthetic humic acid type M1 shows a lower iron content than Aldrich humic acid, it still contains inorganic impurities resulting from chemicals and glassware applied during the synthesis (cf. Tab. 6.2). To reduce the amount of inorganic impurities of the synthetic product we developed a special synthesis method for extremely pure humic acid type M1.

Based on the synthesis described in 6.1.1 we synthesized a humic acid type M1 using highly purified precursors and likewise ultra pure auxiliaries, e.g., highly purified water, hydrochloric acid$_{(min)}$ (Merck) and sodium hydroxide (Merck) solution. The synthesis was carried out in a apparatus made of Teflon.

6.2.1 Characterization

As a result of the „high-purity“ chemistry the amount of inorganic impurities of the humic acid was strongly reduced in comparison to the conventional synthesis. Iron was not detectable in the humic acid fractions. Furthermore, the content of other inorganic constituents was partially reduced by a factor of 10 to 100 and reaches the range of the detection limit. The ash content of this humic acid amounts to < 0.05 %.

The ultra pure synthetic humic acid type M1 shows a somewhat higher content of carboxylic and phenolic OH groups than synthetic humic acid type M1 synthesized by the conventional method (cf. Tab. 6.3). The carboxylic group content determined by calcium acetate exchange amounts to 1.36 ± 0.08 meq/g and the radiometric determined content of phenolic OH groups amounts to 2.5 ± 0.3 meq/g. This result points to the fact, that inorganic impurities of the conventional humic acid type M1 may influence the humic acid functionality by masking functional groups.

Investigations by FTIR spectroscopy show that the ultra pure humic acid of type M1 shows a comparable structure to the conventional humic acid of type M1. FTIR spectra of both humic acids are depicted in Fig. 6.6.

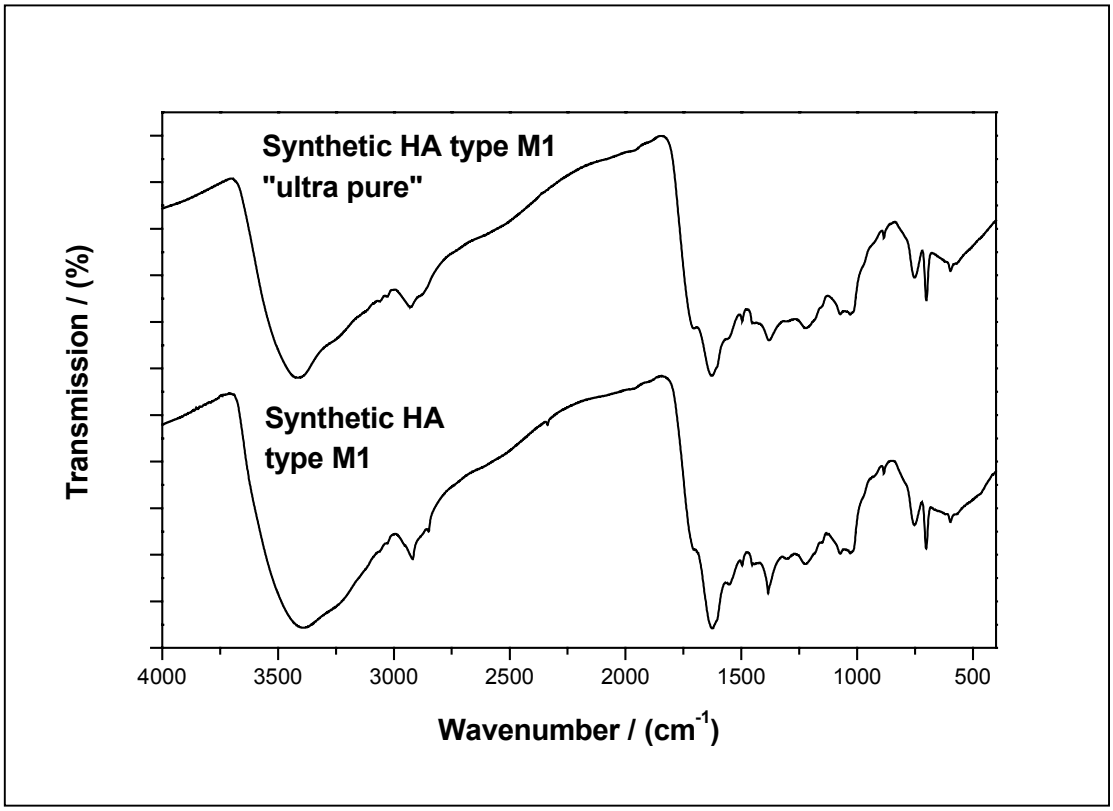

Figure 6.6: FTIR spectra of synthetic humic acid type M1 synthesized by the conventional method and by a special synthesis method for ultra pure humic acids.

6.3 Synthesis of humic acid type M42 with a carboxylic group content comparable to most natural humic acids

In order to simulate the functionality of most natural humic acids, it is necessary to synthesize humic acids with higher amounts of functional groups, especially carboxylic groups compared to synthetic humic acid type M1. Thus we developed a synthesis method for a humic acid with a higher amount of carboxylic groups.

6.3.1 Synthesis

A mixture of 22 g DL-glutamic acid monohydrate (Fluka), 33.3 g xylose (Merck), and 60 mL water was continuously heated for 90 hours at 80 ± 2 °C under reflux and inert gas. The precursor substances are depicted in Fig. 6.7.

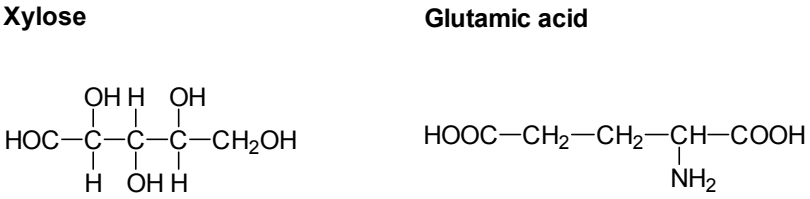

Figure 6.7: Precursor substances of synthetic humic acid type M42.

During the reaction a dark-brown solid and solution were formed. After centrifugation the solid reaction product was ground with ethanol (Merck) and ether (Merck), and then again centrifuged. The solid product was stirred with 150 mL 2 M NaOH (Merck) for 8 hours under inert gas. After centrifugation the remaining solid product was stirred once more with 100 mL 2 M NaOH for 8 hours under inert gas. The alkaline solution, containing the humic acid-like melanoidin fraction, was acidified with 2 M HCl (Merck). The resulting precipitate was washed, dialyzed using dialysis tubes (Thomapor®, exclusion limit MWCO <1000) against purified water, and then lyophilized.

This synthesis was repeated four times. The synthesis products were combined. The yield amounts to 25 g synthetic humic acid type M42 (charge M81).

6.3.2 Characterization

Elemental analysis

The elemental composition of synthetic humic acid type M42 (charge M81), summarized in Tab. 6.4, is comparable to natural humic acids. Differences in the nitrogen and sulfur content compared to Aldrich humic acid are attributed to the precursor substances of the synthetic product.

Table 6.4: Elemental composition of synthetic humic acid type M42 (charge M81) in comparison to natural humic acids.

Element / (%)	Synthetic humic acid type M42 (charge M81)	Aldrich humic acid (charge A2)	Literature [13]
C	58.41 ± 0.53	54.47 ± 1.42	50 - 60
H[a]	4.30 ± 0.22	3.82 ± 0.14	4 - 6
N	4.54 ± 0.12	0.75 ± 0.04	2 - 6
S	-	3.80 ± 0.10	0 - 2
O[b]	27.24 ± 0.53	29.26 ± 1.53	30 - 35
Ash content / (%)	0.3	3.7	-
Moisture content / (%)	5.2	4.2	-

[a] Corrected for water content of the humic acid. [b] The oxygen content was calculated from the difference to 100 %.

Inorganic constituents

The inorganic main constituents of synthetic humic acid type M42 are summarized in Tab. 6.5 in comparison to Aldrich humic acid.

Comparable to synthetic humic acid type M1 humic acid type M42 has only a low amount of inorganic impurities. A great advantage of the synthetic product is the low iron content compared to Aldrich humic acid.

Functional groups

The results of the functional group analysis with different methods are comprised in Tab. 6.6. Due to the fact that this humic acid does not form an insoluble barium salt, the barium hydroxide method for the determination of the total acidity was not applied.

Table 6.5: Inorganic main constituents of synthetic humic acid type M42 in comparison to the purified Aldrich humic acid.

Element / (ppm)	Synthetic humic acid type M42 (charge M81)	Aldrich humic acid (charge A2)
Na	1393 ± 151	2465 ± 418
Mg	19 ± 9	10 ± 5
Al	38 ± 16	78 ± 9
Si	86 ± 40	372 ± 187
Ca	815 ± 357	126 ± 95
Fe	**< 20**	**3651 ± 224**

Table 6.6: Functional groups of synthetic humic acid type M42 (charge M81) determined by different methods.

Functional groups/(meq/g)	Synthetic humic acid type M42 (charge M81)			Aldrich humic acid (charge A2)	Literature [14]
	Radiometric determination	Calcium acetate exchange	Direct titration		
COOH + acidic OH [a]	6.01 ± 0.11	-	-	6.9 ± 0.7	5.6 – 8.9
COOH	3.72 ± 0.28	4.10 ± 0.10	-	4.74 ± 0.05	1.5 – 5.7
acidic OH [a]	2.30 ± 0.36	-	-	3.2 ± 0.7	2.1 – 5.7
PEC [b]	-	-	3.90 ± 0.18	5.33 ± 0.12	-

[a] Acidic hydroxyl groups, e.g., substituted to five-membered heterocycles and aromatics.
[b] PEC = Proton exchange capacity.

In contrast to our synthesized humic acid of type M1, which has only 1.02 ± 0.06 meq/g carboxylic groups, the synthetic humic acid of type M42 shows a carboxylic group content which is comparable to most naturally occurring humic acids. With this results it is shown, that by varying the precursor substances different synthetic humic acids with variable functionality can be designed.

Considering the precursor substances, the unexpectedly high quantity of functional groups determined by the radiometric method, which are capable for methylation and are not hydrolyzable, probably results from H-acidic heterocyclic structures as well as phenolic

structural elements. Phenolic structural elements were determined by pyrolysis-gas chromatography/mass spectrometry.

Capillary electrophoresis

Fig. 6.8 depicts the electropherogram of synthetic humic acid type M42. This synthetic product shows in comparison to synthetic humic acid type M1 (Fig. 6.2) a more heterogeneous charge-to-size-ratio distribution. The higher proton exchange capacity of this humic acid may be a potential reason for this observation. The humic acid carboxylic groups are deprotonated at the experimental conditions applied. A mutual repulsion of the deprotonated carboxylic groups can occur, which can cause an unfolding of the molecule and also a cleavage of smaller fragments due to the overcoming of van der Waals forces.

Due to the higher carboxylic group content of synthetic humic acid type M42 in comparison to humic acid type M1 this humic acid shows a longer migration time. However, in comparison to Aldrich humic acid and other natural humic acids synthetic humic acid type

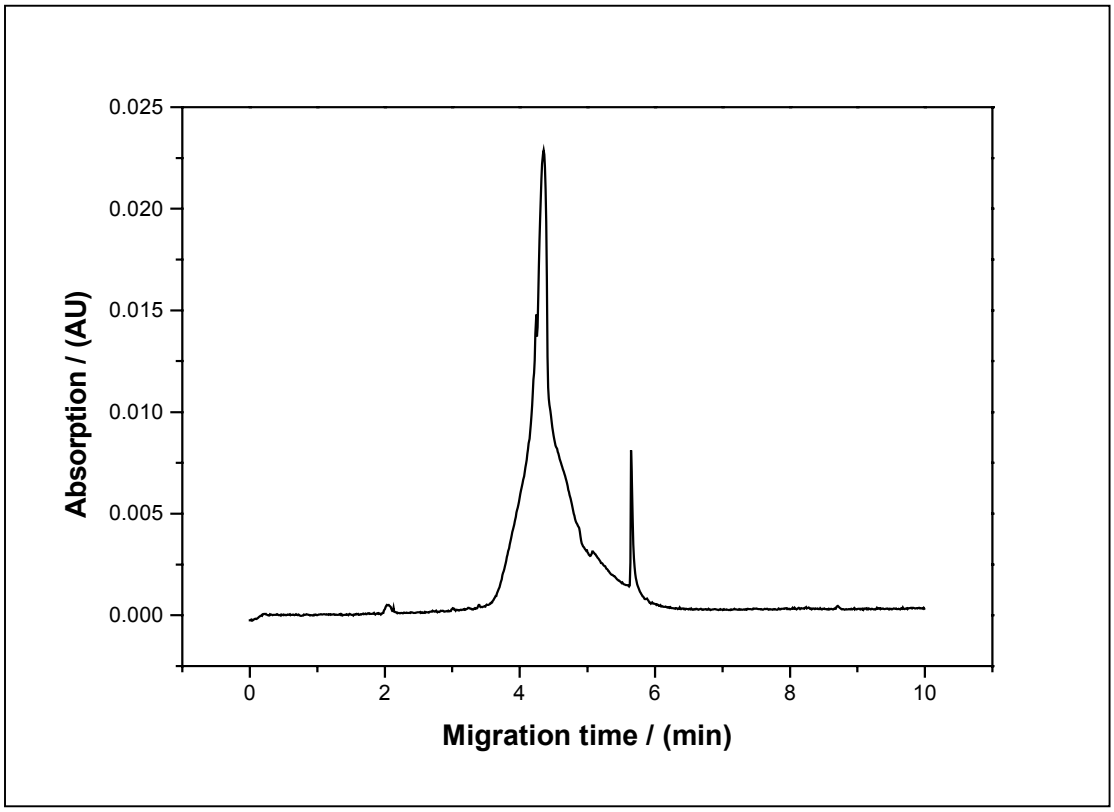

Figure 6.8: Capillary electropherograms of synthetic humic acid type M42 (charge M81). Separation conditions: buffer KH_2PO_4 (3 mM) - $Na_2B_4O_7$ (6 mM), pH 8.9; fused silica capillary 75 µm i.d. x 50 cm effective length, 57 cm total length; separation voltage 30 kV; temperature 30 °C; 15 s pressure injection; detection wavelength 214 nm.

M42 shows a smaller charge-to-size-ratio distribution. This indicates a greater homogeneity of the synthetic product regarding their molecule fractions.

FTIR spectroscopy

Fig. 6.9 compares the FTIR spectra of synthetic humic acid type M42 and type M1. These spectra confirm once more that synthetic humic acid type M42 shows a higher carboxylic group content than synthetic humic acid type M1. The IR absorption band at 1707 cm^{-1} is more pronounced than in the spectrum of humic acid type M1. Furthermore, one can conclude that humic acid type M42 shows IR absorption bands which are characteristic for natural humic acids [9,16].

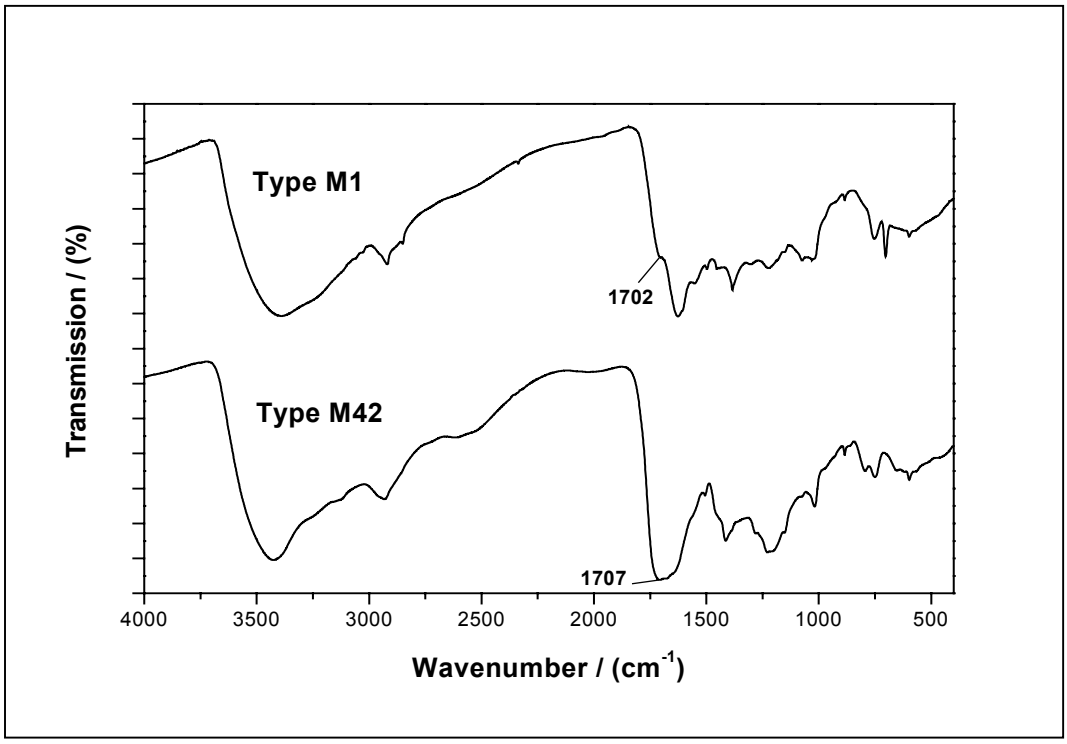

Figure 6.9: FTIR spectrum of synthetic humic acid type M42 (charge M81) in comparison to synthetic humic acid type M1.

6.4 Synthesis of a nitrogen-free humic acid

The ability of humic acids to complex metal ions is mainly due to their high concentration of oxygen-containing functional groups, especially carboxylic and phenolic OH groups. However, also other functional groups, such as nitrogen-containing groups, may contribute as electron-donors to the complexation process. Defined synthetic humic acid model substances,

with or without nitrogen may help to elucidate the influence of nitrogen-containing functional groups on the overall complex formation capability. Therefore, we synthesized a non-nitrogenous humic acid according to our melanoidin concept. Reducing sugars, such as glucose and galactose, can undergo the "Maillard reaction" in hot alkaline solution in absence of amino acids and form the so-called nitrogen-free "pseudo melanoidins" [19].

6.4.1 Synthesis

A mixture of 12 g D(+)-glucose (Fluka), 0.2 g Na_2CO_3 (p.a., Merck) and 18 mL water was refluxed for 15 days under nitrogen (Fig. 6.10). The starting pH was 8.9. In the initial phase of the reaction, the pH decreased to about pH 5 after 24 hours for about one week. Therefore, we adjusted the pH of the reaction mixture to pH 8 by addition of Na_2CO_3 once a day for the first 8 days of the synthesis. The humic acid-like fraction of the reaction product was extracted with 2 M NaOH (Merck) and then precipitated with 2 M HCl (Merck). The resulting precipitate was washed, dialyzed and lyophilized. The synthesis yielded 996 mg of non-nitrogenous synthetic humic acid.

Glucose

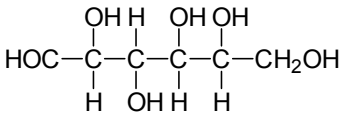

Figure 6.10: Glucose - Precursor for the nitrogen-free humic acid.

6.4.2 Characterization

Elemental analysis

Tab. 6.7 shows the elemental composition of the non-nitrogenous synthetic humic acid and a comparison to literature values for natural humic acids [13]. The synthetic product compares well with natural humic acids.

Table 6.7: Elemental composition of the synthesized non-nitrogenous humic acid in comparison to natural humic acids [13].

Element [a] / (%)	Non-nitrogenous synthetic humic acid	Natural humic acids [13]
C	57.55 ± 0.03	50 – 60
H	5.26 ± 0.01	4 – 6
N	-	2 – 6
O	37.14 ± 0.03	30 – 35

[a] Not corrected for ash and moisture content.

Functional groups

Tab. 6.8 summarizes the functional group content of the non-nitrogenous synthetic product compared to natural humic acids [14]. It is remarkable that the non-nitrogenous synthetic humic acid prepared from glucose shows a higher carboxylic group content than other synthetic humic acids prepared from reducing sugars and α-amino acids. For instance, the synthetic humic acid from type M1 that was discussed in paragraph 6.1, shows only a concentration of 1.0 meq/g carboxylic groups. We conclude from the radiometric determination of the functional groups that the non-nitrogenous product contains both phenolic OH and carboxylic groups.

Table 6.8: Functional group content of the synthesized non-nitrogenous humic acid in comparison to natural humic acids [14].

Functional groups / (meq/g)	Non-nitrogenous synthetic humic acid		Aldrich humic acid (charge A2)	Natural humic acids [14]
	Calcium acetate exchange	Radiometric determination		
COOH + phenolic OH	-	7.23 ± 0.81	6.9 ± 0.7	5.6 – 8.9
COOH	2.64 ± 0.12	2.38 ± 0.14	4.74 ± 0.05	1.5 – 5.7
phenolic OH	-	4.86 ± 0.83	3.2 ± 0.7	2.1 – 5.7

FTIR spectroscopy

Fig. 6.11 shows the FTIR spectrum of the non-nitrogenous synthetic humic acid, which shows characteristic absorption bands for humic acids [9,16]. It is to emphasize that this spectrum shows IR absorption bands which are characteristic for phenolic OH groups (deformation vibrations of phenolic OH groups, e.g., 1281 cm^{-1}).

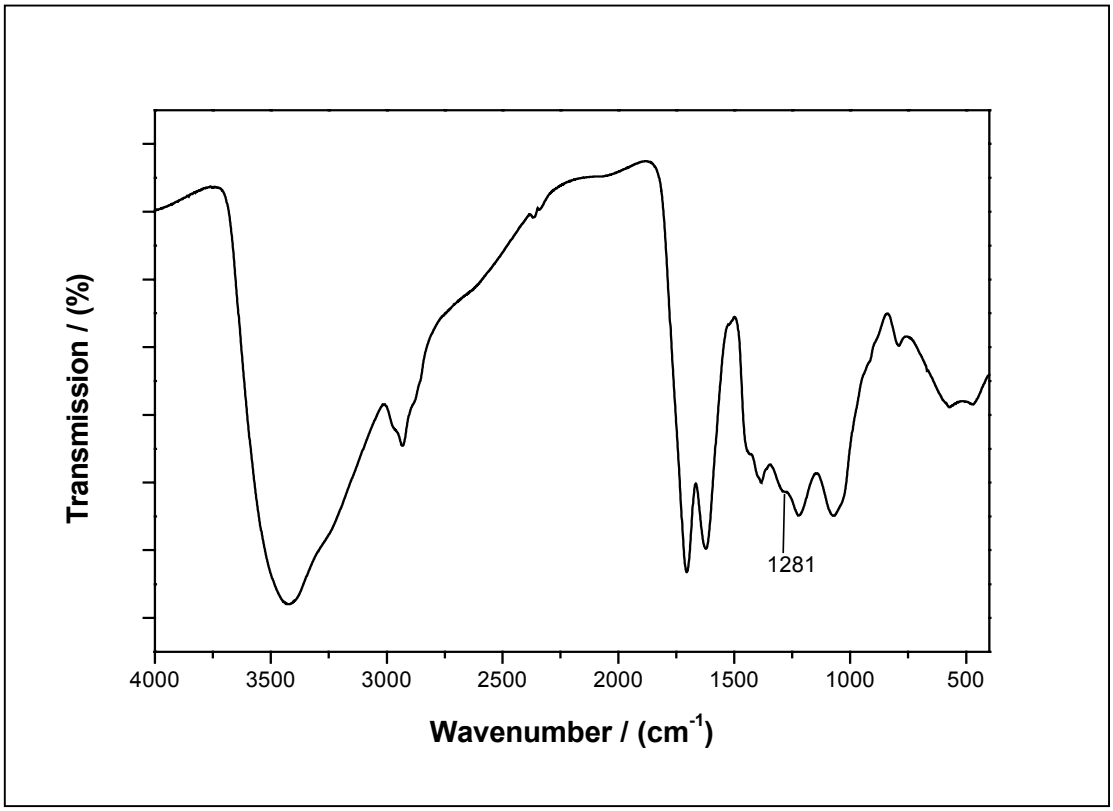

Figure 6.11: FTIR spectrum of the non-nitrogenous synthetic humic acid.

Additionally, the fact that this humic acid contains phenolic OH groups was confirmed by pyrolysis-gas chromatography/mass spectrometry. With this method we detected phenol and phenolic substitution products as thermolysis fragments.

Capillary electrophoresis

Capillary zone electrophoresis showed that the non-nitrogenous humic acid has a more homogeneous charge-to-size ratio distribution than natural humic acids. Fig. 6.12 depicts an electropherogram for the synthetic product.

The results of the different characterization methods show that it is possible to synthesize non-nitrogenous humic acid model substances from glucose.

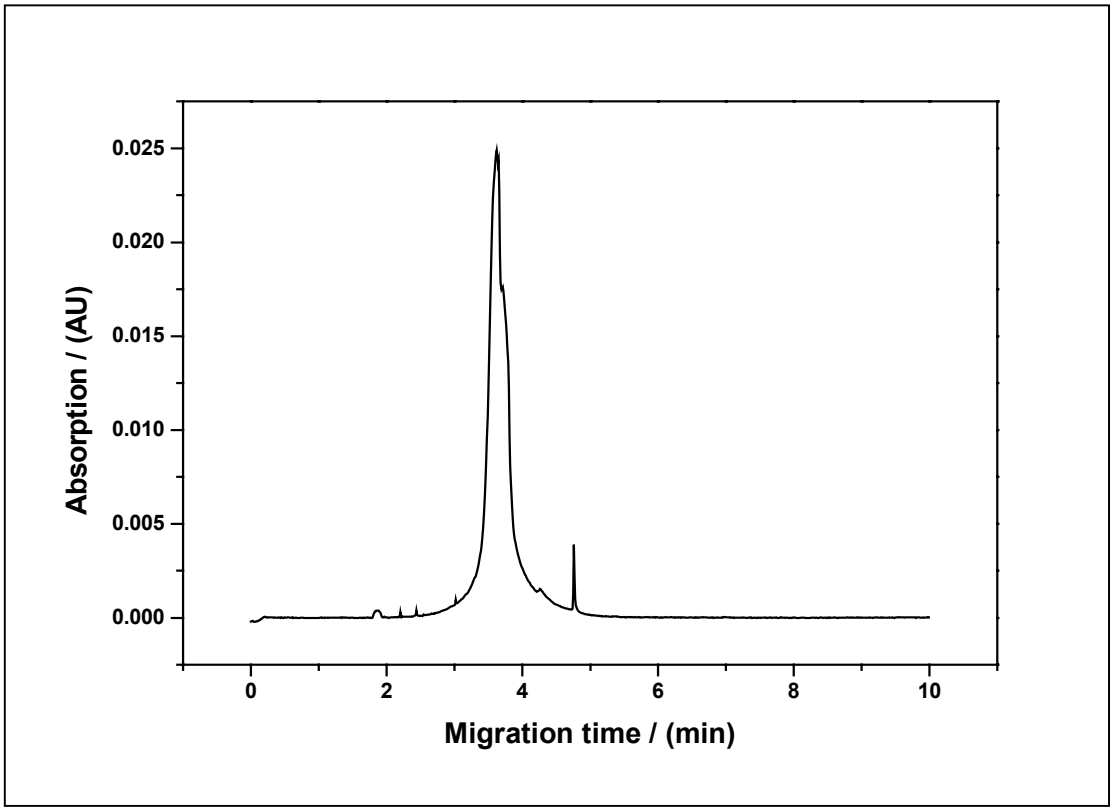

Figure 6.12: Capillary electropherograms of the non-nitrogenous synthetic humic acid.

Separation conditions: buffer KH_2PO_4 (3mM) – $Na_2B_4O_7$ (6mM), pH 8.9; fused silica capillary 75 µm i.d. x 50 cm effective length, 57 cm total length; separation voltage 30 kV; temperature 30 °C; 15 s pressure injection; detection wavelength 214 nm.

6.5 Conclusions

We have shown that the synthesis of melanoidins starting from reducing sugars and α-amino acids results in humic acid-like substances. These can be used as humic acid model substances. The humic acid-like melanoidins show functional and structural properties which are comparable to natural humic acids. Nevertheless, they show a higher homogeneity regarding their molecule fractions and a lower amount of inorganic constituents than their natural analogous. It was shown experimentally that the amount of inorganic constituents can

be decreased to the detection limit applying an “high purity” synthesis method. “Ultra-pure“ synthetic humic acids can be used to study the influence of inorganic impurities and constituents on humic acid properties, for instance on the complexation behavior.

The functional and structural properties of synthetic humic acids can be varied by varying the precursor substances. We have shown that the synthesis starting from xylose, glycine and phenylalanine results in a synthetic humic acid type M1 having a high amount of mono-substituted aromatic structural elements and only a low number of carboxylic groups. Starting from xylose and glutamic acid it is possible to synthesize a humic acid, which shows a carboxylic group content comparable to most natural humic acids. Besides the functional group content, the elemental composition of the synthetic humic acids can also be varied. A nitrogen-free synthetic humic acid model substance was synthesized from an aqueous glucose solution.

7 Synthesis of modified humic acids with blocked phenolic hydroxyl groups

We synthesized modified humic acids with blocked phenolic OH groups with regard to the investigation of the influence of phenolic OH groups on the complexation behavior of humic acids with metal ions.

The modification process is comparable to the radiometric determination of functional groups (cf. paragraph 5) and comprised two steps (Fig. 7.1): a) the permethylation of carboxylic and phenolic OH groups with diazomethane resulting in methyl ester and methyl ether groups and b) the hydrolysis of the ester groups in alkaline solution.

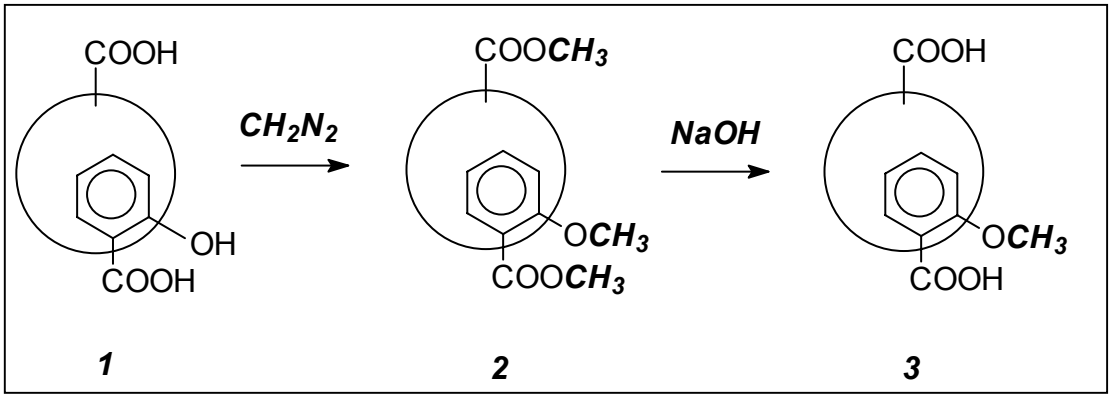

Figure 7.1: Reaction scheme for the synthesis of humic acids with blocked phenolic OH groups. (1) – unmodified humic acid, (2) – permethylated humic acid, (3) – humic acid with blocked phenolic OH groups.

7.1 Synthesis

We synthesized modified humic acids with blocked phenolic OH groups starting from the synthetic humic acids type M1 and M42 and from Aldrich natural humic.

First, the suspension of the original humic acid in methanol was reacted under stirring for three hours at –5 to 5 °C with diazomethane, generated from Diazald® (Sigma-Aldrich). After three hours the solvent was distilled. The permethylation procedure was repeated for several times and stopped when the incorporation of diazomethane into the humic acid was completed. The solvent, that was distilled from the reaction mixture then showed the yellow color of the non-reacted excess of diazomethane. Then the permethylated sample was lyophilized. The functional group content of the permethylated humic acid, was determined radiometrically.

For hydrolysis of the ester groups we applied two different pathways, (a) the hydrolysis with methanolic NaOH under reflux and (b) the hydrolysis with 2 M NaOH at room temperature.

(a) The permethylated humic acid was refluxed under stirring for 8 hours with an excess of methanolic NaOH solution. Following, the methanol was removed by distillation. The distillation residue was taken up in water. The alkali non-soluble components were separated by centrifugation and the modified synthetic humic acid was precipitated from the aqueous solution by adding 1 M HCl. This method was exclusively used for the permethylated humic acid type M1.

(b) The permethylated humic acid was stirred for 8 hours with 2 M NaOH in a nitrogen atmosphere. The alkali non-soluble residue was separated by centrifugation. Following, the modified humic acid was precipitated by addition of 2 M HCl. This method was applied for all permethylated humic acids.

In both cases the modified humic acid precipitate was centrifuged, washed, dialyzed using dialysis tubes (Thomapor®, exclusion limit MWCO < 1000), and then lyophilized.

It is to consider that with this method also other H-acidic OH groups, e.g., OH groups substituted to five-membered heterocycles may be methylated with diazomethane, resulting in nonhydrolizable methyl ether groups.

7.2 Characterization

The permethylated humic acids as well as the humic acids with blocked phenolic OH groups were characterized for their functional group content using different methods. Tab. 7.1 summarizes the results of these investigations. The humic acids were also investigated by FTIR spectroscopy.

Table 7.1: Functional group content of the modified humic acids (HA) in comparison to the unmodified humic acids.

Humic acid	Modification	Phenolic OH / (meq/g)	COOH / (meq/g)	PEC / (meq/g) [a]
Aldrich (charge A2/97)	original	3.4 ± 0.5	4.41 ± 0.11	5.06 ± 0.17
	permethylated	0.6 ± 0.3	< 0.1 [b]	n.m. [c]
	blocked phenolic OH groups	1.1 ± 0.4	3.25 ± 0.05	3.58 ± 0.21
Type M1 (charge R36/95) [d]	original	2.3 ± 0.1	1.02 ± 0.06	1.36 ± 0.08
	permethylated	0.3	< 0.1 [b]	n.m.
	blocked phenolic OH groups	1.1 ± 0.2	1.91 ± 0.07	1.94 ± 0.13
	original HA saponified	1.7 ± 0.1	2.03 ± 0.02	2.12 ± 0.06
Type M1 (charge M100A) [e]	original	2.4 ± 0.1	1.34 ± 0.05	1.69 ± 0.10
	permethylated	0.3	< 0.1 [b]	n.m.
	blocked phenolic OH groups	0.9 ± 0.3	1.16 ± 0.03	1.35 ± 0.23
Type M42 (charge M81)	original	2.3 ± 0.4 [f]	4.10 ± 0.10	3.90 ± 0.18
	permethylated	0.6 ± 0.1	< 0.1 [b]	n.m.
	blocked acidic OH groups [g]	0.6 ± 0.3	3.21 ± 0.08	3.28 ± 0.06

[a] PEC: Proton Exchange Capacity. [b] Radiometrically determined. [c] n.m. : not measured. [d] Hydrolysis method (a). [e] Hydrolysis method (b). [f] cf. chapter 6.3. [g] Blocked acidic OH groups, e.g., substituted to five-membered heterocycles and aromatics (cf. chapter 6.3).

From the results summarized in Tab. 7.1 one can conclude that the phenolic OH groups are only partially modified during the derivatization process. The humic acids with blocked phenolic OH groups have 52 % to 74 % less phenolic OH groups compared to the original humic acids. In the permethylated humic acids we still determined by the radiometric method functional groups which are capable for methylation but are not hydrolyzable, i.e., these are no carboxylic groups. However, it is still not confirmed if these functional groups are unmodified phenolic OH or other unmodified H-acidic OH groups or functional groups which are produced during the derivatization of the humic acids and that are capable for methylation

but not hydrolyzable. It is obvious that in some cases the number of functional groups that are capable for methylation and not hydrolyzable is increased during the saponification step.

Applying method (a) for the hydrolysis of ester groups, the carboxylic group content of the humic acid was increased probable due to the hydrolysis of ester groups of the original humic acid (see Tab. 7.1). Also hydrolysis of amide groups may occur under the applied conditions which also results in the formation of carboxylic groups. Therefore, an alkaline treatment of the original humic acid type M1 was performed in the same manner as the saponification of the permethylated humic acid of type M1. The functional group analysis of the resulting humic acid (original humic acid saponified) is also shown in Tab. 7.1. The resulting humic acid has a carboxylic group content that is comparable with the modified synthetic humic acid with blocked phenolic OH groups but has a higher content of phenolic OH groups. The amount of phenolic OH groups is somewhat lower than in the original humic acid. This may be caused by condensation reactions during refluxing with methanolic NaOH.
The hydrolysis method (b) represents a more sensitive method. However, comparing the amount of carboxylic groups of the modified humic acids with the unmodified humic acids one can observe that the modified humic acids show a lower carboxylic group content than the original humic acids. Possible causes may be:

- a decomposition of the humic acid molecules in acid-soluble components during the modification;
- a leaching of smaller humic acid molecules with higher carboxylic group content from the humic acid mixture during reprocessing of the modified humic acids or
- decarboxylation reactions during the derivatization process.

The smallest differences in the carboxylic group content were observed for the modified synthetic humic acid type M1 (-13 %) and type M42 (-22 %) compared to the original humic acids. This points to the fact that both humic acid materials are more homogenous than Aldrich humic acid.

The modification process of phenolic OH groups was further investigated by FTIR spectroscopy, which allows the observation of the two different derivatization steps, i.e., first the formation of the permethylated humic acid and second the saponification of the permethylated product resulting in the humic acid with blocked phenolic OH groups.
IR absorption bands, which point to the formation of methyl ether groups, including phenylmethylethers, were identified especially in the finger-print region of the spectra of the

modified humic acids with blocked phenolic OH. However, due to the overlapping of IR absorption bands of different humic acid functional groups resulting in a few broad IR absorption bands as well as due to strong interactions between different functional groups of the humic acid it is difficult to clearly establish these absorption bands in some cases.

Fig. 7.2 shows the FTIR spectra of the unmodified and the modified humic acid type M1. An indication for the modification of phenolic OH groups is the absence of the absorption band at 1292.8 cm^{-1} in the spectrum of the modified humic acid, which corresponds to these functional groups. The spectrum of the unmodified humic acid type M1 shows this band. The ether group absorption bands (1023.9 cm^{-1}, 1097.4 cm^{-1} and 1246.8 cm^{-1}) present in the spectrum of the modified humic acid also confirm that phenolic OH groups are blocked. Additionally, the increase of the intensity of the absorption band at 2862.8 cm^{-1} indicates the formation of methyl ethers. The increase of the intensity of the absorption band at 1453.5 cm^{-1} (C-H deformation vibrations) results from the incorporation of CH_3-groups into the molecule as a result of the methyl ether formation. Furthermore, the synthetic humic acid type M1-B has a significantly higher amount of carboxylic groups (1712.2 cm^{-1}) than the original humic acid.

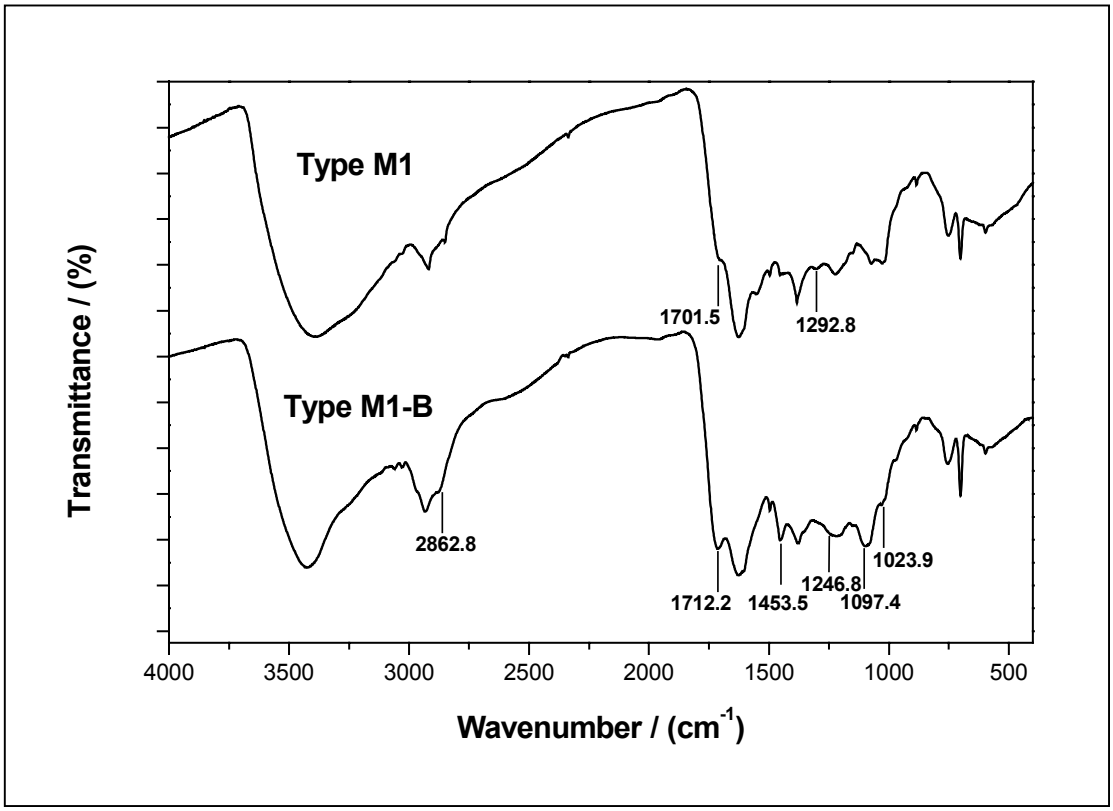

Figure 7.2: FTIR spectra of the unmodified synthetic humic acid of type M1 and the synthetic humic acid with blocked phenolic OH groups (Type M1-B; hydrolysis (a)).

From the characterization results one can conclude that there is the possibility to synthesize humic acids with blocked phenolic OH groups. With the modified humic acid type M1 we investigated for the first time the influence of phenolic OH groups on the complexation behavior of humic acids with UO_2^{2+} ions. These investigations are described in paragraph 11.

8 Synthesis of isotopically labelled humic acids

Migration and sorption experiments are performed to predict the migration behavior of radionuclides in the presence of humic substances. One of the decisive questions, that has to be answered concerns the fate of humic acids during the interaction of humic-acid-metal-complexes with sediments. In order to study the migration and sorption behavior of actinides in the presence of humic acids, i.e., in laboratory batch and column experiments it is advantageous to label the humic material with radionuclides. Thus, it is possible to detect and to balance very precisely the fate of humic acids in the investigated system.

Requirements on a radioactive labelling of humic acids are the use of long-living radionuclides, e.g., ^{14}C, the irreversibility of the labelling, the preservation of the humic acid functionality and a high isotopic enrichment. The stability of the labelled material is essential for its successful use in experiments over long times. Decomposition of the labelled humic acid and loss of radioactivity during such experiments would lead to incorrect results and an incorrect interpretation of the processes under investigation. The incorporation of a radioactive label into humic materials must be accomplished by methods which do not change the characteristics of the humic material.

There are some possibilities to introduce radioactive labels, e.g., ^{14}C, ^{125}I, into the humic acid molecule. For instance, the chemical derivatization of functional groups using a radioactive reagent, e.g., [^{14}C]methylamine or the enzymatically mediated incorporation of [^{14}C]phenol in the humic material [20,21]. However, this reactions may alter the humic acid, especially the functionality of humic acids by derivatization of functional groups. Such derivatives often are not sufficiently stable for long-time experiments [20,22]. Furthermore, there is the possibility to synthesize isotopically labelled humic acid model substances according to our melanoidin concept using isotopically labelled precursor substances, e.g., α-amino acids. The greatest advantages of the synthesis of isotopically labelled melanoidins compared to other labelling methods are the stable labelling of the humic acid in the backbone structure without any changes in the humic acid functionality and the possibility to synthesize humic acids with different functionalities as described in chapter 6.1. to 6.4.

Within the scope of this project, we investigated the synthesis of ^{14}C-labelled humic acid model substances with different functionalities starting from ^{14}C-labelled α-amino acids. The aim of this work was the selection of the optimal labelling position of the amino acid to obtain humic acids with high specific radioactivity [23].

8.1 Synthesis and results

We synthesized ^{14}C-labelled humic acids of type M1 and type M42 according to the synthesis procedures described in 6.1 and 6.3, respectively. The ^{14}C-labelled α-amino acids used are depicted in Fig. 8.1.

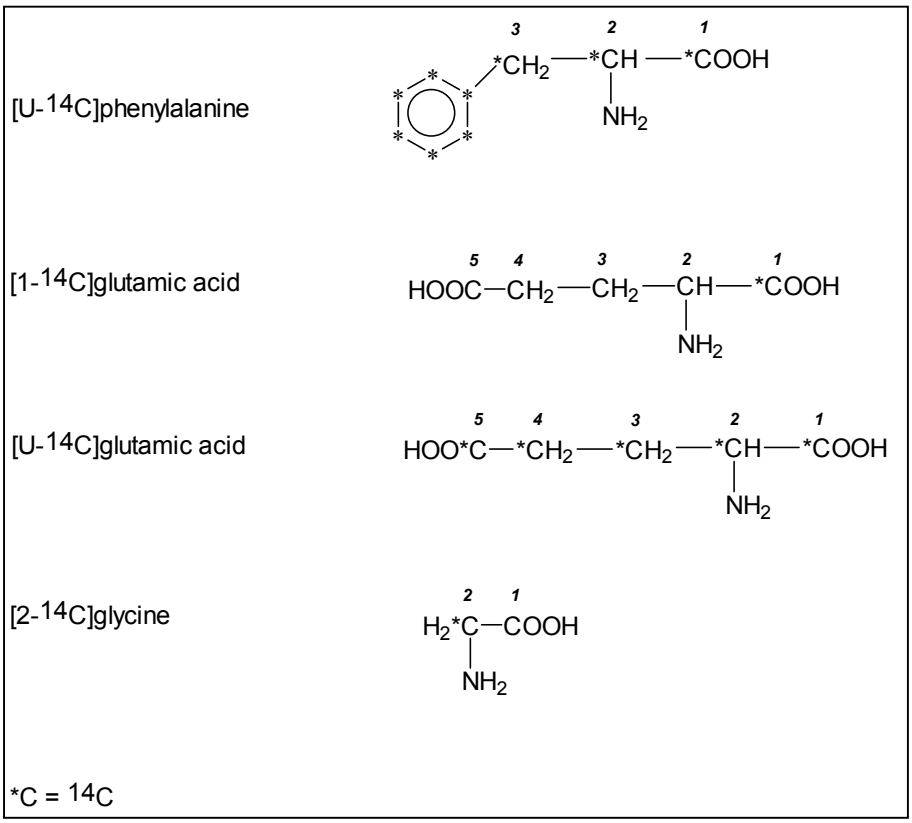

Figure 8.1: ^{14}C-labelled amino acids used for the synthesis of ^{14}C-labelled synthetic humic acids type M1 and type M42.

Tab. 8.1 summarizes the starting materials, the specific activities of the amino acids and the activity yields of the synthesized humic acids.

The radiochemical yield depends on the experimental conditions and is limited by the formation of insoluble humin-like substances. The yields as well as the specific activity of CO_2 which is eliminated during the reaction allow conclusions with regard to the reaction

course. The nitrogen content of the humic acid molecule corresponds to the amount of incorporated amino acid. In all cases, the C-1 carboxylic group of the amino acid is eliminated during the melanoidin formation. This elimination is a precondition for the incorporation of the amino acid in the melanoidin molecule. Therefore, [1-^{14}C]-labelled amino acids, e.g., [1-^{14}C]glutamic acid, are not suitable for the synthesis of ^{14}C-labelled humic acids. However, the CO_2 which is released during the reaction originates not only from the amino acid because the specific activity of the eliminated CO_2 is smaller than the specific activity of the amino acid related to the labelling position. CO_2 from xylose is also eliminated during the reaction.

Table 8.1: Starting materials and activity yields for the synthesis of different humic acids. Xylose was the sugar component used in all cases.

Humic acid type	Precursors		Humic acid Yield	
	Amino acids	(MBq/mmol)	(% ^{14}C)	(MBq/g)
M1	[U-^{14}C]phenylalanine, glycine	40	12	36
M1	[2-^{14}C]glycine, phenylalanine	40	30	104
M42	[1-^{14}C]glutamic acid	40	0	0
M42	[U-^{14}C]glutamic acid	40	5	102

The highest activity yields for humic acid type M1 are reached using [2-^{14}C]glycine as precursor substance. Calculations have shown that the maximal specific activity of humic acid type M1, that can be reached starting from [2-^{14}C]glycine with a maximal specific activity of 1.85 GBq/mmol, amounts to 4.8 GBq/g. With this specific activity 100 ng of ^{14}C-labelled humic acid can exactly be detected. That means, that about 1 µg ^{14}C-labelled humic acid per liter can be detected. This detection limit allows the use of this ^{14}C-labelled humic acid in batch and migration experiments.

Furthermore, using [U-^{14}C]glutamic acid, synthetic humic acid type M42 can be synthesized with a comparable high specific activity (like humic acid type M1 starting from [2-^{14}C]glycine). This fact enables us to synthesize ^{14}C-labelled humic acids with a high carboxylic group content comparable to most natural humic acids. However, the yield of ^{14}C of this synthesis is smaller compared to the synthesis of humic acid type M1.

9 Stability of synthetic and natural humic acid stock solutions

Natural humic acids are subjected to permanent alteration reactions. Nevertheless, comparable chemical properties are necessary for all comparative investigations with humic acids. Alterations of humic acids are especially possible in solutions with extreme pH conditions after long storage periods.

The stability of stock solutions from synthetic and natural humic acids were investigated regarding their temperature and light sensitivity under different pH conditions.

9.1 Experimental

Alkaline conditions

Stock solutions of synthetic humic acid type M1 and type M42 as well as Aldrich humic acid were prepared under aerobic conditions with a humic acid concentration of 1 g/L and a NaOH concentration of 10^{-2} mol/L. Three samples of each stock solution were stored under the following conditions:

a) at room temperature and daylight,
b) at room temperature under exclusion of daylight and
c) at 5 °C under exclusion of daylight.

Periodically the absorption of the humic acid solutions at 465 nm were measured with a spectrophotometer (Spekol 11, VEB Carl Zeiss Jena, Germany). Furthermore, the pH values of the solutions were determined.

Acid conditions

A stock solution of synthetic humic acid type M1 (0.5 g HA/L) was investigated at pH 6. Furthermore, stock solutions of synthetic humic acid type M42 and Aldrich humic acid (1 g HA/L) were investigated at pH 4.

The storage conditions and the absorption measurements of the solutions were the same as in the investigations under alkaline conditions.

9.2 Results

Alkaline conditions

Fig. 9.1 shows the absorption intensities at 465 nm for stock solutions of synthetic humic acid type M1 stored under different conditions versus storage time. For all stock solutions a decrease in the absorption intensities was observed with increasing storage time. The highest decrease was determined for solutions which were stored at room temperature and daylight.

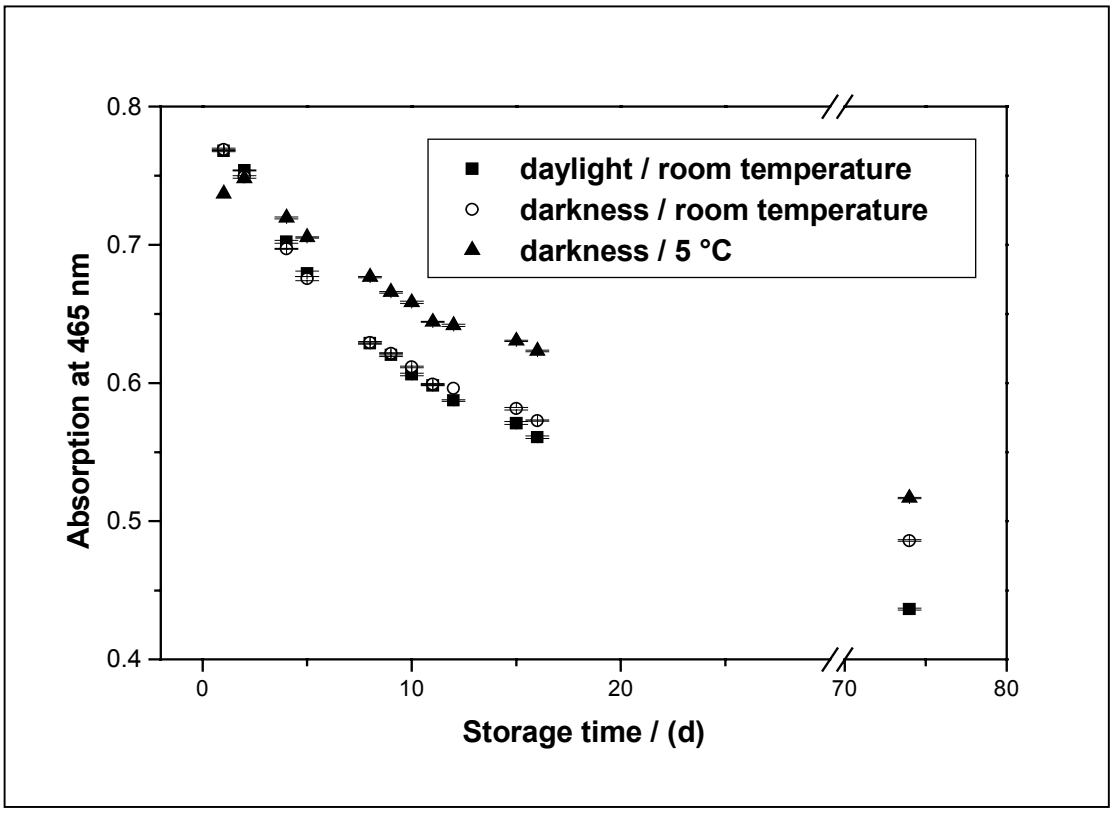

Figure 9.1: Absorption of stock solutions of synthetic humic acid type M1 at 465 nm at different storage conditions versus storage time ([HA]: 1 g/L; [NaOH]: 10^{-2} M).

Comparable trends were determined for synthetic humic acid type M42 and Aldrich humic acid. Fig. 9.2 depicts a comparison of the absorption trend for the investigated humic acid stock solutions stored at room temperature and daylight. For all humic acid solutions a decrease of the absorption at 465 nm with increasing storage time was observed. The lowest percentage decrease in dependence on the storage conditions and storage time was observed for Aldrich humic acid.

Significant changes in the pH values of the solutions of Aldrich humic acid and synthetic humic acid type M1 were not observed. The solutions of synthetic humic acid type M42 show a permanent decrease of their pH values.

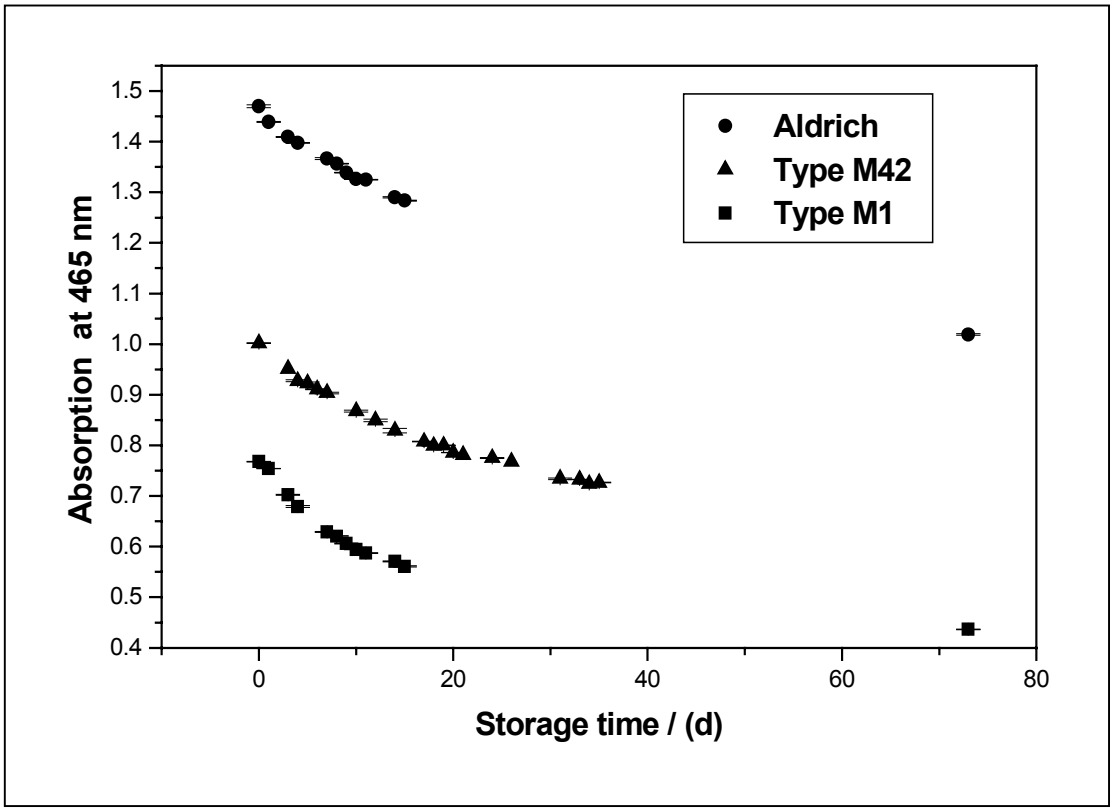

Figure 9.2: Absorption of humic acid stock solutions at 465 nm versus storage time ([HA]: 1 g/L; [NaOH]: 10^{-2} M; storage at room temperature and daylight).

The decrease in the absorption intensities points to the fact that the stock solutions are subjected to alterations under the applied conditions. The alterations may be caused by a hydrolytic decomposition of the humic acids, e.g., due to the hydrolysis of ester groups, because of the high pH values. The alterations of the solutions can be retarded by storing the solutions under cooling and exclusion of daylight.

Acid conditions

Under acid pH conditions all solutions show only an insignificant decrease in the absorption intensities at 465 nm, which lies in the range of the experimental error. Fig. 9.3 shows the trend of the absorption at 465 nm for the humic acid solutions stored at room temperature and daylight versus storage time.

Significant changes in the pH values were not observed for the solutions of synthetic humic acid type M1. Solutions of humic acid type M42 and Aldrich humic acid only show a negligible increase in their pH values.

In contrast to the storage at alkaline conditions no significant dependency between the storage conditions and the stability of the solution was observed.

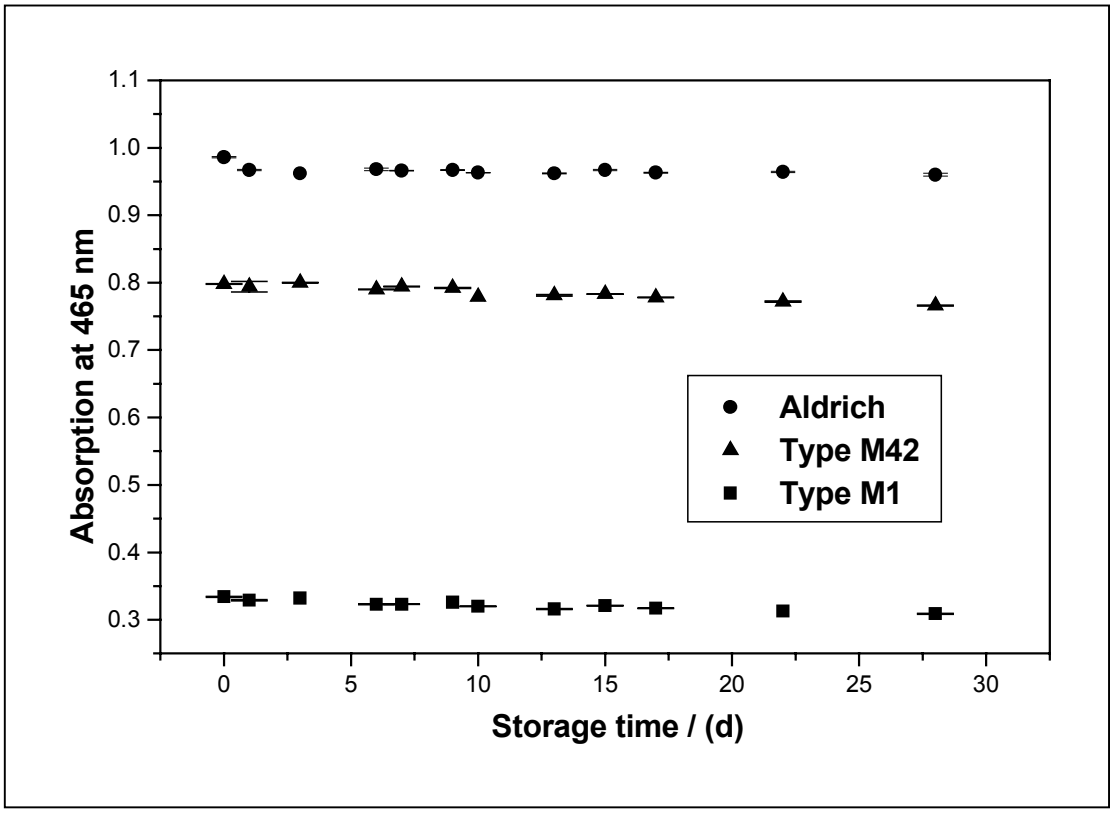

Figure 9.3: Absorption of humic acid solutions at 465 nm versus storage time ([HA]: 1 g/L for Aldrich HA and HA type M42; 0.5 g/L for HA type M1; pH 4 for Aldrich HA and HA type M42; pH 6 for HA type M1; storage at room temperature and daylight).

From that one can conclude, that humic acid stock solutions show a higher stability under acid conditions. However, instabilities of the solutions are expected with increasing storage time, which may be caused by chemical reactions and/or by the growth of fungi.

9.3 Conclusions

Aqueous stock solutions of synthetic and natural humic acids show comparable stabilities under similar storage conditions. They show alterations during the storage over long periods of time, whereby acid solutions show higher stabilities than alkaline solutions. For alkaline solutions we observed a strong dependency between the storage conditions and the stability of the solutions.

Freshly prepared stock solutions of synthetic and natural humic acids should be used to ensure comparable experimental conditions for the investigations of humic acids in solution.

10 Interaction of synthetic and natural humic acids with uranium(VI)

10.1 EXAFS investigations for the determination of structural parameters of uranyl(VI) humates [24]

Extended X-ray absorption fine structure analysis (EXAFS) is an useful tool for analyzing the complexation behavior of humic substances on a molecular level. EXAFS is a standard technique, providing molecular-level information on the nearest neighbor structure of a chosen absorbing atom [25], which also allows the investigation of amorphous materials and liquid substances.

The objective of the EXAFS investigations was to obtain information about the structure of uranyl-humic acid complexes, in particular about the binding of the UO_2^{2+} ion onto humic acid. The EXAFS investigations performed included the following focal points:

- comparison of the interaction between the purified natural humic acid from Fluka and the synthetic humic acid type M1 with UO_2^{2+} ions,
- comparison of uranyl humates with different uranyl loadings,
- comparison of uranyl humates prepared under different conditions and
- comparison of uranyl humates that were measured in the wet or dry form.

10.1.1. Experimental

Sample preparation

We studied uranyl humate complexes prepared under different conditions. The humic acid was either dissolved in aqueous solution or prepared as an aqueous suspension of solid humic acid. These were then reacted with solutions containing varying UO_2^{2+} amounts. After isolation and purification of the uranyl humates the samples were lyophilized. One sample was not dried completely, but measured in the form of a wet paste.

A list of the samples investigated, the concentration of uranyl ions per weight humic acid in the reaction solution during the preparation, the uranyl loadings of the samples regarding their carboxylic group contents and the general preparation method are given in Tab. 10.1. A detailed description of the sample preparation is given in [24].

Table 10.1: Sample preparation and UO_2^{2+} loadings of the uranyl humate complexes investigated.

Sample	Sample preparation		Uranyl humate	
	mg U/g HA in reaction solution	Method of sample preparation	UO_2^{2+} loading[a] (mg U/g HA)	UO_2^{2+} loading [b] (% COOH)
1	540	reaction of UO_2^{2+} with dissolved Fluka-HA; pH = 3.5	392	87
2	400	sorption of UO_2^{2+}; onto an aqueous suspension of Fluka-HA; pH < 1	160	35
3	45	reaction of UO_2^{2+} with dissolved Fluka-HA; pH = 4.0	36	8
4	48	reaction of UO_2^{2+} with dissolved Fluka-HA; pH = 4.0	44	10
5	21	reaction of UO_2^{2+} with dissolved synthetic HA type M1; pH = 4.0	18	14

[a] The UO_2^{2+} loadings of the samples were determined using ICP-MS following digestion of the uranyl humates in HNO_3. The average values from two ICP-MS determinations are shown.
[b] UO_2^{2+} loadings expressed in percent of carboxylic group capacity calculated assuming charge neutralization. The humic acid carboxylic group content was determined by the calcium acetate method.

Although similar amounts of uranyl ions per weight humic acid were used in the preparation of samples 1 and 2, their uranyl loadings differ significantly due to the different pH conditions during sample preparation.

EXAFS measurements

Uranium L_{III}-edge EXAFS transmission spectra were measured at room temperature at the Hamburger Synchrotronstrahlungslabor HASYLAB, experimental station RÖMO II, beamline X1.1, using a Si(311) double-crystal monochromator detuned ~ 50 % of the maximum incident flux. Fig. 10.1 shows schematically the experimental set-up.

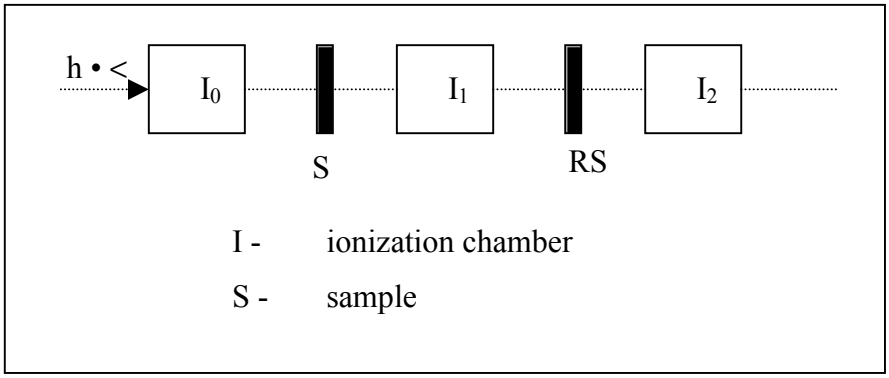

Figure 10.1: Experimental set-up of the EXAFS measurements.

The samples were dispersed in Teflon and pressed as 1.3 cm diameter pellets. The amount of sample corresponding to 18-30 mg U, calculated from the experimentally determined uranyl loadings given in Tab. 10.1, was introduced into the pellets. The jump over the U L_{III}-edge for these samples averaged 0.8. Sample 4 was measured as a wet paste, loaded into a polyethylene sample holder having thin windows in the direction of the synchrotron beam. The edge jump for this sample was only 0.2 so that the signal-to-noise ratio limited the upper range of the spectrum to ~ 17900 eV. To calibrate the energy of the sample spectra, a spectrum from a 0.2 M UO_2Cl_2 solution which was placed behind the sample, was recorded simultaneously. The energy of the first inflection point in the reference spectrum was defined as 17166 eV. Three spectra were recorded for each sample and then averaged. The ionization energy for the U L_{III} electron (E_0) was arbitrarily defined as 17185 eV for all averaged sample spectra.

Data reduction and analysis were performed using the suite of programs EXAFSPAK [26]. Scattering amplitude and phase-shift functions were calculated using the theoretical EXAFS modeling code FEFF6 [27]. A more detailed description of the data analysis is given in [24].

IR spectroscopy

IR spectra of the dried uranyl humate samples as well as the untreated humic acids were measured. Spectra from KBr pellets containing equal amounts of sample were recorded at room temperature between 200 and 4000 cm^{-1}.

10.1.2 Results and discussion

IR Spectroscopy

All IR spectra of the uranyl humate complexes show, in comparison to the uncomplexed humic acids, a decrease in the absorption bands characteristic for C=O and C-O vibrations of carboxylic groups at 1720 cm^{-1} and 1200 cm^{-1}, respectively. At the same time the intensity of bands associated with asymmetric and symmetric stretching vibrations of COO^- groups, found between 1560 cm^{-1} and 1520 cm^{-1} and at 1380 cm^{-1}, increases. As example, the IR spectra of the untreated Fluka humic acid and sample 1 are depicted in Fig. 10.2. For some samples the observed changes were not as great due to the low uranyl loadings. However, the combined decrease in carbonyl band intensity and increase in COO^- band intensity indicate the conversion of humic acid carboxylic groups to carboxylate ions through the loss of protons upon reaction with uranyl ions. This strongly suggests a direct interaction/complexation of the humic acids with the uranyl ions. Furthermore, the results from IR spectroscopy point to a monodentate coordination of the COO^- group onto the UO_2^{2+} ion [24].

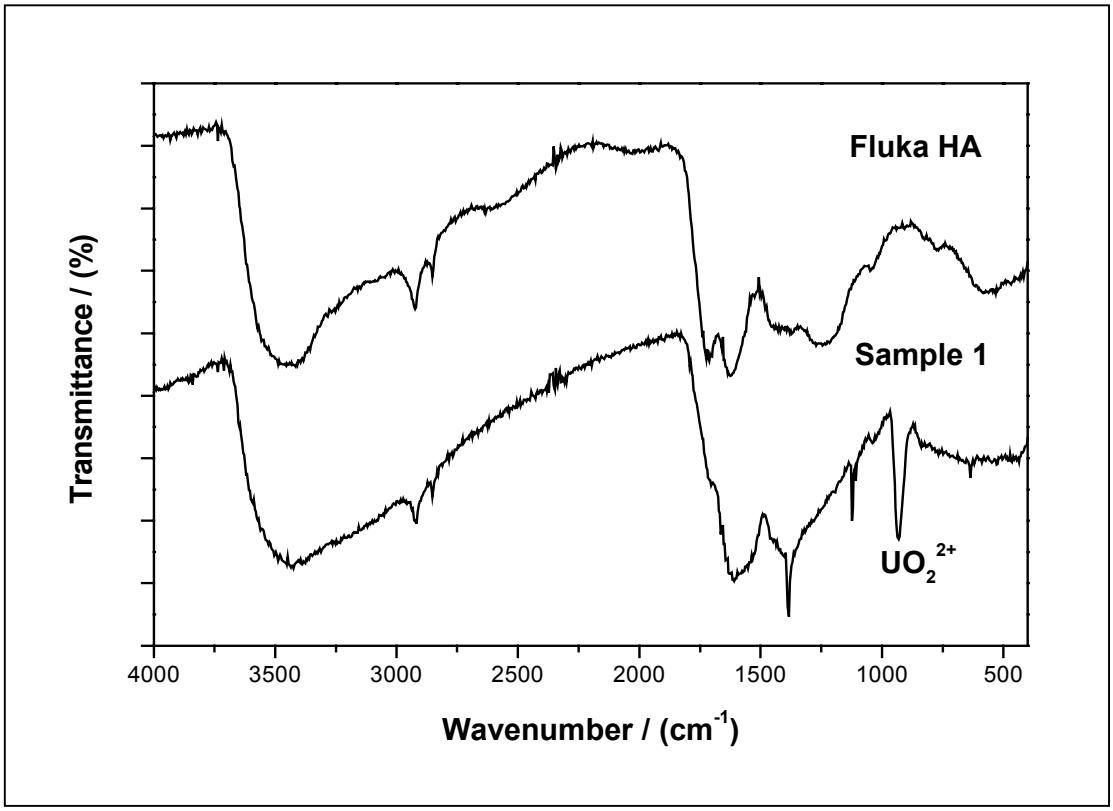

Figure 10.2: IR Spectra of the untreated, purified Fluka humic acid and sample 1, Fluka HA following complexation with uranyl ions.

EXAFS results

The EXAFS oscillations were isolated from the raw, averaged data by removal of the pre-edge background, followed by μ_0-removal via spline fitting techniques and normalization using a Victoreen falloff [25]. As example, Fig. 10.3 shows the U L_{III} absorption spectrum of sample 5, which is already energy calibrated and corrected relative to the pre-edge background.

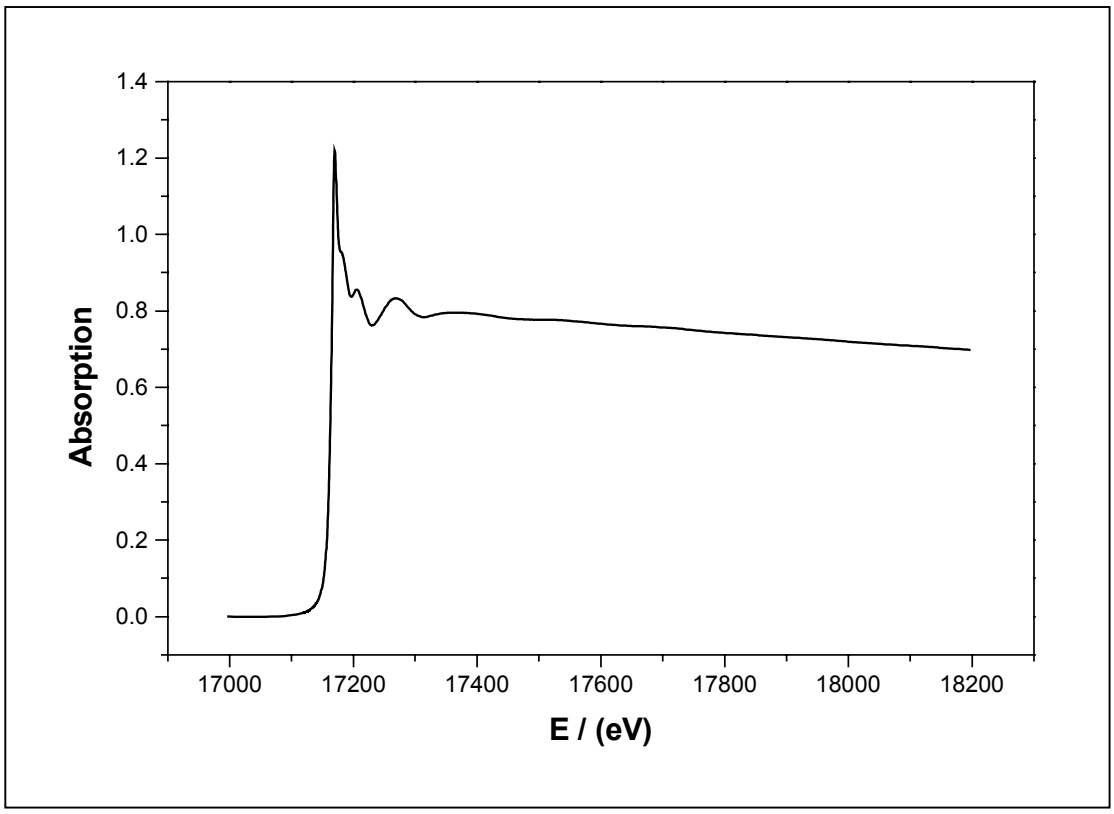

Figure 10.3: U L_{III}-edge absorption spectra of sample 5.

The k^3-weighted EXAFS oscillation of all investigated uranyl humate samples of Fluka humic acid and synthetic humic acid type M1 are depicted in Fig. 10.4.

The contribution of the different coordination shells to the EXAFS oscillation can be separated by Fourier transformation. Fig. 10.5 shows the corresponding Fourier transforms (FT's). The FT's represent pseudo-radial distribution functions of atoms surrounding the central, absorbing uranium atom. The intensity of the peaks corresponds to the coordination number. The peak position gives information about the distances of the atoms. The FT's are not corrected for EXAFS phase-shifts causing peaks to appear at shorter distances (R + Δ) relative to the true near-neighbor distances R.

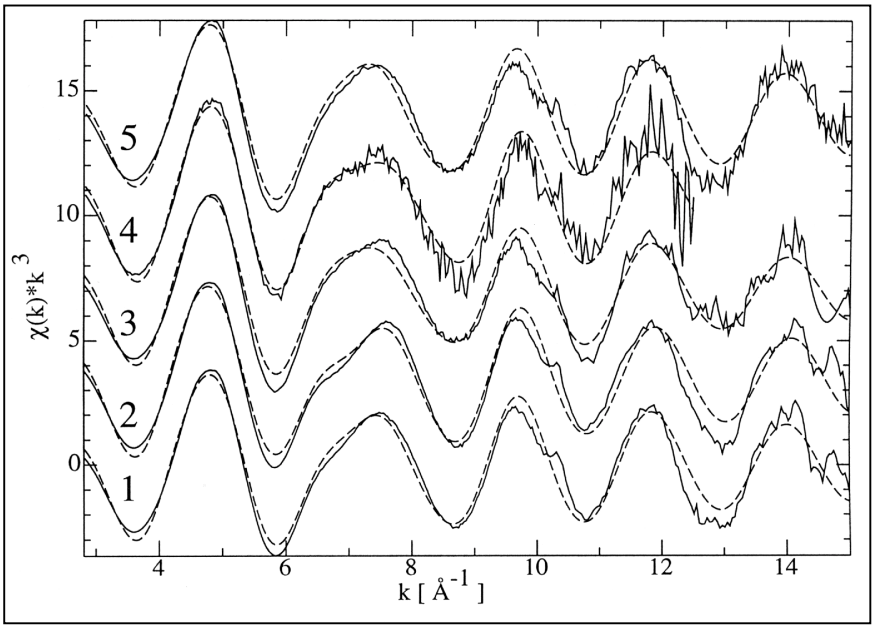

Figure 10.4: k^3-weighted U L_{III}-edge EXAFS for samples 1 – 5 (Tab. 10.1). The solid lines are the experimental spectra, the dashed lines result from the fit described in the text. For clarity, the spectra have been shifted along the y-axis.

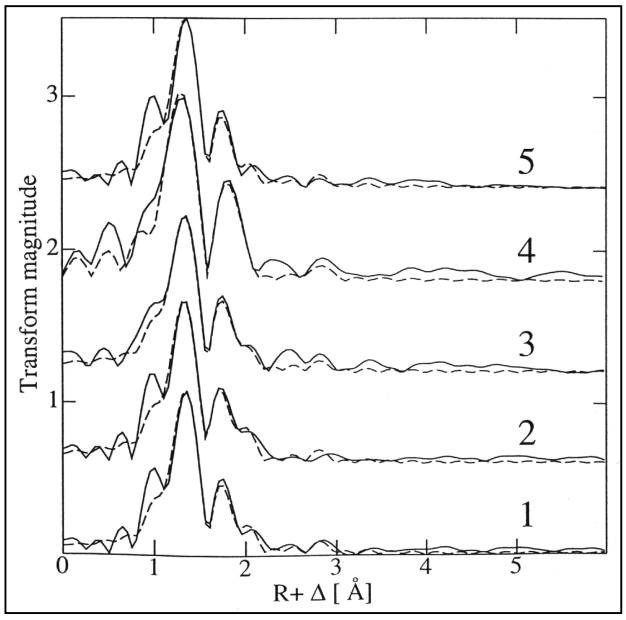

Figure 10.5: Fourier transforms of the EXAFS depicted in Fig. 10.4. The transformation in the k-region shown was performed using a rectangular window. The solid lines are the experimental spectra, the dashed lines results from their fit. For clarity, the spectra have been shifted along the y-axis.

The EXAFS oscillations in Fig. 10.4 show no significant differences except for slight variations in the structure of the shoulder centered at about 7 $Å^{-1}$. Two coordination shells are evident in the FT's in Fig. 10.5. All samples investigated show comparable FT's which are dominated by a peak at approximately 1.3 Å. This peak corresponds to the axial oxygen atoms (O_{ax}) of the uranyl unit. The next peak represents the equatorial oxygen atoms (O_{eq}) coordinated to uranium. The weak peak in the FT's at about 2.9 Å is not from a true coordination shell. It results from multiple scattering along the uranyl unit [28,29]. No peaks with significant intensity indicative of scattering on a strong backscatterer, e.g., a U-U interaction are evident in the spectra.

The EXAFS oscillations were fitted to the EXAFS equation using a structural model with the two coordination shells observed in the FT's, containing oxygen atoms as backscatterer. In addition, multiple scattering involving both axial oxygen atoms of the uranyl unit was included in the fit. The k-range of the fits was 2.8 – 15 $Å^{-1}$. For sample 4 the k-range was limited to 2.8 – 12.5 $Å^{-1}$. The coordination number for the axial oxygen atoms (N_{ax}) was held constant at 2. The shift in threshold energy (ΔE_0) was varied as single value for all paths. A more detailed description of the evaluation of the experimental data including a test of the accuracy of the EXAFS analysis and an exemplary deconvoluted fit of an uranyl humate spectrum is given in [24].

The structural parameters obtained from the fits of the EXAFS oscillations are given in Tab. 10.2.

Table 10.2: Fit parameters for U L_{III}-edge EXAFS data for samples 1-5 (cf. Tab. 10.1) using the model described in the text (N_{ax} = 2). Errors in bond length (R) and coordination numbers (N) are ± 0.02 Å and ~20 %, respectively. (ΔE_0: shift in threshold energy, σ^2 : EXAFS-Debye-Waller factor).

Sample	$U\text{-}O_{ax}$		$U\text{-}O_{eq}$			ΔE_0
(cf. Tab. 10.1)	R (Å)	σ^2 ($Å^2$)	N	R (Å)	σ^2 ($Å^2$)	(eV)
1	1.78	0.002	5.0	2.38	0.013	- 7.5
2	1.77	0.002	5.4	2.39	0.013	- 8.3
3	1.78	0.003	5.2	2.37	0.013	- 8.5
4	1.78	0.002	5.0	2.37	0.010	- 7.9
5	1.78	0.002	5.1	2.37	0.014	- 8.5

The axial U-O_{ax} distances in all samples investigated were determined to be 1.77 – 1.78 Å, equatorial U-O_{eq} distances amount to 2.37 - 2.39 Å. Within the experimental error there are no differences in the U-O bond distances between the samples with large loadings (sample 1 and 2) compared to those with relatively low loadings (sample 3 and 4). Furthermore, the structural parameters obtained for the sample prepared by sorption of UO_2^{2+} onto a suspension of natural humic acid (sample 2) are the same as those for the samples prepared from humic acid in solution. The sample measured as a wet paste (sample 4) shows the same results as the samples measured in the dried form. This indicates that the presence of excess water does not change the average equatorial bond distance surrounding uranium in the uranyl humate complexes. The comparison of the fit results obtained for the samples prepared from Fluka humic acid and the uranyl humate prepared from synthetic humic acid type M1 shows that the synthetic humic acid behaves similarly towards the binding of UO_2^{2+} ions as the natural humic acid. This was already found in former studies of the interaction of UO_2^{2+} ions with the same synthetic humic acid and Fluka humic acid with higher UO_2^{2+}-loadings [10].
The high Debye-Waller-factors are attributed to a high disorder in the arrangement of atoms in the equatorial shell which is caused by the high variety of binding sites of the humic acids. Additional measurements at low temperatures are necessary to distinguish between static disorder, such as the presence of two U-O_{eq} distances close in proximity and thermal disorder.

Assuming that carboxylic groups are the most important functional groups of the humic acid for the complexation of metal ions at pH 4, essentially three important bonding modes of carboxylate ions to metal ions are possible, as depicted in Fig. 10.6.

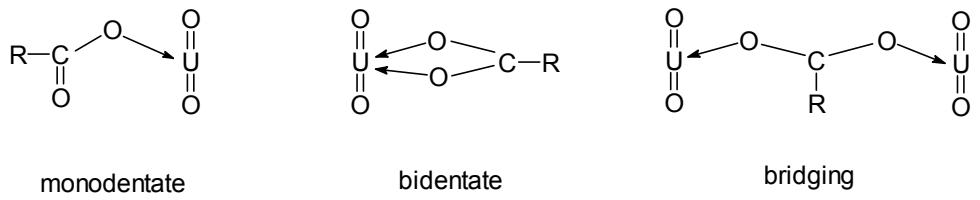

Figure 10.6: Schematic representation of the possible coordination modes of the carboxylate ion onto the UO_2^{2+} unit.

Nineteen crystalline uranyl carboxylate complexes with known structures, having ligands that may serve as models for humic acid structural elements, were considered regarding their axial and equatorial U-O bond distances [24]. The averaged bond distances are 1.76 ± 0.03 Å for

$U\text{-}O_{ax}$, 2.48 ± 0.05 Å for $U\text{-}O_{eq}$ (bidentate carboxylate oxygen atoms), 2.39 ± 0.05 Å for $U\text{-}O_{eq}$ (monodentate carboxylate oxygen atoms) and 2.36 ± 0.05 Å for $U\text{-}O_{eq}$ (bridging carboxylate oxygen atoms).

The observed binding distances for the axial oxygen atoms of the uranyl unit for sample 1 – 5 are comparable to the averaged bond distance observed for the crystalline uranyl carboxylate complexes [24]. Furthermore, the $U\text{-}O_{eq}$ distances in the uranyl humates lie closer to the averaged values typical for monodentate or bridging carboxylate groups, than to the averaged value for bidentate coordination. So we conclude that the number of monodentate and/or bridging carboxylate ligands must be greater than the number of bidentate ligands. Otherwise the average $U\text{-}O_{eq}$ distance would exceed the measured value of 2.37 ± 0.02 Å. Nevertheless, this result is in contrast to IR results published by Koglin et al. [30], who interpreted a bidentate coordination of humic acid carboxylic groups onto uranium.

The EXAFS fits of the uranyl humate spectra show the presence of five oxygen atoms in the equatorial sphere around the uranyl unit. Assuming charge neutralization two negative charged complexing groups are required to neutralize the charge of the uranyl unit. If two monodentate carboxylate groups are considered as the bonding partners three neutral ligands are necessary to fulfill the coordination requirement of five equatorial atoms. The binding of two bidentate carboxylate anions or four bridging groups would also attain charge neutralization. In both cases, four equatorial oxygen atoms are contributed by the carboxylate ligands and the coordination number of five is still not reached. However, in the case of bidentate ligation the resulting average bond distance would be much longer. This is of course assuming that the bond length between any neutral ligands and uranium is not extremely short. As example, the average $U\text{-}O_{eq}$ bond distance for water ligands in the crystalline complexes considered in [24] is 2.43 Å. If water is considered as the neutral ligand/s then the average $U\text{-}O_{eq}$ bond length from a neutral complex involving bidentate carboxylate groups is exceedingly longer than the distances observed for samples 1-5.

If not only carboxylate ligands but also acidic hydroxyl groups, e.g., phenolic OH or hydroxyl groups in α-position to a carboxyl group, are included as possible ligands for charge neutralization several neutral ligands must be present to obtain a coordination number of five. Which kind of neutral ligands contribute to the coordination is not known. However, it is possible that protonated phenolic OH groups contribute to the complexation process.

The possibility of any coordination involving bridging of two uranyl ions via a single carboxylate oxygen atom (μ-oxo-bridging) was excluded because no typical U-U distance for

such coordination was observed. However, from our analysis the presence of bridging carboxylate groups cannot be excluded [24].

10.2 Determination of uranyl complexation constants with natural and synthetic humic acids at pH 4

Laser-induced fluorescence spectroscopy offers a very good possibility to investigate the complexation behavior of metal ions with humic acids. This method renders the possibility for a direct quantification and characterization of the investigated system with very low detection limits. In contrast to other methods like ultrafiltration, ion exchange or solvent extraction, a further advantage of this method represents the possibility for a direct determination of the metal ion speciation without any disturbance of the thermodynamic equilibrium.
The objective of the investigation was to determine the ability of synthetic humic acid type M42, which has a carboxylic group content comparable to most natural humic acids, to mimic the complexation behavior of natural humic acids with UO_2^{2+} ions.

10.2.1 Experimental

Preparation of uranyl humate solutions

To characterize the interaction of the UO_2^{2+} ion with synthetic and natural humic acids, we measured the fluorescence signal of the UO_2^{2+} ion as a function of the total uranyl concentration at a constant humic acid concentration. All experiments were performed in air at 20 ± 1 °C in 0.1 M $NaClO_4$ at pH 3.98 ± 0.01 for synthetic humic acid type M42 (charge M81) and pH 3.96 ± 0.03 for Aldrich humic acid. The humic acid concentration was kept constant at 5 mg/L. The uranyl concentration was varied from $1.0 \cdot 10^{-6}$ to $9.7 \cdot 10^{-6}$ M for synthetic humic acid type M42 and $6.5 \cdot 10^{-7}$ to $8.3 \cdot 10^{-6}$ M for Aldrich humic acid. The sample solutions were prepared from stock solutions of humic acid and $UO_2(ClO_4)_2$. The concentration of UO_2^{2+} in the solutions was determined with ICP-MS analysis. The ionic strength was adjusted to 0.1 M with 1 M $NaClO_4$ (p.a., Merck). Calibration of the relative fluorescence signal as a function of the UO_2^{2+} concentration was done with solutions that were identical to the solutions of the complexation experiments but did not contain any humic acid. The pH values were adjusted with NaOH (Merck) and $HClO_4$ (Merck).

The uranyl species distribution from pH 3 to 9 ([UO_2^{2+}]: $1 \cdot 10^{-5}$ M; pCO_2: $10^{-3.5}$ atm; 0.1 M $NaClO_4$) was calculated with the EQ3/6 program [31] based on complex formation constants compiled by Grenthe et al. [32] (NEA data base). Under these conditions, the first uranyl hydrolysis species, UO_2OH^+, occurs besides the free UO_2^{2+} ion at pH 4 with a relative concentration of 2.7 %. Thus, the uranyl hydroxo species concentrations in the experiments performed are lower than the experimental error and were therefore not considered for calculating the complexation constants.

Laserfluorescence spectroscopic measurements

A detailed description of the laser instrumentation is given in [33]. The spectroscopic light source was a Nd:YAG laser, pulsed with a repetition rate of 10 Hz (GCR 230, Spectra Physics, Mountain View, CA, USA). The fourth harmonic oscillation of the Nd:YAG laser (266 nm) at laser energies below 700 μJ was applied to excite the uranyl fluorescence. At these energies, no significant photolytic decomposition of the humic acid occurs [33]. The emission signal was focused into the spectrograph (Model 1235 Acton Research, Acton, MA, USA) by a fiber optic cable. For fluorescence detection, we used a time controlled photodiode array detector (Model 1455 EG&G Instruments, Princeton Applied Research, Princeton, NJ, USA), cooled to – 30 °C. Using a delay generator (Model 9650, EG&G Instruments), the time gate of fluorescence detection was set to open at 200 ns after the excitation pulse for an interval of 1000 ns. Time resolved measurements allow the discrimination of uranyl fluorescence signal against excitation pulse and short humic acid fluorescence emission (fluorescence lifetime < 10 ns [10]). The fluorescence signal was measured from 408 to 634 nm. Ten spectra of each sample were collected over 100 laser pulses in each case. The spectra were standardized relative to the pulse energy. An average spectrum was calculated from 10 emission spectra.

10.2.2 Results and discussion

The measured fluorescence spectra represent the sum of the free UO_2^{2+} ion fluorescence, the fluorescence of the first hydrolytic uranyl species (UO_2OH^+) and a residue of scattered laser light of the excitation pulse (second order) at 532 nm produced in the spectrograph. The spectra were deconvoluted by a non-linear least square method using spectra from earlier measurements [33] to calculate the contribution of the free UO_2^{2+} ion to the fluorescence signal. The spectrum of UO_2OH^+ was included in the peak deconvolution because of the strong fluorescence yield of UO_2OH^+ in comparison to the free UO_2^{2+} ion. The amount of

UO_2OH^+ (< 2.7 %) that was present in the experiment was neglected in the stability constant calculations because its concentration was below the experimental error for the UO_2^{2+} concentration determination. For all cases no emission of the uranyl humate complex was directly observed. Furthermore, we did not observe any quenching effects of the UO_2^{2+} ion by self quenching or quenching by the humic acid in the investigated concentration range.

The uranyl fluorescence intensity for each sample was integrated between 465 and 570 nm. Equivalent results from the solutions without humic acid were used to determine the free UO_2^{2+} concentration when uranyl humate is present.

The evaluation of the experimental data was performed based upon the metal ion charge neutralization model [34], which considers the complexation reaction of a given metal ion with humic acid as a metal ion charge neutralization process. According to this model, the UO_2^{2+} ion occupies two proton exchanging sites of the humic acid molecule [Eq. (10.1)]:

$$UO_2^{2+} + HA(II) \equiv UO_2HA(II) \tag{10.1}$$

where HA(II) represents the humic acid ligand and $UO_2HA(II)$ stands for the uranyl humate complex.

$$\beta = \frac{[UO_2HA(II)]}{[UO_2^{2+}]_{free} \bullet [HA(II)]_{free}} \tag{10.2}$$

β - complexation constant; $[UO_2HA(II)]$ - uranyl humate concentration; $[UO_2^{2+}]_{free}$ – free uranyl ion concentration; $[HA(II)]_{free}$ – free humic acid concentration

The model was chosen because it offers the possibility to determine complexation constants which are independent of the humic acid origin, the metal ion concentration, and the pH value. Based on this concept, stability constants of uranyl complexes with natural humic acids and their synthetic analogues are expected to be similar.

Because not all complexing sites of the humic acid are available for the UO_2^{2+} ion binding the loading capacity (LC), which represents the mole fraction of maximal available complexing sites of the humic acid, is introduced by this model. The LC represents a humic acid specific value which depends on the experimental conditions.

The LC and the complexation constants were determined graphically by linear regression of the experimental data after rearranging Eq. (10.3) for the free UO_2^{2+} ion concentration [34]:

$$\beta = \frac{[UO_2HA(II)]}{[UO_2^{2+}]_{free} \bullet ([HA(II)]_{total} \bullet LC - [UO_2HA(II)])} \tag{10.3}$$

where β represents the complexation constant, $[UO_2HA(II)]$ the uranyl humate concentration, $[UO_2^{2+}]_{free}$ the free uranyl ion concentration, $[HA(II)]_{total}$ the total molar humic acid concentration [34] and LC stands for the loading capacity.

$$[UO_2^{2+}]_{free} = LC \bullet \frac{[UO_2^{2+}]_{free} \bullet [HA(II)]_{total}}{[UO_2HA(II)]} - \frac{1}{\beta} \qquad (10.4)$$

Fig. 10.7 shows the analysis for synthetic humic acid type M42.

Considering the graphically determined LC, we computed a complexation constant for each experimental point. The results of these calculations, the analytical data of the starting concentrations and the data derived from the spectroscopic measurements are summarized in Tab. 10.3. Tab. 10.4 gives the graphically determined complexation constants and the LC in comparison to the values published by Czerwinski et al. [35] obtained by using a natural humic acid from the Gorleben site.

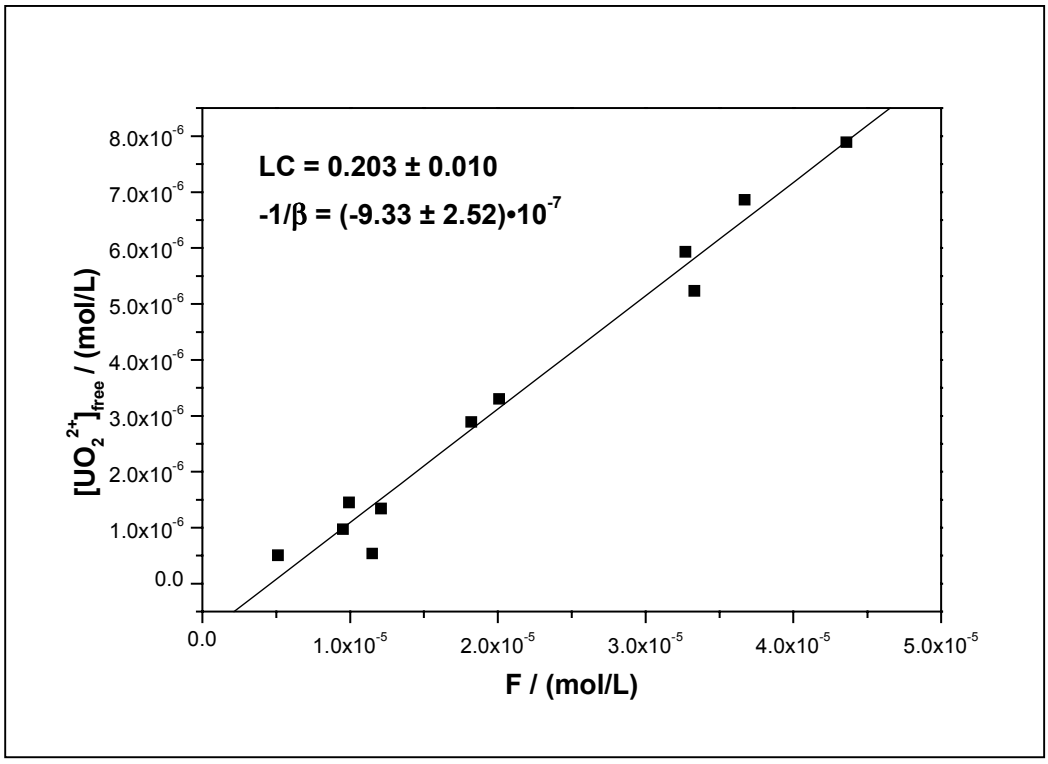

Figure 10.7: Graphically determination of the loading capacity (LC) and the complexation constant for the complexation of synthetic humic acid type M42 with the UO_2^{2+} ion by linear regression of experimental data.

$$F = \frac{[UO_2^{2+}]_{free} \bullet [HA(II)]_{total}}{[UO_2HA(II)]}$$

Table 10.3: Analytical data of the starting concentrations, the spectroscopically determined data of each component, and log β for the complexation of synthetic humic acid of type M42 and Aldrich humic acid.

$[HA(II)]_{total}$ (μmol/L)	$[UO_2^{2+}]_{total}$ (μmol/L)	$[UO_2^{2+}]_{free}$ (μmol/L)	$[UO_2HA(II)]$ (μmol/L)	$[HA(II)]_{free}$ (μmol/L)	log β
Synthetic humic acid type M42 (charge M81)					
(PEC[a]: 3.90 ± 0.18 meq/g; pH 3.98 ± 0.01; I: 0.1 M $NaClO_4$; LC: 0.203 ± 0.010)					
9.8 [b]	1.00	0.54	0.46	1.53	5.74
9.8	1.47	0.51	0.97	1.02	6.27
9.8	1.97	0.97	1.00	0.99	6.02
9.8	2.42	1.34	1.08	0.90	5.95
9.8	2.88	1.45	1.43	0.56	6.25
9.8	4.44	2.89	1.55	0.43	6.09
9.8	4.90	3.30	1.60	0.38	6.10
9.8	6.76	5.23	1.54	0.45	5.82
9.8	7.71	5.93	1.78	0.21	6.16
9.8	8.70	6.86	1.83	0.15	6.24
9.8	9.66	7.89	1.77	0.21	6.03
Aldrich humic acid (charge A2)					
(PEC: 5.33 ± 0.12 meq/g; pH 3.96 ± 0.03; I: 0.1 M $NaClO_4$; LC: 0.217 ± 0.022)					
13.3	0.65	0.27	0.38	2.51	5.76
13.3	1.24	0.48	0.77	2.12	5.88
13.3	2.42	1.23	1.19	1.70	5.76
13.3	2.96	1.45	1.51	1.38	5.88
13.3	4.80	2.87	1.93	0.96	5.84
13.3 [b]	6.07	3.58	2.49	0.40	6.24
13.3	6.99	4.95	2.04	0.85	5.68
13.3	8.27	5.79	2.48	0.41	6.01

[a] PEC: Proton exchange capacity.
[b] Value was not considered for validation.

Table 10.4: Complexation constants and loading capacities of synthetic humic acid type M42 and purified natural humic acid from Aldrich in comparison to a Gorleben humic acid.

	Synthetic humic acid type M42 (charge M81)	Aldrich humic acid (charge A2)	GoHy humic acid GoHy-537 [35]
	Complexation constants log β [a]		
Graphical [b]	6.04 ± 0.24	5.86 ± 0.28	-
Calculated [c]	6.06 ± 0.35	5.88 ± 0.35	6.16 ± 0.13
	Loading capacities (LC) [%] [a]		
Graphical [b]	20 ± 2	22 ± 4	18.5 ± 0.3

[a] Deviations = 2 σ.
[b] Calculated by linear regression of experimental data.
[c] Mean values from Tab. 10.3.

Within the experimental errors we found a remarkable agreement between the LC and complexation constants of the synthetic humic acid type M42 and Aldrich humic acid, which indicates a similar complexation behavior for both investigated systems. This fact was already observed comparing the complexation behavior of the natural humic acids from Fluka and Aldrich with a previous sample of synthetic humic acid type M42 published in [36].
For validation of the postulated complexation reaction [Eq. (10.1)], Eq. (10.2) was rearranged to:

$$\log\frac{[UO_2HA(II)]}{[UO_2^{2+}]_{free}} = \log[HA(II)]_{free} + \log\beta \quad . \tag{10.5}$$

The slope of the linear regression function of Eq. (10.5) represents the metal ion to ligand ratio and will result of unity, when Eq. (10.1) is valid. The determined values are 0.92 ± 0.17 for synthetic humic acid and 0.81 ± 0.16 for Aldrich humic acid. These results verify the postulated complexation reaction.

Although there are several literature values for the uranyl humic acid complexation, a direct comparison of our complexation data is only possible with data published by Czerwinski et al. [35] given in Tab. 10.4, because these were also treated with the metal ion charge neutralization model. The complexation constants of our synthetic humic acid and Gorleben humic acid agree very well within the experimental errors. There are small differences in the loading capacity of our product and of Gorleben humic acid which may be due to their different origin.

From these results we conclude that the synthetic humic acid type M42 appropriately simulates the functionality of natural humic acids although there are differences in their elemental composition and structural elements

10.3 Structure of uranyl(VI) humate complexes of synthetic and natural humic acids studied by FTIR spectroscopy

IR spectroscopy is a useful tool for the characterization of humic acids regarding their functionality. Functional and structural changes of humic acids are reflected by changes in the intensity, position or occurrence of characteristic absorption bands. In addition, IR spectroscopy offers the possibility to investigate functional variations of humic acids due to complex formation processes with metal ions [24].

The objective of this work was to proof the similar coordination of UO_2^{2+} ions onto synthetic and natural humic acids and to confirm previous results obtained by EXAFS and laser-induced fluorescence spectroscopy. For the first time uranyl humate complexes were investigated in the far infrared range (FIR) beside the middle infrared range (MIR) [37].

10.3.1 Experimental

Preparation of uranyl humates

For the preparation of the uranyl humate complexes synthetic humic acid type M1 and type M42 as well as natural humic acid from Aldrich were suspended in water. On the basis of their carboxylic group contents uranyl acetate (type M1, Aldrich) or uranyl perchlorate (type M42) solutions were added to the aqueous humic acid suspensions for the complex formation. The pH values were adjusted to pH 4 for synthetic humic acid type M1 and Aldrich humic acid and to pH 2 for humic acid type M42. The uranyl humate complexes were isolated by centrifugation, purified and lyophilized. The uranyl loadings of the complexes were determined by ICP-MS after digestion of the complexes with HNO_3. Assuming charge neutralization, the uranyl humates of humic acid type M1, type M42 and Aldrich show regarding their carboxyl group contents uranyl loadings of 120 %, 29 % and 129 %, respectively. The low uranyl loading of humic acid type M42 compared to humic acid type M1 and humic acid Aldrich results from the different pH values during sample preparation.

FTIR measurements

FTIR measurements were carried out with the spectrometer mod. SPECTRUM 2000 (Perkin Elmer, Nieuwerke, NL). The humic acids as well as their uranyl complexes were measured in the solid form as KBr pellets (MIR range) and PE pellets (FIR range).

10.3.2 Results and discussion

Fig. 10.8 shows a comparison of the FTIR spectra of the humic acids investigated in the range between 4000 cm^{-1} and 50 cm^{-1} (MIR-FIR).

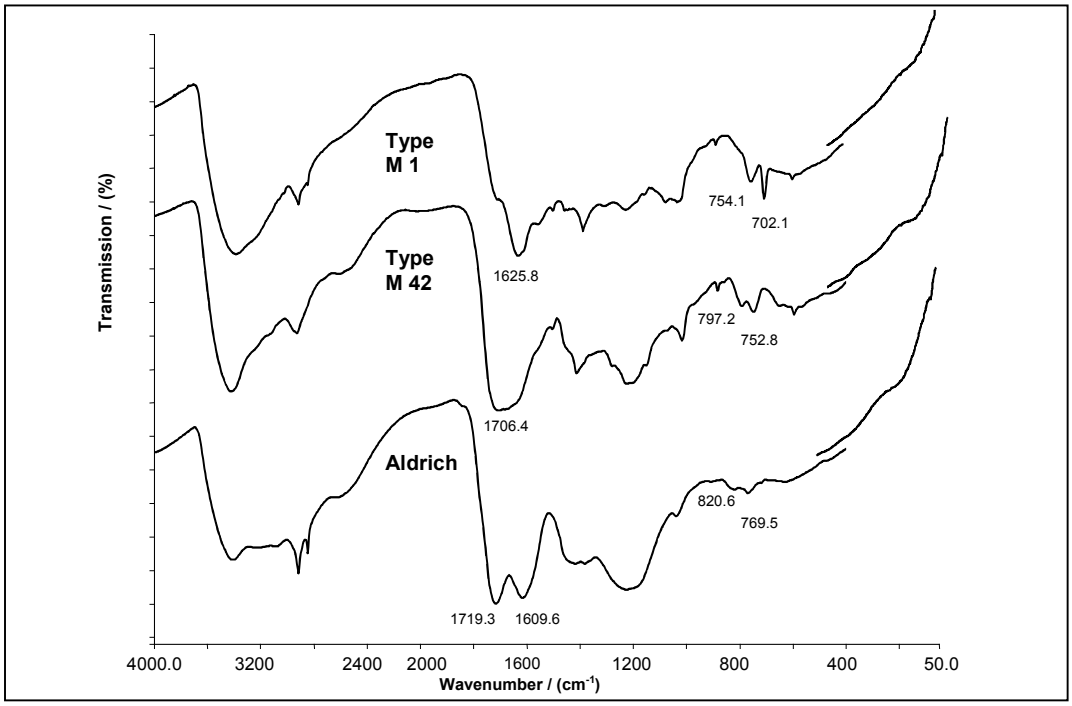

Figure 10.8: FTIR spectra (MIR and FIR) of synthetic humic acid type M1 and type M42 and Aldrich humic acid.

The humic acids show comparable IR absorption bands. However, some differences occur in the MIR. Synthetic humic acid type M1 exhibits clear δ(C-H) out of plane vibrations at 702.1 cm^{-1} and 754.1 cm^{-1} which corresponds to mono-substituted aromatic structures caused by the use of phenylalanine as precursor substance. In contrast to synthetic humic acid type M1, synthetic humic acid type M42 and Aldrich humic acid show more pronounced C=O stretching vibrations at 1706.4 cm^{-1} (M42) and 1609.6 cm^{-1}, 1719.3 cm^{-1} (Aldrich) due to their higher carboxylic group contents. All humic acids show absorption bands which correspond to aliphatic structural elements. As expected, in the FIR the humic acids exhibit no characteristic absorption bands.

Fig. 10.9 depicts the FTIR spectra of the solid uranyl humate complexes. The FTIR spectra of all uranyl humates show in comparison to the untreated humic acids comparable variations due to the complex formation. All FTIR spectra of the uranyl humate complexes show in consequence of the complexation reaction a decrease of the absorption bands characteristic for C=O and C-O vibrations of non-dissociated carboxylic groups at about 1720 cm^{-1} and 1200 cm^{-1}.

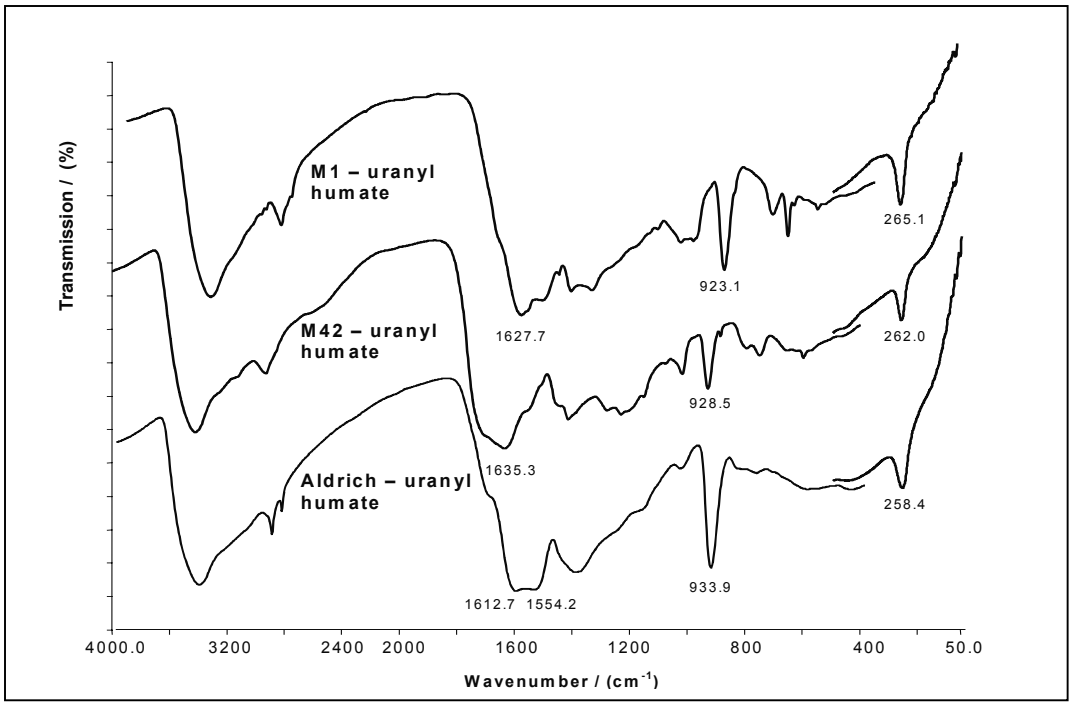

Figure 10.9: FTIR spectra of uranyl humate complexes of synthetic humic acid type M1, type M42 and Aldrich humic acid.

For all complexes the asymmetric UO_2^{2+} stretching vibration was observed in the MIR range (923.1 cm^{-1} (M1), 928.3 cm^{-1} (M42) and 933.1 cm^{-1} (Aldrich)). The position of this band is shifted significantly to higher wavenumbers with decreasing aromatic character of the complexing humic acid. Furthermore, characteristic UO_2^{2+} bending frequencies were first detected in the FIR range at 265.1 cm^{-1} (M1), 262.0 cm^{-1} (M42) and 258.4 cm^{-1} (Aldrich). These bands show a significant shift to lower wavenumbers with decreasing aromatic character of the humic acid.

From the results obtained one can conclude that the UO_2^{2+} coordination onto humic acids is comparable for the investigated synthetic and natural humic acids. The observed shifts of the absorption bands of the UO_2^{2+} unit in the MIR and FIR range may be explained by differences in the aromaticity of the humic acids. However, these differences do not indicate significant differences in the UO_2^{2+} coordination.

The FTIR spectroscopic results agree with our previous investigations by EXAFS and laser-induced fluorescence spectroscopy and show once more that the synthetic humic acids mimic the functionality of natural humic acids very well.

11 Influence of phenolic hydroxyl groups on the complexation behavior of humic acids with uranium(VI)

The influence of phenolic OH groups on the complexation behavior of humic acids under acid and neutral conditions is not known up to now. Often it is assumed that only humic acid carboxylic groups act as complexing groups in the complexation process with metal ions at pH values lower pH 9 because of the high pK_a values of phenolic OH groups [38]. Nevertheless, phenolic OH groups may contribute to the complexation process as chelating agents. Beyond it they are able to form hydrogen bonds, e.g., with oxygen atoms coordinated to the complexing metal ion.

For the first time, we investigated the influence of phenolic OH groups on the complexation behavior of humic acids with UO_2^{2+} ions using a modified synthetic humic acid type M1 with blocked phenolic OH groups as well as a additional alkali treated synthetic humic acid of type M1 (see paragraph 7; type M1, charge R36/95). The investigations were performed at pH 4 by laser-induced fluorescence spectroscopy.

11.1 Experimental

The preparation of the uranyl humates corresponds to the procedure described in paragraph 10.2.1. The composition of the investigated uranyl humate solutions as well as the main characteristics of the humic acids applied are shown in Tab. 11.1.

The calibration of the relative fluorescence signal as a function of the UO_2^{2+} concentration was done with solutions that were identical to the solutions of the complexation experiments but did not contain any humic acid.

Table 11.1: Characteristics of the applied humic acids and composition of the investigated uranyl humate solutions.

	Type M1-V [a]	Type M1-B [b]
phenolic OH / (meq/g)	1.7 ± 0.1	1.1 ± 0.2
PEC [c] / (meq/g)	2.12 ± 0.06	1.94 ± 0.13
COOH / (meq/g)	2.03 ± 0.02	1.91 ± 0.07
UO_2^{2+} / (µmol/L)	1.1 – 10.3	1.1 – 10.3
HA / (mg/L)	10	10
pH	3.96 ± 0.04	3.94 ± 0.05
I_{NaClO4} / (mol/L)	0.1	0.1

[a] Type M1-V: humic acid type M1 directly saponified. [b] Type M1-B: humic acid type M1 with blocked phenolic OH groups. [c] PEC: Proton exchange capacity.

The experimental conditions of the spectroscopic measurements were the same as described in paragraph 10.2.1.

11.2 Results and discussion

The experimental data were evaluated applying the charge neutralization model by Kim and Czerwinski [34]. This model was chosen because it renders, due to the introduction of the loading capacity as normalizing term, the possibility for the description of the complexation behavior of humic acids independent of the experimental conditions and of the origin of the humic acids. Applying this complexation model comparable complexation constants will be determined for different humic acids. That means, in contrast to other thermodynamic complexation models, differences in the complexation behavior of humic acids will not be reflected in different stability constants. However, differences in the complexation behavior of humic acids will result in different loading capacities, which depend on the humic acid and the experimental conditions.

A significant lower loading capacity for the humic acid with blocked phenolic OH groups should result, if the blocking of the phenolic OH groups shows an influence on the complexation behavior of humic acids with UO_2^{2+} ions.

Tab. 11.2 shows the analytical data of the starting concentrations, the spectroscopically determined data for each component and the complexation constants which were determined for each measurement. The loading capacities (LC, Eq. (11.1)) for both humic acids were determined graphically as described in paragraph 10.2.2. An illustration of the LC (Eq. (11.1))

for both humic acids with UO_2^{2+} ions, which represents the mole fraction of maximal available complexing sites of the humic acids under the applied experimental conditions, is given in Fig. 11.1.

$$LC = \frac{[UO_2HA(II)]_{max}}{[HA(II)]_{tot}} \qquad (11.1)$$

$[UO_2HA(II)]_{max}$ represents the maximal concentration of humic acid complex which can be formed under the applied experimental conditions and $[HA(II)]_{tot}$ stands for the total molar humic acid concentration.

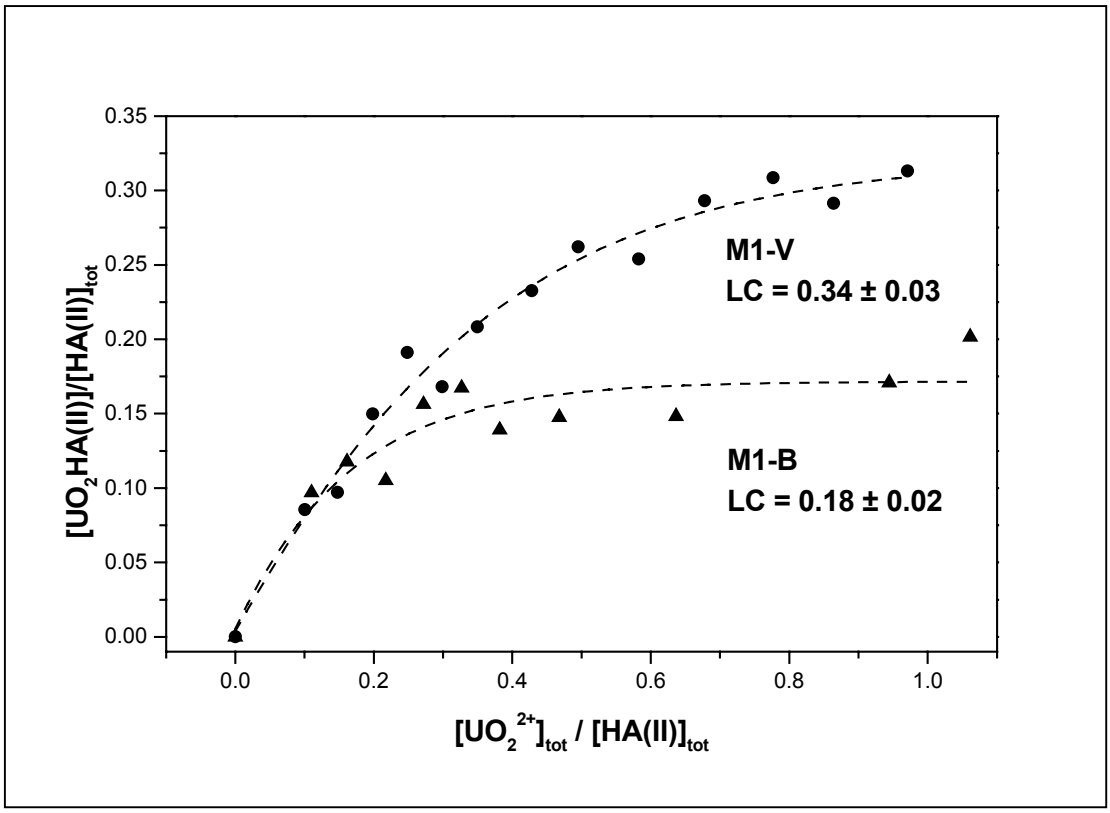

Figure 11.1: Loading capacities for humic acid M1-V and M1-B.

Tab. 11.3 summarizes the LC and the calculated complexation constants for humic acid M1-V and M1-B.

Table 11.2: Analytical data of the starting concentrations, the spectroscopically determined data of each component, and log β for the complexation of the alkali treated synthetic humic acid type M1 (M1-V) and the modified synthetic humic acid type M1 with blocked phenolic OH groups (M1-B).

$[HA(II)]_{total}$ (µmol/L)	$[UO_2^{2+}]_{total}$ (µmol/L)	$[UO_2^{2+}]_{free}$ (µmol/L)	$[UO_2HA(II)]$ (µmol/L)	$[HA(II)]_{free}$ (µmol/L)	log β
Type M1-V (unmodified phenolic OH)					
(PEC[a]: 2.12 ± 0.06 meq/g; pH 3.96 ± 0.04; I: 0.1 M $NaClO_4$; LC: 0.34 ± 0.03)					
10.6	1.07	0.16	0.91	2.69	6.32
10.6	1.56	0.53	1.03	2.56	5.88
10.6	2.10	0.52	1.59	2.01	6.18
10.6	2.63	0.61	2.03	1.57	6.33
10.6	3.17	1.39	1.78	1.81	5.85
10.6	3.70	1.50	2.21	1.39	6.03
10.6	4.54	2.07	2.47	1.13	6.02
10.6	5.25	2.47	2.78	0.82	6.14
10.6	6.18	3.48	2.69	0.90	5.93
10.6	7.18	4.08	3.11	0.49	6.19
10.6	8.23	4.96	3.27	0.32	6.31
10.6	9.16	6.07	3.09	0.51	6.00
10.6	10.29	6.98	3.32	0.28	6.23
Type M1-B (modified phenolic OH groups)					
(PEC: 1.94 ± 0.13 meq/g; pH 3.94 ± 0.05; I: 0.1 M $NaClO_4$; LC: 0.18 ± 0.02)					
9.7	1.07	0.13	0.94	0.86	6.94
9.7	1.56	0.42	1.14	0.65	6.62
9.7	2.10	1.09	1.02	0.78	6.08
9.7	2.63	1.12	1.52	0.28	6.69
9.7	3.17	1.54	1.62	0.17	6.78
9.7	3.70	2.36	1.35	0.45	6.11
9.7	4.54	3.10	1.43	0.36	6.10
9.7	6.18	4.74	1.44	0.36	5.93
9.7	9.16	7.50	1.66	0.14	6.20
9.7 [a]	10.29	8.34	1.96	-	-

[a] Value was not considered for determination of log β and validation.

Table 11.3: Complexation constants and loading capacities of the synthetic humic acid with unmodified phenolic OH groups (M1-V) and with blocked phenolic OH groups (M1-B).

	Synthetic humic acid M1-V	Synthetic humic acid M1-B
	Complexation constants log β [a]	
Calculated [b]	6.11 ± 0.34	6.38 ± 0.74
	Loading capacities (LC) [%] [a]	
Graphical [c]	34 ± 3	18 ± 2

[a] Deviations = 2 σ.
[b] Mean values from Tab. 9.2.
[c] Determined by linear regression of experimental data.

Within their experimental errors both humic acids show comparable complexation constants. Nevertheless, humic acid M1-B shows a significant lower LC at pH 4 than humic acid M1-V. This indicates that the blocking of the phenolic OH groups changes the complexation behavior of the humic acid. From these results one can conclude that phenolic OH groups may be involved in the complexation process with UO_2^{2+} ions under the applied conditions.
At pH 4, the humic acid phenolic OH groups are likely protonated due to their high pK_a values. We assume that intramolecular hydrogen bonds between the hydrogen atoms of the unmodified phenolic OH groups and the oxygen atoms of the UO_2^{2+} ions contribute to the complex formation. However, also steric effects, i.e., steric hindrances, may contribute to the change of the complexation behavior of the humic acid after blocking the phenolic OH groups. Currently we are investigating the influence of phenolic OH groups on the complexation behavior of humic acids using other modified synthetic and natural humic acids. Furthermore, EXAFS investigations are planned to confirm this result.

12 Complexation behavior of uranium(VI) with humic acids at pH 7

Predicting the environmental behavior of uranium in aquifer systems requires knowledge about the complexation behavior of uranium in the presence of humic substances at environmental relevant pH values, i.e., in the neutral pH range. Up to now the uranium complexation with humic substances has been mostly studied under conditions where

competing reactions such as carbonate complexation and hydrolysis are excluded. The investigations were carried out at pH #4. However, it is known, that in the environmental relevant pH range the uranium speciation is determined by carbonate complexation and hydrolysis. Thus, mixed ligand complexes consisting of uranium, humic acid and a secondary ligand, e.g., carbonate or hydroxide can be formed. From that the requirement for the investigation of the complexation behavior of uranium in the presence of humic acids at pH values greater than pH 4 results.

There are only few studies describing the formation of ternary uranium complexes in the presence of humic acids. Zeh et al. [39] described a ternary complex of uranyl hydroxo humate ($UO_2(OH)HA$, $\log \beta = 14.7 \pm 0.5$). Glaus et al. [40] reported a UO_2CO_3HA complex with a stability constant of $\log \beta \approx 5$.

Within this project we investigated the complexation behavior of uranium in the presence of humic acids at pH 7 by means of time-resolved laser-induced fluorescence spectroscopy. The experiments were performed under exclusion of CO_2 to prevent the formation of carbonate complexes.

12.1 Experimental

Sample preparation

We investigated the complexation behavior of uranium with the purified natural humic acid from Aldrich at pH 7.00 ± 0.04 in 0.1 M $NaClO_4$ solution. The fluorescence signal of the uranium species as a function of the total uranium concentration was measured at a constant humic acid concentration (5 mg/L). The uranium concentration was varied from $4.8 \cdot 10^{-6}$ to $1.8 \cdot 10^{-5}$ mol/L. The calibration of the relative fluorescence signal as a function of the uranium concentration was done on solutions that were identical to the solutions of the complexation experiments but did not contain any humic acid.

To exclude the formation of carbonate complexes the sample preparation was performed using CO_2 free water as well as carbonate-free chemicals in a glove box under inert gas conditions (N_2). The uranium concentration of the solutions was determined by ICP-MS analysis.

Laserspectroscopic measurements

The spectroscopic investigations were performed in a glove box under inert gas conditions (N_2). For fluorescence excitation we used a excitation wavelength of 410 nm produced in an optical parametric oscillator (MOPO-730-10, Spectra Physics, USA), which was pumped with

the third harmonic (355 nm) of a Nd:YAG laser. The laser light was transferred into the glove box applying a fiber optic cable. The laser energies for fluorescence excitation only reached amounts of about 150 µJ because of an energy loss in the fiber optic cable. The fluorescence signal was focused into the spectrograph (Model 1235 Acton Research, Acton, MA, USA) by a fiber optic cable. For the detection we used a time controlled photodiode array detector (model 1455 EG&G Instruments, Princeton Applied Research, Princeton, NJ, USA), cooled to –30 °C. The time gate of fluorescence detection was set to open at 200 ns after the excitation pulse for an interval of 2 µs. The fluorescence signal was measured from 408 to 634 nm. Ten spectra of each sample were collected over 100 laser pulses in each case. The spectra were standardized relative to the pulse energy. An average spectrum was calculated from 10 emission spectra. Because of the excitation wavelength of 410 nm and the low laser energies used for the excitation we only observed a weak fluorescence signal. The errors of the fluorescence measurements amounted to about 10 %.

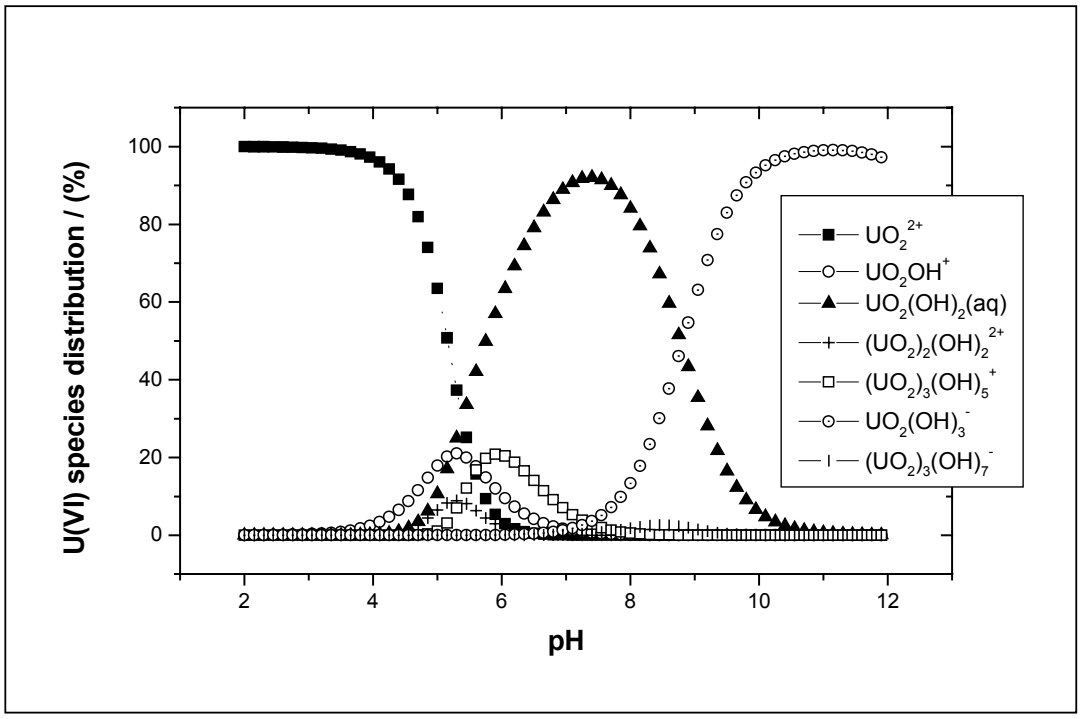

Figure 12.1: Uranium(VI) species distribution in aqueous solution in the absence of CO_2 and humic acid ($[UO_2^{2+}]$: $1 \cdot 10^{-5}$ mol/L; I: 0.1 M $NaClO_4$).

Uranium species distribution

The uranium species distribution from pH 2 to 12 ($[UO_2^{2+}]$: $1 \cdot 10^{-5}$ mol/L; I: 0.1 M $NaClO_4$) in absence of humic acid and CO_2 was calculated (Fig. 12.1) with the EQ3/6 program [31] based on complexation constants compiled by Grenthe et al. (NEA data base) [32].

In absence of CO_2 and humic acid, the uranium speciation in the neutral and alkaline pH range is dominated by uranyl hydroxo complexes. At pH 7 uranium occurs to 89.6 % as $UO_2(OH)_2(aq)$, 6.4 % as $(UO_2)_3(OH)_5^+$, 1.5 % as UO_2OH^+, and 1.4 % as $UO_2(OH)_3^-$.

12.2 Results and discussion

The measured uranyl fluorescence intensities of the solutions with humic acid as well as without humic acid were integrated between 450 and 570 nm. Fig. 12.2 shows the results of this integration in dependence on the total uranium concentration.

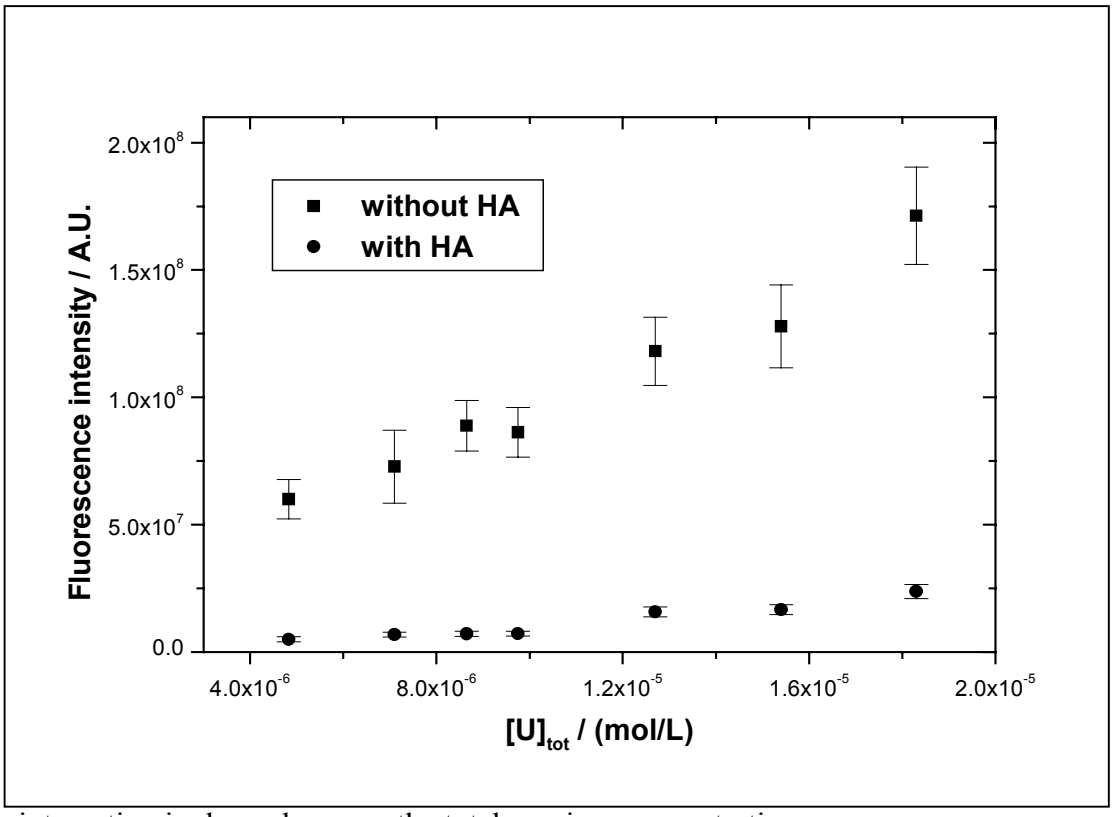

Figure 12.2: Integral fluorescence intensities of U(VI) of the investigated solutions with and without humic acid in dependence on the total uranium concentration.

Due to the complex formation between humic acid and uranium species at pH 7 a strong decrease in the fluorescence intensities of the solutions containing humic acid compared to the fluorescence intensities of the solutions without humic acid was obtained.

Under consideration of the uranium speciation at pH 7 we assume that the complex formation with humic acid starts from the aqueous $UO_2(OH)_2$ complex, that reacts with the humic acid under ligand exchange to a ternary uranyl hydroxo humate complex. The strong decrease in the fluorescence intensities of the solutions with humic acid compared to the solutions without humic acid confirms the assumption that the aqueous $UO_2(OH)_2$ complex basically contributes to the complex formation between uranium(VI) and humic acid at pH 7. Nevertheless, it is not known to which extent other uranium species, that are also present in the solution (with about 10 %) besides the main species $UO_2(OH)_2$, contribute to the complex formation with humic acid. However, in our evaluation we did not consider these additional complex formation possibilities because the amounts of these species are lower than the experimental errors of the fluorescence measurements used for the determination of the concentration of non-complexed uranium as well as for the determination of the total uranium concentration.
For the individual complexation reaction we assumed, comparable to Zeh et al. [39], that UO_2OH^+ reacts with the humic acid under charge neutralization [Eq. (12.1)].

$$UO_2OH^+ + HA(I)^- \equiv UO_2(OH)HA(I) \qquad (12.1)$$

The complex stability constant for the postulated complex formation can be defined as follows:

$$\beta = \frac{[UO_2(OH)HA(I)]}{[UO_2OH^+]_{free} \bullet [HA(I)^-]_{free}} \qquad (12.2)$$

where $[UO_2(OH)HA(I)]$ represents the concentration of the postulated ternary uranyl hydroxo humate complex, $[UO_2OH^+]_{free}$ stands for the free uranium hydroxide concentration in solution and $[HA(I)^-]_{free}$ represents the concentration of the free humic acid ligand in solution. The concentration of $UO_2(OH)HA(I)$ can be derived according to Eq. (12.3).

$$[UO_2(OH)HA(I)] = [UO_2OH^+]_{tot} - [UO_2OH^+]_{free} \qquad (12.3)$$

$[UO_2OH^+]_{tot}$ represents the total uranium concentration in solution determined by ICP-MS. The concentration of free uranium hydroxide, $[UO_2OH^+]_{free}$, was calculated from the fluorescence intensities of the solutions without and with humic acid (Fig. 12.2).
The total humic acid concentration $[HA(I)]_{tot}$ in mol/L was determined according to the definition in the metal ion charge neutralization model [34]:

$$[HA(I)]_{tot} = \frac{[HA] \cdot PEC}{1} \tag{12.4}$$

where [HA] is the concentration of humic acid in g/L, PEC is the proton exchange capacity of the humic acid in eq/g and 1 stands for the charge of the postulated complexing uranium species, UO_2OH^+. Introducing the loading capacity (LC) according to Eq.(12.5), whereby $[UO_2(OH)HA(I)]_{max}$ represents the maximal concentration of the uranyl hydroxo humate complex which can be formed under the applied conditions, the free humic acid concentration in solution can be defined according to Eq. (12.6).

$$LC = \frac{[UO_2(OH)HA(I)]_{max}}{[HA(I)]_{tot}} \tag{12.5}$$

$$[HA(I)]_{free} = [HA(I)]_{tot} \cdot LC - [UO_2(OH)HA(I)] \tag{12.6}$$

The combination of Eqs. (12.2) and (12.6) results in:

$$\beta = \frac{[UO_2(OH)HA(I)]}{[UO_2OH^+]_{free} \cdot ([HA(I)]_{tot} \cdot LC - [UO_2(OH)HA(I)])} \tag{12.7}$$

As already shown in paragraph 10.2.2 the LC as well as the complexation constant can be determined graphically by rearranging Eq. (12.6) for the free $[UO_2OH^+]$ concentration in solution (Fig. 12.3).

Applying the graphically determined LC we calculated for each experimental point a complexation constant according Eq. (12.7). The results of these calculations are summarized in Tab. 12.1 together with the analytical data of the initial concentrations as well as the data derived from the laserspectroscopic measurements.

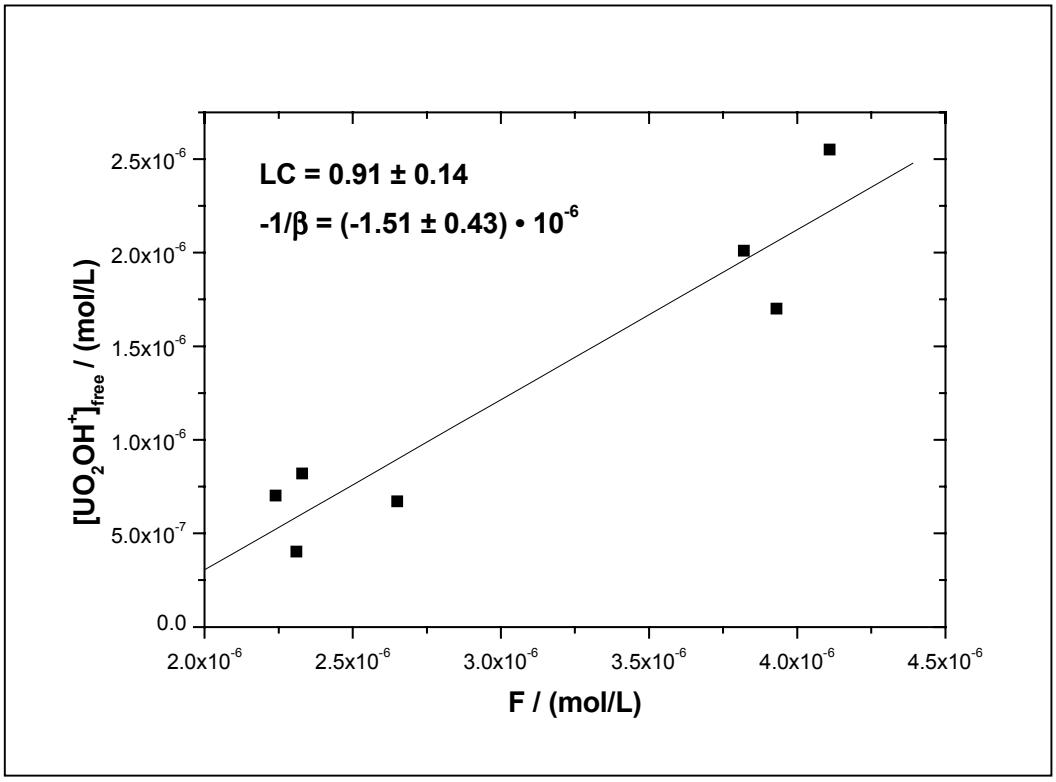

Figure 12.3: Graphical determination of the loading capacity (LC) and the complexation constant for the complexation of Aldrich humic acid with U(VI) at pH 7 by linear regression of experimental data.

$$F = \frac{[UO_2OH^+]_{free} \bullet [HA(I)]_{tot}}{[UO_2(OH)HA(I)]}$$

Table 12.1: Analytical data of the initial concentrations, the spectroscopically determined data of each component, and log β for the complexation of Aldrich humic acid with U(VI) at pH 7.

$[HA(I)]_{tot}$ (µmol/L)	$[UO_2OH^+]_{tot}$ (µmol/L)	$[UO_2OH^+]_{free}$ (µmol/L)	$[UO_2(OH)HA(I)]$ (µmol/L)	$[HA(I)]_{free}$ (µmol/L)	log β
Aldrich humic acid (charge A2/97)					
PEC: 5.06 ± 0.17 meq/g; pH 7.00 ± 0.04; I: 0.1 M $NaClO_4$; LC: 0.91 ± 0.14					
25.4	4.83	0.40	4.43	18.67	5.77
25.4	7.10	0.67	6.43	16.67	5.76
25.4	8.65	0.70	7.95	15.14	5.87
25.4	9.75	0.82	8.93	14.17	5.89
25.4	12.73	1.70	11.02	12.07	5.73
25.4	15.38	2.01	13.37	9.73	5.84
25.4[a]	18.32	2.55	15.77	7.33	5.93

[a] Value was not considered for validation.

The results of the evaluation of the experimental data applying the metal ion charge neutralization model are summarized in Tab. 12.2.

Table 12.2: Results of the laserspectroscopic investigation of the complexation between U(VI) and Aldrich humic acid at pH 7, I: 0.1 M $NaClO_4$.

Complexation data	Aldrich humic acid (± 2 σ)
Loading capacity (LC)	0.91 ± 0.28
log β – calculated[a]	5.83 ± 0.14
log β – graphical[b]	5.83 ± 0.25

[a] Mean value from Tab. 12.1.
[b] Calculated by linear regression of experimental data.

The graphical as well as the calculated complex formation constants agree very well. For validation of the postulated complexation reaction, Eq. (12.2) was rearranged to:

$$\log \frac{[UO_2(OH)HA(I)]}{[UO_2OH^+]_{free}} = \log[HA(I)]_{free} + \log \beta \qquad (12.8)$$

The slope of the linear regression function of Eq. (12.8) for our experimental data was determined with 0.9. The deviation of this value from the ideal value of one and also the relatively high standard deviations obtained for log β (graphical) and for LC are mainly due to the propagation of experimental errors, which were described above. Nevertheless, the result of the validation verifies the postulated complexation reaction.

In addition to the described evaluation of the experimental data applying the metal ion charge neutralization model, we determined a conventional complex stability constant without the introduction of the loading capacity. With this method we determined a complex stability constant of log β = 5.76 ± 0.28 (± 2 σ). This result agrees very well with the complexation constants summarized in Tab. 12.2.
A direct comparison of our complexation constant with the complexation constant published by Zeh et al. [39] is not possible because the stability constant determined by Zeh et al. was calculated using other presumptions.

The total reaction for the complexation of $UO_2(OH)_2$ with humic acid can be divided into different partial reactions [Eq. (12.9)-(12.13)]. Under consideration of the complex stability

constants of the partial reactions as well as the dissociation constant of the humic acid the stability constant of the total reaction can be derived. Therefore, the complexation constants for the hydrolysis of uranium [32] were converted for an ionic strength of 0.1 M applying the Davies equation [41]. The dissociation constant pKa (I: 0.1 M) of Aldrich humic acid was determined from the direct titration of the humic acid (cf. paragraph A.2.4) at half deprotonation and amounts to 4.58 ± 0.03.

Reaction			**log $\beta_{0.1\ M}$**	
$UO_2(OH)_2 + 2\ H^+$	≡	$UO_2^{2+} + 2\ H_2O$	10.08	(12.9)
$UO_2^{2+} + H_2O$	≡	$UO_2OH^+ + H^+$	-4.98	(12.10)
HHA(I)	≡	$H^+ + HA(I)^-$	-4.58 ± 0.03	(12.11)
$UO_2OH^+ + HA(I)^-$	≡	$UO_2(OH)HA(I)$	5.83 ± 0.14	(12.12)
$UO_2(OH)_2$ + HHA(I)	**≡**	**$UO_2(OH)HA(I) + H_2O$**	**6.35**	**(12.13)**

From the partial reactions above we derived a complex stability constant for the total complexation reaction of $UO_2(OH)_2$ with Aldrich humic acid of log $\beta_{0.1M}$ = 6.35.
However, to verify these first results and to determine the contribution of the other uranium species present in the solution to the complexation process at pH 7 it is necessary to continue these investigations with additional laserspectroscopic measurements above and below pH 7. Furthermore, EXAFS investigations should be performed to validate the formation of the $UO_2(OH)HA(I)$ complex.

13 Migration behavior of uranium in an aquifer system rich in humic substances[1]

Laboratory flow through column experiments contribute essential knowledge to assess the influence of humic substances on the migration behavior of actinide ions. There is the possibility to investigate the migration behavior of actinides depending on different parameters, e.g., groundwater flow velocity and column length.

[1] This work was performed in cooperation with Dr. R. Artinger (INE, Forschungszentrum Karlsruhe).

There are some publications which describe flow through column experiments for the investigation of the migration behavior of radionuclides in geological formations, for instance investigations regarding the migration behavior of Am(III) [42], Eu(III), Np(IV)/(V) and Pa(IV)/(V) [43]. Up to now, the migration behavior of uranium was studied by Kim et al. by means of column experiments [44,45]. Migration experiments with a sediment/groundwater (GoHy-2227) system from the Gorleben site (Germany) were performed. The investigations were carried out under inert gas conditions (Ar + 1 % CO_2) with columns of 25 cm length and 5 cm inner diameter.

The present study focuses on flow through column experiments to investigate the migration behavior of uranium in a sandy humic colloid-rich aquifer system, i.e., in the system sediment/groundwater GoHy-532 from Gorleben. We investigated the uranium migration behavior as a function of uranium/groundwater equilibration time before injection into the column, groundwater flow velocity and column length. Ultrafiltration experiments were used for the determination of the uranium size distribution.

13.1 Experimental

Experimental set-up

The experiments were performed in a glove box under inert gas conditions (Ar + 1 % CO_2, 22 ± 2 °C). The columns were tightly packed with sand and equilibrated with groundwater (GoHy-532) from the Gorleben site over several months. The sediment and groundwater characterization was described by Artinger [42,46]. The groundwater has a dissolved organic carbon content (DOC) of about 30 mg C/L, a pH value of 7.2 ± 0.1 and a Eh value of - 220 mV. The monitoring of the experiments and the recording of the experimental data was performed on-line by a personal computer. The experimental set-up is shown in Fig. 13.1.

Tracers

The uranium isotope Uranium-232 ($t_{1/2}$ = 72 years) in form of $^{232}UO_2Cl_2$ (Isotopendienst M. Blaseg GmbH, Waldburg, Germany) was applied because of its high specific activity. The ^{232}U stock solution showed a specific activity of 841 kBq/mL which corresponds to an uranium concentration of $4.6 \cdot 10^{-6}$ mol/L. Furthermore, tritiated water (HTO) was used as a conservative tracer to determine the hydraulic properties of the columns.

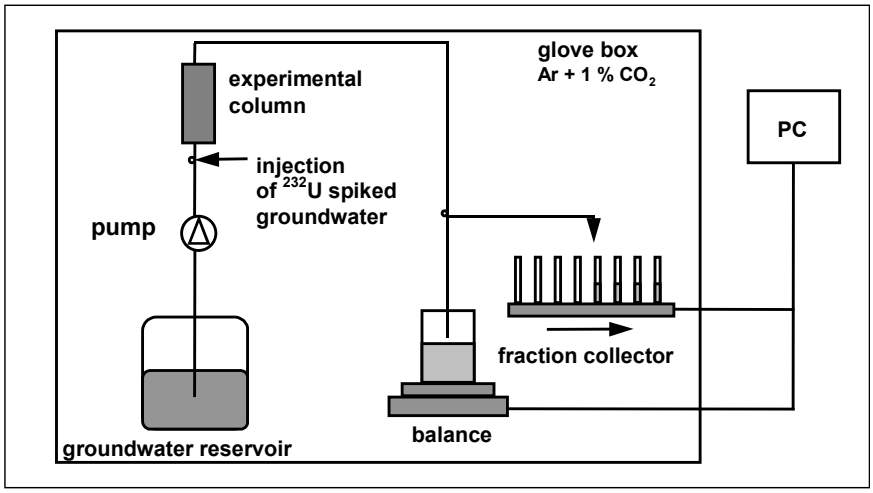

Figure 13.1: Experimental set-up of the column experiments.

Procedure

The column experiments were performed in dependence on:

^{232}U/groundwater pre-equilibration time before the injection into the column,

groundwater flow velocity and column length.

Prior to the experiments aliquots of the ^{232}U stock solution were reacted with the groundwater corresponding to the studied pre-equilibration time. Different pre-equilibration times from 1 hour to 82 days were investigated. The groundwater flow velocity was varied from 0.04 m/d to 2.03 m/d. The column length was varied between 25 cm and 75 cm. The experimental parameters and the hydraulic properties of the individual migration experiments are summarized in Tab. 13.1.

For all experiments 1 mL of the ^{232}U spiked initial solution and 200 µL HTO were simultaneously injected into the column. The eluted water was collected in a polypropylene flask. In addition to this, fractions of the eluate were collected by a fraction collector at certain times during the experiment. The eluate, the eluate fractions and the initial solutions were analyzed for their ^{232}U and HTO concentrations by liquid scintillation counting. Additionally, alpha-spectroscopy was applied to determine the concentration of ^{232}U daughter nuclides. Thus, it was possible to correct the alpha-activities determined by liquid scintillation counting with regard to the alpha-activity contributed by the daughter nuclides. The breakthrough curves for HTO and ^{232}U result from the ^{232}U and HTO concentration in the eluate fractions.

Furthermore, investigations regarding the size distribution of uranium in the initial solutions and in different eluate fractions were performed by ultrafiltration. Ultrafilters with molecular weight cutoffs of 1 kD to 1000 kD (MICROSEP, Filtron, Northborough, MA, USA) were applied.

Table 13.1: Experimental conditions for the column experiments.

Experiment number	U / groundwater equilibration time (d)	Column length (cm)	Uranium concentration (mol/L)	Darcy velocity ν_D (m/d)	Pore water flow velocity ν (m/d)	Effective porosity ε	Longitudinal dispersion coefficient D_L (cm^2/s)
1	0.04	25	$5.1 \cdot 10^{-7}$	0.321	0.970	0.331	$8.64 \cdot 10^{-5}$
2	0.63	25	$4.5 \cdot 10^{-7}$	0.314	0.949	0.331	$3.73 \cdot 10^{-5}$
3	11	25	$4.9 \cdot 10^{-7}$	0.312	0.943	0.331	$3.70 \cdot 10^{-5}$
4	82	25	$4.2 \cdot 10^{-7}$	0.310	0.934	0.332	$3.34 \cdot 10^{-5}$
5	5	25	$4.4 \cdot 10^{-7}$	2.030	6.078	0.334	$2.14 \cdot 10^{-4}$
6	6	25	$4.7 \cdot 10^{-7}$	0.038	0.114	0.333	$1.58 \cdot 10^{-5}$
7	5	50	$4.1 \cdot 10^{-7}$	0.241	0.724	0.333	$2.55 \cdot 10^{-5}$
8	5	75	$4.3 \cdot 10^{-7}$	0.239	0.697	0.343	$3.24 \cdot 10^{-5}$

^{232}U species distribution

Species calculations for the groundwater GoHy-532 ([UO_2^{2+}]: $5 \cdot 10^{-7}$ mol/L, pH 7.2 ± 0.1, 1 % CO_2) were performed to determine the distribution of uranium species in the investigated groundwater/sediment system. The calculations based on complex formation constants compiled by Grenthe et al. [32] (NEA data base) and stability constants for the complex formation of UO_2^{2+} with humic acids published by Czerwinski et al. (UO_2HA(II)) [35] and Zeh et al. (UO_2OHHA(I)) [39]. Two calculations were performed at Eh = 800 mV and Eh = -220 mV, respectively. Uranium(VI) occurs at Eh = 800 mV and pH 7.2 to about 72 % as $UO_2(CO_3)_2^{2-}$, 21 % as $UO_2(CO_3)_3^{4-}$, 2 % as $UO_2(OH)_{2(aq)}$ and only to about 3 % as UO_2OHHA(I) complex. Considering the experimental determined redox potential of the groundwater of –220 mV and assuming thermodynamic equilibration uranium shows a totally different species distribution. The initially added U(VI) should be present in reduced form as U(IV) in form of the $U(OH)_{4(aq)}$ complex. Possibly occurring U(IV) humate complexes were not considered in the calculation because there are no reliable thermodynamic data. Generally it is known from literature that tetravalent actinides like Th(IV) [1] interact stronger with humic substances than hexavalent uranium.

In contrast to the calculated species distribution, ultrafiltration experiments of the ^{232}U labelled groundwaters showed for uranium roughly the size distribution of the humic substances in the groundwater [46]. Fig. 13.2 shows the ^{232}U size distribution in different initial solutions (alpha-activity contribution by daughter nuclides #10 %). From this one can conclude that ^{232}U is mainly associated with humic colloids. Approximately 85 - 90 % of ^{232}U are associated with colloids greater than 1000 D and about 20 - 30 % occur in form of ionic species, probable carbonato complexes.

Up to now it can not definitely be stated whether and to what extend the humic colloid-bound uranium is present in the reduced tetravalent state. From neptunium experiments performed recently [47] it is known that the oxidation state has an essential influence on the neptunium size distribution. The reduction of Np(V) causes a decrease of ionic NpO_2^+ species in solution. Np(IV) is almost quantitatively associated to humic colloids. From that one may expect that the reduction of U(VI) to U(IV) also influences the uranium size distribution. However, no significant changes in the ^{232}U size distribution were observed. Therefore, it can be concluded that there is no significant uranium reduction in the initial solutions.

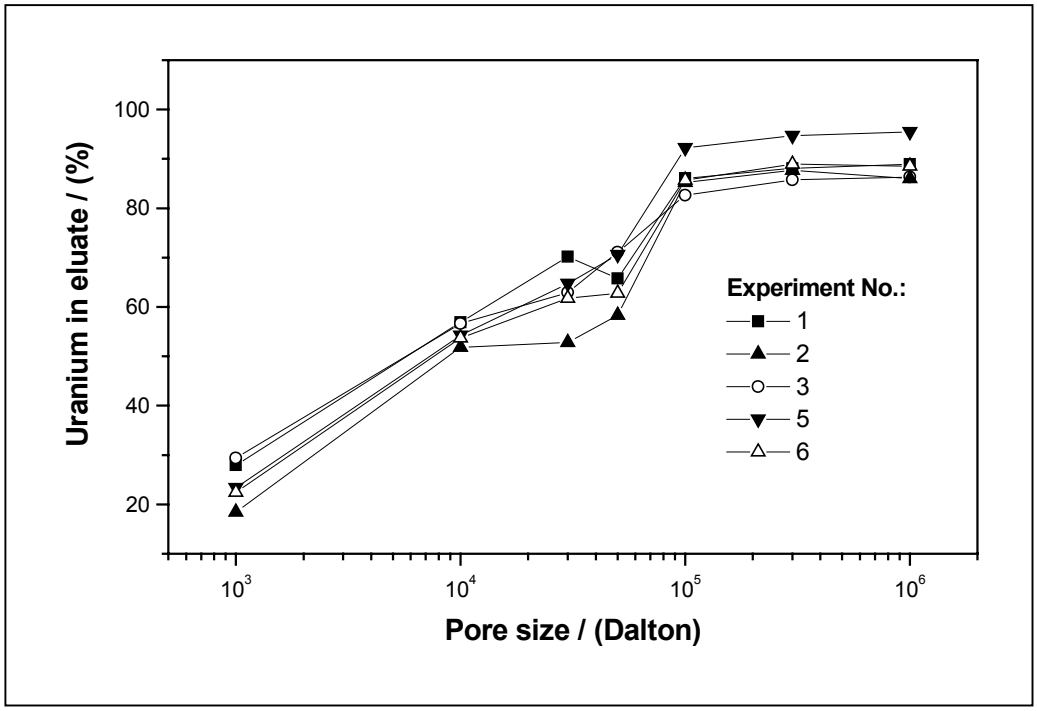

Figure 13.2: ^{232}U size distribution in the initial solutions (GoHy-532, 1 % CO_2, [U]: $4.1 \cdot 10^{-7}$–$5.1 \cdot 10^{-7}$mol/L, activity contribution of daughter nuclides #10 %).

13.2 Results and discussion

13.2.1 Comparison of ^{232}U and HTO breakthrough curves

From the breakthrough curves of ^{232}U and HTO one can conclude how far the ^{232}U migration differs from the groundwater flow.

The migration behavior is characterized by the retardation factor, R_f [Eq. (13.1)], where V represents the volume of the eluate and V_P stands for the effective pore volume of the column.

$$R_f = \frac{V}{V_P} \tag{13.1}$$

$R_f > 1$ indicates a delayed transport of an injected metal ion trough the column compared to that of the conservative tracer with a retardation factor of one, whereas $R_f < 1$ means an accelerated migration.

For example, the ^{232}U and HTO breakthrough curves of experiment No. 7 are depicted in Fig. 13.3. These curves are typical for the experiments carried out under varied experimental

conditions. In addition, a ^{241}Am breakthrough curve is shown in Fig. 13.3 that was measured under comparable conditions [42].

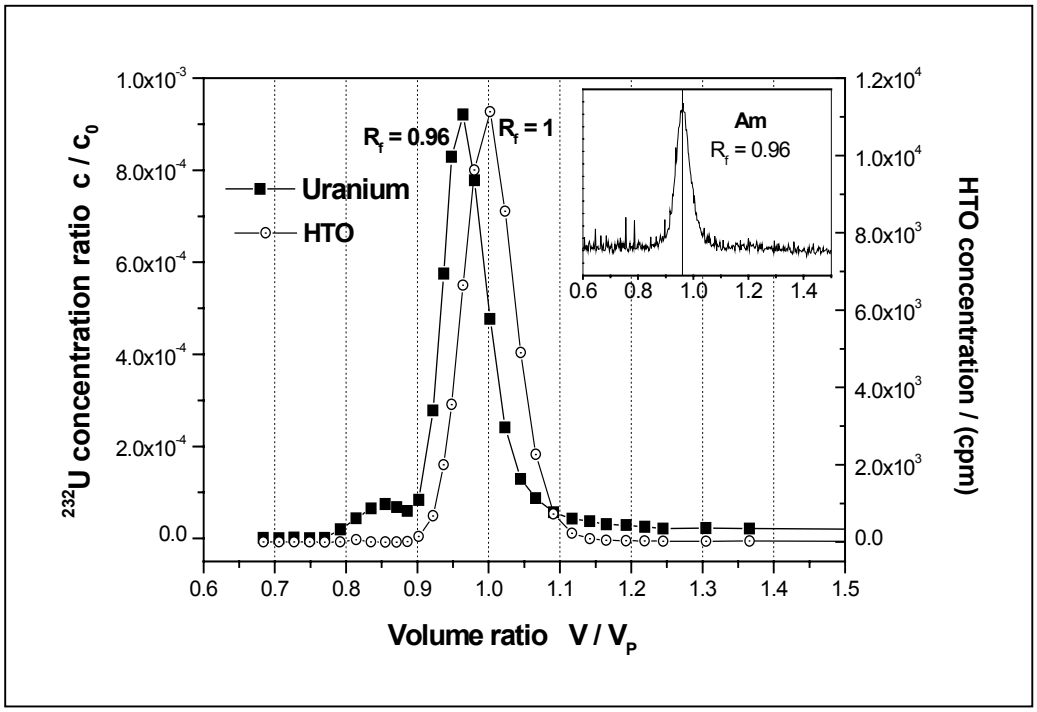

Figure 13.3: ^{232}U and HTO breakthrough curves in comparison to an ^{241}Am breakthrough curve determined under comparable conditions [42].

Fig. 13.3 shows that a fraction of ^{232}U is eluted with the retardation factor $R_f = 0.96$ meaning that this part of uranium is transported slightly faster through the column than the conservative tracer. This accelerated transport is attributed to the association of uranium with humic colloids, which move faster than the conservative water-tracer due to size exclusion processes.

The humic colloid-borne transport is confirmed by ultrafiltration experiments. Fig. 13.4 shows exemplary for experiment No. 7 the size distribution of uranium in fraction 13, eluted at $R_f = 0.92$. In this fraction ^{232}U shows roughly the size distribution of the DOC in the groundwater [46]. No significant fraction of ionic uranium species was obtained.

In addition, the humic colloid-borne ^{232}U transport is confirmed by the R_f value of 0.96 ± 0.01 which is also found in ^{241}Am migration experiments.

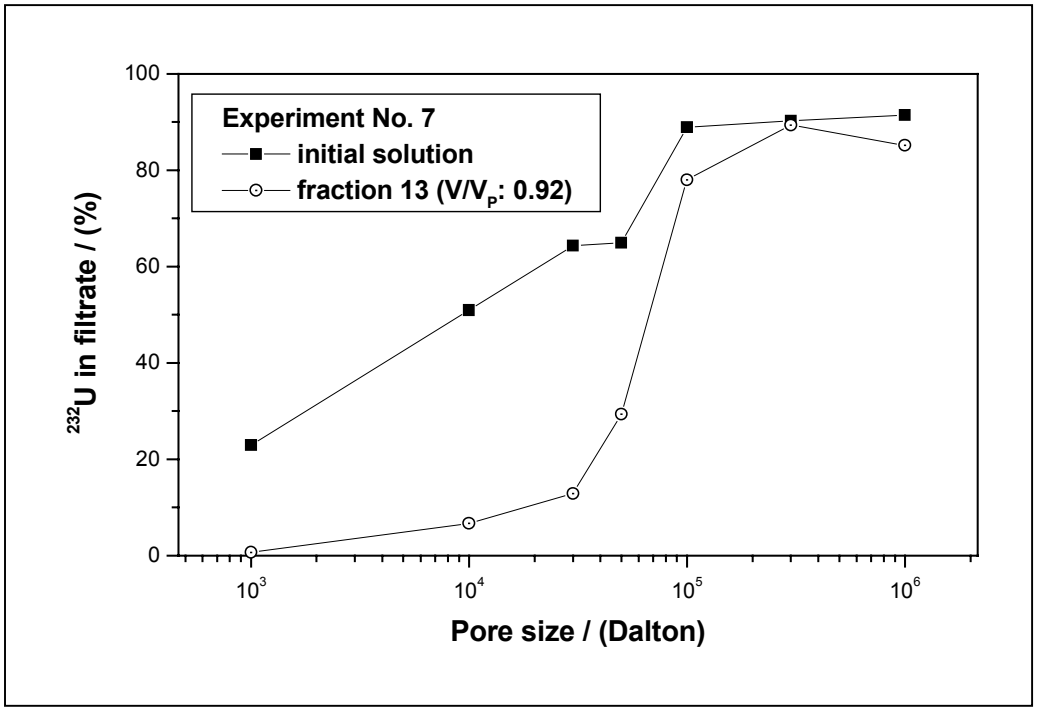

Figure 13.4: Size distribution of ^{232}U in fraction 13, experiment No. 7.

Furthermore, the ^{232}U breakthrough curves show the elution of a smaller fraction of ^{232}U at $R_f = 0.84 \pm 0.01$ and a different strong pronounced tailing after the breakthrough maximum (Fig. 13.3). The early eluted uranium fraction at $R_f = 0.84 \pm 0.01$ is attributed to the association of uranium with much larger colloids, that was shown by filtration experiments. For example, in experiment No. 4 about 50 % of ^{232}U and its daughter nuclides, eluted from $R_f = 0.78$ to $R_f = 0.88$, are bound to colloids > 450 nm. Merely 20 % of the nuclides are associated with colloids smaller than 10^6 Dalton, which is typical for humic colloids. Whether this transport is mediated by enlarged coagulated humic substances, inorganic colloids, or eventual microorganisms, is not known up to now.

There are some indications that the uranium transport with larger colloids is related to a reduction of U(VI) to U(IV). An example for this is the enhancement of the ^{228}Th/^{232}U isotope ratio in the early eluted fraction at $R_f = 0.84 \pm 0.01$. Breakthrough curves of ^{228}Th, which was formed during the experiments with concentrations between 10^{-10} and 10^{-9} mol/L from the radioactive decay of ^{232}U, were determined for two experiments by alpha-spectrometry. As illustrated in Fig. 13.5 the maximum of the ^{228}Th breakthrough curves occurs at a R_f value of about 0.9. This thorium fraction migrates distinctly faster through the column than the humic

colloid-bound non-retarded ^{232}U fraction at $R_f = 0.96 \pm 0.01$. This points to the fact that the tetravalent ^{228}Th migrates with larger colloids.

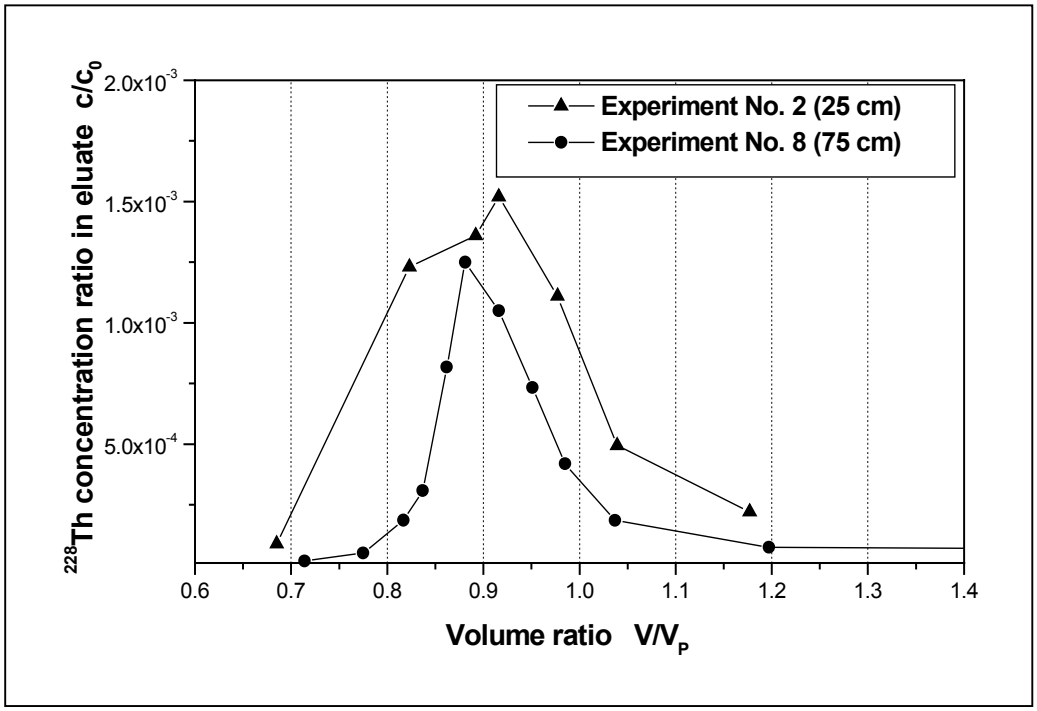

Figure 13.5: ^{228}Th breakthrough curves determined by alpha-spectrometry.

Experiment No. 4 with the highest ^{232}U/groundwater pre-equilibration time of 82 days gives another indication for the possible accelerated transport of U(IV). Here, the uranium fraction with $R_f = 0.84$ is especially pronounced (cf. Fig. 13.7), which points to a faster migration of ^{232}U associated to larger molecules.

13.2.2 Determination of the ^{232}U recovery

As mentioned before, colloid-borne ^{232}U is not only eluted with $R_f = 0.96 \pm 0.01$ (mean value for all experiments) but also earlier at $R_f = 0.84 \pm 0.01$. Beyond it, a different strong pronounced tailing is observed after the breakthrough maximum. To be able to compare the recovery of humic colloid-borne uranium with $R_f = 0.96 \pm 0.01$ for all experiments, a Gaussian distribution with $R_f = 0.96 \pm 0.01$ as center, and a dispersion derived from the HTO migration was taken as a basis. As second component a Gaussian distribution with $R_f = 0.84 \pm 0.01$ (exception experiment No. 8: $R_f = 0.88$) as center was fitted. For example, Fig. 13.6

shows the analysis of the breakthrough curves regarding the recovery of humic colloid-borne ^{232}U for experiment No. 4.

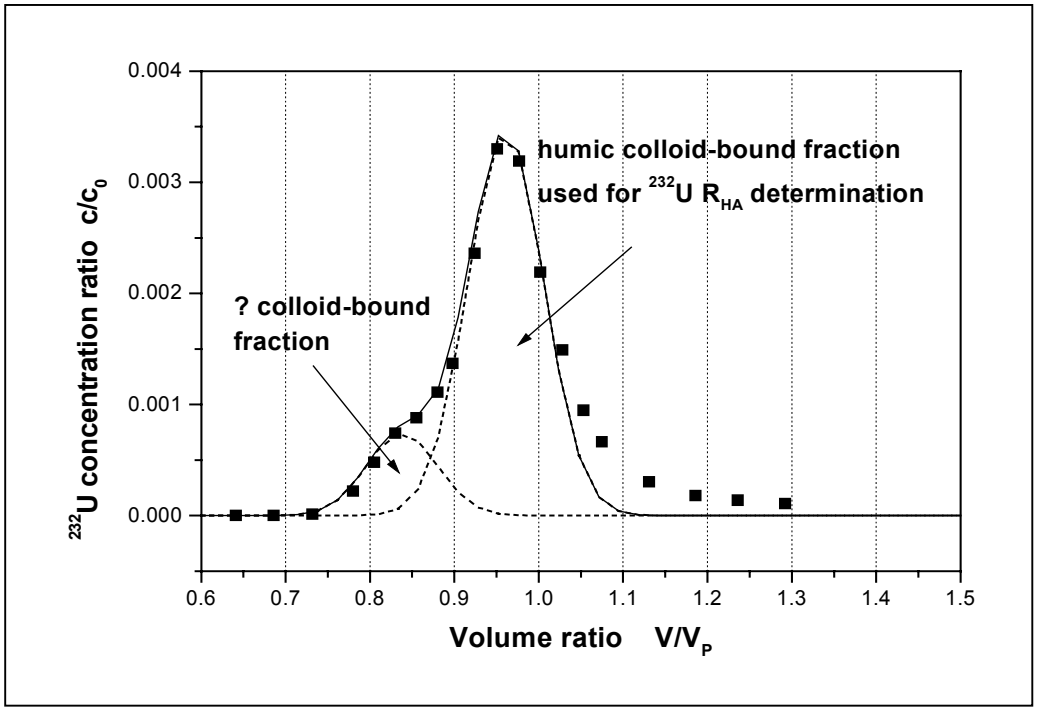

Figure 13.6: Determination of the humic colloid-borne ^{232}U fraction.

Furthermore, we determined the total recovery of ^{232}U after about 5 pore volumes, which includes the recovery of colloid-borne uranium fractions with R_f values of 0.84 ± 0.01 and 0.96 ± 0.01 as well as the recovery of retarded ^{232}U in the tailing. It is calculated according to Eq. (13.2):

$$R = \frac{U_{eluted}}{U_{injected}} \bullet 100\% \qquad (13.2)$$

where U_{eluted} represents the eluted uranium after about 5 pore volumes and $U_{injected}$ stands for the injected uranium.

The total recoveries (R_{tot}) and the recoveries of humic colloid-borne ^{232}U (R_{HA}), which includes only the fraction eluted at R_f = 0.96 ± 0.01 are summarized in Tab. 13.2 for all experiments. As mentioned before, the attachment of the ^{232}U fraction with R_f = 0.96 ± 0.01 to the humic colloid-borne fraction was confirmed by ^{241}Am experiments [42].

Table 13.2: Recovery of ^{232}U in column experiments.

Experiment number	Pre-equilibration time (d)	Darcy velocity v_D (m/d)	Column length (cm)	Total ^{232}U recovery R_{tot} (%)	Humic colloid-borne ^{232}U recovery R_{HA} (%)	Retardation of humic colloid-borne ^{232}U R_f (± 0.01)
Variation of pre-equilibration time						
1	0.04	0.321	25	2.0 ± 0.5	0.4 ± 0.1	0.97
2	0.63	0.314	25	3.5 ± 0.9	1.4 ± 0.3	0.97
3	11	0.312	25	5.2 ± 1.3	3.3 ± 0.8	0.96
4	82	0.310	25	14.2 ± 3.6	7.6 ± 1.9	0.96
Variation of Darcy velocity						
5	5	2.030	25	9.1 ± 2.3	6.5 ± 1.6	0.95
3	11	0.312	25	5.2 ± 1.3	3.3 ± 0.8	0.96
6	6	0.038	25	6.0 ± 1.5	1.5 ± 0.4	0.97
Variation of column length						
3	11	0.312	25	5.2 ± 1.3	3.3 ± 0.8	0.96
7	5	0.241	50	3.5 ± 0.9	2.4 ± 0.6	0.96
8	5	0.239	75	6.4 ± 1.6	2.0 ± 0.5	0.96

13.2.3 Influence of the pre-equilibration time on the migration behavior of uranium

Fig. 13.7 depicts the ^{232}U breakthrough curves for the experiments applying different ^{232}U/groundwater pre-equilibration times before injection into the column. The ^{232}U recoveries are summarized in Tab. 13.2.

Fig. 13.7 shows that a significant increase of the humic colloid-bound ^{232}U fraction occurs with increasing ^{232}U/groundwater pre-equilibration. This observation is confirmed by the recoveries summarized in Tab.13.2. The comparison of the recovery of colloid-borne uranium and the total recovery after about 5 pore volumes as a function of the pre-equilibration time (Tab. 13.2) shows that both recoveries increase with increasing pre-equilibration time. This fact suggests that uranium binding onto the humic colloids becomes stronger with increasing equilibration time. Consequently, uranium becomes less available for an interaction with the sediment surface during the migration through the column. Comparable results were found for americium [42]. In addition, Rao et al. [48] studied the interaction between Eu(III) and humic acids using cation exchange. They described a time-dependent stronger binding of trivalent metal ions with humic substances. However, the cause of this phenomenon is not known up to now.

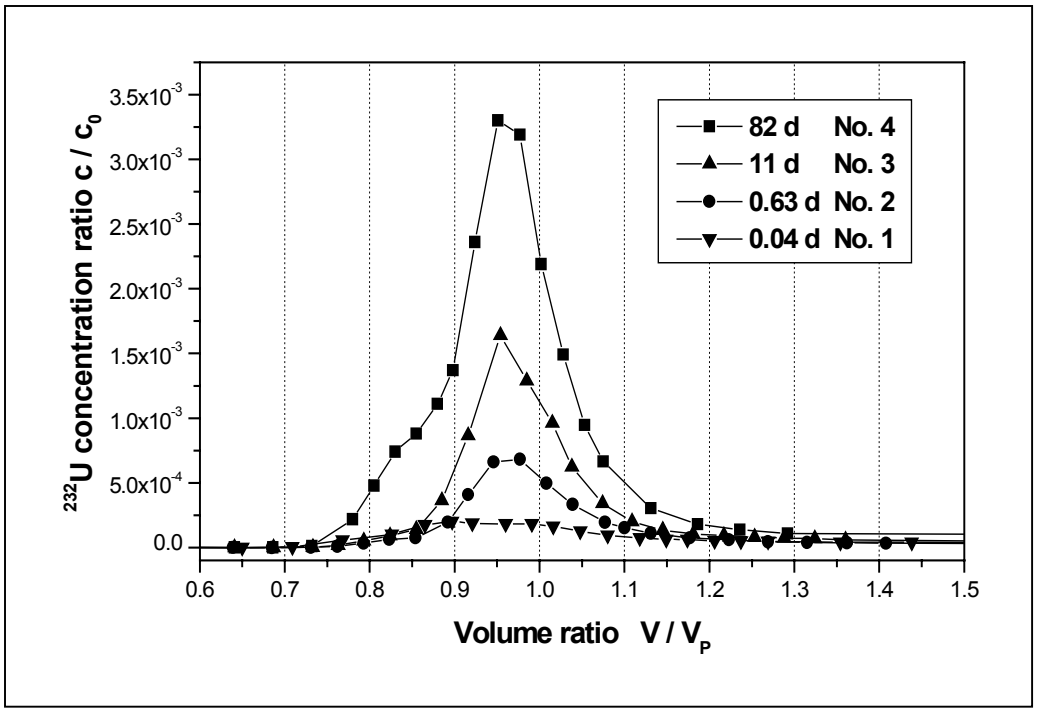

Figure 13.7: ^{232}U breakthrough curves in dependence on the ^{232}U/groundwater equilibration time before injection into the column.

The relatively large fraction of ^{232}U eluted at $R_f = 0.84$ after a equilibration time of 82 days (experiment No. 4) can possibly be attributed to the reduction of uranium(VI) to uranium(IV). The fact that the breakthrough curve of the tetravalent uranium daughter nuclide thorium shows a maximum at $R_f \sim 0.9$ (cf. paragraph 13.2.1) represents a possible reference for that. Nevertheless, an experimental proof for a reduction of uranium(VI) does not exist.

13.2.4 Influence of the groundwater flow velocity and the column length on the migration behavior of uranium

Variations in the groundwater flow velocity and the column length cause variations in the residence time of the colloid-bound uranium in the column. Fig. 13.8 shows the ^{232}U breakthrough curves obtained with different groundwater flow velocities. Increasing the groundwater flow velocity from 0.04 m/d to 2.03 m/d, an increase of the recovery of colloid-bound ^{232}U from 1.5 % to 6.5 % was obtained (Tab. 13.2). This tendency was also found for Am(III) [42].

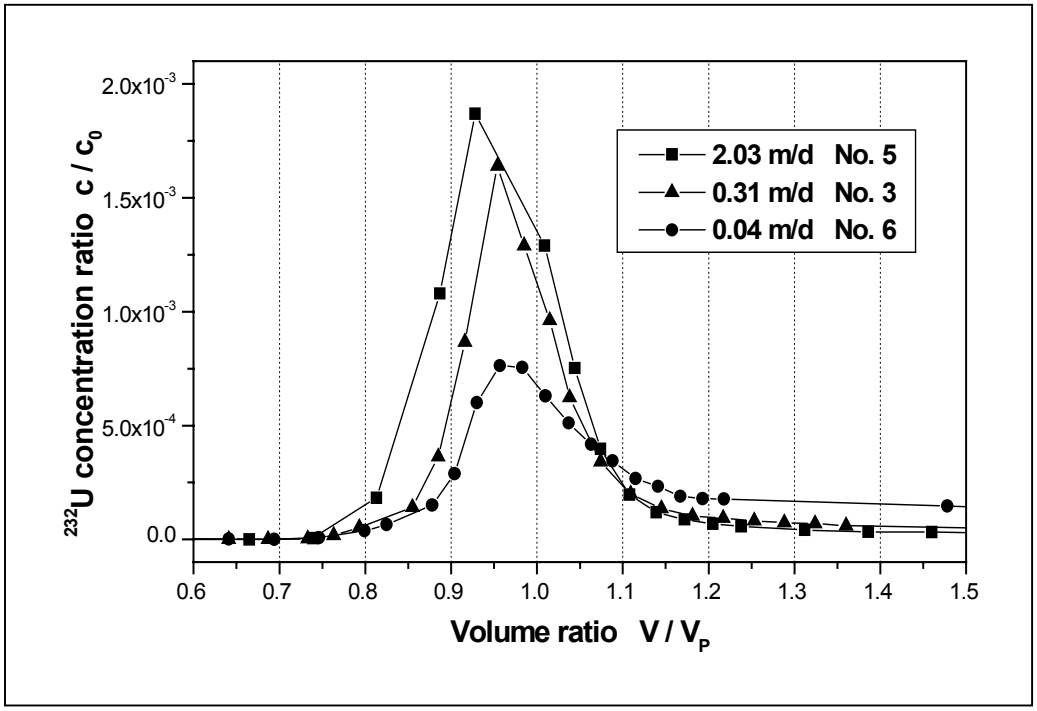

Figure 13.8: ^{232}U breakthrough curves in dependence on the groundwater flow velocity.

Furthermore, a decrease in the recovery of colloid-borne uranium was observed with increasing column length (Tab. 13.2).

Fig. 13.9 depicts the recovery of non-retarded colloid-borne ^{232}U as a function of the residence time in the column. The results consists of the results obtained by varying the groundwater flow velocity and the column length. The recovery of non-retarded colloid-bound transported uranium decreases continuously with increasing residence time in the column, which points to a time-dependent stronger interaction of uranium with the sediment surface. This dependence may be explained by a time-dependent dissociation of uranium from the colloids followed by an interaction with the sediment surface.

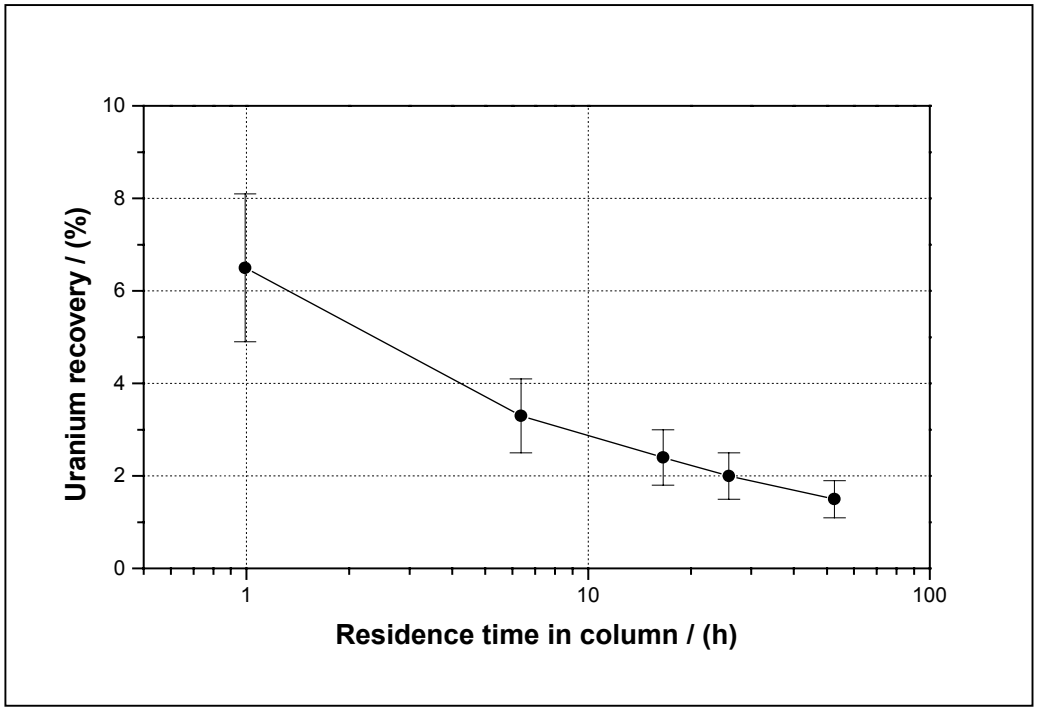

Figure 13.9: Recovery of humic colloid-borne ^{232}U (R_f = 0.96 ± 0.01) in dependence on the residence time in the column. The pre-equilibration time is constant.

In contrast to this fact, the total recovery of eluted ^{232}U shows no distinct trend depending on the migration period (Tab. 13.2). This may be due to the different strong tailing and the varying amount of the colloid-borne uranium fraction at R_f = 0.84 ± 0.01. From data in Fig. 13.8 one can derive that the tailing of the breakthrough curves increases with increasing migration time. That means the interaction of uranium with the sediment shows an increasing influence on the uranium migration.

13.3 Conclusions

The results of the migration experiments in a sandy humic colloid rich groundwater/sediment system show that depending on the experimental conditions a portion of 0.4 up to 7.6 % of the injected uranium migrates non-retarded and colloid bound. Due to size exclusion effects, the migration velocity of the humic colloid-borne uranium is found to be up to 5 % faster than the groundwater flow velocity.

The migration behavior of uranium is strongly influenced by kinetically controlled processes. The recovery of humic colloid-borne uranium depends on the uranium/groundwater equilibration time prior to the injection into the column. The recovery increases with increasing pre-equilibration time, which is attributed to a time-dependent binding of uranium onto the humic colloids with different strength. Furthermore, the recovery of uranium depends on the residence time of humic colloid-borne uranium in the column, determined by the groundwater flow velocity and the column length. With increasing residence time a decreasing recovery of humic colloid-borne uranium was observed. These observations are due to a time-dependent dissociation of uranium from the humic colloids followed by an interaction of uranium with the sediment. Up to now it is not known to what extent U(VI) is reduced to U(IV) during the experiments. First indications point to the reduction of uranium and a colloid-borne transport of U(IV).

^{228}Th, which was formed from ^{232}U by radioactive decay during the migration experiments, also migrates colloid-bound through the groundwater/sediment system. The mean migration velocity of the colloid-borne thorium fraction is about 10 % higher than the groundwater flow velocity.

The column experiments reveal important kinetic effects controlling the humic colloid-borne migration of uranium. These kinetic effects are comparable to those found for instance for the migration behavior of Am(III). Consequently one can conclude that the K_D concept, which is based on thermodynamic equilibrium, is not suitable to describe the humic colloid-borne uranium migration. Therefore, the uranium migration experiments provide a first basis to describe and to predict the subsurface migration of colloidal uranium in natural aquifers. Additional experiments are necessary to further improve the understanding of the basic processes controlling uranium migration, especially experiments investigating the influence of the uranium reduction to the tetravalent oxidation state on the migration behavior of uranium.

14 Effect of humic acid on the uranium(VI) sorption onto phyllite

For the safety assessment of uranium mining areas and for the far field of nuclear waste repositories it is crucial to understand the interaction of uranium with site-specific rock material and furthermore, to know all processes and substances that may influence this interaction. Such processes are, for instance, possible chemical reactions inside a rock pile. Organic materials, such as humic and fulvic acids, may interact with dissolved inorganic contaminants and may affect the sorption behavior of such contaminants on geological materials. Due to complex formation reactions between radionuclides and humic substances the solubility of contaminants can be enhanced. The sorption of the formed species can be either stronger or weaker than the sorption of the uncomplexed species. Thus, the uranium migration in aquifers is affected. Consequently, it is necessary to quantify the influence of humic material on radionuclide sorption.

Phyllite was chosen as a site-specific rock material because it is quite common in the Western Erzgebirge in Saxony, Germany, and because it is closely associated with the uranium deposits of the uranium mining areas in East Germany. Phyllite is a low-grade metamorphic rock that is mainly composed of the minerals quartz, muscovite, chlorite, and albite.

Batch experiments were conducted in order to determine the effect of humic acid on the uranium(VI) sorption onto phyllite in the pH range of 3.5 to 9.5. A site-specific natural humic acid (Kranichsee humic acid), isolated from the bog 'Kleiner Kranichsee' [49], and a ^{14}C-labelled synthetic humic acid type M1 (^{14}C-M1) were used for the experiments. Both humic acids were compared with regard to their sorption behavior on phyllite and their influence on the uranium sorption onto phyllite.

The effect of humic substances of different origin on the uranium(VI) sorption onto various rock materials and minerals, e.g., clay, hematite, silica and ferrihydrite, has been described in the literature [50-55].

14.1 Experimental

Materials

The light-colored phyllite, used for the sorption experiments, was obtained from the uranium mine 'Schlema-Alberoda' near Aue in Western Saxony (Germany). It was collected at a depth of 540 m. The phyllite is composed of 48 vol.% of quartz, 25 vol.% of chlorite, 20 vol.% of muscovite, 5 vol.% of albite, and 2 vol.% of brownish opaqueous material, identified as Ti-

and Fe-oxides [56]. The 63 to 200 µm grain size fraction of the phyllite was used for batch sorption experiments. Its specific surface area, determined by means of the BET method, is 4.0 m^2/g.

The natural humic acid (Kranichsee humic acid) used for the sorption experiments was isolated from surface water of the mountain bog 'Kleiner Kranichsee' that is located in the vicinity of uranium mining sites at Johanngeorgenstadt in Western Saxony (Germany) [49].

The ^{14}C-labelled synthetic humic acid type M1 (^{14}C-M1) was synthesized as described in paragraph 8.

Sorption experiments

The sorption experiments were conducted under atmospheric conditions. 20 mL of a 0.1 M $NaClO_4$ (Merck) solution were added to 500 mg of the rock material (63 to 200 µm fraction) in 50 mL polypropylene centrifuge tubes (Cellstar). Then, the samples were aged for 24 h. After that, additional 18 mL of 0.1 M $NaClO_4$ solution were added. The desired pH was adjusted by addition of dilute $HClO_4$ (Merck) or NaOH (Merck). For studies at pH values higher than 7, a calculated amount of $NaHCO_3$ was added to accelerate the equilibration process with atmospheric CO_2. In the following days the pH was readjusted until the pH was stable. Then 2 mL of a humic acid stock solution (100 mg humic acid/L, 0.1 M $NaClO_4$) was added to reach the final volume of 40 mL and a humic acid concentration of 5 mg/L. The humic acid/mineral contact time was 14 days. The pH was checked and adjusted every day. Then, the experiment was started by adding 84 µL of a $4.8 \cdot 10^{-4}$ M uranyl perchlorate stock solution, prepared in $5 \cdot 10^{-3}$ M $HClO_4$, to obtain a uranyl concentration of $1 \cdot 10^{-6}$ M. The pH was readjusted immediately after the addition of the perchlorate solution. Then, the samples were rotated end-over-end at room temperature for about 60 hours. After this time, the final pH values were determined. Subsequently, the samples were centrifuged at 10000 rpm for 30 minutes. The supernatant was filtered using Minisart N membranes (Sartorius) with a pore size of 450 nm. To avoid contamination caused by conservation agents in the filter membranes the membranes were washed five times with 20 mL of Milli-Q water (Milli-RO/Milli-Q-System, Millipore).

The supernatant (non-filtered solution) and the 450 nm filtrate were analyzed for the final uranium and humic acid concentration. It could be shown that there was no significant difference between the concentrations determined for the supernatant and the 450 nm filtrate. The uranium concentration was determined by ICP-MS (Inductive Coupled Plasma-Mass Spectrometry, Mod. ELAN 5000, Perkin Elmer). The concentration of the natural humic acid

was determined by UV/Vis spectrophotometry (Mod. 8452A, Hewlett Packard) at 254 nm. The concentration of the ^{14}C-labelled synthetic humic acid was determined both by UV/Vis spectrophotometry and by Liquid Scintillation Counting (LSC, Beckman Instruments) after combustion of the material with a sample oxidizer (Mod. P 307, Canberra-Packard).

In addition, the uranium sorption onto the wall of the centrifuge tubes was determined. The effect was about 2-3 % at pH 5 to 7.7. In the acid and alkaline pH range, the vial wall sorption was 0.2-1 %.

The amount of uranium adsorbed to the mineral surface was calculated as the difference between the initial U(VI) concentration ($1 \cdot 10^{-6}$ M) and the sum of the final uranium concentration in the 450 nm filtrates and the amount of uranium adsorbed onto the wall of the experimental vials.

The difference between the initial humic acid concentration (5 mg/L) and the sum of the corresponding final concentration in the 450 nm filtrates and the amount of humic acid sorbed onto the centrifuge tube walls was attributed to humic acid sorption onto the mineral. In case of the ^{14}C-labelled synthetic humic acid the amount of humic acid sorbed onto the phyllite was additionally determined by LSC.

14.2 Results and discussion

In Fig. 14.1 and 14.2 the results of the uranium sorption experiments carried out in the presence of 5 mg/L humic acid are depicted. For the ^{14}C-labelled synthetic humic acid (^{14}C-M1) the humic acid uptake was determined by UV/Vis spectrophotometry of the solution and by LSC measurements both of the solution and of the phyllite. The results of both methods agree well (relative standard deviation: 5 % (2σ)).

Fig. 14.1 shows the humic acid uptake by phyllite for Kranichsee humic acid and for ^{14}C-M1 as a function of pH. Both humic acids are strongly taken up over the entire pH range. From pH 3.6 to 7.7: 86 to 94 % of the Kranichsee humic acid are adsorbed. Above pH 8, the humic acid sorption decreases to 78 % at pH 9.4. The sorption of the synthetic ^{14}C-M1 is in the pH range from 3.6 to 7.7 somewhat lower (4 to 6 %) than the sorption of the Kranichsee humic acid and above pH 8 higher (2 to 5 %) than the sorption of the Kranichsee humic acid.

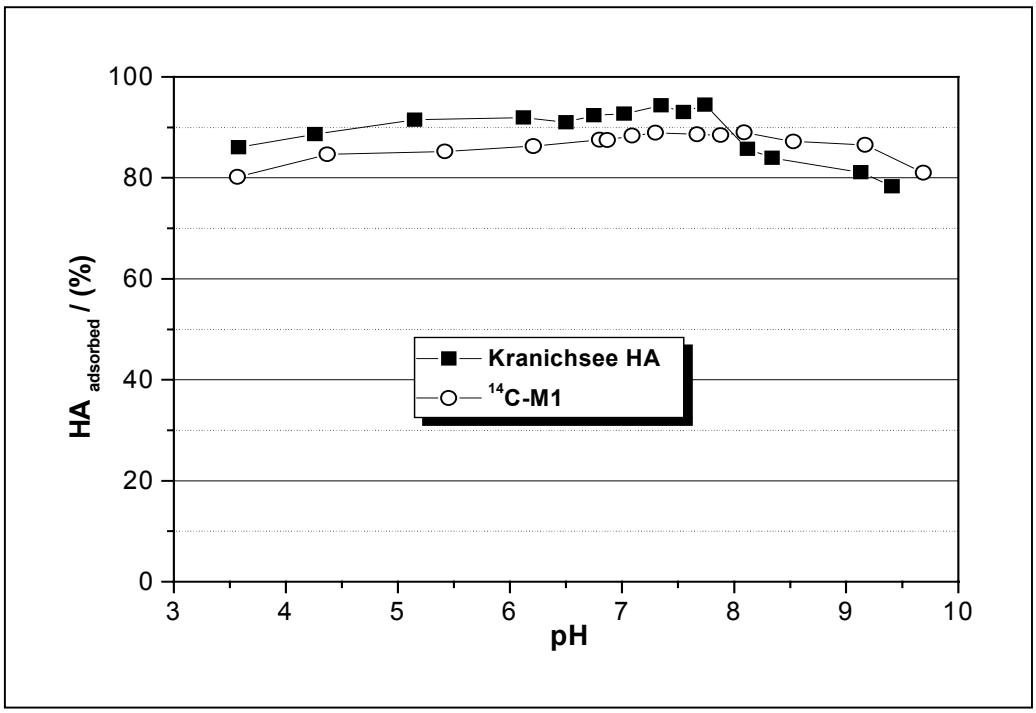

Figure 14.1: Humic acid uptake by phyllite in experiments conducted in the presence of 5 mg HA/L.(Kranichsee humic acid: determined by UV/Vis spectrophotometry; ^{14}C-M1: determined by LSC).

This high humic acid sorption onto phyllite cannot only be attributed to the specific surface area of phyllite of 4.0 m^2/g which was determined by the BET method. Instead of that, we believe that ferrihydrite is responsible for the high humic acid adsorption onto phyllite. Ferrihydrite ($Fe_2O_3 \cdot 1.8\ H_2O$) as secondary mineral phase is formed in the course of the sorption experiments (proved by Arnold et al. [57]) and is visible as precipitate with a slight reddish-brownish color. It has a high specific surface area of 600 m^2/g and thus, it is expected to offer a significant sorption potential both to uranium and to humic acid. This assumption is supported by results found by Payne et al. [53] who investigated the uranium adsorption on ferrihydrite in the presence of humic acid. They found that the humic acid uptake by ferrihydrite as a function of pH was generally strong (approx. 82 to 90 % between pH 3.5 to 9) and decreased only at pH values higher than pH 9.

When discussing the results of the sorption experiments further, it has to be taken into account that the rock material had already been contacted with humic acid for 14 days before uranium(VI) was added. That means, the mineral surfaces are likely to be coated with humic acid at the beginning of the sorption experiments. Thus, sorption sites of the solids may either be blocked by adsorbed humic acid from other aqueous species or the humic acid may provide additional sorption sites due to its complexing ability.

The uranyl sorption onto phyllite in the presence of humic acid was compared to the uranyl sorption found by previously conducted experiments where the sorption of U(VI) onto phyllite was studied in the absence of humic material [57]. The experimental conditions of these experiments were the same as described in paragraph 14.1.2. Fig. 14.2 shows the pH-dependent U(VI) uptake onto phyllite in the absence and in the presence of the natural and the synthetic humic acid.

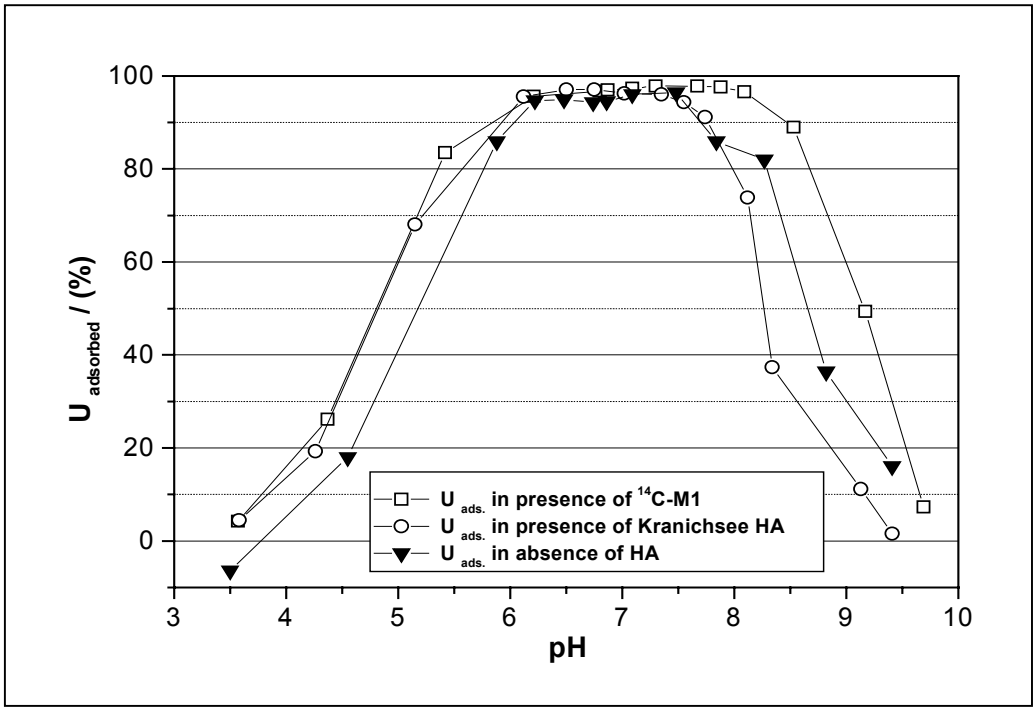

Figure 14.2: Uranium uptake by phyllite in experiments conducted in the presence of 5 mg HA/L. Data for uranium uptake in the absence of humic acid [57] are also shown.

The pH-dependent uranium adsorption on phyllite in the presence of the natural and the synthetic humic acid is similar to the uranium adsorption on phyllite in experiments conducted in the absence of humic acid. The strong uranyl sorption on phyllite (95 - 97 % in the absence of humic acid) is not significantly changed by humic acid in the pH range from 6 to 7.5. This very strong uranium adsorption on phyllite can also be attributed to the component ferrihydrite. Oxidic iron present in solution is known to form coatings on the surface of other minerals and to adsorb uranium well in composite minerals [58]. The small amount of dissolved humic acid (6-7 % of the total humic acid content) is not able to decrease the uranyl uptake on the solid by forming aqueous uranyl humate complexes. Consequently, the maximum of the uranium sorption on phyllite is not shifted to lower pH values, as known for the mineralogical constituents of the phyllite (muscovite, albite and quartz) [59], but

remains unchanged in the pH range from 6 to 7.5 when humic acid is present at 5 mg/L. On the other hand, the large amount of humic acid sorbed onto the mineral surface can only induce a very small enhancement of the uranium sorption. That means, the influence of humic acid on the uranium sorption is suppressed in the near neutral pH range.

In the pH range from 3.6 to 6, the uranium uptake on phyllite is somewhat higher when humic acid is present. This may be attributed to the fact that humic acid is sorbed on the mineral surface thereby providing additional sorption sites due to their complexing ability and/or due to adsorption of uranyl humate complexes on the mineral surface. The enhancement of the uranium uptake is almost the same for Kranichsee humic acid and for ^{14}C-M1. However, above pH 7.5, the influence of the two humic acids on the uranyl uptake by phyllite is different. The Kranichsee humic acid slightly reduces the uranyl sorption on phyllite whereas the synthetic humic acid, ^{14}C-M1, increases the uranyl sorption on phyllite compared to experiments carried out in the absence of humic acid. According to the speciation calculation considerable amounts of HCO_3^- are available to form complexes with uranyl ions ($UO_2(CO_3)_3^{4-}$, $UO_2(CO_3)_2^{2-}$). The inorganic carbonates have a higher complexing ability towards uranyl ions than humic acid. Nevertheless, the weakly sorbing uranyl carbonate complexes [60,61] are not able to predominate the influence of humic acid. Although the uptake of ^{14}C-M1 on phyllite at alkaline pH values is somewhat higher than the uptake of Kranichsee humic acid, there should be additional reasons for their different influence on the uranium sorption.

We conclude that the influence of humic acid on the uranium sorption depends on the pH of the solutions and on the humic acid in question. We conclude further that the ^{14}C-labelled synthetic humic acid (^{14}C-M1) is suitable for future experiments studying the kinetics and reversibility of the uranium and humic acid sorption onto minerals.

15 Conclusions

Within this project four different humic acid model substances with different functionality were developed according the melanoidin concept: a synthetic humic acid with a high content of aromatic structural elements and a low number of carboxylic groups (type M1), a synthetic humic acid type M1 of high purity, a synthetic humic acid with a carboxylic group content comparable to most natural occurring humic acids (type M42), and a nitrogen-free synthetic humic acid.

All synthesized humic acid model substances were characterized for their functional and structural properties and compared to purified commercially available natural humic acid from Aldrich. A radiometric method for determination of functional groups was applied beside conventionally direct and indirect potentiometric titration methods.

The synthetic model substances show structural and functional properties which are comparable to natural humic acids. The functional and structural properties of the synthetic humic acids can be varied by varying the precursor substances. One great advantage of the humic acid model substances represents their low up to not detectable content of inorganic impurities, especially iron, compared to natural humic acids. Furthermore, the synthetic humic acids show a more homogenous distribution of their charge-to-size ratios indicating a higher homogeneity.

Modified humic acids with blocked phenolic hydroxyl groups were also synthesized. They can be used to study the influence of phenolic hydroxyl groups on the complexation behavior of humic acids.

^{14}C-labelled humic acids were synthesized according to the melanoidin concept. They show a stable isotopic labelling in their molecular structure. Applying this synthetic pathway, it is possible to obtain humic acid model substances with specific activity levels, that enables their use in migration and sorption experiments under environmentally relevant conditions.

Synthetic humic acid type M1 and synthetic humic acid type M1 with blocked phenolic hydroxyl groups were distributed to the project partners for comparative studies.

Comparative studies for the interaction of synthetic and natural humic acids with uranium(VI) at pH 4 were performed by extended X-ray absorption fine structure spectroscopy (EXAFS), laser-induced fluorescence spectroscopy, and FTIR spectroscopy.

The analysis of U L_{III}-edge EXAFS data of different uranyl humates using Fluka humic acid and synthetic humic acid type M1 yielded axial U-O distances of 1.77 – 1.78 Å and five equatorial oxygen atoms at distances of 2.37 – 2.39 Å. The equatorial U-O distances for the uranyl humates indicate predominately monodentate coordination of the humic acid carboxylic groups with the uranium. Assuming charge neutralization for the complexation of uranyl ions with humic acid, neutral ligands contribute to the coordination number of five. Similar structural parameters were determined for synthetic humic acid type M1 and Fluka humic acid which indicate a similar complexation behavior. In addition, FTIR spectroscopy showed a comparable coordination of UO_2^{2+} ions with Aldrich humic acid and the synthetic humic acids type M1 and type M42.

Applying laser-induced fluorescence spectroscopy, we determined a similar complexation behavior for synthetic humic acid type M42 and Aldrich humic acid. We determined corresponding loading capacities and complexation constants for the complexation with UO_2^{2+} ions at pH 4.

The spectroscopic methods showed that the synthetic humic acid model substances simulate very well the functionality of natural humic acids. This allows their application in model investigations to improve the knowledge about the complexation process between humic acids and metal ions.

For the first time, we investigated the influence of phenolic hydroxyl groups on the complexation behavior of humic acids with UO_2^{2+} ions. We used the modified humic acid type M1 with blocked phenolic hydroxyl groups as well as the unmodified synthetic humic acid type M1. Applying the charge neutralization model, both humic acids showed comparable complexation constants. However, significant differences exist in their loading capacities with uranyl ions at pH 4. From this we conclude that the blocking of the phenolic hydroxyl groups changes the humic acid complexation behavior with UO_2^{2+} ions.

First laserspectroscopic studies were performed to investigate the complexation behavior of uranium(VI) with humic acid in the absence of CO_2 at pH 7. The complexation experiments showed that uranium(VI) reacts with humic acids under formation of a ternary uranyl hydroxo humate complex. We assumed that $UO_2(OH)_2$ reacts under ligand exchange with the humic acid. For the total complexation reaction, we determined a complexation constant of $\log \beta_{0.1M} = 6.35$. For the charge neutralization reaction of UO_2OH^+ with humic acid at pH 7 in 0.1 M $NaClO_4$, we determined a loading capacity for the humic acid with UO_2OH^+ of 0.91 ± 0.28

and a complexation constant of log $\beta_{0.1M}$= 5.83 ± 0.14. However, to verify these first results additional measurements are recommended.

The migration behavior of uranium in a sandy aquifer system rich in humic substances (Pleistocene quartz sand, groundwater GoHy-532 from Gorleben site, Germany) was studied in laboratory column experiments. A part of the injected uranium migrates non-retarded, slightly faster than the groundwater. This migration behavior can be attributed to the association of uranium with humic colloids, which move faster due to size exclusion processes. The migration behavior of uranium is strongly influenced by the kinetically-controlled interaction processes of uranium with humic colloids. The recovery of non-retarded uranium increases with increasing uranium/groundwater contact time before injection into the column. Furthermore, the recovery of humic colloid-borne uranium decreases with decreasing groundwater flow velocity and increasing column length which corresponds to an increasing residence time of uranium in the column.

Batch experiment were performed to investigate the influence of humic acids on the sorption behavior of uranium onto phyllite, a rock material from the uranium mine 'Schlema-Alberoda' in Western Saxony (Germany). The batch experiments were conducted applying a natural site-specific humic acid (Kranichsee humic acid) as well as a ^{14}C-labelled synthetic humic acid type M1. The natural humic acid and the synthetic humic acid have a similar sorption behavior on phyllite. Their influence on the uranyl sorption is also comparable, especially in the acidic and neutral pH range. In the pH range from 3.6 to 6, the uranium uptake on phyllite is somewhat increased when humic acid is present. In the neutral pH range, the uranium adsorption on phyllite in the presence of humic acids is similar to the uranium adsorption in the absence of humic acids. In the pH range between 7.7 and 9.7, the synthetic humic acid increases the uranyl sorption whereas the natural humic acid decrease the uranyl sorption compared to experiments conducted in the absence of humic acid.

We conclude from the batch experiments that the influence of humic acids on the uranium sorption mainly depends on the pH of the solutions. Furthermore, we conclude that it is useful to use ^{14}C-labelled synthetic humic acid model substances for sorption experiments.

The results of these studies improve the knowledge of the complexation behavior of humic acids with uranium(VI) under aerobic conditions. Nevertheless, in future it will be necessary to investigate the complexation behavior of uranium and other actinides, e.g., thorium and neptunium with humic acids under anaerobic, i.e., reducing conditions. This includes studying

the complexation behavior of these actinides in the tetravalent oxidation state with humic materials as well as studying their sorption and migration behavior in the presence of humic materials. Furthermore, the knowledge about the redox properties of humic substances requires improvement.

Our study also showed the necessity to study kinetic processes controlling the migration behavior of uranium and other actinides in the presence of humic substances. Furthermore, it is necessary to include complexation models of humic acids with actinides in existing modeling codes for geochemical transport. A more detailed knowledge is needed of the interaction of humic acids with actinide ions other than uranium. This knowledge can be obtained using unmodified and modified synthetic and natural humic acids, for instance humic acid with blocked phenolic hydroxyl groups.

This increased knowledge will lead to a better modeling of the geochemical interaction of actinides and to an significantly improved risk assessment for the long-term storage of nuclear waste in underground repositories.

16 References

[1] Choppin, G.R.: The Role of Natural Organics in Radionuclide Migration in Natural Aquifer Systems. Radiochim. Acta **58/59**, 113 (1992).

[2] Jensen, B.S., Halken, T., Jestin, I., Jorgensen, D.*: The role of colloids in the migration of radioelements.* Final report, EUR 16763 EN, 1996, p. 36.

[3] Pompe, S.: *Entwicklung huminsäureähnlicher Melanoidine als Funktionalitätsmodelle für Huminsäuren und ihr Vergleich mit Fluka-Huminsäure hinsichtlich ihres Komplexbildungsverhaltens gegenüber Uran(VI)*. Doctoral thesis, TU Dresden, 1997.

[4] Hänninen, K.I., Klöcking, R., Helbig, B.: Synthesis and Characterization of Humic Acid-Like Polymers. Sci. Tot. Environm. **62**, 201 (1987).

[5] Maillard, L.C.: Synthèse des Matières Humique par Action des Acides Aminès sur les Sucres Réducteurs. Ann. Chim. (Paris) **5**, 258 (1916).

[6] Enders, C., Theis, K.: Die Melanoidine und ihre Beziehung zu den Huminstoffen. Brennstoff Chemie **19**, 360 (1938).

[7] Angrick, M., Rewicki, D.: Die Maillard-Reaktion. Chemie in unserer Zeit **14**, 149 (1980).

[8] Hodge, J.E.: Chemistry of Browning Reactions in Model Systems. J. Agric. Food Chem. **1**, 928 (1953).

[9] Stevenson, F.J.: *Humus Chemistry*. John Wiley & Sons, New York, 1994.

[10] Pompe, S., Bubner, M., Denecke, M.A., Reich, T., Brachmann, A., Geipel, G., Nicolai, R., Heise, K.H., Nitsche, H.: A comparison of natural humic acids with synthetic humic acid model substances: characterization and interaction with uranium(VI). Radiochim. Acta **74**, 135 (1996).

[11] Kim, J.I., Buckau, G.: *Characterization of reference and site specific humic acids.* RCM-Report 02188, TU München, 1988.

[12] Bubner, M., Heise, K.H.: Characterization of Humic Acids. II. Characterization by Radioreagent-Derivatization with [^{14}C]Diazomethane. Forschungszentrum Rossendorf, Institute of Radiochemistry Annual Report 1993, **FZR-43**, 22 (1994).

[13] Stevenson, F.J.: *Humus Chemistry*. John Wiley&Sons, New York, 1982.

[14] Grauer, R.: *Zur Koordinationschemie der Huminstoffe*, Paul Scherrer Institut, Switzerland, Bericht Nr. 24, 1989, p. 7.

[15] Pompe, S., Heise, K.H., Nitsche, H.: Capillary electrophoresis for a "finger-print" characterization of fulvic and humic acids. J. Chromatogr. A **723**, 215 (1996).

[16] MacCarthy, P., Rice, J.A.: Spectroscopic Methods (Other Than NMR) for Determining Functionality in Humic Substances. In: *Humic Substances in Soil, Sediment, and Water*. G.R. Aiken, D.M. McKnight, R.L. Wershaw and P. MacCarthy (eds.). Wiley&Sons, New York, 1985, ch. 21.

[17] Bayer, E., Albert, K., Bergmann, W., Jahns, K., Eisener, W., Peters, K.: Aliphatische Polyether, Grundbausteine von natürlichen Huminstoffen: Nachweis durch Festkörper-^{13}C-NMR-Spektroskopie. Angew. Chem. **96**, 151 (1984).

[18] Ikan, R., Rubinsztain, Y., Ioselis, P., Aizenshtat, Z., Pugmire, R., Anderson, L.L., Woolfenden, W.R.: Carbon-13 cross polarized magic-angle samples spinning nuclear magnetic resonance of melanoidins. Org. Geochem. **9**, 199 (1986).

[19] Ishiwatari, R., Morinaga, S., Yamamoto, S., Machihara, T., Rubinsztain, Y., Ioselis, P., Aizenshtat, Y., Ikan, R.: A Study of the formation mechanism of sedimentary humic substances. – I. Characterization of synthetic humic substances (melanoidins) by alkaline potassium permanganate oxidation. Org. Geochem. **9**, 11 (1986).

[20] Carlsen. L., Lassen, P., Warwick, P., Randall, A.: Radio-Labelled Humic and Fulvic Acids: A New Approach to Studies on Environmental Fate of Pollutants. In: *Humic Substances in the Global Environment and Implications on Human Health.* (N. Senesi, T.M. Miano, eds.), Elsevier Science, 1994, p. 1107.

[21] Warwick, P., Carlsen, L., Randall, A., Zhao, R., Lassen, P.: ^{14}C and ^{125}I Labelling of Humic Materials for Use in Environmental Studies. Chemistry and Ecology **8**, 65 (1993).

[22] Carlsen, L., Lassen, P., Christiansen, J.V., Warwick, P., Hall, A., Randall, A.: Radiochim. Acta **58/59**, 371 (1992).

[23] Bubner, M., Pompe, S., Meyer, M., Heise, K.H., Nitsche, H.: Synthesis of Isotopically Labeled Synthetic Humic Acids. Forschungszentrum Rossendorf, Institute of Radiochemistry Annual Report 1998, **FZR-247**, 25 (1999).

[24] Denecke, M.A., Pompe, S., Reich, T., Moll, H., Bubner, M., Heise, K.H., Nicolai, R., Nitsche, H.: Measurement of the Structural Parameters for the Interaction of Uranium(VI) with Natural and Synthetic Humic Acids using EXAFS. Radiochim. Acta **79**, 151 (1997).

[25] Koningsberger, D.C., Prins, R. (eds.): *X-Ray Absorption: Principles, Applications, Techniques of EXAFS, SEXAFS and XANES*. John Wiley and Sons, New York, 1988.

[26] George, G.N., Pickering, I.J.: *EXAFSPAK: A suite of Computer Programs for Analysis of X-ray Absorption Spectra*. Stanford Synchrotron Radiation Laboratory, Stanford, CA, USA, 1995.

[27] Rehr, J.J., Albers, R.C., Zabinsky, S.I.: High-Order Multiple-Scattering Calculations of X-ray-Absorption Fine Structure. Phys. Rev. Lett. **69**, 3397 (1992).

[28] Hudson, E.A., Allen, P.G., Terminello, L.J., Denecke, M.A., Reich, T.: Polarized X-Ray-Absorption Spectroscopy of the Uranyl Ion: Comparison of Experiment and Theory. Phys. Rev. B **54**, 156 (1996).

[29] Denecke, M.A., Reich, T., Pompe, S., Bubner, M., Heise, K.H., Nitsche, H., Allen, P.G., Bucher, J.J., Edelstein, N.;., Shuh, D.K.: Differentiating between Monodentate and Bidentate Carboxylate Ligands Coordinated to Uranyl Ions Using EXAFS. J. Physique IV 7, C2-637-8 (1997).

[30] Koglin, E., Schenk, H.J., Schwochau, K.: Spectroscopic Studies on the Binding of Uranium by Brown Coal. Appl. Spectrosc. **32**, 486 (1978).

[31] Wolery, T.J.: *EQ3/6, A Software Package for the Geochemical Modeling of Aqueous Systems.* UCRL-MA-110662 Part 1, Lawrence Livermore National Laboratory, 1992.

[32] Grenthe, I., Fuger, J., Konings, R.J.M., Lemire, R.J., Muller, A.B., Nguyen-Trung, Cregu, C., Wanner, H.: *Chemical Thermodynamics of Uranium*, 1st ed., Elsevier Science, Amsterdam, 1992.

[33] Brachmann, A.: *Zeitaufgelöste laser-induzierte Fluoreszenzspektroskopie zur Charakterisierung der Wechselwirkung des Uranylions mit Huminsäuren und Carboxylatliganden.* Doctoral thesis, TU Dresden, 1997.

[34] Kim, J.I., Czerwinski, K.R.: Complexation of Metal Ions with Humic Acids: Metal Ion Charge Neutralization Model. Radiochim. Acta **73**, 5 (1996).

[35] Czerwinski, K.R., Buckau, G., Scherbaum, F., Kim, J.I.: Complexation of the Uranyl Ion with Aquatic Humic Acid. Radiochim. Acta **65**, 111 (1994).

[36] Pompe, S., Brachmann, A., Bubner, M., Geipel, G., Heise, K.H., Bernhard, G., Nitsche, H.: Determination and Comparison of Uranyl Complexation Constants with Natural and Synthetic Humic Acids. Radiochim. Acta **82**, 89 (1998).

[37] Heise, K.H., Nicolai, R., Pompe, S., Bubner, M., Nitsche, H.: FTIR-Untersuchungen zur Komplexierung von Uran(VI) durch huminsäureähnliche Melanoidine. GDCh-Tagung, FG Nuklearchemie, Dresden, 07.-09.09.1998.

[38] Choppin, G.R., Allard, B.: Complexes of Actinides with Naturally Occurring Organic Compounds. In: *Handbook on the Physics and Chemistry of the Actinides.* Vol. 3, (A.J. Freeman and C. Keller, eds.), Elsevier Sci. Publ., Amsterdam, 1985, p. 407.

[39] Zeh, P., Czerwinski, K.R., Kim, J.I.: Speciation of Uranium in Gorleben Groundwaters. Radiochim. Acta **76**, 37 (1997).

[40] Glaus, M.A., Hummel, W., Van Loon, L.R.: Stability of Mixed-Ligand Complexes of Metal Ions with Humic Substances and Low Molecular Weight Ligands. Environ. Sci. Technol. **29**, 2150 (1995).

[41] Davies, C.W.: Ion Association: Butterworths, London, 1962.

[42] Artinger, R., Kienzler, B., Schüßler, W., Kim, J.I.: Effects of humic substances on the ^{241}Am migration in a sandy aquifer: column experiments with Gorleben groundwater/sediment systems. J. Contam. Hydrol. **35**, 261 (1998).

[43] Kim, J.I., Delakowitz, B., Zeh, P., Klotz, D., Lazik, D.: A Column Experiment for the Study of Colloidal Radionuclide Migration in Gorleben Aquifer Systems. Radiochim. Acta **66/6**7, 165 (1994).

[44] Kim, J.I., Zeh, P., Runde, W., Mauser, C., Paskalidis, B., Kornprobst, B., Stöwer, C.: *Nuklidmigration (99Tc, 237Np, 238Pu, 241Am) im Deckgebirge und Salzstsock des geplanten Endlagers Gorleben*. RCM-Report 01495, TU München, 1995.

[45] Kim, J.I., Delakowitz, B., Zeh, P.: *Migration behaviour of radionuclides. In: Colloid migration in groundwaters: geochemical interactions of radionuclides with natural colloids*. Final report, EUR 16754EN, 1996, p. 63.

[46] Artinger, R., Kienzler, B., Schüßler, W., Kim, J.I.: Sampling and Characterization of Gorleben Groundwater/Sediment Systems for Actinide Migration Experiments. In: *Effects of Humic Substances on the Migration of Radionuclides: Complexation and Transport of Actinides*. First Technical Progress Report of the EC Project No. FI4W-CT96-0027 (G. Buckau, ed.). Forschungszentrum Karlsruhe, Wissenschaftliche Berichte, FZKA 6124, Karlsruhe, 1998, p. 23.

[47] Artinger, R., Seibert, A., unpublished.

[48] Rao, L., Choppin, G. R., Clark, S. B.: A study of metal-humate interactions using cation exchange. Radiochim. Acta **66/67**, 141 (1994).

[49] Schmeide, K., Zänker, H., Heise, K.H. and Nitsche, H.: Isolation and Characterization of Aquatic Humic Substances from the Bog ″Kleiner Kranichsee″. In: *Effects of Humic Substances on the Migration of Radionuclides: Complexation and Transport of Actinides.* First Technical Progress Report of the EC Project No. FI4W-CT96-0027

(G. Buckau, ed.). Forschungszentrum Karlsruhe, Wissenschaftliche Berichte, FZKA 6124, Karlsruhe, 1998, p. 161.

[50] Beneš, P., Kratzer, K., Vlcková, Š. and Šebestová, E.: Adsorption of Uranium on Clay and the Effect of Humic Substances. Radiochim. Acta **82**, 367 (1998).

[51] Ho, C.H. and Miller, N.G. (1985) Effect of Humic Acid on Uranium Uptake by Hematite Particles. J. Colloid Interf. Sci. **106**, 281 (1985).

[52] Labonne-Wall, N., Moulin, V. and Vilarem, J.-P.: Retention Properties of Humic Substances onto Amorphous Silica: Consequences for the Sorption of Cations. Radiochim. Acta **79**, 37 (1997).

[53] Payne, T.E., Davis, J.A. and Waite, T.D.: Uranium Adsorption on Ferrihydrite - Effects of Phosphate and Humic Acid. Radiochim. Acta **74**, 239 (1996).

[54] Payne, T.E., Shinners, S. and Twining, J.R.: Uranium Sorption on Tropical Wetland Sediments. In: *Uranium Mining and Hydrogeology II. Proceedings of the International Conference and Workshop. Freiberg, Germany, September 1998*, (ed. B. Merkel, C. Helling and St. Hurst), von Loga, Köln, 1998, pp. 298.

[55] Ticknor, K.V., Vilks, P. and Vandergraaf, T.T.: The effect of fulvic acid on the sorption of actinides and fission products on granite and selected minerals. Appl. Geochem. **11**, 555 (1996).

[56] Arnold, T., Zorn, T., Bernhard, G. and Nitsche, H.: Characterization of Phyllite with SEM/EDS, PIXE, and Thin Section Microscopy. Forschungszentrum Rossendorf, Institute of Radiochemistry Annual Report 1997, **FZR-218**, 1 (1998).

[57] Arnold, T., Zorn, T., Bernhard, G. and Nitsche, H.: Sorption of Uranium(VI) onto Phyllite. Chem. Geol. **151**, 129 (1998).

[58] Payne, T.E., Davis, J.A. and Waite, T.D.: Uranium Retention by Weathered Schists - The Role of Iron Minerals. Radiochim. Acta **66/67**, 297 (1994).

[59] Schmeide, K., Jander, R., Heise, K.H. and Bernhard, G.: Effect of Humic Acid on the Uranium(VI) Sorption onto Phyllite and its Mineralogical Constituents. In: *Effects of Humic Substances on the Migration of Radionuclides: Complexation and Transport of Actinides.* Second Technical Progress Report of the EC Project No. FI4W-CT96-0027 (G. Buckau, ed.). Forschungszentrum Karlsruhe, Wissenschaftliche Berichte, FZKA 6324, Karlsruhe, 1999, p. 199.

[60] Ticknor, K.V.: Uranium Sorption on Geological Materials. Radiochim. Acta **64**, 229 (1994).

[61] Waite, T.D., Davis, J.A., Payne, T.E., Waychunas, G.A. and Xu, N.: Uranium(VI) Adsorption to Ferrihydrite: Application of a Surface Complexation Model. Geochim. Cosmochim. Acta **58**, 5465 (1994).

[62] Schnitzer, M., Khan, S.U.: *Humic substances in the environment.* A.D. McLaren, (Hrsg.), Marcel Dekker, Inc., New York, 1972.

17 Acknowledgment

The authors would like to thank Monika Meyer, Rosemarie Ruske, Renate Jander and Andrea Schubert for their valuable help in synthesizing, purification and characterization of the humic acids, Dr. Gerhard Schuster for thermoanalytical investigations, Dr. Waltraud Wiesener for ICP-MS analyses as well as Roswita Nicolai and Heidemarie Görner from the Institute of Bioinorganic and Radiopharmaceutical Chemistry for FTIR spectroscopic measurements and elemental analyses, respectively.

Thanks are given to Dr. Gerhard Geipel for the very good cooperation and his support during the performance and evaluation of laserspectroscopic investigations.

We thank Dr. Melissa Denecke and Dr. Tobias Reich for the very good collaboration in the performance and evaluation of the EXAFS measurements. We would also like to thank HASYLAB for the allotment of measurement time.

Dr. Vinzenz Brendler we thank for speciation calculations.

We would like to thank Dr. Klaus Albert and Matthias Pursch from the Institute of Organic Chemistry of the University Tübingen for recording of ^{13}C-CP/MAS-NMR spectra and for their support in the interpretation of these spectra.

The authors thank Prof. Dr. J.I. Kim for giving us the possibility to perform column experiments at the Institute of Nuclear Waste Management in Karlsruhe. In particular we thank Dr. Robert Artinger for the very good cooperation in performing and evaluating the column experiments.

At this place we would like to thank all colleagues who contributed to the success of this work.

A Appendix - Analytical methods used for the characterization of humic acids

A.1 Elemental analysis

The determination of the carbon, hydrogen and nitrogen content of the humic acids was performed with an elemental analyzer (model CHNS-932, Leco, St. Joseph, MI, USA).
Ash and moisture contents of the humic acids were determined thermoanalytically with the CH-analyzer RC 412 (Leco, St. Joseph, MI, USA) and the thermoanalyzer STA 92 (Setaram, Lyon, France). The samples were heated in a stream of oxygen. The amount of water, which was released up to about 150 °C, was measured for the estimation of the moisture content. The ash content corresponds to the ignition residue after heating the sample to 700 °C.
The inorganic constituents of the humic acids were determined by ICP-MS analyses after digestion of the humic acids with HNO_3 in a microwave.

A.2 Functional groups

A.2.1 Radiometric determination of functional groups [12]

[^{14}C]diazomethane with a known specific activity was used for the radiometric determination of humic acid carboxylic and phenolic OH groups. It was produced from diazald-N-methyl-[^{14}C] with a specific activity of 1.9 GBq/mmol (Sigma, Aldrich) that was diluted with inactive Diazald® (Aldrich). The methylation of the humic acid was carried out under reduced pressure at –10 to 0 °C in a vacuum apparatus. The specific activity of the humic acids after methylation was determined by liquid scintillation counting (Beckman Instruments, Fullerton, CA, USA) after combustion of the substances with a sample oxidizer (model P307, Canberra-Packard, Warrenville, IL, USA).
The saponification of the permethylated humic acids was done by stirring the humic acid with methanolic NaOH at 70 °C for 4 hours. The activity of the methanol which was released during the saponification was also determined by liquid scintillation counting.

A.2.2 Calcium acetate method

The carboxylic group content of the humic acids was determined with the calcium acetate method according the method described in [62], which allows the humic acid to react with an excess of 1 N $Ca(CH_3COO)_2$. Humic acids liberate acetic acid during the reaction with calcium acetate. The released acetic acid is then titrated with NaOH solution.

$$2R-COOH + Ca(CH_3COO)_2 \rightarrow (R-COO)_2Ca + 2CH_3COOH$$

R: Humic acid molecule

For sample preparation and preparation of the calcium acetate solution CO_2-free water was used. The samples were prepared and titrated under inert gas. For titration, we used the automatic titration system TPC 2000 (Schott, Hofheim, Germany) applying the titration software TR 600, version 5.02.

A.2.3 Barium hydroxide method

The total proton exchange capacity was determined by the barium hydroxide method described in [62], which allows humic acid to react with an excess of $Ba(OH)_2$, followed by titration of the unused base with 0.1 M HCl:

$$Ba(OH)_2 + 2HA \rightarrow BaA_2 + 2H_2O$$

HA: Humic acid

Sample preparation as well as titration were done under inert gas. CO_2-free water was used. For titration, we used the automatic titration system TPC 2000 applying the titration software TR 600, version 5.02.
The difference between the total proton exchange capacity determined by barium hydroxide method and the carboxylic group content determined by calcium acetate exchange corresponds to the number of phenolic OH groups of the humic acid.

A.2.4 Direct titration

The determination of the humic acid proton exchange capacity was performed by acid-base titration of humic acid which was previously dissolved in alkaline solution.
A stock solution of humic acid was made by dissolving humic acid in a known volume of 0.1 M NaOH and diluting this solution with 0.1 M $NaClO_4$ under inert gas conditions. An aliquot of this solution was then titrated against 0.1 M $HClO_4$ under inert gas to determine the excess of NaOH which was not used for dissolving, i.e., deprotonation of the humic acid.

A.3 Capillary electrophoresis

Capillary electrophoretic investigations were performed using the capillary electrophoresis system P/ACE 2050 (Beckman Instruments, Palo Alto, CA, USA) with a variable separation voltage of 1 to 30 kV and an UV photometer detector. Before sample loading, the capillary was conditioned for 2 min with 0.1 M NaOH and then for 2 min with buffer solution. As electrolyte system we used a potassiumdihydrogenphosphate-sodiumtetraborate buffer (3 mM KH_2PO_4, 6 mM $Na_2B_4O_7$) with pH 8.9. The sample was injected into the column by pressure injection for 15 s. The separation was carried out at 30 °C with a voltage of 30 kV. Detection was done on-line at the catodic site of the capillary at 214 nm. The humic acids were dissolved in 10^{-3} M NaOH with a concentration of 400 mg/L. The solutions were used directly for injection. No filtration or other special sample treatment was necessary.

A.4 Structural characterization

A.4.1 FTIR spectroscopy

FTIR measurements were carried out with the spectrometer model SPECTRUM 2000 (Perkin Elmer Europe B.V., Nieuwerke, NL). Spectra were recorded in the MIR range as KBr pellets and in the FIR range as polyethylene pellets with a diameter of 13 mm and optimized sample amounts.

A.4.2 ^{13}C-CP/MAS-NMR spectroscopy

^{13}C-CP/MAS-NMR measurements were performed by a Bruker MSL 200 spectrometer (Bruker, Rheinstetten, Germany). Magic-angle spinning was executed at rates of 10000 Hz. The spectra were recorded using 90° pulse length of 4.4 µs, contact time of 1 ms, and delay time of 1 s.

A.4.3 Pyrolysis-Gas chromatography/Mass spectrometry (Py-GC/MS)

The filament pyrolysis system Pyroprobe (model 2000, CDS Analytical Inc., Oxford, PA, USA) on-line coupled with a gas chromatograph (model HP 5890, Hewlett Packard, Waldbronn, Germany) with a mass selective detector (mass range 20-450 atomar mass units; model HP 5871a) was used. Pyrolysis and separation were done in a helium atmosphere as described in [3].